# SYNTHESIS, CHARACTERIZATION, AND PRELIMINARY APPLICATION OF NEW BIOCOMPATIBLE NANOGELS USEFUL AS ANTICANCER DRUG DELIVERY SYSTEMS

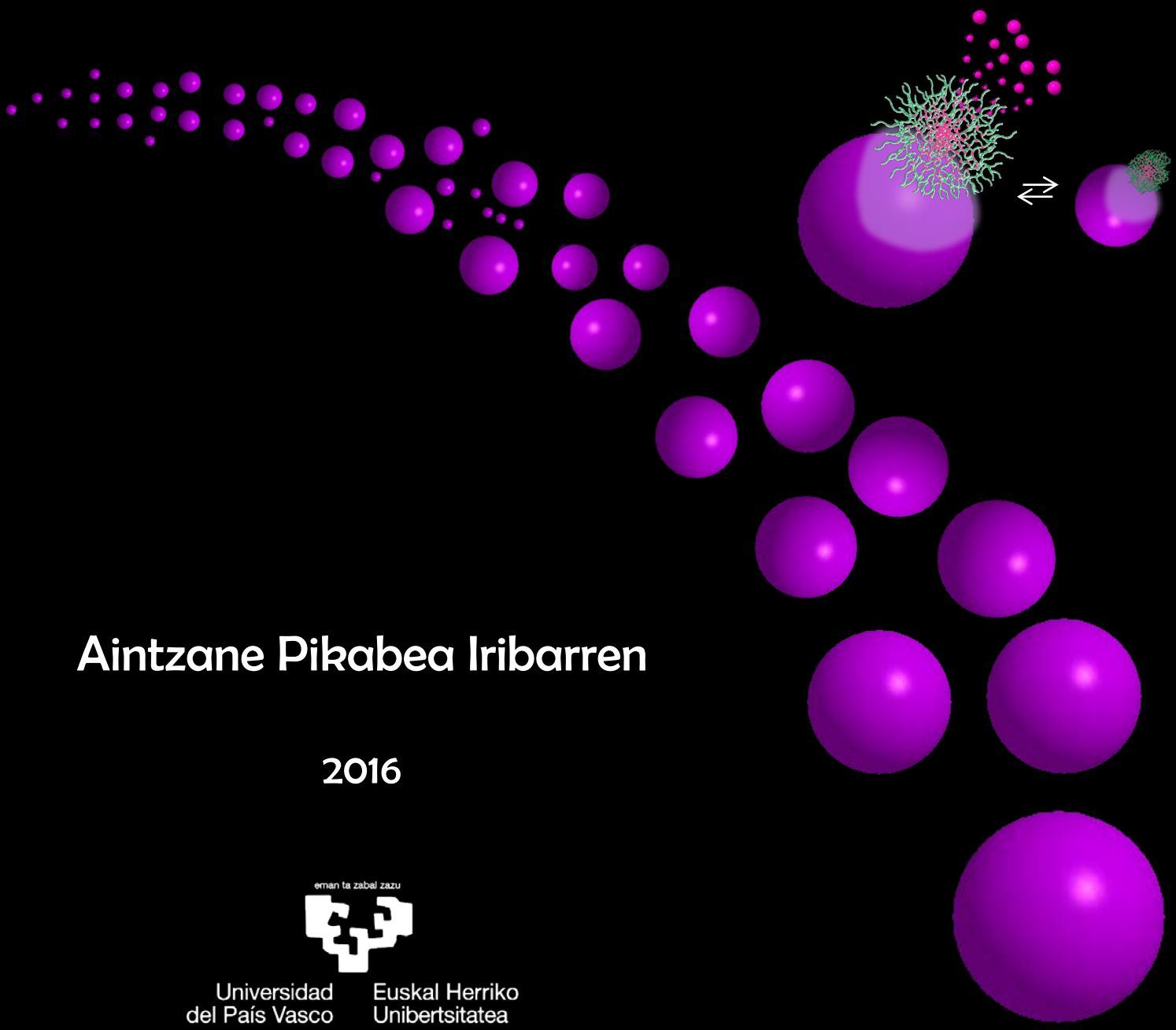

Aintzane Pikabea Iribarren

2016

eman ta zabal zazu

Universidad del País Vasco

Euskal Herriko Unibertsitatea

# SYNTHESIS, CHARACTERIZATION, AND PRELIMINARY APPLICATION OF NEW BIOCOMPATIBLE NANOGELS USEFUL AS ANTICANCER DRUG DELIVERY SYSTEMS

by

Aintzane Pikabea Iribarren

POLYMAT, Ingeniaritza Kimikoa taldea
Kimika Aplikatua Saila
Kimika Zientzien Fakultatea
Euskal Herriko Unibertsitatea UPV/EHU
Donostia-San Sebastián


# Eskerrak

Azkenean! Ailegatu gara akaberara! Ezina ekinez egina! Zuek denak lan honetan duzuen zatiarengatik, ESKERRIK ASKO!!

Lehenik eta behin nire bi zuzendariak eskertu nahiko nituzke: Jacqueline eta Josetxo, MILA ESKER bihotz bihotzez!!! Jacqueline, eskerrik asko benetan hasiera hasieratik nigan jarri duzun konfiantzarengatik, zure hurbiltasunarengatik, zientziaz eta bizitzaz erakutsi dizkidazun gauza guztiengatik, zure laguntza aberatsarengatik, eskaini didazun aukera andanagatik, eta nola ez, azken txanpan tesi honetan jarri duzun indar eta pazientzia guztiarengatik!! Josetxo, muchas gracias a ti también por toda la confianza que has puesto en mí, por todo lo que me has enseñado, y por haberme apoyado y ayudado tanto personalmente como profesionalmente. ¡Te he echado mucho de menos desde que te fuiste a Londres! ¡También agradezco el gran esfuerzo que has tenido que hacer en estos últimos meses! ¡Te deseo muchísima suerte para esta nueva etapa de tu vida! Eskerrik asko biei!! Oraindik hartzeko ditugun ardo kopak eskuan, topa eginen dugu!

Atenasen egin nuen egonaldian zuzendari izan nuen Dimosthenis Stamopoulos ere eskertu nahiko nuke. Θα ήθελα να ευχαριστήσω τον Αναπληρωτή Καθηγητή, Σταμόπουλο Δημοσθένη για την ευκαιρία που που έδωσε να εργαστώ στην ερευνητική του ομάδα για τρεις μήνες. Τον ευχαριστώ πολύ για τις πολύτιμες συμβουλές και την καθοδήγησή του κατα τη διάρκεια της παραμονής μου στην Ελλάδα.

Me gustaría agradecer a Pablo Taboada y su grupo por el trabajo realizado con nuestros nanogeles, por estar siempre dispuestos a ayudarnos y colaborar con nosotros. ¡Muchas gracias por dar un gran empujón a nuestros nanogeles, demostrando su potencial en medicina!

Manolo, agradezco mucho el trabajo que has hecho con nuestros nanogeles, y por haber demostrado que se puede simular cualitativamente su comportamiento. ¡Muchas gracias por ser siempre tan amable y tan atento!

Eskerrik asko gure idazkari eta laguntzaile diren Inés eta Mameni, por ser tan eficaces y amables. Siempre con una sonrisa y la palabra adecuada en la boca, y con la solución en las manos. Zoragarriak zaretelako, mila esker!!

Muchas gracias a Lourdes Cantón por haberme apoyado al principio de la tesis, y también por haberme hecho un sitio en Conta. Miki, zuri ere eskerrik asko, zuen txokoan ongi sentiarazi nauzulako eta behar izan dudanetan lagundu nauzulako. Txapela bezala, *euskara ahoan, ta ibili munduan!* También agradezco a Mario Montes y Oihane Sanz (milesker!) por haberme

aceptado en el garito y haberme dejado formar parte del grupo de Catálisis. Me habéis hecho sentir como en casa. Eskerrik asko! También me gustaría agradecer a José Carlos de la Cal por haberme dejado su despacho en los últimos meses y por su ayuda cuando acabé la carrera. ¡Tus consejos me ayudaron mucho!

Eskerrik asko baita ere Biokimikako Unai Onari eta Oierri zentrifuga erabiltzen uzteagatik, eta orokorrean Biokimika taldeko guztiei, hagitz ongi hartu izan nauzuelako beti. También quiero agradecer a los responsables de TEM. Muchas gracias, Mariano y Maite, por toda la paciencia que habéis tenido, y por todo el trabajo que habéis hecho con nuestros magneto-nanogeles. Parecía imposible, pero después de haber hecho un gran esfuerzo… ¡¡lo hemos conseguido!! Tampoco me quiero olvidar del técnico de RMN, J.I., por todo el trabajo que realizó para entender la morfología de nuestros nanogeles. Muchas gracias por todo el tiempo y paciencia. Agradezco también a Mihail Ipatov por las medidas magnéticas de nuestras partículas y a Alba, Lourdes y Josepi, por haberme ayudado a caracterizar los nanogeles.

¡Cómo me olvidaré de las chicas que han estado y están en nuestro nanogrupo! Muchas gracias Marta, por haberme ayudado cuando lo he necesitado, et merci beaucoup, Laura, pour ta volonté de m´aider. Chicas, ¡me alegro muchísimo de haberos conocido! ¡Estoy segura de que mantendremos nuestra amistad!

Garbiñe, AUNITZ dut zuri eskertzeko, AUNITZ jaso dut zugandik eta!! Tesiarekin hasi nintzenetik izugarrizko babesa, leialtasuna, laguntza, konfiantza, eta indarra sentitu ditut zugandik. Eskerrak aunitz, benetan! Lankide ona, eta lagun ezin hobea izan zara! Behar izan dudan guztietan ondoan egon zara, bazaude, eta egonen zarela ere badakit! Eskerrik asko zure ahizpa ttikia banintz bezala zainddu eta maitatzeagatik!

Garitoko lagunak... Babes ederra eskaini didazue urte hauetan! Porque siempre os he sentido cerca… Ane (eZkerriaZko!), Iñigo eta David… eskerrik asko bihotz bihotzez egunero entzuteko eta laguntzeko prest egoteagatik!! Ha sido un placer haber compartido el despacho con vosotros!! Topa, egin ditugun irri guzti horiengatik!! Iñigo, me quedo a la espera del siguiente pintxopote!

En este punto también quiero agradecer a mis amigos Ion y Óscar… ¡Fue un lujo compartir el despacho con vosotros! Muchísimas gracias por haberme aceptado tan bien en el garito. ¡Es fácil sentirse bien con gente como vosotros! Milesker!

Lizartzako Olatz eta Tolosako Maider ere eskertu nahiko nituzke, tesi honek eman diten gauza aberatsenetariko bat izan delakoz zuen laguntasuna. Hasi nintzenean izugarrizko

babesa izan zineten niretzat eta etxean bezala sentiarazi ninduzuen. Geroztik ondoan sentitu zaituztet eta badut fedea hemendik aitzinera ere horrela segituko dugula! ESKERRAK AUNITZ benetako lagun izateagatik!! Ez dut atzenduko Oñatiko sustrai ttikia… Zu ezagutzeko gogoz nago!

A toda la gente de la Universidad de Granada, por haberme recibido siempre con brazos abiertos y una gran simpatía. Ha sido un placer haberos conocido y compartir momentos con vosotros. ¡Un beso a mis sobrinos granaínos Anibal y Darío!

Karreran zehar ezagutu eta orduz geroztik lagun ditudan haiei… Klasekide izan ziren Irati, Aitziber, Eneko, June eta Nerea, eskerrik asko! Itziar, zenbat urte elkarrekin, ederra sortu den konfiantza! Milesker tesian zehar eman didazun laguntza guztiarengatik! Ane eta Leire, urruti egonda ere hurbil zaudetelako eta lagun onak izatearren, milesker! Eli Oiartzabal, kostaldeko altxorrari, ez dakizu zenbat pozten naizen zu ezagutu izanaz, gustua ematen du horrelako lagun bat ondoan izateak, beti ulertu izan nauzulako, eta lagun hagitz ona izateagatik, esker mila! Tesia hasi aitzinetik ere gidari, egunerokoan babesle eta zaindari, inoiz ez laguntzeko nagi, beti erne eta adi, lagun onaren adibide garbi… ESKERRIK ASKO Amaia beratarrari! Oihane, Eibarko bizilagun, euskaran aldeko borrokan egin ginen izaun, ordutik izan zattut ondun, beti laguntza emateko modun, bihotz bihotzez eskerrik asko lagun!!

Gracias a mi amigo cordobés, una de las personas más maravillosas que he conocido durante la tesis, por su nobleza, positivismo, confianza, apoyo, fuerza, y lealtad. Iré a visitarte a tus tierras, porque ¡siempre nos quedará la penúltima cerveza! Bihotz bihotzez eskerrik asko, Juanjo.

Mendaroko Josebari eskarrik asko, y muchísimas gracias Burgoseko Anari. Egindako irri guztiengatik, por nuestra amistad, inoiz ahaztuko ez ditudan momentu alai horiengatik, y por la confianza que me habéis dado. *Honestamente,* plazer bat zuek ezagutu izana! Vero, lagun bizkaitarra, mila esker zuri ere, hain denbora ttikian eman didazun konfiantzarengatik! Aunitz pozten naiz zu ezagutu izanaz!

Kimika munduan ondoan izan ditudan lagunez gain, kanpokoen babesa ezinbertzekoa izan da eta beraiek ere eskertu nahi ditut bizitza bertze modu batean ikusten eta aitzinera egiten laguntzeagatik, nigan sinestegatik, beti ondoan egoteagatik, eta maitatua eta aske sentiarazteagatik!!

Ameslari zareten Aitziber eta Amaia Telletxeari… zuen ahots eta musika soinuarekin goxatzegatik, badakizuen guzia erakusteagatik, hainbertze momentu aberats eta aske

eskaintzeagatik, eta zuen ahizpa ttikia banintz bezala mattatua sentiarazteagatik… Eskerrak aunitz!! Ailegatu da momentua gitarra hartu eta elkarteko xokoan akaberarik gabeko solasaldi ta kantu saioekin gozatzeko!!!

Ainhoa iruindarra eta Miren iraizoztarra ere eskertu nahi ditut! Hilero egin ditugun egonaldiek eman izan didaten indarrak aunitz balio izan duelakoz, mila esker! Orain dela urte batzuk sortu zenak iraunen duelakoz, toooopa!! Hasta siempre camaradas!! Baztandar mattiak!! Garazi eta Garaxi, eskermile aunitz! Hoi de hoi egitezko lagunek zatela erakustia! Zauntu ginenez geroztik onduan! Ze plazer zuekin elkartzia, zuek lagun izetia… Bihar izen dutenetan laguntzeko prest egotiagatik, ta babes haundie matiagatik, ESKERMILE!!!

Arruzpiko sorginak!!! Sorgin hizkeran, nola ez!! Hapaipimepertzepe mopomepentuputapan gopozaparapaztepeapagapatipik, hapaipimepertzepe apafaparipi, bepestapa, epegoponapaldipi, sopolapas, ipirripi, epelkaparripizkepetapa, epelkaparlapan… Zepe koponfipiapantzapa, zepe gopozapamepen, zepe lapagupuntapasupun! Napahipiz upurtepe hopotapan upurruttipigopo epegopon gaparepen, gepehipixipigopo epelkapartkaparepen epespepentzapan sepegipittkuput! Popollipit hoporipik, epeskeperrapak apaupunipitz!!

Eta azkenik, nire min guztiak zuen min dituzuenei… beti ondoan sentittu zattuztedalakoz, momenturo zuen babesa, konfiantza, maitasuna eta animoak sentittu dittudalakoz, eman didazuen guztiarengatik, eta zuek gabe inondik inora ere ez nintzelakoz akaberara ailegatu izanen… zuentzat tesi hau! ESKERRAK AUNITZ!!!! AUNITZ MATTE ZATTUZTET ama, atta, osaba, anai-arreba aranztar eta azpeitiarrak! eta nola ez, nere bizipoz, inddar eta ilusio diren etxeko bi moñoñuk (gor)aipat nahi dittut… Iluntasunin argi, ittotasunin asnase, hotz dagonin goxotasun, sargori denin freskotasun, estutasunin lasaigarri… Zuen irria izan delakoz difentzikin aitzinera egitteko inddarrik haundina... ESKERRAK AUNITZ, INTZA ta XUBAN!

*Etxekoei…*

# CONTENTS

## CHAPTER 3: FUNCTIONALIZED PDEAEMA-BASED DUAL-STIMULI-RESPONSIVE NANOGELS

## CHAPTER 4: MULTI-STIMULI-RESPONSIVE MAGNETO-NANOGELS

**CHAPTER 5: BIOMEDICAL APPLICATIONS OF PDEAEMA-BASED MULTI-RESPONSIVE NANOGELS**



**CHAPTER 6: CONCLUSIONS**

**APPENDIX I: CHEMICAL STRUCTURES OF THE REAGENTS USED AND LIST OF SYMBOLS**



**APPENDIX II: pH- AND THERMO-SENSITIVITY OF FUNCTIONALIZED PDEAEMA-BASED NANOGELS AND DIFFERENT EFFECTS ON THEIR SWELLING-DE-SWELLING BEHAVIORS**

## APPENDIX III: SYNTHESIS AND CHARACTERIZATION OF MAGNETIC NANOPARTICLES

# 1

# Introduction, General Objectives, and Contents

# 1.1. Introduction

In this PhD thesis, the synthesis, characterization, and preliminary bio-applications of new biocompatible nanogels, are presented. Nanogels are cross-linked polymeric particles in the colloidal range able to swell by absorption of large amounts of solvent, but they do not dissolve due to the constituting structure of the polymer network, physically or chemically cross-linked.[1]

From the biotechnological application's point of view, they represent a highly interesting and unique class of materials mostly due to their stimuli-responsive nature,[2] that is, ability to undergo reversible volume phase transitions in response to stimuli such as pH,[3] temperature,[4,5] ionic strength,[6] magnetic field,[7] biomolecules,[8] photons,[9] redox potential,[10,11] and electric field.[12] Among the different sensitivities, the most relevant to biomedical application are the responses to temperature and pH changes, being thermo- and pH-responsive nanogels useful in the case of releasing a biologically active compound in a physiological medium in which the main variables to consider are changes in temperature and pH, respectively. The stimuli-sensitive swelling-de-swelling behavior of nanogels is governed by the balance and result of the competition between repulsive intermolecular forces (electrostatic and osmotic forces) acting to expand the polymer network, and attractive forces (hydrogen bonds, van der Waals, and hydrophobic interactions) that act to shrink it.[2]

A vast array of polymerization techniques in dispersed media have been described for the preparation of nanogels including emulsion polymerization, inverse mini/microemulsion polymerization, cross-linking between neighbouring chains, and controlled/living radical polymerization.[13-15] Among them, emulsion polymerization is considered one of the most adequate synthetic strategies to produce nanogels, due to its easy control of particle size and size distributions, and ability to simultaneously attain both high molecular weights and high reaction rates.[16-18]

The stimuli-sensitiveness of nanogels could be precisely adjusted to the respective requirements and settings by controlling different characteristics.[1,19] The size of the nanogels governs many functions *in vivo*, including blood circulation time, extravasation, targeting, immunogenicity, internalization, clearance, and uptake mechanisms, and therefore, the optimum size depends on the specific bioapplication. The understanding of the morphology of

nanogels is also interesting to control their swelling-de-swelling behavior. The study of the chemical functionalities distribution would be also beneficial considering that nanogel properties are governed by the interface between the nanoparticles and the surrounding environment. For their successful implementation in biotechnological applications, biocompatibility is also critical.[20]

Nanogels have found their way into the biomedical field through plenty of applications such as drug delivery,[21-23] gene delivery,[24-26] protein uptake,[27] embolic therapies,[28] tissue engineering,[29,30] optical detection,[31] intracellular imaging,[32] cell encapsulation,[33] and carbon dioxide capture and release.[34] Nevertheless, their greatest impact has been in the area of drug delivery, since apart from the stimuli-responsiveness, they benefit from plenty of advantages compared to other nanomaterials.[35] Their straightforward synthetic procedure results in a good control of particle size and surface properties, advantageous for drug uptake and release kinetics. Being small in size, they are able to reach the smallest capillary vessels and penetrate the tissues either through the paracellular or the transcellular pathways. In addition, their porous inner structure leads to high drug loading capacity without any chemical reactions. Moreover, the rapid response to external stimuli results in a sustainable release of drugs, improving the therapeutic efficacy and reducing the side effects. Also, their swollen networks are highly hydrophilic and present a low interfacial energy in a biological environment, reducing interactions with proteins, increasing their bioavailability and biocompatibility, prolonging the circulation time, and thereby improving the chance to target the site.[15,19,36-43] Recently published reviews reflect the practical significance of nanogels as drug carriers.[36,44-49] It has been demonstrated their suitability in anticancer,[50] anti-inflammatory,[51] anti-psoriatic,[52] transdermal,[53] and ocular[54] drug delivery.

Concerning the tumor targeting drug delivery field, an ideal anticancer drug carrier should retain the drug molecules in the bloodstream and normal tissues and release them at the specific tumor sites.[55] So, it would be desirable if drugs could be delivered by a system that sensed the signal caused by the diseases and then acted to release the appropriate amount of drug in response to the signal.[56] In particular, pH is one of the most exploited stimuli for drug delivery applications due to two ubiquitous pH differences. Comparing to the blood and normal tissues (pH 7.4), intracellular compartments (endosomes and lysosomes) are accompanied with a local pH decrease (pH 5.2). The pH of pathological tissues (primary and metastasized tumors) is also slightly more acidic (pH 6.5), mainly because of the accumulation of lactic acid

produced from the high rate of glycolysis in tumor microenvironments.[56-59] These pH variations have provided researchers with a convenient and effective variable for pH-dependent anticancer drug delivery.[60-64] Especially, the use of weak polybases containing ionizable tertiary amine groups has appeared to be of primary importance for the synthesis of pH-responsive nanogels[65] due to the possibility of developing cationic vectors capable of endosome disruption *via* the proton sponge mechanism.[66]

Worth nothing in this regard is the high interest of poly(2-diethylaminoethyl methacrylate) (PDEAEMA)-based nanogels, being biocompatible,[67] showing pH-responsiveness at physiological conditions,[68] and being also able to effectively disrupt endosomes.[57,69] Moreover, amine groups of PDEAEMA allow nanogels to act as a reservoir of therapeutic molecules such as small interfering ribonucleic acids (siRNAs) through coordination or electrostatic interactions.[70] Marek *et al.*[71] and Nagasaki and co-workers[72-78] have reported PDEAEMA-based nanogels with potential utility as endosomolytic agents for nonviral gene delivery, drug delivery carriers, nanoreactors, and skin-specific nanocatalysts for reactive oxygen species.

With the aim of better mimicking biological functions, a system providing multiple specific abilities in response to its surrounding environment is required.[79] Therefore, the current trends are moving toward multi-stimuli-responsive systems, which are sensitive to more than one stimulus, due to their unprecedented control over drug delivery and release, providing superior *in vitro* and/or *in vivo* anticancer efficacy.[80,81] One of these multi-stimuli-sensitive systems are nanogels, as reflected in many recent works.[34,82-87]

Additionally, nanogels could be conveniently hybridized with inorganic nanoparticles, obtaining multifunctionality and novel properties. The adequate design of hybrid nanogels not only improves the probing applications as desirable, but extends their suitability in theranostic, as recently reviewed by several authors.[88-90] Theranostic is a promising field that has proved to be advantageous over conventional medicine, owing to the combination of therapeutic and diagnostic capabilities into a single multifunctional system.[91-93] Hybrid nanogels have shown great potential in biomedical applications such as imaging,[94] chemo-photothermal synergistic therapy,[95] bioseparation,[96] triggered drug release,[97] optical sensing,[98] and hyperthermia,[99] among others. Different nanosized materials such as plasmonics (gold[100] and silver[101]), magnetic (magnetite[102,103] and gadolinium[104]), porous silica[105] and semiconductor (*e.g.* CdSe/CdS core/shell)[89] nanoparticles, nanostructured carbon materials (carbon nanotubes,[106]

graphene,[107] and nanodiamond[108]), and quantum dots[109] have been incorporated to prepare such hybrid nanogels.

Special attention has been focused on magnetic nanoparticles (MNPs) for nanomedicine, mainly because of their biocompatibility, superparamagnetic behavior and stability.[110-117] The large amount of lately published works indicates the tremendous interest in magnetic-labeled nanogels, known as magneto-nanogels (MNGs), for theranostics.[118-133]

## 1.2. General Objectives

The main objective of this PhD thesis is the synthesis and characterization of new multi-stimuli-responsive nanogels.

New different PDEAEMA-based dual stimuli-responsive nanogels were synthesized by surfactant-free emulsion polymerization. The effect of different variables and parameters on the stimuli-responsiveness of the nanogels was studied by analyzing their swelling-de-swelling behavior. Moreover, after performing some *in vitro* cytotoxicity tests with the nanogels, their applicability as potential nanocarriers for drug delivery was examined by studying their ability to uptake and release an anticancer drug (doxorubicin hydrochloride), together with their cellular uptake with a cancer cell line (HeLa).

Magnetic-labeled hybrid nanogels were also prepared by using the previously synthesized PDEAEMA-based nanogels. With the aim of investigating the suitability of the MNGs for biomedical applications, *in vitro* preliminary experiments on their biocompatibility with human blood cells were also performed.

## 1.3. Contents

In Chapter 2, the synthesis of pH- and thermo-sensitive PDEAEMA-based cationic nanogels is reported. Their swelling-de-swelling behavior was thoroughly characterized by using light scattering techniques and potentiometric titrations, and the effect of the ionic strength of the medium on the response to different stimuli was also examined. In addition, $^{1}$H-NMR transverse relaxation measurements were carried out to study the morphology of the nanogel particles.

In Chapter 3, a series of new functionalized dual stimuli-responsive PDEAEMA-based nanogels is presented, which were synthesized by taking the nanogels reported in Chapter 2 as reference and varying different variables such as initiator, cross-linker, and stabilizer concentrations, cross-linker type, and some functionalizations. The effect of those variables was understood by thoroughly characterizing the responsiveness to different stimuli and analyzing the morphology of the nanogels.

In Chapter 4, different magneto-nanogel (MNG) families are presented. Their preparation was carried out by incorporating magnetic nanoparticles (MNPs) into PDEAEMA-based nanogels. First of all, different types of MNPs were synthesized, and their morphological, colloidal, crystallographic and magnetic properties were characterized, together with their chemical composition. Then, the MNPs were encapsulated into the nanogels by using different methodologies. The first family was obtained by mixing citric acid-coated MNPs and PDEAEMA-based nanogels. The second family of MNGs was prepared by encapsulating citric acid-coated MNPs into the primary amine-functionalized nanogels. In the third case, uncoated MNPs were mixed with epoxide-functionalized nanogels. The colloidal, morphological, and magnetic properties of all the MNGs synthesized were characterized.

In Chapter 5, the analysis of the potential bio-application of the previously synthesized nanogels and MNGs is reported. In a first part, *in vitro* experiments on their biocompatibility were carried out. Regarding the PDEAEMA-based nanogels, *in vitro* toxicity tests with cervical cancer cells (HeLa cells) were carried out to evaluate their cytocompatibility. The study of the biocompatibility of MNGs was focused on the interactions between MNGs and human blood cells. As different dispersing media were used to prepare the blood samples, the role of the media on the interactions between MNGs and blood cells was also addressed. In a second part, the suitability of the nanogels synthesized as anticancer drug carriers was studied. After encapsulating the anticancer drug doxorubicin hydrochloride (DOXO) inside the nanogels, the colloidal stability of the DOXO-loaded nanogels in cell culture media was studied. In addition, the study of the DOXO release kinetics was performed and the cellular uptake of the DOXO-loaded nanogels was also investigated. Two different types of nanogels differing in the poly(ethylene glycol) (PEG) concentration used in their syntheses were chosen for this study,

giving the possibility to understand the role of the PEGylation on the nanogels potential application as drug delivery systems.

In Chapter 6 the main conclusions of the work are presented.

Appendix I shows the chemical structures of the main reagents and the list of the symbols used in this work.

Appendix II is a supplementary section of Chapter 3, showing the swelling-de-swelling behaviors of some PDEAEMA-based dual stimuli-responsive nanogels.

Finally, Appendix III is a supplementary section of Chapter 4, showing the synthesis and characterization of the magnetic nanoparticles (MNPs) used for the preparation of the magneto-nanogels (MNGs).

## 1.4. References


1. J. Ramos, J. Forcada, R. Hidalgo-Alvarez, *Chem. Rev.* **2014**, *114*, 367–428.
2. J. Forcada, Chapter 3, *Responsive Polymeric Nanoparticles* In *Controlled Release Systems: Advances in Nanobottles and Active Nanoparticles*, Eds. A. van Herk, J. Forcada, G. Pastorin, ISBN 978-981-4613-22-4, **2016**.
3. S. Sadighian, H. Hosseini-Monfared, K. Rostamizadeh, M. Hamidi, *Adv. Pharm. Bull.* **2015**, *5*, 115-220.
4. J. Dubbert, K. Nothdurft, M. Karg. W. Richtering, *Macromol. Rapid Commun.* **2015**, *36*, 159-164.
5. J. Brijitta, B. V. R. Tata, R. G. Joshi, *J. Polym. Res.* **2015**, *22*, 36, 8 pp.
6. A. Pikabea, J. Ramos, J. Forcada, *Part. Part. Syst. Charact.* **2014**, *31*, 101-109.
7. R. Turcu, V. Socoliuc, I. Craciunescu, A. Petran, A. Paulus, M. Franzreb, E. Vasile, L. Vekas, *Soft Matter* **2015**, *11*, 1008-1018.
8. L. Zhao, L. Wang, G. Gai, *Appl. Mech. Mater.* **2014**, *680*, 42-45.

9. H. Kang, A. C. Trondoli, G. Zhu, Y. Chen, Y.-J. Chang, H. Liu, Y.-F. Huang, X. Zhang, W. Tan, *ACS Nano* **2011**, *5*, 5094-5099.
10. W. Wu, W. Yao, X. Wang, C. Xie, J. Zhang, X. Jiang, *Biomaterials* **2015,** *39*, 260-268.
11. W. Chen, K. Achazi, B. Schade, R. Haag, *J. Controlled Release* **2015**, *205*, 15-24.
12. J. Ge, E. Neofytou, T. J. Cahill, R. E. Beygui, R. N. Zare, *ACS Nano* **2012**, *6*, 227-233.
13. P. Baipaywad, N. Udomluck, S.-G. Pyo, H. H. Park, H. Park, *J. Nanosci. Nanotechnol.* **2014**, *14*, 7363-7373.
14. N. Sanson, J. Rieger, *Polym. Chem.* **2010**, *1*, 965-977.
15. M. Asadian-Birjand, A. Sousa-Herves, D. Steinhilber, J. C. Cuggino, M. Calderón, *Curr. Med. Chem*. **2012**, *19*, 5029-5043.
16. J. Ramos, J. Forcada, *Nanogels,* In *Encyclopedia of Biomedical Polymers and Polymeric Biomaterials*, Eds. M. Mishra, ISBN: 9781439898796, **2013**.
17. J. Forcada, R. Hidalgo-Álvarez, *Curr. Org. Chem.* **2005**, *9*, 1067-1084.
18. R. Pelton, T. Hoare, *Microgels and Their Synthesis: An Introduction,* In *Microgel Suspensions: Fundamentals and Applications,* Eds. A. Fernandez-Nieves, H. M. Wyss, J. Mattsson, D. A. Weitz, ISBN: 978-3-527-32158-2, **2011**.
19. D. Klinger, K. Landfester, *Polymer* **2012**, *53*, 5209-5231.
20. N. M. B. Smeets, T. Hoare, Chapter 8, *Microgels and Nanogels for Drug Delivery* In *Controlled Release Systems: Advances in Nanobottles and Active Nanoparticles*, Eds. A. van Herk, J. Forcada, G. Pastorin, ISBN 978-981-4613-22-4, **2016**.
21. D. Y. Ko, H. J. Moon, B. Jeong, *J. Mater. Chem. B* **2015**, *3*, 3525-3520.
22. M. Mackiewicz, K. Kaniewska, J. Romanski, E. Augustin, Z. Stojek, M. Karbarz, *J. Mater. Chem. B* **2015**, *3*, 7262-7270.
23. K. Nagahama, Y. Sano, T. Kumano, *Bioorg. Med. Chem. Lett.* **2015**, *25*, 2519-2522.
24. P. Cao, X. Sun, Y. Liang, X. Gao, X. Li, W. Li, Z. Shong, W. Li G. Liang, *Nanomedicine* **2015**, *10*, 1585-1597.
25. J. S. Park, S. W. Yi, H. J. Kim, K.-H. Park, *Carbohydr. Polym.* **2016**, *136*, 791-802.
26. H. N. Yang, J. S. Park, S. Y. Jeon, K.-H. Park, *Carbohydr. Polym.* **2015**, *122*, 265-275.
27. B. Zhang, B. Wei, X. Hu, Z. Jin, X. Xu, *Carbohydr. Polym.* **2015**, *124*, 245-253.
28. Y. Ma, J. Wan, K. Qian, S. Geng, N. He, G. Zhou, Y. Zhao, X. Yang, *J. Mater. Chem. B* **2014**, *2*, 6044-6053.

29. D. Steinhilber, T. Rossow, S. Wedepohl, F. Paulus, S. Seiffert, R. Haag, *Angew. Chem. Int. Ed.* **2013**, *52*, 13538-13543.
30. Y. Xia, X. He, M. Cao, C. Chen, H. Xu, F. Pan, J. R. Lu, *Biomacromolecules* **2013**, *14*, 3615-3625.
31. X. Zhou, J. Nie, B. Du, *ACS Appl. Mater. Interfaces* **2015**, *7*, 21966-21974.
32. M. Chan, A. Almutairi, *Mater. Horiz.* **2016,** *3,* 21-40.
33. R.-C. Luo, C.-H. Chen, *Soft* **2012**, *1*, 1-23.
34. P. D. L. Werz, J. Kainz, B. Rieger, *Macromolecules* **2015**, *48*, 6433-6439.
35. R. T. Chacko, J. Ventura, J. Zhuang, S. Thayumanavan, *Adv. Drug Delivery Rev.* **2012**, *64*, 836-851.
36. S. Maya, B. Sarmento, A. Nair, N. S. Rejinold, S. V. Nair, R. Jayakumar, *Curr. Pharm. Des.* **2013**, *19*, 7203-7218.
37. N. M. B. Smeets, T. Hoare, *J. Polym. Sci., Part A: Polym. Chem*. **2013**, *51*, 3027-3043.
38. W. Cheng, G. Wang, J. N. Kumar, Y. Liu, *Macromol. Rapid Commun.* **2015**, *36*, 2102-2106.
39. C. Dispenza, S. Rigogliuso, N. Grimaldi, M. A. Sabatino, D. Bulone, M. L. Bondì, G. Ghersi, *React. Funct. Polym.* **2012**, *73*, 1103-1113.
40. X. Hu, Z. Tong, L. A. Lyon, *Langmuir* **2011**, *27*, 4142-4148.
41. N. Bhuchar, R. Sunasee, K. Ishihara, T. Thundat, R. Narain, *Bioconjugate Chem.* **2012**, *23*, 75-83.
42. S. Wellert, A. Radulescu, A. Carl, R. von Klitzing, K. Gawlitza, *Macromolecules* **2015**, *48*, 4901-4909.
43. A. J. Sivaram, P. Rajitha, S. Maya, R. Jayakumar, M. Sabitha, *Wiley Interdiscip. Rev.: Nanomed. Nanobiotechnol.* **2015**, *7*, 509-533.
44. A. Talevi, M. E. Gantner, M. E. Ruiz, *Recent Pat. Anti-Cancer Drug Discovery* **2014**, *9*, 83-98.
45. F. Sultana, Manirujjaman, Imran-Ul-Haque, M. Arafat, S. Sharmin, *J. Appl. Pharm. Sci.* **2013**, *3*, S95-S105.
46. G. Soni, K. S. Yadav, *Saudi Pharm. J.* **2014**, DOI:10.1016/j.jsps.2014.04.001.
47. S. V. Kapadi, L. Gadhe, S. Talele, G. N. Chaudhari, *World J. Pharm. Res.* **2015**, *4*, 553-566.

48. J. Mudassir, Y. Darwis, P. K. Khiang, *Int. J. Polym. Mater. Polym. Biomater.* **2015**, *64*, 155-167.
49. G. Srinivas, P. Ramnathkar, *Am. J. PharmTech Res.* **2014**, *4*, 269-282.
50. S. Lou, S. Gao, W. Wang, M. Zhang, J. Zhang, C. Wang, C. Li, D. Kong, Q. Zhao, *Nanoscale* **2015**, *7*, 3137-3146.
51. P. P. Shah, P. R. Desai, A. R. Patel, M. S. Singh, *Biomaterials* **2012**, *33*, 1607-1617.
52. V. Avasatthi, H. Pawar, C. P. Dora, P. Bansod, M. S. Gill, S. Suresh, *Pharm. Dev. Technol.* **2015**, DOI: 10.3109/10837450.2015.1026605.
53. G. Aarthi, T. Anusuya, A. M. Paul, V. Pandiyarasan, *Int. J. ChemTech Res.* **2015**, *7*, 786-789.
54. F. H. Nasr, S. Khoee, *Eur. J. Med. Chem.* **2015**, *102*, 132-142.
55. Y. Q. Yang, B. Zhao, Z. D. Li, W. J. Lin, C. Y. Zhang, X. D. Guo, J. F. Wang, L. J. Zhang, *Acta Biomater.* **2013**, *9*, 7679-7690.
56. T. Omura, M. Ebara, J. J. Lai, X. Yin, A. S. Hoffman, P. S. Stayton, *J. Nanosci. Nanotechnol.* **2014**, *14*, 2557-2562.
57. A. S. M. Wong, S. K. Mann, E. Czuba, A. Sahut, H. Liu, T. C. Suekama, T. Bickerton, A. P. R. Johnston, G. K. Such, *Soft Matter* **2015**, *11*, 2993-3002.
58. T. Zhou, C. Xiao, J. Fan, S. Chen, J. Shen, W. Wu, S. Zhou, *Acta Biomater.* **2013**, *9*, 4546-4557.
59. S. Manchun, K. Cheewatanakornkool, C. R. Dass, P. Sriamornsak, *Carbohydr. Polym.* **2014**, *114*, 78-86.
60. Y. Xue, X. Xia, B. Yu, X. Luo, N. Cai, S. Long, F. Yu, *RCS Adv.* **2015**, *5*, 73416-73423.
61. X. Chen, X. Yao, L. Chen, X. Chen, *Macromol. Biosci.* **2015**, *15*, 1563-1570.
62. X. Yao, L. Chen, X. Chen, Z. Zhang, H. Zheng, C. He, J. Zhang, X. Chen, *ACS Appl. Mater. Interfaces* **2014**, *96*, 7816-7822.
63. L. Lin, W. Xu, H. Liang, L. He, S. Liu, Y. Li, B. Li, Y. Chen, *Colloids Surf., B* **2015**, *126*, 459-466.
64. S. Manchun, C. R. Dass, P. Sriamornsak, *Adv. Mater. Res.* **2015**, *1060*, 227-230.
65. W. B. Liechty, R. L. Scheuerle, N. A. Peppas, *Polymer* **2013**, *54*, 3784-3795.
66. E. D. Maximova, M. V. Zhiryakova, E. B. Faizuloev, A. A. Nikonova, A. A. Ezhov, V. A. Izumrudov, V. N. Orlov, I. D. Grozdova, N. S. Melik-Nubarov, *Colloids Surf., B* **2015**, *136*, 981-988.

67. B. H. Tan, P. Ravi, L. N. Tan, K. C. Tam, *J. Colloid Interface Sci.* **2007**, *309*, 453-463.
68. J. I. Amalvy, E. J. Wanless, Y. Li, V. Michailidou, S. P. Armes, *Langmuir* **2004**, *20*, 8992-8999.
69. Y. Hu, T. Litwin, A. R. Nagaraja, B. Kwong, J. Katz, N. Watson, D. J. Irvine, *Nano Lett.* **2007**, *7*, 3056-3064.
70. M. Tamura, S. Ichinohe, A. Tamura, Y. Ikeda, Y. Nagasaki, *Acta Biomater*. **2011**, *7*, 3354-3361.
71. S. R. Marek, C. A. Conn, N. A. Peppas, *Polymer* **2010**, *51*, 1237-1243.
72. M. Oishi, H. Hayashi, T. Uno, T. Ishii, M. Iijima, Y. Nagasaki, *Macromol. Chem. Phys.* **2007**, *208*, 1176-1182.
73. M. Oishi, H. Hayashi, K. Itaka, K. Kataoka, Y. Nagasaki, *Colloid. Polym. Sci.* **2007**, *285*, 1055-1060.
74. M. Oishi, N. Miyagawa, T. Sakura, Y. Nagasaki, *React. Funct. Polym.* **2007**, *67*, 662-668.
75. A. Tamura, M. Oishi, Y. Nagasaki, *J. Controlled Release* **2010**, *146*, 378-387.
76. H. Hayashi, M. Iijima, K. Kataoka, Y. Nagasaki, *Macromolecules* **2004**, *37*, 5389-5396.
77. M. Oishi, Y. Nagasaki, *React. Funct. Polym.* **2007**, *67*, 1311-1329.
78. M. Oishi, H. Hayashi, M. Iijima, Y. Nagasaki, *J. Mater. Chem.* **2007**, *17*, 3720-3725.
79. X. Zhang, S. Lü, C. Gao, C. Chen, X. Zhang, M. Liu, *Nanoscale* **2013**, *5*, 6498-6506.
80. M. S. Strozyk, M. Chanana, I. Pastoriza-Santos, J. Pérez-Juste, L. M. Liz-Marzán, *Adv. Funct. Mater.* **2012**, *22*, 1436-1444.
81. R. Cheng, F. Meng, C. Deng, H.-A. Klok, Z. Zhong, *Biomaterials* **2013**, *34*, 3647-3657.
82. Y. Wang, J. Nie, B. Chang, Y. Sun, W. Yang, *Biomacromolecules* **2013**, *14*, 3034-3046.
83. E. Pérez, R. Olmo, C. Teijón, E. Muñíz, N. Montero, J. M. Teijón, M. D. Blanco, *Colloids Surf., B* **2015**, *136*, 222-231.
84. R. Gui, Y. Wang, J. Sun, *Colloids. Surf., B* **2014**, *116*, 518-525.
85. W.-H. Chiang, W.-C. Huang, Y.-J. Chang, M.-Y. Shen, H.-H. Chen, C.-S. Chern, H.-C. Chiu, *Macromol. Chem. Phys.* **2014**, *215*, 1332-1341.
86. A. Sousa-Herves, S. Wedepohl, M. Calderón, *Chem. Commun.* **2015**, *51*, 5264-5267.
87. M. Li, Z. Tang, H. Sun, J. Ding, W. Song, X. Chen, *Polym. Chem.* **2013**, *4*, 1199-1207.
88. M. Molina, M. Asadian-Birjand, J. Balach, J. Bergueiro, E. Miceli, M. Calderón, *Chem. Soc. Rev.* **2015**, *44*, 6161, 6186.
89. B. H. Juarez, L. M. Liz-Marzán, *Z. Phys. Chem.* **2015**, *229*, 263-282.

90. W. Wu, S. Zhou, *Nano Rev.* **2010**, *1*, 5730, 17 pp.
91. B. Sierra-Martin, A. Fernandez-Barbero, *Soft Matter* **2015**, *11*, 8205-8216.
92. M. J. Sailor, J.-H. Park, *Adv. Mater.* **2012**, *24*, 3779–3802.
93. M. A. Hood, M. Mari, R. Muñoz-Espí, *Materials* **2014**, *7*, 4057-4087.
94. Y. Chen, X. Zheng, X. Wang, C. Wang, Y. Ding, X. Jiang, *ACS Macro Lett.* **2014**, *3*, 74-76.
95. H. Wang, J. Di, Y. Sun, J. Fu, Z. Wei, H. Matsui, A. del C. Alonso, S. Zhou, *Adv. Funct. Mater.* **2015**, *25*, 5537-5547.
96. R. Turcu, V. Socoliuc, I. Craciunescu, A. Petran, A. Paulus, M. Franzreb, E. Vasile, L. Vekas, *Soft Matter* **2015**, *11*, 1008-1018.
97. H. Wang, J. Yi, S. Mukherjee, P. Banerjee, S. Zhou, *Nanoscale* **2014**, *6*, 13001-13011.
98. A. Riedinger, M. P. Leal, S. R. Deka, C. George, I. R. Franchini, A. Falqui, R. Cingolani, T. Pellegrino, *Nano Lett.* **2011**, *11*, 3136-3141.
99. R. Regmi, S. R. Bhattarai, C. Sudakar, A. S. Wani, R. Cunningham, P. P. Vaishnava, R. Naik, D. Oupicky, G. Lawes, *J. Mat. Chem.* **2010**, *2*0, 6158-6163.
100. M. Oishi, A. Tamura, T. Nakamura, Y. Nagasaki, *Adv. Funct. Mater.* **2009**, *19*, 827-834.
101. E. V. Panfilova, B. N. Khlebtsov, N. G. Khlebtsov, *Colloid J.* **2013**, *75*, 333-338.
102. L. Jiang, Q. Zhou, K. Mu, H. Xie, Y. Zhu, W. Zhu, Y. Zhao, H. Xu, X. Yang, *Biomaterials* **2013**, *34*, 7418-7428.
103. J. Liu, C. Detrembleur, A. Debuigne, M.-C. De Pauw-Gillet, S. Mornet, L. Vander Elst, S. Laurent, E. Duguet, C. Jérôme, *J. Mater Chem. B.* **2014**, *2*, 1009-1023.
104. J. Lux, M. Chan, L. V. Elst, E. Schopf, E. Mahmoud, S. Laurent, A. Almutairi, *J. Mater. Chem. B* **2013**, *1*, 6359-6364.
105. G. Liu, C. Zhu, J. Xu, Y. Xin, T. Yang, J. Li, L. Shi, Z. Guo, W. Liu, *Colloids Surf., B* **2013**, *111*, 7-14.
106. Y. Qin, J. Chen, Y. Bi, X. Xu, H. Zhou, J. Gao, Y. Hu, Y. Zhao, Z. Chai, *Acta Biomater.* **2015**, *17*, 201-209.
107. C. Wang, J. Mallela, U. S. Garapati, S. Ravi, V. Chinnasamy, Y. Girard, M. Howell, S. Mohapatra, *Nanomedicine* **2013**, *9*, 903-911.
108. H.-J. Kim, K. Zhang, L. Moore, D. Ho, *ACS Nano* **2014**, *8*, 2998-3005.
109. S. Rejinold N, K. P. Chennazhi, H. Tamura, S. V. Nair, R. Jayakumar, *ACS Appl. Mater. Interfaces* **2011**, *3*, 3654-3665.

110. S. Bucak, B. Yavuztürk, A. D. Sezer, *Magnetic Nanoparticles: Synthesis, Surface Modifications and Application in Drug Delivery* In *Pharmacology, Toxicology and Pharmaceutical Science, Pharmacology, "Recent Advances in Novel Drug Carrier Systems"*, Eds. A. D. Sezer, ISBN: 978-953-51-0810-8, **2012**.
111. A. Aggarwal, P. Chhajer, S. Maheshwari, *Int. J. Pharm. Sci. Res.* **2012**, *3*, 4670-4680.
112. M. Colombo, S. Carregal-Romero, M. F. Casula, L. Gutiérrez, M. P. Morales, I. B. Böhm, J. T. Heverhagen, D. Prosperi, W. J. Parak, *Chem. Soc. Rev.* **2012**, *41*, 4306-4334.
113. B. Issa, I. M. Obaidat, B. A. Albiss, Y. Haik, *Int. J. Mol. Sci.* **2013**, *14*, 21266-21305.
114. M. Mahdvai, M. B. Ahmad, M. J. Haron, F. Namvar, B. Nadi, M. Z. A. Rahman, J. Amin, *Molecules* **2013**, *18*, 7533-7548.
115. M. Mahmoudi, S. Sant, B. Wang, S. Laurent, T. Sen, *Adv. Drug Delivery Rev.* **2011**, *63*, 24-46.
116. J. Estelrich, E. Escribano, J. Queralt, M. A. Busquets, *Int. J. Mol. Sci.* **2015**, *16*, 8070-8101.
117. R. A. Revia, M. Zhang, *Mater. Today* **2015**, DOI: 10.1016/j.mattod.2015.08.022.
118. H. Tabani, K. Khodaei, Y. Bide, F. D. Zare, S. Mirzaei, A. R. Fakhari, *J. Chromatogr. A* **2015**, *1407*, 21-29.
119. R. Gui, H. Jin, *RCS Adv.* **2014**, *4*, 2797-2806.
120. M. K. Jaiswal, M. De, S. S. Chou, S. Vasavada, R. Bleher, P. V. Prasad, D. Bahadur, V. P. Dravid, *ACS Appl. Mater. Interfaces* **2014**, *6,* 6237-6247.
121. C. A. Demarchi, A. Debrassi, F. de Campos Buzzi, R. Corrêa, V. C. Filho, C. A. Rodrigues, N. Nedelko, P. Demchenko, A. Ślawska-Waniewska, P. Dłużewski, J.-M. Greneche, *Soft Matter* **2014**, *10***,** 3441-3450.
122. J. Liu, C. Detrembleur, A. Debuigne, M.-C. De Pauw-Gillet, S. Mornet, L. Vander Elst, S. Laurent, E. Duguet, C. Jérôme, *J. Mater Chem. B.* **2014**, *2*, 1009-1023.
123. G. Liu, D. Wang, F. Zhou, W. Liu, *Small* **2015**, *23*, 2807-2816.
124. J. Zhu, C. Peng, W. Sun, Z. Yu, B. Zhou, D. Li, Y. Luo, L. Ding, M. Shen, X. Shi, *J. Mater. B* **2015**, *3*, 8684-8693.
125. M. Sun, A. Zhou, Q. Zhang, M. Ye, Q. Liu, *Eur. Polym. J.* **2015**, *66*, 569-576.
126. Z. Yuan, Y. Wang, D. Chen, *J. Mater. Sci.* **2014**, *4*9, 3287-3296.
127. M. Boularas, E. Gombart, J-F. Tranchant, L. Billon, M. Save, *Macromol. Rapid Commun.* **2015**, *36*, 76-83.

128. R. Turcu, I. Craciunescu, V. M. Garamus, C. Janko, S. Lyer, R. Tietze, C. Alexiou, L. Vekas, *J. Magn. Magn. Mater.* **2015***, 380,* 307-314.
129. W.-H. Chiang, V. T. Ho, H.-H. Chen, W.-C. Huang, Y.-F. Huang, S.-C. Lin, C.-S. Chern, H.-C. Chiu, *Langmuir* **2013**, *29*, 6434-6443.
130. V. Fischer, M. B. Bannwarth, G. Jakob, K. Landfester, R. Muñoz-Espí, *J. Phys. Chem. C* **2013**, *117*, 5999-6005.
131. M. Behbahani, Y. Bide, S. Bagheri, M. Salarian, F. Omidi, M. R. Nabid, *Microchim. Acta* **2016**, 183, 111-121.
132. L. Chen, Y. Xue, X. Xia, M. Song, J. Huang, H. Zhang, B. Yu, S. Long, Y. Liu, L. Liu, S. Huang, F. Yu, *J. Mater. Chem. B* **2015**, *3*, 8949-8962.
133. K. Kurd, A. A. Khandagi, S. Davaran, A. Akbarzadeh, *Artif. Cells, Nanomed., Biotechnol.* **2015***,* DOI: 10.3109/21691401.2015.1008513.

# 2

# Synthesis and Characterization of dual-stimuli-responsive nanogels

# 2.1. Introduction

The beauty of environmentally-responsive cross-linked colloidal particles, known as nanogels, lies in their unprecedented ability to undergo large reversible volume changes in response to external stimuli such as temperature, pH, and magnetic field.[1] Furthermore, their small size allows them to overcome various biological barriers and achieve passive and active targeting, which reduce adverse reactions in tumor therapy. Due to their porous structure they are able to contain small molecules inside and release them by changing their volume. These properties make them interesting and suitable materials to be used as nanocarriers in drug/gene delivery.[2-10]

The possibility of using multi-stimuli-responsive vehicles to control the response of a single system is considered to be highly advantageous for their future use in the biomedical field, taking into account their enhanced efficacy and ability to direct drugs to the targeted tissue of certain diseases such as tumors and release them in a controlled manner answering to small stimuli variations.[11] Among different biotechnological applications, nanogels present great potential for drug/gene delivery, particularly those that respond when all external stimuli exist simultaneously, obtaining better efficiency, lower side effects, and more controllable delivery of drugs or genes. Special interest is focused on temperature- and pH-sensitive nanogels being these two stimuli of great scientific and technological significance in biomedicine.[9,12-18]

In particular, it is of great practical significance regarding the development of drug delivery systems to produce pH-responsive nanogels. They exhibit large volume changes in response to small pH variations, showing a volume phase transition pH (VPTpH). Considering this interesting property, they can be used at different levels: at organ level, as the gastrointestinal tract is characterized by pH gradients; at tissue level, taking advantage of the characteristic acidic extracellular environment of unhealthy tissues different from healthy tissues; and at cellular level, as endo/lysosomes are more acidic in comparison to the cytoplasm.[12,19-21] The swelling is ascribed to the enhanced electrostatic repulsion among charges within the polymer network that appears due to the ionization of ionizable groups varying the pH. Considering that the extracellular pH of unhealthy tissues is lower than that of healthy tissues,[22] cationic pH-sensitive nanogels will be one of the best options to be used in

the delivery of anti-tumor drugs, as they swell at acidic conditions.[11] Apart from that, positively charged nanogels show higher affinity for negatively charged cell membranes and thus they can be readily internalized by cells.[23] Additionally, amine groups are available for a proton sponge effect during endolysosomal acidification, allowing more efficient endosomal escape.[9] Therefore, a nanogel based on poly(2-diethylaminoethyl methacrylate) (PDEAEMA) results in an appropriate candidate being biocompatible, sensitive to pH, cationic, and presenting a VPTpH in the physiologically relevant pH range of 5.0–7.4.[12,24-27] Fortunately, PDEAEMA-based nanogels also showed thermal response apart from the response to pH variations, enhancing the suitability of these nanogels to be used in bio-applications.[28]

In this work, the synthesis of dual-responsive PDEAEMA-based nanogels was carried out by emulsion polymerization in a batch reactor, taking as reference procedures used by Nagasaki and co-workers,[29-33] Amalvy *et al*.,[34] and Hu *et al*.,[35] but with some modifications. Considering that an enhanced stability should be obtained polymerizing cationic monomers in a cationic system, a cationic initiator was used [2,2′-azobis (*N,N′*-dimethyleneisobutyramidine) dihydrochloride, ADIBA].[36] Moreover, surfactant-free emulsion polymerization was used as most surfactants are potentially toxic to organisms due to their surface activity allowing reactions with biological membranes. Apart from this, the biocompatible cross-linker ethylene glycol dimethacrylate (EGDMA) was used. Furthermore, it is noticeable that the pH-responsive nanogels synthesized were solely based on weakly basic monomer repeating units. In most studies so far the fraction of pH-sensitive moieties within the gel phase was limited to a few percent, resulting in a weak pH-responsive swelling-de-swelling behavior that is strongly influenced by the distribution of the pH-sensitive co-monomer. The preparation of pH-responsive nanogels/microgels based solely on pH-sensitive monomers has been recently reported.[37]

In order to better exploit the technological promise of responsive materials, an improved understanding of the microstructure of nanogels is required. To date, the heterogeneous nanogel structure has been investigated by using static light scattering,[38] small angle neutron scattering,[39-41] and $^{1}$H-Nuclear Magnetic Resonance (NMR) transverse relaxation measurements.[42-46] Comparing with the other techniques mentioned, in addition to the microstructure, NMR measurements give detailed information about the chemical structure of the polymer chains conforming the nanoparticles. The heterogeneity in nanogel microstructure

would be reflected in $^{1}$H-transverse magnetization relaxation because the cross-linking density gradient causes different degrees of proton mobilities.[42,43]

In this Chapter, the synthesis of new biocompatible, pH- and temperature-sensitive PDEAEMA-based cationic nanogels is described. The inner structure of the nanogels synthesized was investigated by high-resolution proton transverse relaxation NMR measurements. Their response to pH and temperature changes was also examined thoroughly by using light scattering techniques and potentiometric titrations. Considering that physiological conditions imply a specific ionic strength, the effect of the ionic strength on both sensitivities was also studied.

## 2.2. Experimental

### 2.2.1. Materials

All the following materials were used as received:

- 2-(diethylamino)ethyl methacrylate (DEAEMA), supplied by Sigma-Aldrich, was used as a main monomer.
- Ethylene glycol dimethacrylate (EGDMA), supplied by Sigma-Aldrich, was used as a cross-linker.
- 2,2′-azobis (*N,N′*-dimethyleneisobutyramidine) dihydrochloride (ADIBA), supplied by Wako Chemical GmbH, was used as a cationic initiator.
- Glycine, γ-aminobutyric acid, pyridine, bis-tris, sodium phosphate monobasic, and dibasic, Trizma®, triethylamine and sodium chloride (NaCl), supplied by Sigma-Aldrich, were used to prepare the buffers.
- Deuterium oxide ($D_2O$), supplied by Sigma-Aldrich, and deuterium chloride (DCl), supplied by Eurisotop, were used for NMR characterization.
- Hydrochloric acid (HCl) and sodium hydroxide (NaOH), supplied by Sigma-Aldrich, were used for potentiometric titrations.
- Double deionized (DDI) water was used throughout the work.

## 2.2.2. Synthesis of the nanogels

Nanogel particles were synthesized by batch emulsion polymerization of DEAEMA. The experimental set-up used is shown in Figure 2.1. The equipment consists of a 250-mL jacketed glass reactor, fitted with a reflux condenser, stainless steel stirrer, sample device, and nitrogen inlet tube. Once 20 g of DEAEMA as a main monomer, 0.2 g of EGDMA as a cross-linker, and 170 g of water were charged into the reactor, the reaction mixture was heated at 70 °C, stirred at 300 rpm, and purged with nitrogen for 40 min before starting the polymerization reaction. After adding the initiator (2 wt% of ADIBA with respect to the main monomer, in 10 g of DDI water), the polymerization reaction was allowed to continue under nitrogen atmosphere stirring for 2 h at 70 °C. The reaction mixture was subsequently cooled to 25 °C maintaining the stirring.

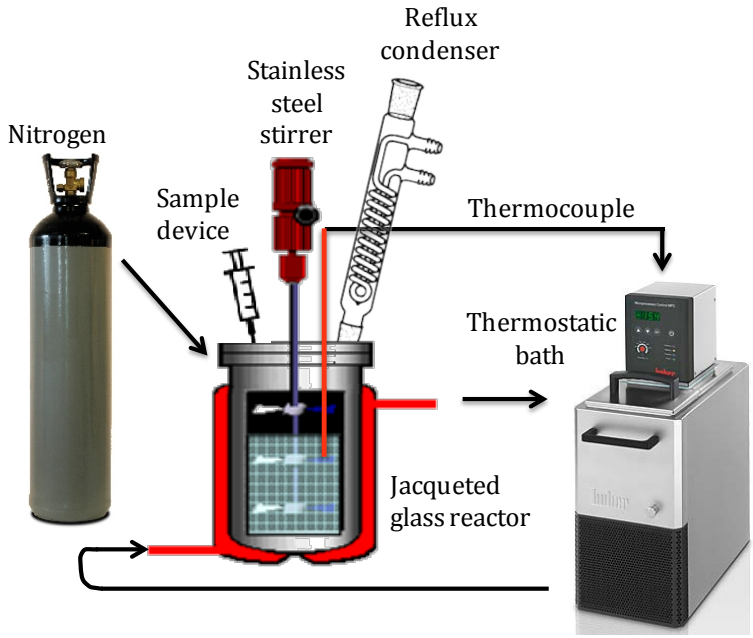


**Figure 2.1.** Batch polymerization reaction equipment for the synthesis of nanogels.

## 2.2.3. Characterization of the nanogels

The final dispersion was filtered through glass wool and dialyzed (MW Cut-off (MWCO) of 12-14 KDa) against DDI water at acidic conditions during the first two days to ensure the removal of the unreacted DEAEMA (being more soluble at acidic conditions). Then, the entire dialysate volume was changed for DDI water at least once a day until the conductivity of the dialysate was close to that of the DDI water (2 µC/cm).

### 2.2.3.1. Microstructure of nanogels

Before analyzing the morphology and inner structure of the nanogels synthesized, samples were lyophilized using a Telstar Cryodos-50 lyophilizer and dispersed in acidic $D_2O$ solution (pH ≈ 3) at a concentration of 2 wt%. In order to study the inner structure of the nanogels, $^1$H-NMR technique was used. $^1$H transverse relaxation ($T_2$) measurements were made on a Bruker Avance 500 NMR spectrometer using the protocol presented by other authors with some modifications.[42,44] The decay of transverse magnetization relaxation was measured using Hahn-echo pulse sequence: $90^{\circ}_{x}$-t-$180^{\circ}_{x}$-t-Hahn echo-(adquisition), where t is the echo time. Half of the Hahn echo decay was detected and Fourier transformed. The number of the echo times employed was 25 between 0.54 ms and 4860 ms. The normalized integral intensity of various resonances was fitted by two-exponential decay functions.

### 2.2.3.2. Colloidal characterization

Colloidal characteristics of the nanogel particles synthesized, such as the average hydrodynamic particle diameters at different pHs and temperatures were measured by Photon Correlation Spectroscopy (PCS, Zetasizer Nano ZS, Malvern Instruments). In all the measurements ionic strength and pH of the medium were controlled using different buffered media depending on the pH of the solution.

In order to investigate the pH- and thermo-sensitivity, samples were dispersed at different pHs at a certain ionic strength of the medium and at a polymer concentration of 0.005 wt%. To study the pH-sensitivity, measurements were carried out at 25 °C from pH 3 to pH 10 taking three measurements every pH unit, except on the critical pH range, where measurements were carried out every 0.5 pH unit. To study the thermal behavior,

measurements were carried out at different pHs from 10 to 80 °C, taking measurements every 2 °C. The optimized stabilizing time of the measurements was 10 min.

Volume phase transition pH and temperature (VPTpH and VPTT) were determined and established as the pH and temperature corresponding to the inflection point in the average hydrodynamic diameter versus pH or temperature curves, respectively.

Electrophoretic mobility measurements were carried out by Electrophoretic Light Scattering (ELS), using a Zetasizer Nano ZS. Previously lyophilized particles were resuspended in buffered water solution at a concentration of 0.05 wt%. Each sample was subjected to five measurements at 25 °C, with a 60 s delay between them.

To study the effect of the ionic strength on both sensitivities, 10 mM of cationic buffer and an appropriate concentration of NaCl salt were added to obtain ionic strengths of 100 and 150 mM. Furthermore, in order to simulate real physiological conditions and study the behavior of the nanogel at these conditions, Phosphate Buffered Saline (PBS) was used as buffer: 10 mM of phosphate salts and an appropriate concentration of NaCl salt up to 150 mM were used.

Potentiometric titrations of the nanogels were performed using T90 titrator (Mettler Toledo). Briefly, 0.05 g of lyophilized nanogel was resuspended in 100 mL of DDI with 10 mM of NaCl. The pH was increased to 10.0 using NaOH water solution, and the titration was carried out using HCl (10 mM) as titrant. It is remarkable that the acid-base titration was carried out slowly (control of the equilibrium given by dE/dt = 0.5 mV/s, in which dE/dt is the time derivative of the potential, and $t_{min}$ = 120 s and $t_{max}$ = 600 s) to facilitate a complete equilibration between the aqueous and gel phases.[47] The potentiometric titration data were analyzed using the method of Kawaguchi *et al*.[48] The value of degree of protonation (α) was determined by the moles of titrated polyelectrolyte and the titrant added, where α ranged from zero at the un-ionized state of amine groups to one at the full protonated state. The pH/α curves were determined from the obtained titration curves. Henderson-Hasselbalch equation could subsequently be used to calculate the apparent $pK_a$ of the protonated amine groups as a function of the degree of protonation (α):

$$pK_a = pH + \log\left(\frac{\alpha}{1-\alpha}\right) \qquad (2.2)$$

# 2.3. Results and discussion

## 2.3.1. Morphology of the nanogels

In spite of the large number of publications on PDEAEMA-based micro/nanogels appeared in the last years, little interest has been devoted to their inner morphology.[12,34,49] Nevertheless, the morphology of nanogel particles plays an important role in the understanding of the swelling properties.

In the case of using batch emulsion polymerization to produce nanogels, the general concept for nanogel structure is a core/shell model in which core and shell, separated by diffuse boundaries, have different structures and cross-linking degrees due to the specificity of the polymerization/cross-linking processes involved.[42,43] The reason behind this morphology is the faster reaction rate of the cross-linker comparing to that of the main monomer,[12,14-18,50] resulting in a heterogeneous cross-linking density distribution. Figure 2.2 depicts the polymerization and cross-linking reactions occurred during the synthesis of the nanogel particles. As can be observed, DEAEMA copolymerizes with the two double bonds of EGDMA, generating cross-linking points between the polymeric chains.

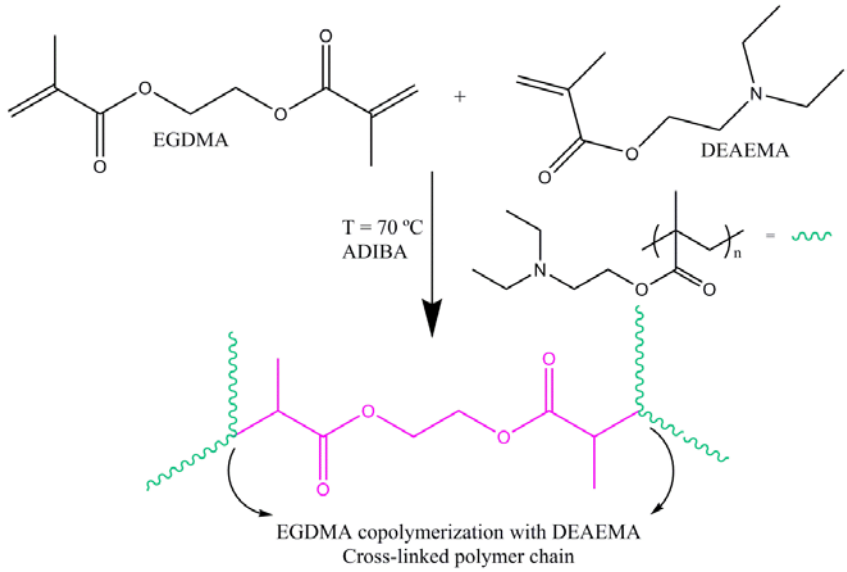


**Figure 2.2.** Scheme of the polymerization and cross-linking reactions occurred during the synthesis of the nanogel particles.

In order to analyze the morphology of the nanoparticles, high-resolution transverse relaxation ($T_2$) $^1$H-NMR measurements were used for the first time with PDEAEMA-based nanoparticles. The heterogeneity of PDEAEMA chains distribution in the nanoparticles would be reflected in the $^1$H transverse magnetization relaxation due to PDEAEMA chains proton mobility gradient caused by different cross-linking densities. From transverse magnetization ($T_2$) decay, it is possible to show a bimodal distribution of the PDEAEMA chain mobility inside the nanogel particles from which the morphological core-shell model can be derived.

A proton high-resolution NMR spectrum of PDEAEMA-based nanogel particles is shown in Figure 2.3. The resonance peak relative to the methyl protons of PDEAEMA chains that appears at 1.2 ppm (R1) was used to investigate the heterogeneity in microstructure of nanogels, being the least sensitive to noise interference, due to its high intensity.

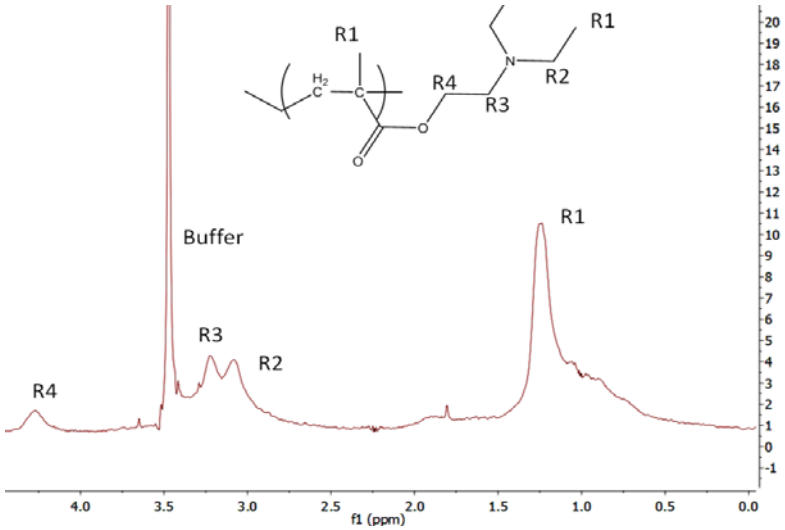


**Figure 2.3.** Proton high-resolution spectrum of a PDEAEMA-based nanogel dispersed in $D_2O$ at acidic conditions and 25 °C.

The best fitting for the integral of this resonance peak was resulted to be a biexponential decay:[42]

$$\frac{S(t)}{S(0)} = C_s \exp\left\{-\frac{t}{T_{2S}}\right\} + C_L \exp\left\{-\frac{t}{T_{2L}}\right\} \qquad (2.3)$$

where S(t)/S(0) is the normalized NMR signal integral as a function of spin-echo time t, $C_S$ and $C_L$ are the relative amounts of methyl protons of PDEAEMA in core and shell, respectively, and $T_{2S}$ and $T_{2L}$ are the short and long transverse relaxation times, respectively.

By adjusting the decay curve to equation 2.3, values of $C_S$ and $C_L$, which describe quantitatively the bimodal heterogeneity of the polymer network in nanogel particles and the ones of $T_{2S}$ and $T_{2L}$ can be obtained. Furthermore, the ratio of the cross-linking densities of the nanogel in core and shell $\left(\frac{CLD^{core}}{CLD^{shell}}\right)$ could be also determined by using equation 2.4.

$$\frac{CLD^{core}}{CLD^{shell}} = \left(\frac{T_{2L}}{T_{2S}}\right)^{1/2} \qquad (2.4)$$

The obtained values of the $^{1}$H-NMR transverse relaxation times ($T_{2S}$ and $T_{2L}$), relative amounts of PDEAEMA chains ($C_S$ and $C_L$) and the ratio of the cross-linking densities ($CLD^{core}/CLD^{shell}$) in nanogel particles are shown in Table 2.1.

| $T_{2S}$ (ms) | $T_{2L}$ (ms) | $C_S$ | $C_L$ | $CLD^{core}/CLD^{shell}$ |
|---|---|---|---|---|
| 4.0 | 72.8 | 0.64 | 0.46 | 4.27 |

**Table 2.1.** Short ($T_{2S}$) and long ($T_{2L}$) proton transverse relaxation times and the relative weight coefficients ($C_S$ and $C_L$) obtained by $^{1}$H-NMR transverse relaxation measurements, together with the calculated cross-linking density ratio ($CLD^{core}/CLD^{shell}$).

Apart of confirming the heterogeneous core–shell microstructure, as represented in Figure 2.4, the ratio of the average cross-linking density between core and shell was calculated, being 4.3, which means that the core was 4.3 times more cross-linked than the shell.

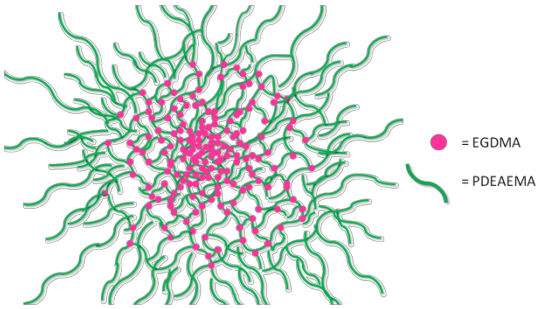


**Figure 2.4.** Schematic representation of the morphology of a nanogel particle.

This is the first time that the morphology of PDEAEMA-based nanoparticles was studied using $^{1}$H-NMR technique, and nanogel particles with a core–shell-type heterogeneous microstructure were obtained in agreement with the results reported with thermo-responsive nanogels based on poly(*N*-isopropylacrylamide) (PNIPAM) or based on poly(*N*-vinyl caprolactam) (PVCL).[42,43,51] In this way, the starting hypothesis was corroborated, confirming a faster reaction rate of the cross-linker (EGDMA) than that of the main monomer (DEAEMA).

## 2.3.2. Dual-stimuli-sensitivity of the nanogels

### 2.3.2.1. pH-sensitivity

In order to analyze the response of the nanogel particles to pH variations, the final average hydrodynamic diameters of dialyzed nanogel particles at different pHs and at 25 °C were measured by PCS. In Figure 2.5, the average hydrodynamic diameter as a function of pH for the nanogel particles dispersed in a cationic-buffered medium with an ionic strength of 10 mM is presented. The inflection point of the hydrodynamic diameter versus pH curve shows the VPTpH from swollen to a collapsed state at pH 6.5. Below the VPTpH, nanogel particles were highly swollen due to the protonation of amine groups causing charge repulsion in the polymer network. Above that critical pH, particles were shrunken reducing their size due to the deprotonation of amine groups and the weakened electrostatic repulsion. This swelling-de-swelling behavior occurred due to the alterations in the internal osmotic balance of the gel brought about by changes in the ionic composition of the external solution. The protonation of the amine groups at acidic conditions triggering the water uptake and nanogel swelling due to an increase in the ion osmotic pressure was opposed by the inherent hydrophobicity of the nanogel particles, which dominated at high pHs and favored the exclusion of water.[52] This phenomenon was previously observed by Marek *et al*.[24] for nanoparticle hydrogels based on PDEAEMA and poly(ethyleneglycol)-*N*-monomethyl ether monomethacrylate cross-linked with tetraethylene glycol dimethacrylate and polyethylene glycol 400 dimethacrylate and Hayashi *et al*.[29] for PDEAEMA-based nanogels possessing heterotelechelic PEG tethered chains and cross-linked with EGDMA.

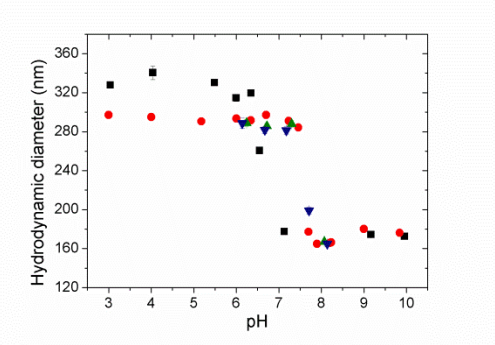


**Figure 2.5.** Average hydrodynamic particle diameters as a function of pH at 25 °C using ionic strengths of 10 mM (cationic buffer) (■), 100 mM (10 mM cationic buffer + NaCl) (●), 150 mM (10 mM cationic buffer + NaCl) (▲), and PBS 150 mM (10 mM phosphate buffer + NaCl) (▼).

This fact was confirmed by electrophoretic mobility measurements. Figure 2.6 shows the obtained values at different pHs. As can be seen, nanogel particles possessed positive electrophoretic mobility values at acidic pHs attributed to the positively charged amine groups. Worth noting is a significant decrease in the electrophoretic mobility at around pH 6, reflecting the deionization of PDEAEMA groups close to the $pK_a$ and the weakening of the electrostatic repulsion that provoked the decrease in size. Above the isoelectric point (pH 8, approximately), the electrophoretic mobility values were negative. These negative values were given by adsorption of hydroxide ions, and not due to the hydrolysis of ester groups, since the behavior was reversible from basic to acidic conditions. Similar tendency was also seen by Marek *et al.*[24] in PDEAEMA-based nanogels cross-linked with tetraethylene glycol dimethacrylate (TEGDMA), by Shahalom *et al*.[53] in poly[DEAEMA-*co*-poly(ethylene glycol) methacrylate (PEGMA)]-based copolymers, and also by Fujii *et al*.[54] in PDEAEMA-based aqueous foams.

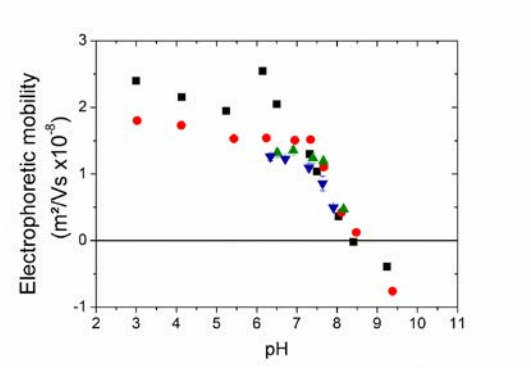


**Figure 2.6.** Electrophoretic mobilities as a function of pH at 25 °C using ionic strengths of 10 mM (cationic buffer) (■), 100 mM (10 mM cationic buffer + NaCl) (●), 150 mM (10 mM cationic buffer + NaCl) (▲), and PBS 150 mM (10 mM phosphate buffer + NaCl) (▼).

In the case of nanogels containing weakly acidic or basic groups, the presence of charged groups in the polymer network affects the osmotic balance between the nanogel and the surrounding medium, making the swelling dynamics highly dependent on the ionic strength and the type of ions of the surrounding medium.[9,55,56] Thus, the effect of the ionic strength on pH-sensitivity was also examined (see Figures 2.5 and 2.6).

On the one hand, increasing the ionic strength from 10 to 100 mM by the addition of NaCl to the dispersion, both size and electrophoretic mobility of the nanogel particles decreased at acidic conditions. This was attributed to an electrostatic and osmotic screening caused by the increase in ionic strength. Similar results were previously obtained in other systems. Nagasaki and co-workers[30,31] remarked the decrease in size by increasing the ionic strength in PEGylated PDEAEMA-based nanogels. Plamper *et al*.[57] found the contraction of the polyelectrolyte arms due to an electrostatic and osmotic screening in poly(2-dimethylaminoehyl) methacrylate (PDMAEMA) and its quaternized ammonium salts. It is important to consider that the decrease in particle size can affect the electrostatic and frictional forces and thereby the electrokinetic behavior of nanogel particles. However, Fernández-Nieves[58] found that an increase in ionic strength yields to variations in the electrophoretic mobility, irrespective of the particle swelling-de-swelling behavior.

Nevertheless, hydrodynamic diameter under alkaline conditions was not affected by the ionic strength. On the basis of these data, it can be confirmed that the pH-dependent swelling-

de-swelling behavior was mainly governed by the gel osmotic pressure but not the interparticle interaction.[17] This difference in ionic strength-dependence between swollen and collapsed nanogels could be understood taking into account that collapsed nanogels behave as hard spheres, while swollen particles acted as spherical polyelectrolytes. Fernández-Nieves[58] suggested that collapsed nanogels are impermeable to the solvent, so that the ionic strength does not affect their elektrokinetic behavior. However, in the case of swollen particles, electrophoretic mobility decreases increasing the electrolyte concentration, irrespective of the charge state.

Additionally, an increase in ionic strength shifted the transition to more basic conditions. This was most likely related to shielding of the repulsion between charged amine groups provoked by the large amounts of electrolytes, enhancing the energy required to deprotonate them (increase in $pK_a$). Oishi and Nagasaki[28] also observed a shift in the transition pH in nanogels composed of PDEAEMA and PEG chains, ascribing it to the increase in $pK_a$. In order to confirm the increase in $pK_a$ at higher ionic strengths, potentiometric titrations carried out at different ionic strengths will be studied and discussed later.

However, increasing the ionic strength above 100 mM, neither the size nor the electrophoretic mobility was affected, and the transition was unaltered. This fact suggests that 100 mM was enough to cause the maximum shielding of the repulsion between charged amine groups, this is, the energy required to deprotonate the charged amine groups was maximum at this point since the surface was saturated by ions. This result is in agreement with the results obtained by Chang *et al.*[59] in P(NIPAM-*co*-methacrylic acid)-coated magnetic mesoporous silica nanoparticles. They observed a shift of $pK_a$ to more basic pHs increasing the NaCl concentration from 0 to 50 mM, but at higher salt concentrations, $pK_a$ remained almost constant. He *et al*.[60] also observed an increase in $pK_a$ increasing the salt concentration to 100 mM and a constant $pK_a$ above this ionic strength in PEG-*b*-PDEAEMA-based four-arm star copolymers. Zhang *et al.*[61,62] also reported an exponential decrease in swelling ratio increasing the ionic strength in carboxymethyl cellulose-based microgels.

This fact could be better understood if we consider some features of the electrical behavior of soft nanoparticles such as nanogel particles, which are different from those of hard nanoparticles. In the case of soft particles, the interpretation of the dielectric behavior becomes more delicate, due to the difficulty to define the nature of the interface between the particle and the outer electrolyte solution.[63-66] In particular, according to Ohshima,[67] the magnitude and the

electrolyte concentration-dependence of the electrophoretic mobility of soft particles differ considerably from those of hard particles. The characteristic of the electrokinetic behavior of soft particles is that the electrophoretic mobility does not reduce to zero at high electrolyte concentrations, tending to a non-zero limiting value.[68] In fact, this limiting value was observed in the nanogels synthesized, since the colloidal characteristics were no longer affected by increasing the ionic strength.

Furthermore, in order to be as close as possible to real physiological conditions and to study the effect of the buffer type on the swelling-de-swelling behavior, samples were dispersed in Phosphate Buffered Saline (PBS). Figures 2.5 and 2.6 also show hydrodynamic diameters and electrophoretic mobilities of the particles dispersed in PBS as a function of pH, respectively. As can be observed, neither the size nor the electrophoretic mobility was affected by the medium and the transition occurred at pH 7.6. The ideal drug carrier requirement for the pH-sensitive nanogels is that PDEAEMA-based nanogels undergo a unique transition at physiological conditions —*i.e.*, a collapsed state in bloodstream and a swollen state in tumor tissues— thus meaning that almost no premature drug release occurs during blood circulation while allowing rapid release on reaching the tumor tissue.[11,27] This is indeed the reason why the nanogel particles synthesized are interesting for bio-applications, giving a volume phase transition at physiological pH range.[59]

In order to better understand the pH-responsiveness of nanogel particles, potentiometric titrations were also carried out. In polyelectrolyte-based micro/nanogels, long time for the equilibrium is needed in order to achieve full distribution of the titrant between the aqueous continuous phase and the gel, due to the diffusion limitations associated with the penetration of titrant ions in the gel.[47] Thus, the stabilization time was firstly optimized in order to achieve successful titrations.

The buffering capacity of PDEAEMA depends on the synthesis method used, but according to several works, the $pK_a$ of the homopolymer is located in the pH range of 7–7.5.[24,34,53,69] The dissociation equilibrium of the polyelectrolyte PDEAEMA is illustrated in Figure 2.7.

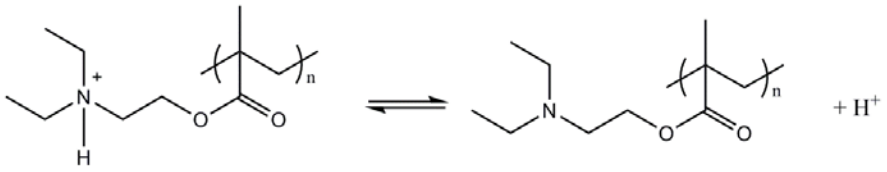

**Figure 2.7.** Dissociation equilibrium of PDEAEMA.

The potentiometric titration curve of the nanogel particles shown in Figure 2.8 indicates that these nanoparticles showed buffering capacity in the pH range of 5.3–7.3.

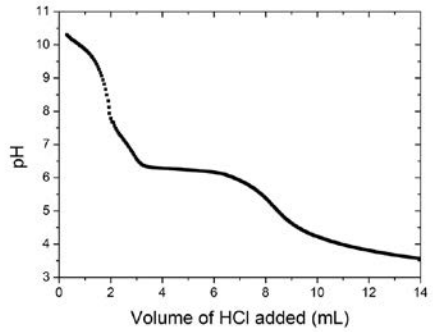


**Figure 2.8.** Potentiometric titration curve of the PDEAEMA nanogel particles.

To further analyze the pH-sensitivity of the nanogel particles and the related dissociation of the polyelectrolyte, potentiometric curve was plotted against the fraction of charged amines or degree of protonation (α). Figure 2.9a displays the pH as a function of the fraction of charged amines (α), which was calculated based on the moles of HCl (titrant) used. As can be observed, the overall degree of protonation (α) of the tertiary amine residues increased from zero to unity as the solution pH was decreased from 8.3 to 5.3. The acidity constant for PDEAEMA segments was estimated from the pH at the half-neutralization point (α = 0.5) as $pK_a$ 6.23, which is lower than that of PDEAEMA homopolymer ($pK_a$ 7–7.5).[24,34,53,69] This might be due to the local high chain density of PDEAEMA sequences within the nanogel particles that makes the protonation more difficult.[70,71]

Moreover, the effective protonation constant ($pK_a$) calculated using Henderson-Hasselbalch equation (see equation 2.2) was plotted against the degree of protonation (α) (see

Figure 2.9b). Figure 2.9 also shows the schematic representation of the charge distribution over nanogel particles during potentiometric titrations.

The regions in the potentiometric curve (see Figure 2.8) above pH 8.3 and below pH 5.3 corresponded to the excess of NaOH and HCl present in the nanogel dispersion, respectively. Apart from that, four regions can be distinguished in Figure 2.9. Considering the pH-dependence of the nanogel, these results can be related to its swelling-de-swelling behavior (see the pH-sensitivity results of the nanogel particles dispersed in a medium of an ionic strength of 10 mM -Figures 2.5 and 2.6-).

Region A ($\alpha \simeq 0$-$0.1$) corresponds to the protonation of the first amine groups located on the outer shell or surface of the nanogel particles. On the one hand, as can be observed in Figure 2.5, nanogels were in their collapsed state in the pH range of 7.2–8.3, and thus only the amine groups located at the surface were accessible. On the other hand, Figure 2.6 shows a little increase in electrophoretic mobility from pH 8.3 to 7.2, suggesting the protonation of amine groups located at the surface of the nanoparticles. As can be seen in Figure 2.9b, the $pK_a$ was near-constant in region A. Such a $pK_a$ profile is only possible if the functional groups are relatively well isolated from each other, being all in a similar chemical environment. Thus, this could be attributed to the amine groups located on the hairs of the shell that were not affected by the electrostatic repulsion of adjacent amine groups.[72]

In the range of $\alpha \simeq 0.1$-$0.22$ (Region B), nanogel particles swelled (see pH range of 6.3-7.2 in Figure 2.5) and so, an enormous volume change must be considered. While nanogel particles are swelling, titrant ions must penetrate deeper inside the structure of the nanogel in order to proceed with the titration. The hindered protonation at the deepest parts of the nanogel particles is reflected on the $pK_a$ decrease up to $\alpha \approx 0.2$, where the nanogel was completely swollen and all the amine groups were totally accessible. In this region, the electrophoretic mobility increased (see Figure 2.6) since all the amine groups located in the shell of the nanogel protonated.

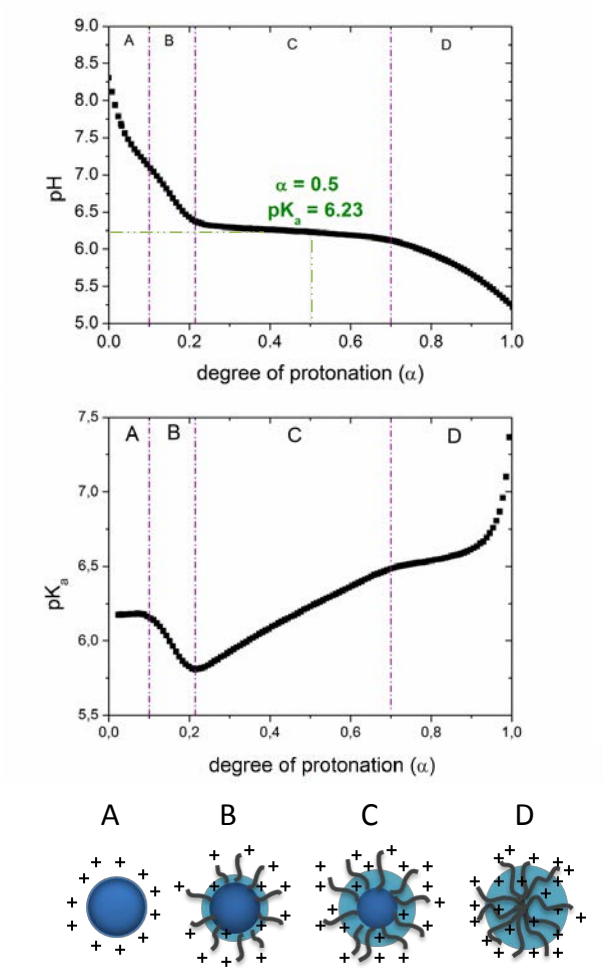


**Figure 2.9.** pH (a) and effective protonation constant $pK_a$ (b) as a function of the degree of protonation (α) for the nanogel particles. A schematic representation of the charge distribution inside nanogel particles during the potentiometric titration is also shown.

Concerning region C ($\alpha \simeq 0.22$-$0.7$), nanogel was completely swollen and the electrophoretic mobility was constant (see pH range of 6.1-6.3 in Figures 2.8 and 2.9, respectively). First of all, in this region, increasing the degree of protonation, $pK_a$ increased. As nanogel particles were swollen, the amine groups were more accessible, being easier their protonation. This is the reason why $pK_a$ increased. The protonation of amine groups located inside the core of the nanogel is confirmed by the constant electrophoretic mobility values, since the electrophoretic mobility is only affected by the groups located in the outer part (being the electrophoretic mobility considered to be on the outermost surface of the particles[73]).

In addition, a fourth region (D) could be defined, equivalent to the pH range of 6.2–5.3, where the pH decreased by increasing the degree of protonation, and the increase of $pK_a$ became less pronounced (see Figure 2.9a and 2.9b, respectively). These results suggest that there is another opposite effect hindering the protonation of amine groups: further protonation enhanced the polymer charge density, resulting in stronger electrostatic repulsive forces. In the presence of adjacent ionized functional groups, the ionization of amine groups at higher degrees of ionization was hindered due to the polyelectrolyte effect.[74,75] Mechanistically, this effect was induced by changes in the electronic environment around the protonated amine groups and the increased electrostatic repulsion of the titrating $H^+$ ions as more amine groups became ionized ($[NH(Et)_2]^+$). Considering that the protonation was more difficult, the addition of the titrant resulted in a pH decrease. Additionally, as expected, electrophoretic mobility remained constant since the protonation of amine groups inside the particles did not contribute to it.

Concerning the suitability of these nanogel particles to be used as drug/gene carriers, when electrostatic interactions are the main force controlling the encapsulation/release of drug/genes, the $pK_a$ gradient within the nanogel particles could be interesting since the behavior would be more tunable.

Additionally, with the aim of studying the effect of the ionic strength on the $pK_a$ value, a potentiometric titration was carried out at an ionic strength of 150 mM. Figure 2.10 shows the comparison of pH as a function of the degree of protonation in the case of the nanogels dispersed at 10 mM and 150 mM. Increasing the ionic strength, the $pK_a$ was also increased ($pK_a = 7.4$). This result corroborated the hypothesis given to understand the shift in VPTpH of nanogel particles increasing the salt concentration.

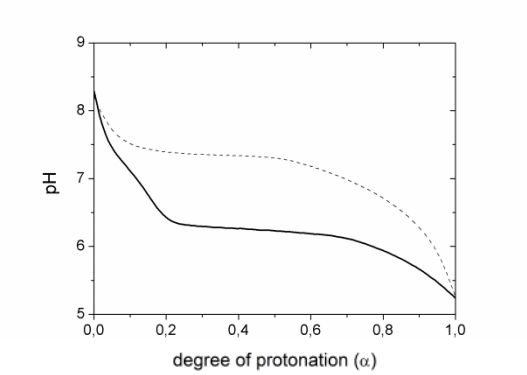


**Figure 2.10.** pH as a function of the degree of protonation (α) for the nanogel particles dispersed at an ionic strength of 10 mM (—) and 150 mM (- - -).

### 2.3.2.2. Thermo-sensitivity

Interestingly, PDEAEMA-based nanogel particles presented pH-dependent thermo-sensitivity. It is well known that the thermo-sensitivity is governed by the balance of hydrophobic/hydrophilic interactions.[9] In the case of PDEAEMA-based nanogels, hydrophilic interactions (H-bonds) are formed between the deprotonated amine groups of PDEAEMA and the water molecules, and the hydrophobic interactions are given between ethyl groups (hydrophobic segments) of the polymeric chains. Being nanogel particles pH-responsive, the adjustment in pH will alter the ionic interactions, hydrogen bonding, and hydrophobic interactions, and thereby, the thermo-responsiveness.[76] Hence, the thermal behavior of the nanogel particles was studied at different pH ranges and these results were related to the pH response. Figure 2.11 displays the variation of the hydrodynamic diameter as a function of temperature at different pH values and at an ionic strength of 10 mM. It is remarkable that all the thermal behaviors obtained were reversible, *i.e.*, no hysteresis between heating and subsequent cooling cycles was observed.

On the one hand, at pH < 6, nanogel particles did not present any temperature-induced swelling-de-swelling behavior because all the amine groups of the nanogel were protonated and there was not any possibility to form H-bonds. Nanoparticles were totally swollen in all the temperature range, because of the electrostatic repulsion between the charged polymer chains. On the other hand, at more basic pH than pH 8, hydrophobic interactions became

strengthened, and nanogel particles were collapsed independently of the temperature. However, in the pH range from 6 to 8, nanoparticles showed temperature-responsiveness. The shrinking of the particles by the temperature increase was related to the disruption of the existing H-bonds and the strengthening of the hydrophobic interactions.[10]

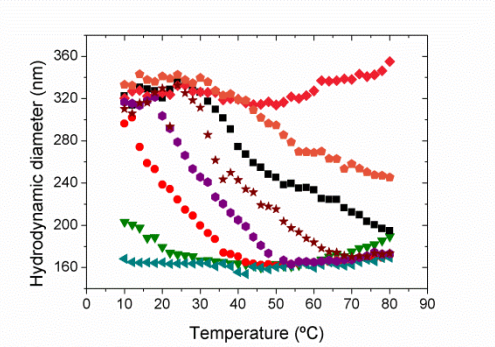


**Figure 2.11.** Average hydrodynamic particle diameters as a function of temperature at different pH and in a cationic buffered medium with an ionic strength of 10 mM. pH 5.6 (◆), pH 5.9 (⬟), pH 6.1 (■), pH 6.3 (★), pH 6.5 (⬢), pH 6.8 (●), pH 7.2 (▼), and pH 7.5 (◀).

The curves shown in Figure 2.11 evidently point out the huge pH-dependence of the thermal response. In order to scrutinize the swelling-de-swelling behavior, the pH influence on the VPTT was evaluated. At more acidic conditions, the temperature-induced volume phase transition occurred at higher temperatures. This result could be ascribed to the protonation of the amine groups and the stronger electrostatic repulsion between charged polymeric chains that makes the solvation by water molecules easier. Therefore, higher temperatures were needed to disrupt H-bonds and cause the collapse of the polymeric network. Remarkable is the huge variation of VPTT (20-50 °C) in a small pH range (pH 6-7).

Similar effects of pH on the temperature-induced behavior of systems based on PDEAEMA were reported by other authors. Yuk *et al*.[77] and Plamper *et al*.[78] found an increase in the transition temperature at lower pH values in copolymer chains based on PDMAEMA and poly(ethylacrylamide) and in star-shaped and linear PDMAEMA polymers, respectively. Beltran *et al*.[79] and de Souza *et al*.[80] also observed the same dependence of the transition temperature on the pH in hydrogels based on PNIPAM and weakly based PDMAEMA and in poly(methyl

methacrylate (PMMA)-*b*-PDMAEMA) copolymers, respectively. In all the cases the results were related to the strengthening/weakening of electrostatic forces.

Additionally, considering the effect of the surrounding ions on the pH-dependent swelling-de-swelling behavior, the influence of the ionic strength on the thermal behavior of the nanogel particles was also studied. Figures 2.12 and 2.13 show thermo-sensitivity curves as a function of pH at ionic strengths of 100 mM (cationic buffer at 10 mM + NaCl) and 150 mM (phosphate buffer at 10 mM + NaCl), respectively.

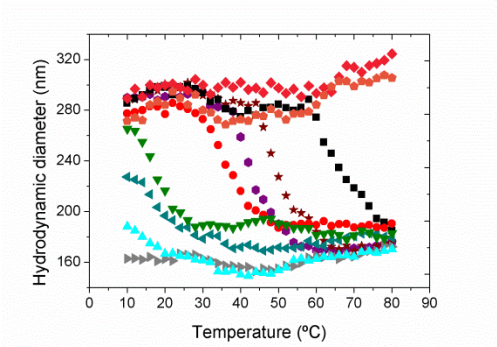


**Figure 2.12.** Average hydrodynamic particle diameters as a function of temperature at different pHs and in a cationic buffered medium with an ionic strength of 100 mM. pH 3.0 (◆), pH 6.5 (⬟), pH 6.7 (■), pH 6.9 (★), pH 7.1 (⬢), pH 7.3 (●), pH 7.5 (▼), pH 7.7 (◀), pH 7.9 (▲), and pH 8.2 (▶).

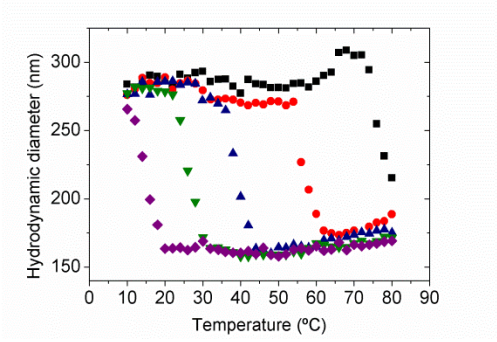


**Figure 2.13.** Average hydrodynamic particle diameters as a function of temperature at different pHs, in PBS medium at 150 mM (phosphate buffer 10 mM + NaCl). pH 6.0 (■), pH 6.5 (●), pH 6.9 (▲), pH 7.5 (▼), and pH 7.9 (◆).

For a clearer study of the ionic strength's influence on the thermal behavior, the VPTT values of the nanogel particles dispersed at different ionic strengths and media were plotted as a function of pH of the medium (see Figure 2.14 and Table 2.2). Regardless of the medium and ionic strength, a linear decrease in VPTT was observed increasing the pH. However, some differences underwent varying the ionic strength. First of all, increasing the ionic strength of the medium up to 100 mM, nanogels revealed temperature-dependent swelling at more basic conditions. In the same way, for a given pH, the temperature-induced transition was moved toward higher temperature values. This behavior could be caused by the higher $pK_a$ at higher ionic strengths. These observations agree with previously reported results by Hirotsu *et al*.[81] They found an increase in VPTT for ionic microgels based on PNIPAM and sodium acrylate increasing the ionic strength and suggested that the VPTT was affected by the alterations in the ionic osmotic pressure.

| | VPTT (°C) | | |
|---|---|---|---|
| **pH** | **Cationic buffer (10 mM)** | **Cationic buffer (10 mM) + NaCl (90 mM)** | **PBS (10 mM) + NaCl (140 mM)** |
| **5.9** | 46.3 | - | - |
| **6.1** | 47.1 | - | 75.8 |
| **6.3** | 39.3 | - | - |
| **6.5** | 29.4 | - | 56.7 |
| **6.7** | 19.2 | 66.7 | - |
| **6.9** | - | 50.3 | - |
| **7.1** | - | 43.2 | 38.3 |
| **7.3** | - | 36.9 | - |
| **7.5** | - | 17.2 | 26.3 |
| **7.9** | - | - | 14.9 |

**Table 2.2.** VPTT values as a function of pH at different ionic strengths and media.

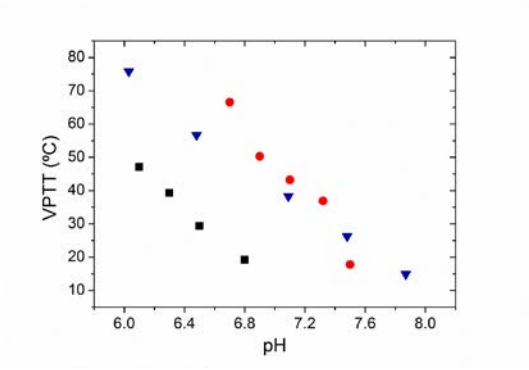


**Figure 2.14.** VPTT values as a function of pH using different ionic strengths: 10 mM cationic buffer (■), 100 mM (10 mM cationic buffer + NaCl) (●), and PBS 150 mM (10 mM phosphate buffer + NaCl) (▼).

Moreover, it is of utmost importance to take into account the nature of the ions that affects the interactions and thus, the response of the nanogel to different stimuli.[79] First of all, as can be seen in Figure 2.14 and Table 2.2, it is worth noting that nanoparticles dispersed in PBS exhibited thermo-sensitivity in a much broader pH range. This fact could be explained considering that ions such as phosphate affect the interactions between the polymer chains and water in different ways: changing the $pK_a$, strengthening the interactions (H-bonds and others) between water and the polymers with the hydrated co-ions, changing the hydrophilicity of PDEAEMA anions pairs, etc.[80] Consequently, as the thermal response was affected in different ways, different swelling-de-swelling behaviors could be expected in nanogel particles dispersed in PBS, broadening the pH range where nanogels showed thermo-sensitivity.

Furthermore, temperature transitions were sharper in the case of using PBS as buffer compared to those seen by using cationic buffers (see Figure 2.13). These results could be explained taking into account the effect of temperature on the $pK_a$ of the buffer. According to the information given by Windbacher[82] and Dawson *et al*.,[83] PBS is much less sensitive to temperature changes than other cationic buffers. The variation of the $pK_a$ of PBS with temperature ($dpK_a/dT$) is much lower ($dpK_a/dT = -3 \cdot 10^{-3}$) than that of the cationic buffer used in the pH range of 6–7 (bis-Tris ($dpK_a/dT = -12 \cdot 10^{-3}$)). Thus, in the case of using cationic buffers, the increase in temperature caused a small decrease in pH, delaying the shrinking of the PDEAEMA-based nanoparticles. By this way, the transition of nanogel particles dispersed in PBS was more defined.

## 2.4. Conclusions

New PDEAEMA-based monodisperse nanogels were successfully prepared by batch emulsion polymerization presenting both temperature- and pH-sensitivity. The heterogeneity of PDEAEMA-based nanogel morphology was also demonstrated by using high-resolution transverse $^{1}$H-NMR measurements. Their dual and tunable sensitivity was studied throughtly. As well as investigating the swelling-de-swelling behavior of the nanogels in response to pH variations. Their buffering capacity was confirmed by potentiometric titrations, suggesting the ability to disrupt endosomes *via* an osmotic pressure buildup (proton sponge hypothesis). Apart from the pH-sensitivity, nanogels showed a tunable pH-dependent thermo-sensitivity: an increase in the pH value led to a significant decrease in VPTT, which could be adjusted as desired close to human body temperature (37 °C). Furthermore, the effect of the ionic strength of the medium on the response to different stimuli was studied. It is remarkable that the transition temperature of the nanogel particles dispersed in PBS was given at physiological conditions (38 °C and pH 7.1), demonstrating the potential use of these nanoparticles in several bio-applications.

In summary, their tunable and dual sensitivity at physiological conditions makes them attractive and potentially applicable in drug delivery, as they can be tailored to suit the needs of this particular bio-application.

*The content of this Chapter has been published in Particle and Particle Systems Characterization,* ***2014****, 31, 101-109.*

## 2.5. References

1. J. Ramos, J. Forcada, R. Hidalgo-Alvarez, *Chem. Rev.* **2014**, *114*, 367–428.
2. G. Soni, K. S. Yadav, *Saudi Pharm. J.* **2014**, DOI:10.1016/j.jsps.2014.04.001.
3. S. Maya, B. Sarmento, A. Nair, N. S. Rejinold, S. V. Nair, R. Jayakumar, *Curr. Pharm. Des.* **2013**, *19*, 7203-7218.
4. N. M. B. Smeets, T. Hoare, *J. Polym. Sci., Part A: Polym. Chem*. **2013**, *51*, 3027-3043.

5. R. T. Chacko, J. Ventura, J. Zhuang, S. Thayumanavan, *Adv. Drug Delivery Rev.* **2012**, *64*, 836-851.
6. A. L. Behera, S. V. Patil, S. K. Sahoo, *Der Pharm. Sin.* **2010**, *1*, 20-28.
7. A. V. Kabanov, S. V. Vinogradov, *Angew. Chem. Int. Ed.* **2009**, *48*, 5418-5429.
8. J. K. Oh, R. Drumright, D. J. Siegwart, K. Matyjaszewski, *Prog. Polym. Sci.* **2008**, *33*, 448-477.
9. K. Raemdonck, J. Demeester, S. S. De Smedt, *Soft Matter* **2009**, *5*, 707-715.
10. B. R. Saunders, B. Vincent, *Adv. Colloid Interface Sci.* **1999**, *80*, 1-25.
11. S. Mura, J. Nicolas, P. Couvreur, *Nat. Mater.* **2013**, *12*, 991-1003.
12. B. H. Tan, P. Ravi, L. N. Tan, K. C. Tam, *J. Colloid Interface Sci.* **2007**, *309*, 453-463.
13. L. Zha, B. Banik, F. Alexis, *Soft Matter* **2011**, *7*, 5908-5916.
14. P. Papaphilippou, M. Christodoulou, O.-M. Marinica, A. Taculescu, L. Vekas, K. Chrissafis, T. Krasia-Christoforou, *ACS Appl. Mater. Interfaces* **2012**, *4*, 2139-2147.
15. W. Xiong, W. Wang, Y. Wang, Y. Zhao, H. Chen, H. Xu, X. Yang, *Colloids Surf., B* **2011**, *84*, 447-453.
16. X. Liu, H. Guo, L. Zha, *Polym. Int.* **2012**, *61*, 1144-1150.
17. Y. Chen, Y. Chen, J. Nan, C. Wang, F. Chu, *J. Appl. Polym. Sci.* **2012**, *124*, 4678-4685.
18. S. Bhattacharya, F. Eckert, V. Boyko, A. Pich, *Small* **2007**, *3*, 650-657.
19. W. Gao, J. M. Chan, O. C. Farokhzad, *Mol. Pharmaceutics* **2010**, *7*, 1913-1920.
20. T. Yoshida, T. C. Lai, G. S. Kwon, K. Sako, *Expert Opin. Drug Delivery* **2013**, *10* (11) 17pp.
21. K. Loomis, K. McNeeley, R. V. Bellamkonda, *Soft Matter* **2011**, *7*, 839-856.
22. L. E. Gerweck, K. Seetharaman, *Cancer Res.* **1996**, *56*, 1194-1198.
23. J.-Z. Du, T.-M. Sun, W.-J. Song, J. Wu, J. Wang, *Angew. Chem. Int. Ed*. **2010**, *49*, 3621-3626.
24. S. R. Marek, C. A. Conn, N. A. Peppas, *Polymer* **2010**, *51*, 1237-1243.
25. M. Tamura, S. Ichinohe, A. Tamura, Y. Ikeda, Y. Nagasaki, *Acta Biomater*. **2011**, *7*, 3354-3361.
26. S. Dai, P. Ravi, K. C. Tam, B. W. Mao, L. H. Gan, *Langmuir* **2003**, *19*, 5175-5177.
27. M. R. Aguilar, C. Elvira, A. Gallardo, B. Vázquez, J. San Román, *Smart Polymers and Their Applications as Biomaterials* In *Topics in Tissue Engineering*, *Vol. 3*, Eds. N.

Ashammakhy, R. L. Reis , E. Chiellini, BTE, Oulu, Finland, ISBN: 978-0-85709-695-1, **2007.**

28. M. Oishi, Y. Nagasaki, *React. Funct. Polym.* **2007**, *67*, 1311-1329.
29. H. Hayashi, M. Iijima, K. Kataoka, Y. Nagasaki, *Macromolecules* **2004**, *37*, 5389-5396.
30. M. Oishi, H. Hayashi, M. Iijima, Y. Nagasaki, *J. Mater. Chem.* **2007**, *17*, 3720-3725.
31. M. Oishi, H. Hayashi, T. Uno, T. Ishii, M. Iijima, Y. Nagasaki, *Macromol. Chem. Phys.* **2007**, *208*, 1176-1182.
32. M. Oishi, N. Miyagawa, T. Sakura, Y. Nagasaki, *React. Funct. Polym.* **2007**, *67*, 662-668.
33. M. Oishi, H. Hayashi, K. Itaka, K. Kataoka, Y. Nagasaki, *Colloid. Polym. Sci.* **2007**, *285*, 1055-1060.
34. J. I. Amalvy, E. J. Wanless, Y. Li, V. Michailidou, S. P. Armes, *Langmuir* **2004**, *20*, 8992-8999.
35. Y. Hu, T. Litwin, A. R. Nagaraja, B. Kwong, J. Katz, N. Watson, D. J. Irvine, *Nano Lett.* **2007**, *7*, 3056-3064.
36. J. Ramos, Á. Costoyas, J. Forcada, *J. Polym. Sci., Part A: Polym. Chem.* **2006**, *44*, 4461-4478.
37. K. E. Christodoulakis, M. Vamvakaki, *Macromol. Symp*. **2010**, *291-292*, 106-114.
38. I. Varga, T. Gilányi, R. Mészáros, G. Filipcsei, M. Zrínyi, *J. Phys. Chem*. B **2001**, *105*, 9071-9076.
39. B. R. Saunders, *Langmuir* **2004**, *20*, 3925–3932.
40. M. Stieger, W. Richtering, J. S. Pedersen, P. Linder, *J. Chem. Phys*. **2004**, *120*, 6197–6206.
41. A. Fernández-Barbero, A. Fernández-Nieves, I. Grillo, E. López-Cabarcos, *Phys. Rev. E.* **2002**, *66*, 051803/1-9.
42. A. Balaceanu, D. E. Demco, M. Möller, A. Pich, *Macromolecules* **2011**, *44*, 2161–2169.
43. A. Balaceanu, D. E. Demco, M. Möller, A. Pich, *Macromol. Chem. Phys*. **2011**, *212*, 2467–2477.
44. G. Aguirre, J. Ramos, J. Forcada, *Soft Matter* **2013**, *9*, 261–270.
45. A. Guillermo, J. P. Cohen Addad, J. P. Bazile, D. Duracher, A. Elaissari, C. Pichot, *J. Polym. Sci., Part B: Polym. Phys.* **2000**, *38*, 889–898.
46. S. Schachschal, A. Balaceanu, C. Melian, D. E. Demco, T. Eckert, W. Richtering, A. Pich, *Macromolecules* **2010**, *43*, 4331–4339.

47. T. Hoare, R. Pelton, Langmuir **2004**, *20*, 2123-2133.
48. S. Kawaguchi, A. Yekta, M. A. Winnik, *J. Colloid Interface Sci.* **1995**, *176*, 362-369.
49. M. Oishi, A. Tamura, T. Nakamura, Y. Nagasaki, *Adv. Funct. Mater.* **2009**, *19*, 827-834.
50. X. Wu, R. H. Pelton, A. E. Hamielec, D. R. Woods, W. McPhee, *Colloid. Polym. Sci.* **1994**, *272*, 467-477.
51. M. Andersson, S. L. Maunu, *J. Polym. Sci., Part B: Polym. Phys.* **2006**, *44*, 3305-3314.
52. B. A. Firestone, R. A. Siegel, *J. Appl. Polym. Sci.* **1991**, *43*, 901-914.
53. S. Shahalom, T. Tong, S. Emmett, B. R. Saunders, *Langmuir* **2006**, *22*, 8311-8317.
54. S. Fujii, M. Mochizuki, K. Aono, S. Hamasaki, R. Murakami, Y. Nakamura, *Langmuir* **2011**, *27*, 12902-12909.
55. N. A. Peppas, A. R. Khare, *Adv. Drug Delivery Rev.* **1993**, *11*, 1-35.
56. K. Podual, F. J. Doyle III, N. A. Peppas, *Polymer* **2000**, *41*, 3975-3983.
57. F. A. Plamper, A. Schmalz, E. Penott-Chang, M. Drechsler, A. Jusufi, M. Ballauff, A. H. E. Müller, *Macromolecules* **2007**, *40*, 5689-5697.
58. A. Fernández-Nieves, M. Marquez, *J. Chem. Phys.* **2005**, *122*, 084702/6.
59. B. Chang, X. Sha, J. Guo, Y. Jiao, C. Wang, W. Yang, *J. Mater. Chem.* **2011**, *21*, 9239-9247.
60. E. He, P. Ravi, K. C. Tam, *Langmuir* **2007**, *23*, 2382-2388.
61. B. Zhang, B. Sun, X. Li, Y. Yu, Y. Tian, X. Xu, *Int. J. Biol. Macromol.* **2015**, *79*, 392-397.
62. B. Zhang, B. Wei, X. Hu, Z. Jin, X. Xu, Y. Tian, *Carbohydr. Polym.* **2015**, *124*, 245-253.
63. H. Ohshima, *J. Colloid Interface Sci.* **1994**, *163*, 474-473.
64. H. Ohshima, *Colloid Surf., A*. **1994**, *103*, 249-255.
65. C. Cametti, *Soft Matter* **2011**, *7*, 5494-5506.
66. H. Ohshima, *Adv. Colloid Interface Sci*. **1995**, *62*, 189-235.
67. H. Ohshima, *Soft Matter* **2012**, *8*, 3511-3514.
68. H. Ohshima, *Colloid. Polym. Sci*. **2007**, *285*, 1411-1421.
69. S. Liu, S. P. Armes, *Angew. Chem. Int. Ed.* **2002**, *41*, 1413-1416.
70. C. Li, Z. Ge, J. Fang, S. Liu, *Macromolecules* **2009**, *42*, 2916-2924.
71. M. Li, Z. Tang, H. Sun, J. Ding, W. Song, X. Chen, *Polym. Chem.* **2013**, *4*, 1199-1207.
72. T. Hoare, R. Pelton, *Macromolecules* **2004**, *37*, 2544-2550.
73. I. Tsoneva, T. Tomov, *Bioelectrochem. Bioenerg.* **1984**, 12, 253-258.
74. T. Hoare, R. Pelton, *Langmuir* **2006**, *22*, 7342-7350.

75. P. Sheikholeslami, C. Ewaschuk, S. U. Ahmed, B. A. Greenlay, T. Hoare, *Colloid Polym. Sci.* **2012**, *290*, 1181-1192.
76. S. Dai, P. Ravi, K. C. Tam, *Soft Matter* **2008**, *4*, 435-449.
77. S. H. Yuk, S. H. Cho, S. H. Lee, *Macromolecules* **1997**, *30*, 6856-6859.
78. F. A. Plamper, M. Ruppel, A. Schmalz, O. Borisov, M. Ballauff, A. H. E. Müller, *Macromolecules* **2007**, *40*, 8361-8366.
79. S. Beltran, J. P. Baker, H. H. Hooper, H. W. Blanch, J. M. Prausnitz, *Macromolecules* **1991**, *24*, 549-551.
80. J. C. P. de Souza, A. F. Naves, F. H. Florenzano, *Colloid Polym. Sci.* **2012**, *290*, 1285-1291.
81. S. Hirotsu, Y. Hirokawa, T. Tanaka, *J. Chem. Phys.* **1987**, *87*, 1392-1395.
82. T. Windbacher, *Engineering Gate Stacks for Field-Effect Transistors*, PhD Thesis, Technischen Universität Wien, Austria, **2010.**
83. R. M. C. Dawson, D. C. Elliott, W. H. Elliot, K. M. Jones, *Data for Biochemical Research, Vol. 15*, Oxford University Press, Oxford, ISBN: 9780198552994, **1987.**

# 3

# Functionalized PDEAEMA-based dual-stimuli-responsive nanogels

# 3.1. Introduction

Since nanogels for a specific application call for a well defined stimuli-responsive behavior precisely adjusted to the respective requirements and settings, it can be stated that the key point for the successful development of such materials is the design of specific synthetic pathways by precisely regulating the synthesis variables such as the synthesis temperature and the amount and type of initiator used, and characteristics such as the cross-linking density, the heterogeneity in microstructure, and the type and localization of chemical functional groups, among others.[1-6]

Owing to the biocompatibility and tunable and dual-stimuli-responsive swelling-de-swelling behavior, nanogels based on poly(2-diethylaminoethyl methacrylate) (PDEAEMA) described in Chapter 2 are considered to be promising candidates on several biomedical applications.[7-9] Besides, another interesting point was the synthesis methodology used, since no purification processes are needed when using the surfactant-free emulsion polymerization approach.[10] These nanogels were taken as a reference for the preparation of new functionalized nanogels.

Many efforts have been made to investigate the synthesis variables with the aim of controlling the properties of the nanogels. Among them, it is well known that the initiator concentration used has a high impact on the size of nanogel particles synthesized by emulsion polymerization, being useful tool to modify the particle dimensional characteristics.[11,12] Thus, first of all, nanogel particles were synthesized and characterized by using different amounts of initiator.

As the internal structure of the nanogels strongly influences their swelling-de-swelling behavior, the adjustment of the number and distribution of cross-linking points within the nanogel particles by using different cross-linker types gives additional possibility to tune their size and swelling properties.[13,14] In view of their biocompatibility, two ethylene glycol (EG)-based cross-linkers were used for the syntheses of nanogel particles: ethylene glycol dimethacrylate (EGDMA) and poly(ethylene glycol) diacrylate (PEGDA). The influence of the cross-linker type and concentration on the dual-stimuli-sensitivity and inner structure of the nanogels was studied thoroughly.

The incorporation of degradable linkages into nanogels allows the nanogel to break down into sufficiently small fragments to facilitate renal clearance and offers additional control

over the drug release rates. One of the simplest ways to introduce degradability into the design of a nanogel is to select a cross-linker that can be cleaved at specific physiological conditions. For example, the use of disulfide groups offers further advantages since the degradation can be targeted to occur in intracellular compartments because of the significantly different reduction potential from the extracellular matrix.[7,9,10,15,16] So as to add degradability to the nanogels, different nanogel families were prepared by using two different disulfide-based cross-linkers: *N,N'*-Bis(acryloyl)cystamine (BAC) and bis(2-methacryloyl)oxyethyl disulfide (DSDMA). The role of the type and concentration of the cross-linkers was investigated.

Furthermore, methodologies to modify the surface can impart to nanogels the ability to control, at least in part, their pharmacokinetics and biodistribution. For example, PEGylation refers to the modification of a particle surface by entrapping, covalently grafting or adsorbing polyethylene glycol (PEG). This modification increases the stability of nanogels preventing them from aggregation, and endows them with *in vivo* longevity and specific capability of extravasation in tumor cells and/or tissues (the so-called enhanced permeability and retention effect) by the induced steric repulsion of blood opsonins.[8,9,17,18,19] Considering the advantages of PEGylation for *in vivo* biomedical applications, nanogel particles were PEGylated by using different amounts of a PEG-based stabilizer: poly(ethylene glycol) methacrylate (PEGMA).

The functionalization of nanogels offers some benefits towards them since it enables targeted and/or triggered drug delivery, immobilization, protection and release of proteins or conjugation to critical genetic markers associated with certain disease states for diagnostic and/or active targeting purposes.[2,8] For instance, epoxide and amine groups have received high interest due to their high reactivity and easy modification.[20-22] Therefore, epoxide- and primary amine-functionalization was incorporated to the previously synthesized nanogels.

In this Chapter, syntheses and characterizations of a series of different functionalized PDEAEMA-based nanogels were described. Different parameters such as the initiator concentration and cross-linker type and concentration, and different functionalizations were thoroughly studied by means of the swelling-de-swelling behavior and morphology of nanogels. The broad selection of response mechanisms of such dual-stimuli-sensitive nanogels increases the interest of them across the multidisciplinary field of biomedical applications.

# 3.2. Experimental

## 3.2.1. Materials

All the following materials were used as received:

- 2-(diethylamino)ethyl methacrylate (DEAEMA), supplied by Sigma-Aldrich, was used as a main monomer.
- 2,2′-azobis (*N,N′*-dimethyleneisobutyramidine) dihydrochloride (ADIBA), supplied by Wako Chemical GmbH, was used as a cationic initiator.
- Tetramethylethylenediamine (TEMED) together with potassium persulfate (KPS), both of them supplied by Sigma-Aldrich, were used as a redox initiator system.
- Ethylene glycol dimethacrylate (EGDMA, E), *N,N′*-Bis(acryloyl)cystamine (BAC) and bis(2-methacryloyl)oxyethyl disulfide (DSDMA, DM), all of them supplied by Sigma-Aldrich, and poly(ethylene glycol) diacrylate (PEGDA, PD, n=400), supplied by Polysciences, Inc., were used as cross-linkers.
- Poly(ethylene glycol) methacrylate (PEGMA, PM, $M_n$=526), supplied by Sigma-Aldrich, was used as a polymeric stabilizer.
- Glycidyl methacrylate (GM), supplied by Sigma-Aldrich, was used as a comonomer for the synthesis of epoxide-functionalized nanogels.
- (2-Boc-amino)ethyl methacrylate (A-Boc), supplied by Sigma-Aldrich, was used as a comonomer in the synthesis of primary amine-functionalized nanogels.
- Trifluoroacetic acid (TFA), diethylether, and sodium hydroxide (NaOH), all of them supplied by Sigma-Aldrich, were used for the removal of Boc protecting groups in the synthesis of primary amine-functionalized nanogels.
- Glycine, γ-aminobutyric acid, pyridine, bis-tris, sodium phosphate monobasic, and dibasic, Trizma®, triethylamine and sodium chloride (NaCl), supplied by Sigma-Aldrich, were used to prepare the buffer solutions at different ionic strengths.
- Deuterium oxide ($D_2O$), supplied by Sigma-Aldrich, and deuterium chloride (DCl), supplied by Eurisotop, were used for NMR characterization.
- Double deionized (DDI) water was used throughout the work.

## 3.2.2. Synthesis of nanogels

Different series of nanogel particles were synthesized by surfactant-free emulsion polymerization of DEAEMA. The experimental set-up was described in Chapter 2 (see Figure 2.1). Concerning the synthesis methodology, two main families of nanogels can be distinguished: the ones synthesized by using a thermal initiator system and the ones synthesized by using a redox initiator system.

### 3.2.2.1. Thermal initiator system

Table 3.1 summarizes the reaction conditions and recipes used to obtain the different nanogels by using a thermal initiator system. In the first column the nomenclature used for each reaction is shown. The number and/or X following AD indicate the amount of ADIBA (AD) added with respect to DEAEMA (wt%M). The following letter and number are the cross-linker type (E=EGDMA, PD=PEGDA, BAC) and the mol amount of cross-linker added with respect to DEAEMA (mol%M). The number and/or Y following PM refer to the amount of PEGMA (PM) with respect to DEAEMA (wt%M). Finally, GM and the following number Z indicate the amount of glycidyl methacrylate (wt%M) used. A-Boc refers to (2-Boc-amino)ethyl methacrylate. Being the reference the type of nanogel presented in Chapter 2 will be also shown and used for comparisons in this Chapter as E0.93PM0.

Briefly, once the main monomer DEAEMA, the comonomer if necessary, the cross-linker, the stabilizer PEGMA, and 170 g of water were charged into the reactor, the reactor content was heated at 70 °C, stirred at 300 rpm, and purged with nitrogen for 40 min before starting the polymerization reaction. After adding the initiator (a certain amount of ADIBA in 10 g of DDI water), the polymerization reaction was allowed to continue under nitrogen atmosphere, under stirring for 2 h at 70 °C. The reaction mixture was subsequently cooled to 25 °C maintaining the stirring.

| NANOGEL | ADIBA | Cross-linker | | PM | GM | A-Boc |
|---|---|---|---|---|---|---|
| | wt%M | Type | mol%M | wt%M | wt%M | wt%M |
| **ADXE0.93PM0** | 1/4 | E | 0.93 | - | - | - |
| **E/PD/BAC0.93PMY** | 2 | E/PD/BAC | 0.93 | 0/10/20 | - | - |
| **E/PD0.33PMY** | | E/PD | 0.33 | 10/20 | - | - |
| **E0.93PM10GMZ** | | E | 0.93 | 10 | 10/20 | - |
| **E0.93PM10ABoc** | | | | | - | 5 |

**Reaction conditions:** 300 rpm, 70 °C, 2 h
20 g DEAEMA, 180 g DDI water
**Variables:** type and concentration of cross-linker and concentrations of ADIBA, PEGMA, GM and A-Boc

**Table 3.1.** Recipes and reaction conditions used in the batch emulsion polymerizations of nanogels using ADIBA as initiator.

So as to obtain functionalization by primary amine groups, after the synthesis of E0.93PM10ABoc, Boc groups had to be removed. For that purpose, the procedure described by Ji *et al.*[23] was followed. Firstly, nanogels were dialyzed against fresh DDI water to ensure the removal of impurities and nonreacted reagents and then, they were lyophilized by using Telstar Cryodos-50 lyophilizer. 2 g of lyophilized PDEAEMA-based nanogel was dispersed in 12.5 mL of trifluoroacetic acid (TFA) and stirred for 2 h at room temperature by using a magnet. The reaction mechanism of the deprotection of Boc groups by using TFA is illustrated in Figure 3.1. TFA was then removed by using a rotary evaporator, and the residue was rinsed three times with diethyl ether. The resultant precipitate was collected by filtration, washed twice by diethyl ether, and dried overnight in vacuum. The nanogel was then washed with NaOH water solution at pH 9 and dialyzed by using dialysis membranes [MW Cut-off (MWCO) of 3500] against DDI water. After the deprotection of Boc groups, the nanogel was named E0.93PM10AEMA.

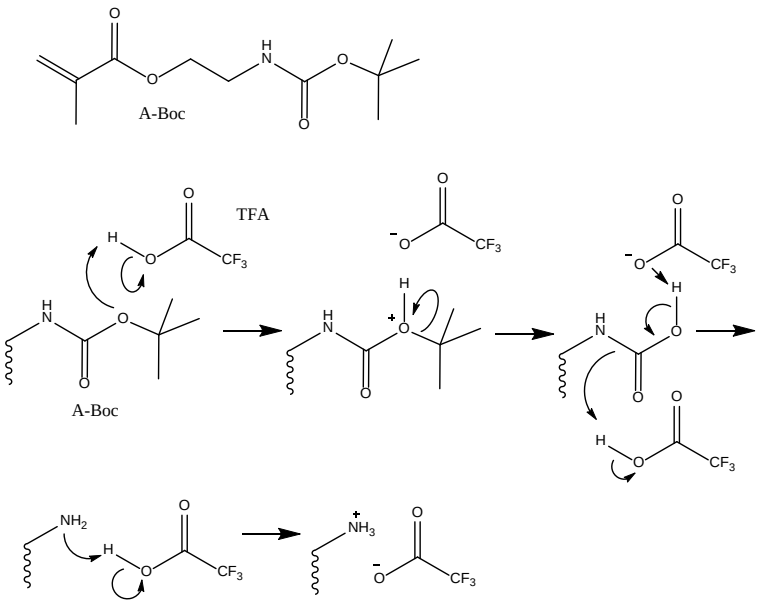


**Figure 3.1.** Reaction mechanism of the deprotection of Boc groups by using TFA.

### 3.2.2.2. Redox initiator system

Some nanogels were synthesized by using a redox initiator system. Briefly, 15 g of the main monomer DEAEMA, a certain amount of PEGMA and 165 g of DDI water were placed into a 250-mL jacketed glass reactor. The reactor content was heated at 50 °C, stirred at 300 rpm, and purged with nitrogen for 40 min before starting the polymerization reaction. Then, 0.174 g of TEMED in 5 g of DDI water was added, and after 10 min, 1.042 g of KPS as initiator in 10 g of DDI water and a certain amount of cross-linker in 5 g of DEAEMA were added. The polymerization reaction was allowed to continue under nitrogen atmosphere while stirring for 2 h, and the reaction mixture was subsequently cooled to 25 °C maintaining the stirring. The final dispersion was filtered through glass wool. Table 3.2 summarizes the reaction conditions and recipes used for the syntheses. The first letter R refers to the initiator system used (R, Redox). The following letters and numbers indicate the cross-linker type (BAC and DM=DSDMA) and the mol amount of cross-linker used with respect to DEAEMA (mol%M). The last letters and numbers describe the amount of PEGMA (PM) added to the reaction recipe with respect to DEAEMA (wt%M).

| NANOGEL | Cross-linker | | PM |
|---|---|---|---|
| | Type | mol%M | wt%M |
| **RBAC/DM0.93** | BAC/DM | 0.93 | 0 |
| **RBACXPMY** | BAC | 0.33/0.93 | 10/20 |
| **RDMZPM10** | DM | 0.93/3.2/6.3 | 10 |
| **Reaction conditions:** 300 rpm, 50 °C, 2 h<br>20 g DEAEMA, 180 g DDI water, 1.042 g KPS, 0.174 g TEMED<br>**Variables:** type and concentration of cross-linker and concentration of PEGMA | | | |

**Table 3.2.** Recipes and reaction conditions used in the batch emulsion polymerizations of nanogels using KPS/TEMED as a redox initiator system.

## 3.2.3. Characterization of nanogels

### 3.2.3.1. Polymeric characterization

Morphology of nanogels. The morphology of nanogels E0.93PM10 and PD0.93PM10 was examined performing $^{1}H$ transverse relaxation ($T_2$) measurements on a Bruker Avance 500 NMR spectrometer. The protocol presented in Chapter 2 was taken as reference, but some modifications were made.[24] To study the microstructure at different temperatures, previously lyophilized nanogel particles were dispersed in buffered media at a concentration of 2 wt% and an ionic strength of 10 mM. Measurements were taken every 5 °C (from 25 °C to 60 °C) and employing a recycle delay of 10 s and a dwell time of 62 μs. The decay of transverse magnetization relaxation was measured using Hahn-echo pulse sequence and the number of the echo times employed was 29 between 0.54 ms and 16.2 s. The normalized integral intensity of various resonances was fitted by two-exponential decay functions and a biexponential decay for the integral of the most intense resonance peak for the different nanogels was assumed. The values of the short ($T_{2S}$) and long ($T_{2L}$) $^{1}H$ transverse relaxation times and the relative amount of methyl protons of PDEAEMA in core ($C_S$) and shell ($C_L$) were obtained, using the equations suggested by Balaceanu *et al.*[25] and explained in Chapter 2 (see 2.2.3.1 Microstructure of nanogels). The ratio between the cross-linking densities ($CLD^{core}/CLD^{shell}$) of the nanogel particles was also determined (see equation 2.4).

Moreover, in the case of nanogel particles with a heterogeneous morphology, the ratio between the number of subchains (*i.e.*, chains between two cross-linking points) in core ($N^{core}$) and shell ($N^{shell}$) can be calculated. Pich and co-workers[25,26] related this ratio to the parameters $C_S$, $C_L$, $T_{2S}$, and $T_{2L}$, by equation 3.1.

$$\frac{N^{core}}{N^{shell}} = \frac{C_S}{C_L} \cdot \left(\frac{T_{2L}}{T_{2S}}\right)^{1/2} = \frac{C_S}{C_L} \cdot \left(\frac{CLD^{core}}{CLD^{shell}}\right) \qquad (3.1)$$

FTIR analysis. With the aim of validating the functionalization of nanogels by epoxide groups, Fourier Transform Infrared (FTIR) spectroscopy (Nicolet 6700 FTIR) was employed. Nanogel particles were dispersed in water and some drops of the dispersion were placed in a sheet made of Thallium Bromoiodide (KSR-5). Sample of nanogel particles dispersion was analyzed after evaporating the water.

$^1$H-NMR analysis. $^1$H-NMR analysis (Bruker Avance 500 NMR spectrometer) was used to confirm the functionalization of nanogel particles by primary amine groups and the complete disappearance of Boc groups. For that purpose, nanogel particles before and after the removal of Boc groups were dispersed in $D_2O$.

### 3.2.3.2. Colloidal characterization

To study the pH- and thermo-sensitivity of the nanogel particles and to determine the volume phase transition pH and temperature (VPTpH and VPTT), the same procedure reported in Chapter 2 was used. For that purpose, Photon Correlation Spectroscopy (PCS, Zetasizer Nano ZS, Malvern Instruments) was used. Nanogels synthesized by using a thermal initiator system (see Table 3.1) were dispersed at different ionic strengths: 10 mM (cationic buffer) or 150 mM (Phosphate Buffered Saline, PBS). When using a redox initiator system (see Table 3.2), nanogels were dispersed at an ionic strength of 150 mM (PBS).

The swelling ratio was calculated by using the following equation:

$$\text{Swelling ratio} = \left(\frac{dp_X}{dp_S}\right)^3 \qquad (3.2)$$

where $dp_X$ is the hydrodynamic diameter at a given pH or temperature (for pH- and temperature-responsive curves, respectively), and $dp_S$ is the smallest hydrodynamic diameter in all the pH or temperature range.

Electrophoretic mobility measurements were conducted by Electrophoretic Light Scattering (ELS, Zetasizer Nano ZS, Malvern Instruments) as explained in Chapter 2. Besides, with the aim of studying the pH-dependent ionization degree of nanogels, potentiometric titrations were performed by using T90 titrator (Mettler Toledo). The same procedure as the one described in Chapter 2 was used for the titrations and analyzing the data obtained.[27,28]

## 3.3. Results and discussion

### 3.3.1. Effect of the initiator concentration

Final conversions were obtained gravimetrically being higher when increasing the initiator concentration as expected [76% (AD1E0.93PM0), 81% (E0.93PM0) and 86% (AD4E0.93PM0)]. An increase in the initiator concentration led to a higher concentration of free radicals which increases the consumption rate of the main monomer (DEAEMA).[29] Hazot *et al.*[30] observed the same effect in poly(*N*-ethylmethacrylamide)-based nanoparticles by using KPS as initiator. Figure 3.2 shows the evolution of particle size of nanogels AD1E0.93PM0, E0.93PM0, and AD40.93PM0 as a function of the partial conversion of DEAEMA. As can be seen, nanogels synthesized with higher initiator concentrations were smaller in size. The increase in initiator concentration and thereby number of growing oligoradicals led to an increase in the number of nanogel particles, being these particles smaller in size.[11,12,31]

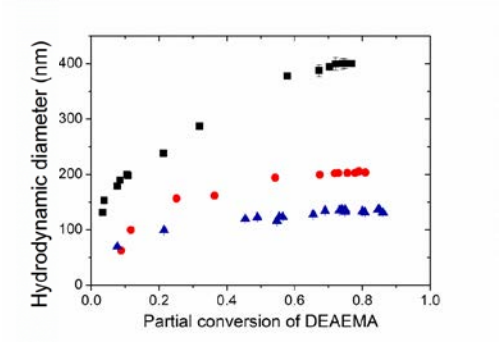


**Figure 3.2.** Evolution of the hydrodynamic diameters of nanogels in the polymerization reactions. AD1E0.93PM0 (■), E0.93PM0 (●), and AD4E0.93PM0 (▲).

The influence of the initiator concentration on pH-sensitivity of nanogel particles was also analyzed by PCS measurements. Figure 3.3 shows the pH-dependence of hydrodynamic diameters, swelling ratios, and electrophoretic mobilities of nanogel particles obtained by using different ADIBA concentrations. In all the cases, the pH-responsive behavior of the nanogel particles was similar. Nanogel particles were swollen below the VPTpH (at around pH 6.5) and collapsed above it. The transition was governed by electrostatic interactions, as confirmed by electrophoretic mobility results shown in Figure 3.3c.

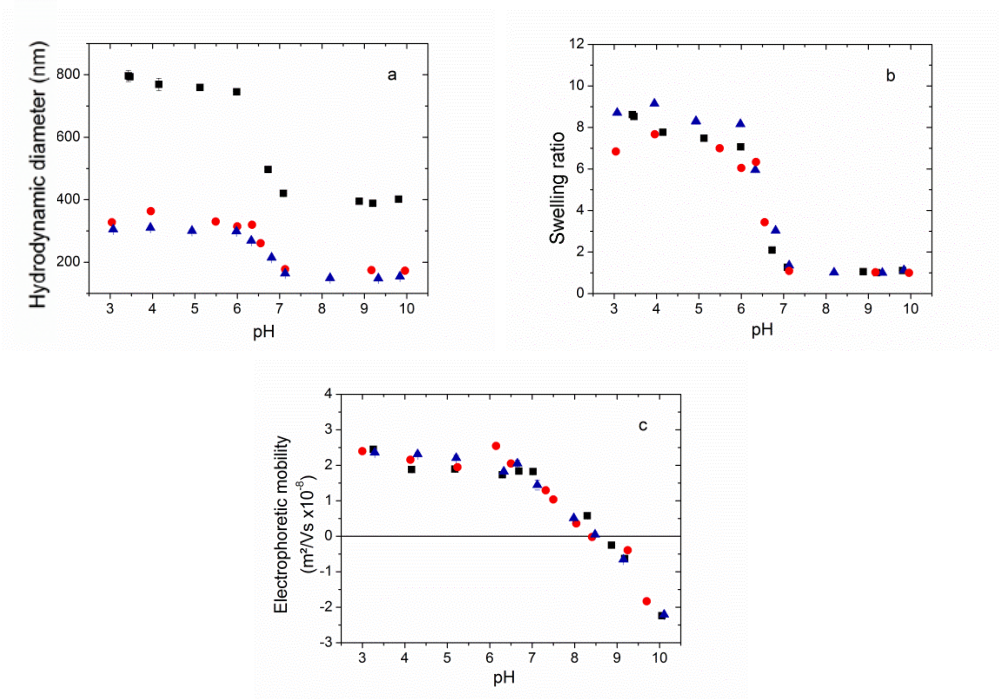


**Figure 3.3.** Hydrodynamic diameters (a), swelling ratios (b), and electrophoretic mobilities (c) of nanogel particles as a function of pH at an ionic strength of 10 mM. AD1E0.93PM0 (■), E0.93PM0 (●), and AD4E0.93PM0 (▲).

Concerning the effect of initiator concentration, despite particles with lower hydrodynamic diameters were obtained at higher initiator concentrations, the swelling ratio was not overly sensitive to initiator concentration (see Figure 3.3b), suggesting a similar cross-linking density in all the cases. This result indicates that the electrostatic interactions balance was not affected by the initiator concentration. Moreover, there was no distinct difference in electrophoretic mobility values varying the initiator concentration. Even though the initiator was positively charged, considering the low amount used compared to the main monomer DEAEMA (0.6, 1.2, and 2.4 mol%M), its contribution was very low in terms of the charge.

## 3.3.2. Effect of the cross-linker type

### 3.3.2.1. Ethylene glycol-based cross-linkers

It is well known that the cross-linker type gives additional possibility to tune the size and swelling properties of nanogels.[14,32,33] Considering this, PDEAEMA-based nanogels differing only in the type of cross-linker used were the subject of this section. For that purpose, EGDMA was substituted by PEGDA for the cross-linking of the polymeric chains forming the nanogels and the influence of the cross-linker type on nanogels properties was investigated.

Even though both cross-linkers (EGDMA and PEGDA) are bifunctional and based on ethylene glycol (EG) units, they have different lengths between the cross-linking points (1 and 9 EG repetitive units in the case of EGDMA and PEGDA, respectively), and they differ in reactive groups (PEGDA contains two acrylate groups while EGDMA contains two methacrylate groups), and hydrophilicity [water solubilities: EGDMA (1 mg/mL)[34] and PEGDA (22 mg/mL)[35]].

#### 3.3.2.1.1. pH- and thermo-sensitivity of nanogels

Figure 3.4 serves to compare the pH-responsive swelling-de-swelling behavior of nanogels PD0.93PM0 and E0.93PM0. As can be seen, the nanoparticles formed did not show pH-sensitive swelling-de-swelling behavior when PEGDA was used as cross-linker.

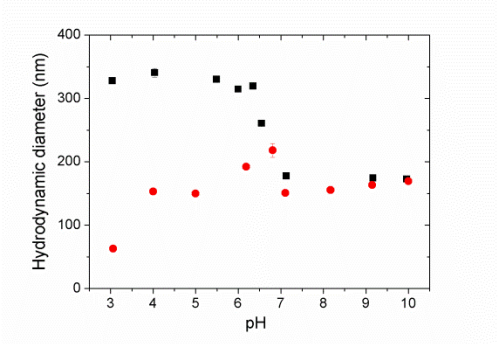


**Figure 3.4.** Hydrodynamic diameters of nanogels E0.93PM0 (■) and PD0.93PM0 (●) as a function of pH at 25 °C at an ionic strength of 10 mM.

It is of paramount importance to take into account not only the reactivity of the main monomer but also the reactivity of the cross-linker used for the synthesis of nanogel particles.[36] To the best of our knowledge, the reactivity ratios of EGDMA and PEGDA with DEAEMA are unknown. However, according to the literature, when copolymerizing monomers containing methacrylate groups with monomers having acrylate ones, the reactivity of these latter is generally lower than the ones having methacrylate groups.[32] The reactivity ratio values of methyl methacrylate with different monomers are shown in Table 3.3.[37]

| **Monomer 1** | **Monomer 2** | $r_{12}$ | $r_{21}$ |
|---|---|---|---|
| Methyl methacrylate | Ethyl methacrylate | 1.16 | 1.00 |
| | Ethyl acrylate | 2.04 | 0.22 |
| | *N*-methyl acrylamide | 1.14 | 0.05 |

**Table 3.3.** Reactivity ratio values of methyl methacrylate and some monomers.

Moreover, PEGDA has much higher water solubility value (22 mg/mL)[35] than DEAEMA (11 mg/mL),[38] implying high incompatibility with DEAEMA and poor incorporation of PEGDA into the PDEAEMA-based nanoparticles. Smith *et al.*[6] reported that the cross-linker (1,2-dihydroxylethylene)bisacrylamide was poorly incorporated in poly(*N*-isopropylacrylamide) (PNIPAM)-based nanogels because of its hydrophilicity. Moreover, Imaz and Forcada studied nanogels based on poly(*N*-vinylcaprolactam) (PVCL) cross-linked with *N,N'*-methyl bisacrylamide and PEGDA. The lower conversion of *N*-vinylcaprolactam (VCL) by using PEGDA as cross-linker was attributed to the incompatibility of PEGDA with the main monomer (VCL) due to the high water solubility of PEGDA.[39] Therefore, due to the incompatibilities between PEGDA and DEAEMA, PDEAEMA polymer chains were not cross-linked.

With the aim of obtaining nanogel particles by using PEGDA as cross-linker, the adding of the stabilizer PEGMA was studied. As can be seen in Figure 3.5a, pH-responsive nanogels cross-linked with PEGDA were formed by adding 10 wt%M of PEGMA (nanogel PD0.93PM10). Owing both methacrylate and EG groups, PEGMA could improve the compatibility between DEAEMA and PEGDA, favoring in this way the formation of cross-linked nanoparticles.

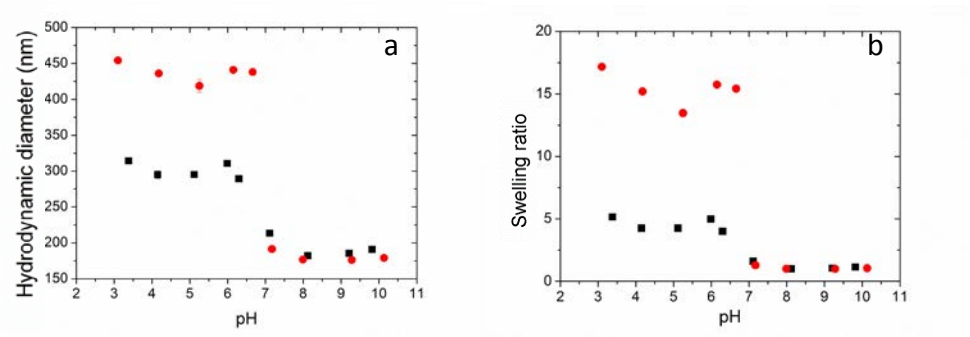


**Figure 3.5.** Hydrodynamic diameters (a) and swelling ratios (b) of nanogels E0.93PM10 (■) and PD0.93PM10 (●), as a function of pH at 25 °C and at an ionic strength of 10 mM.

As in the case of the corresponding nanogel synthesized by using EGDMA as cross-linker (E0.93PM10), nanogel particles underwent a volume phase transition pH (VPTpH) at around pH 6–7: below it, nanogel particles were highly swollen and above it, particles were shrunken reducing their size due to the deprotonation of amine groups of PDEAEMA and the weakened electrostatic repulsion.

Nevertheless, closer attention to Figure 3.5a reveals that the transition sharpness was different depending on the type of cross-linker: nanogels synthesized using PEGDA underwent the transition in a narrower pH range, compared to the ones cross-linked with EGDMA. The difference could be explained in terms of the heterogeneity in microstructure which will be analyzed in section 3.3.2.1.2.

Furthermore, Figure 3.5b reflects the effect of the type of cross-linker on the swelling ratio of the final PDEAEMA-based nanogel particles. Cross-linker-dependent parameters that affect the swelling ratio are (i) the length between the cross-linking points, (ii) the hydrophilicity of the cross-linker, and (iii) the morphology of the nanogel particles.[32,40,41]

Remarkable was the difference between the swelling ratios of the nanogels synthesized: the swelling capability of PD0.93PM10 was much higher than the one of E0.93PM10. Firstly, considering the water solubilities of the cross-linkers, being PEGDA much more water-soluble[35] than EGDMA,[34] it facilitated the access of the water, increasing the swelling ratio. Likewise, PEGDA has a much larger length between the cross-linking points (nine repetitive units of EG) than EGDMA (one repetitive unit of EG), providing higher flexibility, and thus, higher swelling.

Moreover, as can be seen in Figure 3.6, nanogel PD0.93PM10 showed pH-dependent thermo-sensitivity, being swollen at acidic conditions, collapsing at alkaline conditions, and showing pH-dependent thermal response in the pH range of 6-8 due to the formation/disruption of H-bonds between deprotonated amine groups and water molecules. As expected, the lower the pH, the higher the transition temperature was, since the energy needed to disrupt the H-bonds and collapse the nanogel was higher because of the stronger electrostatic interactions.

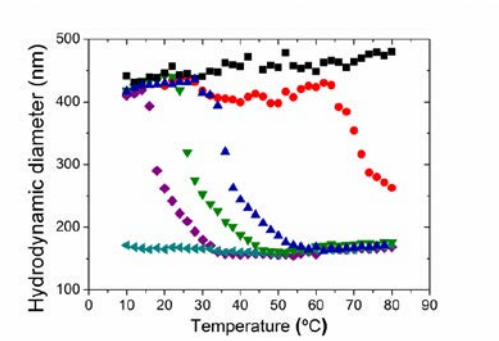


**Figure 3.6.** Hydrodynamic diameters of nanogel PD0.93PM10 as a function of temperature at different pHs at an ionic strength of 10 mM. pH 3.0 (■), pH 6.2 (●), pH 6.6 (▲), pH 6.8 (▼), pH 7.0 (◆), and pH 8.1 (◀).

In order to analyze the effect of the type of cross-linker on the thermal response, a throughout attention should be paid on Figure 3.7, where the variation of the VPTT as a function of pH for the nanogels E0.93PM10 and PD0.93PM10 is shown. Comparing to nanogel PD0.93PM10, nanogel E0.93PM10 was thermo-sensitive at more acidic conditions or related to that, for a given pH, the VPTTs appeared at lower temperatures. To understand this difference, the water solubility of the cross-linkers[34,35] should be taken into account. It is foreseeable that the higher hydrophilicity of PEGDA compared to EGDMA caused an increase in VPTT for a given pH, since higher thermal energy was needed to disrupt H-bonds. Obeso-Vera *et al.*[42] also observed variations in the VPTT of PNIPAM-based nanogels by changing the cross-linker type. According to them, the most water soluble cross-linker imparted hydrophilicity to nanogels, increasing the VPTT. Many authors have remarked the major impact of the cross-linker type on the size and swelling-de-swelling behavior of the nanogels.[39,42]

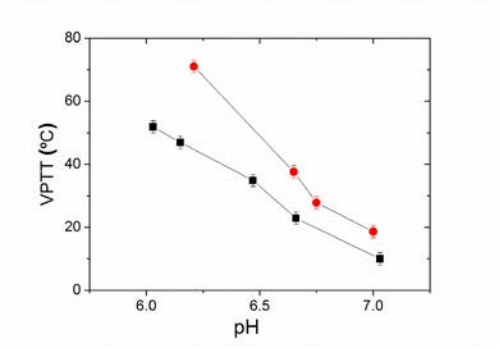


**Figure 3.7.** VPTT values of E0.93PM10 (■) and PD0.93PM10 (●) as a function of pH at an ionic strength of 10 mM.

The effect of the cross-linker type on the colloidal characteristics of all the nanogels synthesized by using different cross-linker types and different concentrations of cross-linker and stabilizer (PEGMA) is summarized in Appendix II. Their pH- and thermo-responsive swelling-de-swelling behaviors are also shown in Appendix II.

Moreover, so as to mimic physiological conditions, those nanogels were also dispersed at an ionic strength of 150 mM in PBS, giving the possibility to study the effect of the ionic strength and type of buffer on their dual stimuli-sensitive swelling-de-swelling behavior. This effect is also described in Appendix II.

#### 3.3.2.1.2. Morphology of nanogels

After an in-depth study of the dual-stimuli-responsive behavior depending on the type of cross-linker, the challenge was the understanding of the inner morphology of the swollen and collapsed nanogel particles varying the type of cross-linker.

The cross-linking density distribution for nanogels prepared by emulsion polymerization was expected to be heterogeneous due to the specificity of the polymerization/cross-linking processes involved, resulting in a core–shell model in which core and shell have different cross-linking degrees.[25,43-45] In the limit of experimental errors, neither the use of PEGMA nor the type of cross-linker used in the syntheses modified the resonances assignment. Thus, the resonance peak R1 at 1.2 ppm (see the $^{1}$H-NMR spectrum of E0.93PM0 in Figure 2.3)

corresponding to methyl protons of PDEAEMA chains was used in the following measurements to investigate the heterogeneity in microstructure, being the least sensitive to noise interference due to its high intensity.

To understand the inner morphology of the nanogels and relate it with the stimuli-responsive swelling-de-swelling behavior, the effect of the temperature on the microstructure was analyzed at different pHs. Firstly, nanogels were dispersed at pH 3 (swollen state at any temperature) and at pH 8 (collapsed state at any temperature). This way, the values of $^1$H transverse relaxation times ($T_{2L}$ and $T_{2S}$) and the relative weight fractions of methyl protons of PDEAEMA ($C_S$ and $C_L$) were obtained for both nanogels. Also the ratio between the cross-linking densities ($CLD^{core}/CLD^{shell}$) was calculated by means of equation 2.4.

Efforts were made for the purpose of optimizing the conditions to carry out $^1$H-NMR transverse relaxation measurements ($T_2$) and ensure the whole relaxation of PDEAEMA protons. The $^1$H-NMR transverse relaxation decay for PDEAEMA-based nanogels at different temperatures was obtained using the conditions described in Chapter 2. However, it was observed that longer echo time was needed at higher temperatures, because the decay was given more slowly (data not shown). This is the reason why acquisitions were taken between 0.54 ms and 16.2 s to obtain the total relaxation in all the temperature range. The best fitting for the integral of the resonance peak was resulted to be a biexponential decay, confirming a core-shell type heterogeneous morphological model, aside from the cross-linker type used. The fittings with two exponentials had $\chi^2$ = 0.0010 and a coefficient of correlation of $R^2$ = 0.99, reflecting that they were quantitative.

Figure 3.8 shows the normalized $T_{2S}$ and $T_{2L}$ values (normalized to $T_2$ values at 25 °C) of the nanogel cross-linked with PEGDA as a function of temperature. The same tendency was observed in the case of the nanogel E0.93PM10. The relaxation time values (both $T_{2S}$ and $T_{2L}$) were increased by increasing the temperature. This was due to the decrease in water viscosity[46] that made the movement of PDEAEMA chains in the medium easier.[47] Considering that the effect of the temperature (given by the decrease in water viscosity) on both $T_2$ values was identical, the ratio $T_{2L}/T_{2S}$ was not affected by the variations in water viscosity.

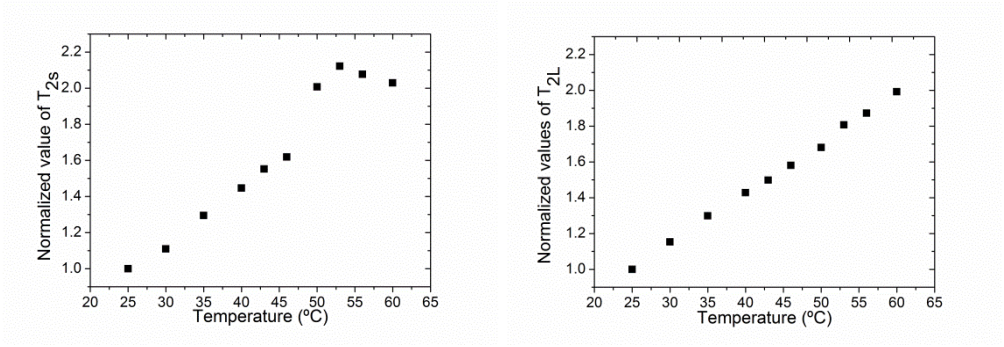


**Figure 3.8.** Temperature dependence of the normalized short ($T_{2S}$, left) and long ($T_{2L}$, right) relaxation times for the collapsed nanogel PD0.93PM10.

The cross-linking density ratios ($CLD^{core}/CLD^{shell}$) of swollen and collapsed nanogel particles were calculated using the values of $T_{2S}$ and $T_{2L}$ (equation 2.4). This ratio provides information about the morphological heterogeneity in nanogel particles, that is, the difference of cross-linking densities between core and shell. In this sense, nanogel particles with the most heterogeneous morphology would have the highest $CLD^{core}/CLD^{shell}$ value.

For the sake of comparison, Figure 3.9 shows the temperature dependence of the cross-linking density ratios for nanogels E0.93PM10 and PD0.93PM10. Irrespective of the cross-linker type used, nanogels showed some similarities. They had a heterogeneous morphology, confirming the faster reaction rate of the cross-linker compared to that of the main monomer.[1] In addition, the ratio between the cross-linking densities of swollen nanogel particles was higher comparing to that of the collapsed nanogel particles. This was due to the fact that PDEAEMA chains were extended in swollen nanogel particles (higher $T_{2L}$ values), making the difference in apparent cross-linking degrees between core and shell more pronounced.

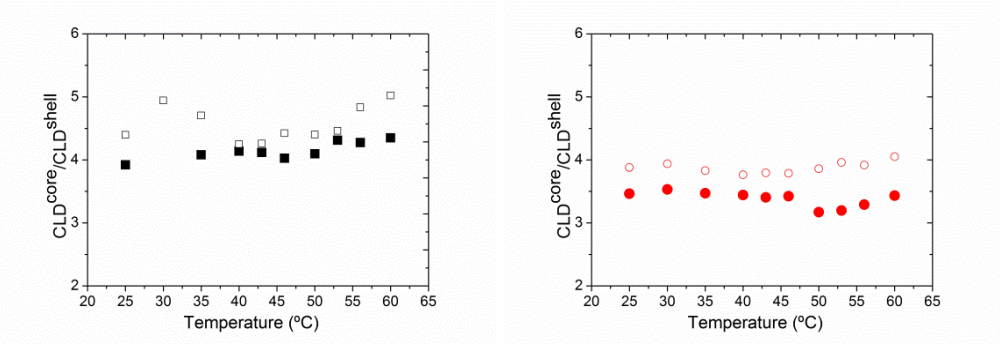


**Figure 3.9.** Temperature dependence of the cross-linking density ($CLD^{core}/CLD^{shell}$) of nanogels E0.93PM10 (■ collapsed, at pH 8 and □ swollen, at pH 3) and PD0.93PM10 (● collapsed, at pH 8 and ○ swollen, at pH 3).

However, the comparison between both nanogels suggests that the cross-linking density ratio was lower in the case of PD0.93PM10 than in the case of E0.93PM10. This result can be understood taking into account that methacrylate and acrylate groups have different reactivities when copolymerizing with methacrylates, in this case, DEAEMA, as explained before (see Table 3.3).[32,37] Containing methacrylate groups, EGDMA is more reactive than PEGDA when copolymerizing with methacrylates leading to a nanogel with a more heterogeneous morphology. These results are in agreement with the ones reported by Lally *et al.*[32] They suggested a more heterogeneous cross-linking points' distribution within the particles when reactivity ratios of cross-linker and monomer were similar. Acciaro *et al.*[40] reported that the comonomer distributions varied significantly depending on their reactivity ratios, affecting the heterogeneity in inner structure and thus, nanogel swelling properties.

Additionally, the different heterogeneities in morphology of nanogels could be related with their swelling capabilities. The comparison between the results shown in Figures 3.5b and 3.9 indicates that nanogels with the highest heterogeneity of the inner structure showed the lowest swelling ratio and the broadest pH-transition. The lower swelling arose from the restricted movement of PDEAEMA chains due to the more heterogeneous distribution of the cross-linking points (covalent bonds between PDEAEMA chains and cross-linker chains). Acciaro *et al.*[40] also reported that nanogels with more homogeneous inner structure and more uniform cross-linking points' distribution showed larger swelling. On the other hand, the starting hypothesis was corroborated, confirming that the heterogeneity in morphology made the

transition broader, since different parts of a gel with heterogeneous inner structure underwent the phase transition at different temperatures.

Taking these results into account and for the sake of a visual representation, schematic representations of the different cross-linking density distributions together with the corresponding average hydrodynamic diameters at the swollen state are shown in Figure 3.10. The most homogeneous distribution of cross-linking points between core and shell is represented in the case of PD0.93PM10.

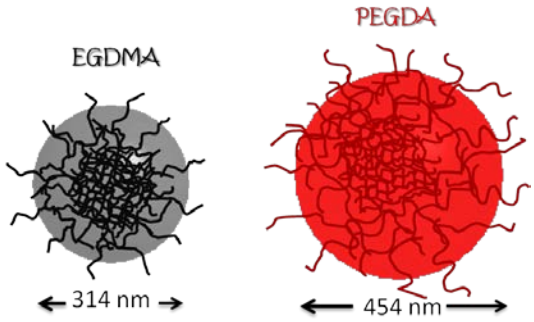


**Figure 3.10.** Schematic representations of the different cross-linking density distributions (morphologies) within nanogel particles together with the corresponding average hydrodynamic diameters at the swollen state. E0.93PM10 (left) and PD0.93PM10 (right).

Another piece of information regarding the inner morphology of these PDEAEMA-based nanogel particles could be the relative weight coefficients of PDEAEMA chains in core ($C_S$) and shell ($C_L$), describing the bimodal heterogeneity of the polymer network in the nanogel. Table 3.4 shows the values of $C_S$ and $C_L$ of collapsed and swollen nanogels (E0.93PM10 and PD0.93PM10) at 25°C.

| NANOGEL | COLLAPSED | | SWOLLEN | |
|---|---|---|---|---|
| | $C_S$ | $C_L$ | $C_S$ | $C_L$ |
| **E0.93PM10** | 0.58 | 0.41 | 0.58 | 0.47 |
| **PD0.93PM10** | 0.55 | 0.46 | 0.53 | 0.47 |

**Table 3.4.** Relative weight coefficients of PDEAEMA chains in the core ($C_S$) and shell ($C_L$) of collapsed (pH 8) and swollen (pH 3) nanogels E0.93PM10 and PD0.93PM10 at 25 °C.

It can be confirmed that regardless of the cross-linker used, the relative weight coefficients of PDEAEMA in core and shell were approximately 0.55 and 0.45, respectively. The fact that the PDEAEMA chains were distributed in a similar way aside from the cross-linker used could be understood by taking the polymerization kinetics into account. The consumption rate of DEAEMA was not affected by the cross-linker type resulting in the same distribution of PDEAEMA chains inside the nanogel. Thus, although the cross-linking points' distribution in nanogel particles and the inner morphology were different, 55 wt% of PDEAEMA chains was located in the core and the rest in the shell. In this manner, it was demonstrated that the type of cross-linker did not affect the polymerization kinetics of the main monomer and neither the PDEAEMA chains distribution, at least at the studied concentration of cross-linkers.

In addition, it is foreseeable that the distribution of PDEAEMA chains will not be affected neither by the pH nor by temperature due to the impossibility for the PDEAEMA chains to migrate from core to shell, or vice versa. This was confirmed by calculating the relative weight coefficients of PDEAEMA chains at different pHs (see Table 3.4). Furthermore, it was also observed that the temperature did not affect these values (data not shown).

Briefly, $C_S$ and $C_L$ were related with the polymerization kinetics of DEAEMA, obtaining the same values regardless of the cross-linker type used. Nevertheless, the $CLD^{core}/CLD^{shell}$ ratio was influenced by the properties of the cross-linkers: water solubilities and different reactivities when copolymerizing with DEAEMA.

Moreover, the ratio of the number of PDEAEMA subchains (chains between two cross-linking points) in core and shell ($N^{core}/N^{shell}$, equation 3.1) was subsequently calculated, being 5.36 and 4.35 for the nanogels E0.93PM10 and PD0.93PM10, respectively. It was noticeable the difference between the amount of PDEAEMA subchains in core and in shell, confirming the heterogeneous cross-linking points distribution, in both cases. This fact could be understood in terms of the higher reactivity of the cross-linker with respect to that of the main monomer,[14,43] leading to a higher amount of cross-linking points and thereby PDEAEMA subchains in the core comparing to the shell.

Nevertheless, PD0.93PM10 had a lower $N^{core}/N^{shell}$ ratio value than E0.93PM10. This could be elucidated in reference to the ratio between the cross-linking densities ($CLD^{core}/CLD^{shell}$) (see Figure 3.9), considering that $C_S$ and $C_L$ did not vary. As expected, the higher the cross-linking density ratio, the higher the difference between the amounts of PDEAEMA subchains in core and shell was, increasing the $N^{core}/N^{shell}$ ratio.

These results underlined the high impact of the cross-linker type on the morphology and therefore, on the swelling properties of nanogel particles.

*The content of this section was published in the Journal of Polymer Science, Part A: Polymer Chemistry, **2015**, 53, 2017-2025.*

### 3.3.2.2. Disulfide-based cross-linkers

It is noteworthy that redox degradable nanogel particles have appeared to be highly advantageous and promising for bio-applications.[48-51] One of the main strategies to prepare redox-sensitive nanogel particles is the incorporation of disulfide bonds in the cross-linker.[52] The use of cross-linkers containing disulfide bonds was envisioned as a potentially useful approach, since disulfide linkages would enable degradation of nanogel particles in a triggered fashion.[15,53] Owing to these advantages, this section is focused on the synthesis and characterization of nanogels cross-linked with disulfide-based cross-linkers.

At a first stage, some preliminary studies were carried out in order to optimize the reaction conditions. The synthesis procedure used for the nanogels E0.93PM10 and PD0.93PM10 was taken as reference, but replacing EGDMA and PEGDA by the disulfide-based cross-linker BAC [bis(acryloyl)cystamine]. For the sake of comparison, being all bifunctional, the same molar concentration of cross-linker was used so as to have the same number of cross-linking points.

Figures 3.11 and 3.12 show the hydrodynamic diameters of nanogels BAC0.93PM0, BAC0.93PM10, and BAC0.93PM20 as a function of pH. The corresponding nanogels synthesized by using EGDMA and PEGDA as cross-linkers are also plotted for the sake of comparison.

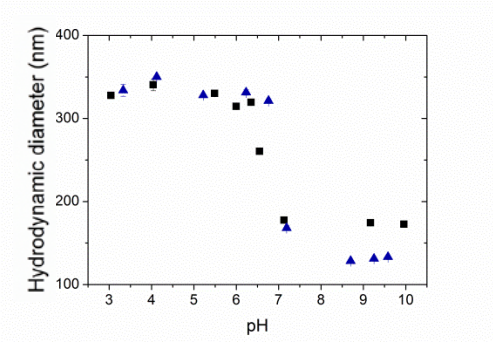


**Figure 3.11.** Hydrodynamic diameters of nanogels E0.93PM0 (■) and BAC0.93PM0 (▲) as a function of pH at an ionic strength of 10 mM.

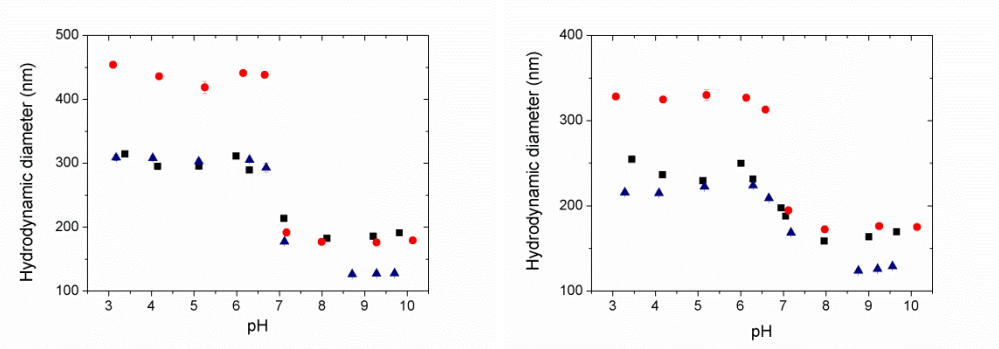


**Figure 3.12.** Hydrodynamic diameters of nanogels E0.93PM10 (■), PD0.93PM10 (●), and BAC0.93PM10 (▲) (left) and E0.93PM20 (■), PD0.93PM20 (●), and BAC0.93PM20 (▲) (right) as a function of pH at an ionic strength of 10 mM.

After confirming the swelling capability of nanogels cross-linked with BAC in response to pH variations, it is interesting to remark the role of the cross-linker type on the pH-responsive swelling-de-swelling behavior of the nanogels.

It could be seen that regardless of the amount of PEGMA used, smaller particle diameters at the collapsed state were obtained by using BAC as cross-linker than in the case of using EGDMA and PEGDA. The reason of this could be found in polymerization kinetics. The conversions in the syntheses of nanogels cross-linked with BAC were calculated gravimetrically, and a final conversion of 60 % was obtained, approximately. So, the

considerable decrease in the final conversion from 80 to 60 % led to smaller nanogel particle sizes (data not shown).[39,54]

This low conversion could be explained taking into account that disulfide bond may be disrupted by numerous side reactions at high temperatures (see Figure 3.13). On the one hand, it can be homolytically cleaved, resulting in sulfur radical formation during the synthesis (Figure 3.13a). Moreover, it may enable a chain-transfer reaction, wherein radical attack at the disulfide bond leads to the formation of a thioether, with a sulfur radical released as a result (Figure 3.13b). In addition, any conversion of the disulfide to thiol during synthesis would promote a Michael addition between the thiol and the vinyl groups of the monomers, again generating a thioether (Figure 3.13c).[15,53,55] All of these possible side reactions would lead to stop the polymerization of growing oligomer chains, decreasing the conversion of the monomer.

It is remarkable that unlike the case of using PEGDA (Figure 3.4), PDEAEMA chains were cross-linked enough and nanogels with a typical stimuli-responsive swelling-de-swelling behavior were formed by using BAC as cross-linker and without the use of PEGMA (see Figure 3.11). As can be seen in Table 3.3, monomers with acrylamide groups (BAC) have similar reactivity as acrylate groups (PEGDA) when copolymerizing with monomers containing methacrylate groups (such as DEAEMA). Considering this, due to the low reactivity with the main monomer, one could not expect that the compatibility of BAC with DEAEMA would be good enough to obtain cross-linked polymeric chains and form nanogels. However, in the case of using BAC as cross-linker, the abovementioned side-reactions of the disulfide groups favoured the cross-linking of polymeric chains, forming a cross-linked inner structure. Gaulding *et al.*[53] synthesized poly(*N*-isopropylmethacrylamide)-based microgels cross-linked with BAC and reported that in the case of using a thermal initiator system, nanogels exhibited a higher apparent cross-linking density as a result of the chain transfer reactions related to the disulfide bonds. In short, the side reactions of disulfide groups are found to be the responsible for cross-linking the PDEAEMA-based chains and obtaining nanogels with a typical swelling-de-swelling behavior in response to pH variations.

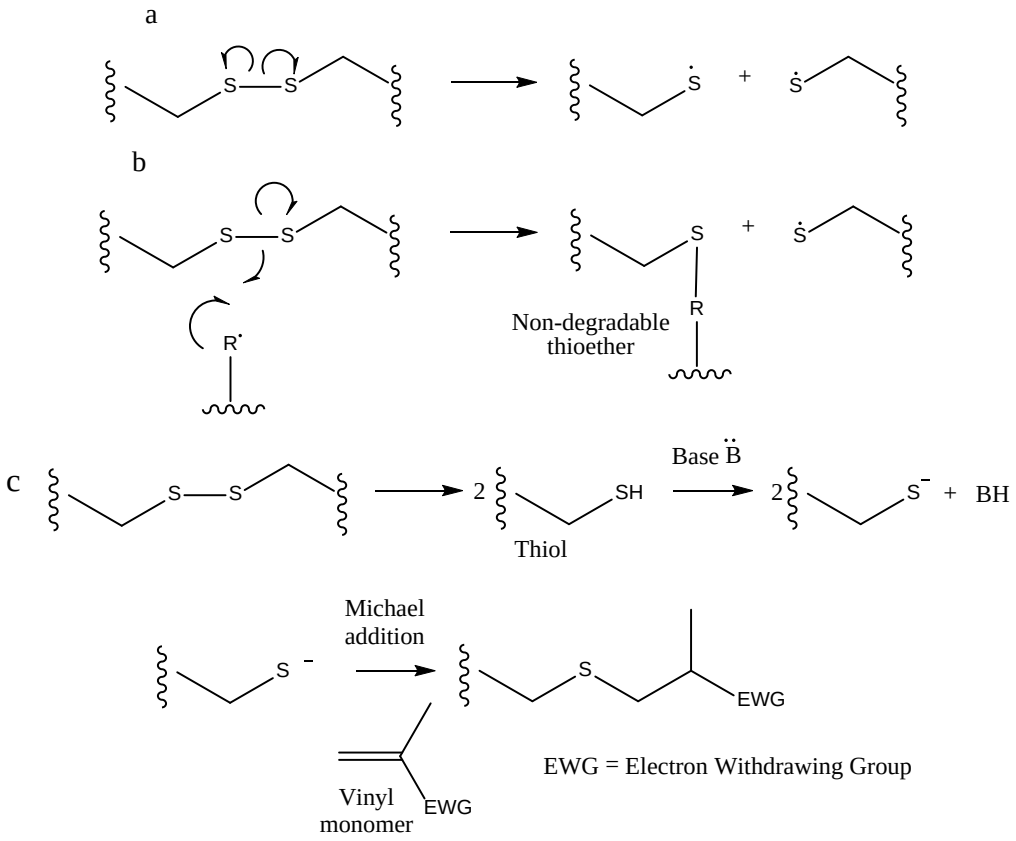


**Figure 3.13.** Reaction mechanisms of potential side reactions of a disulfide bond.

To attempt to avoid the possible side reactions of the disulfide bond and increase the conversion, a redox initiator system was used, as an alternative for the thermal initiator ADIBA. Redox systems are characterized by having a relatively low energy activation (10-20 Kcal/mol), as compared to the thermal initiation (30 Kcal/mol). This enable the polymerization to be carried out at lower temperatures, thereby decreasing the possibility of side reactions which change the reaction kinetics and the properties of the resulting colloidal particles.[56,57]

For this reason, as explained in the experimental part, the syntheses were carried out by using KPS and TEMED as a redox initiator pair at 50 °C (see Table 3.2) and the conversion increased considerably, since a value of 80 % was obtained. It has to be remarked that

PDEAEMA chains at pH 9-10 (reaction conditions) are hydrophobic regardless of the temperature, confirming the adequacy of the reaction temperature used for the syntheses, since polymeric chains must be hydrophobic enough in order to precipitate and form stable particles.[23] The reaction mechanism for the redox system KPS/TEMED is illustrated in Figure 3.14. TEMED is activated by KPS and it is able to react with monomers from the unpaired valence electron, accelerating the rate of formation of free radicals from KPS.

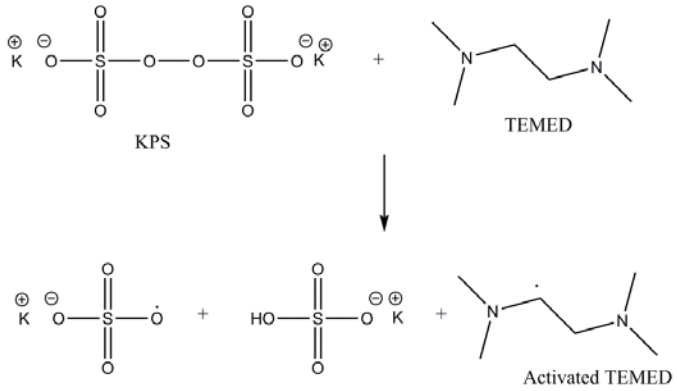


**Figure 3.14.** Reaction mechanism between KPS and TEMED (redox initiator pair used).

However, with the aim of minimizing the interactions between TEMED and BAC, some considerations had to be followed in the synthesis methodology, as reported by Gaulding *et al*.[53] TEMED was firstly added following by an excess of KPS with respect to TEMED and BAC was added immediately after the addition of KPS. Taking into account that BAC is scarcely soluble in water, it was dispersed in a certain amount of DEAEMA so as to add it to the reactor.

Figure 3.15 shows the pH-responsive swelling-de-swelling behaviors of the nanogels cross-linked with BAC and synthesized by using a redox initiator system and different PEGMA concentrations. These results inferred that in the absence of the stabilizer PEGMA the nanoparticles formed did not show a pH-sensitive swelling-de-swelling behavior, while pH-responsive nanogels were obtained when some stabilizer was added to the mixture. The use of PEGMA to obtain nanogel particles was also compulsory in the case of using PEGDA as cross-linker. As in that case, the result could be understood in terms of the low reactivity of the cross-linker BAC with DEAEMA.

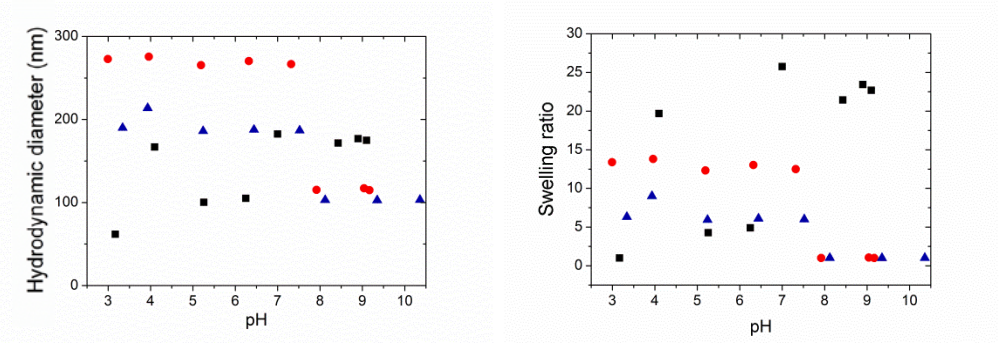


**Figure 3.15**. Hydrodynamic diameters (left) and swelling ratios (right) of nanogels RBAC0.93PM0 (■), RBAC0.93PM10 (●), and RBAC0.93PM20 (▲) as a function of pH at an ionic strength of 150 mM in PBS.

Nevertheless, it is interesting to point out the effect of the initiator system on the final properties of the nanogel particles obtained. Actually, in the case of using a thermal initiator, the side-reactions of disulfide groups helped the cross-linking of polymer chains and nanogels were formed even without PEGMA stabilizer (see Figure 3.11). However, in the case of RBAC0.93PM0, lower temperatures were used, minimizing the transfer reactions of disulfide groups to a considerable extent. Thereby, the cross-linking degree was also decreased and the polymeric chains were not cross-linked. These results confirmed the role of the side reactions on the cross-linking of the nanogel particles, when using a thermal initiator system and BAC as cross-linker.

The PDEAEMA-based nanogels synthesized containing disulfide linkages also showed pH-dependent temperature-responsive swelling-de-swelling behavior, as presented in Figure 3.16. There is no distinct difference in pH-dependency of the thermal behavior from the other PDEAEMA-based nanogels studied above.

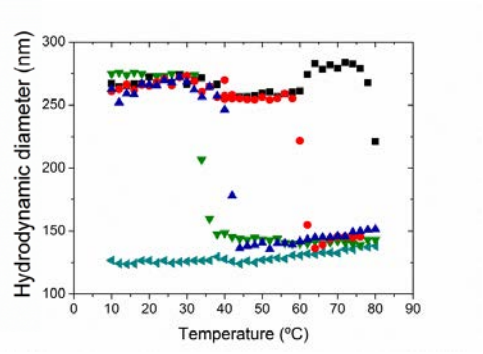


**Figure 3.16.** Hydrodynamic diameters of nanogel RBAC0.93PM10 as a function of temperature at different pHs at an ionic strength of 150 mM in PBS. pH 6.2 (■), pH 6.6 (●), pH 7.1 (▲), pH 7.4 (▼), and pH 7.8 (◄).

The pH-dependence of hydrodynamic diameters and swelling ratios of all the nanogels synthesized by using BAC as cross-linker and a redox initiator system, are shown in Appendix II.

Considering that the type of cross-linker greatly affects the swelling characteristics of nanogels,[58] another family of nanogels was synthesized by using a cross-linker with disulfide linkages but containing methacrylate groups as reactive groups: DSDMA [bis(2-methacryloyl)oxyethyl disulfide]. The same synthesis procedure as in the case of nanogels RBAC0.93PM0/10 was followed, but BAC was replaced by DSDMA. Figure 3.17 shows the pH-responsive swelling-de-swelling behavior of nanogels RDM0.93PM0 and RDM0.93PM10.

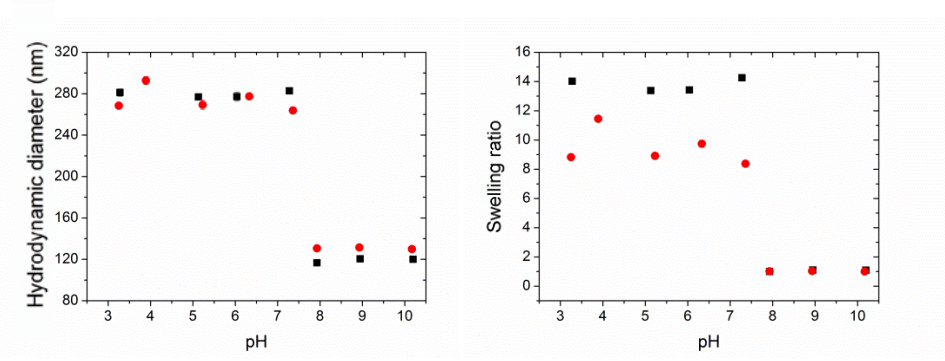


**Figure 3.17.** Hydrodynamic diameters (left) and swelling ratios (right) of nanogels RDM0.93PM0 (■), and RDM0.93PM10 (●) as a function of pH at an ionic strength of 150 mM in PBS.

It is interesting to note that the use of PEGMA was not compulsory to obtain cross-linked nanoparticles when DSDMA was used as cross-linker, remarking the role of the cross-linker type on the formation of nanogels. Considering that DSDMA contains methacrylate groups, it was expected that it would react faster than acrylamide and acrylate groups, obtaining enough cross-linking degree to form cross-linked polymeric nanoparticles (see Table 3.3).

In short, comparing all the cross-linker types used, due to the incompatibilities between the cross-linker and the main monomer, BAC and PEGDA were not able to obtain enough cross-linking degree to obtain nanogels without using any PEGMA (nanogels PD0.93PM0 and RBAC0.93PM0). By contrast, the cross-linkers EGDMA and DSDMA were able to form nanogel particles, being more compatible with the main monomer (nanogels E0.93PM0 and RDM0.93PM0).

Apart from the abovementioned difference between nanogels synthesized by using different cross-linker type (BAC and DSDMA) in the absence of PEGMA, it is appealing to study the differences between them when PEGMA was added as stabilizer to the recipe. For the sake of comparison, pH-responsive swelling-de-swelling behaviors of nanogels RBAC0.93PM10 and RDM0.93PM10 are plotted in Figure 3.18. It is foreseeable that the pH-responsive swelling-de-swelling behavior was similar in both cases, as the transition was given at pH 7.5 and nanogels with the same size were obtained.

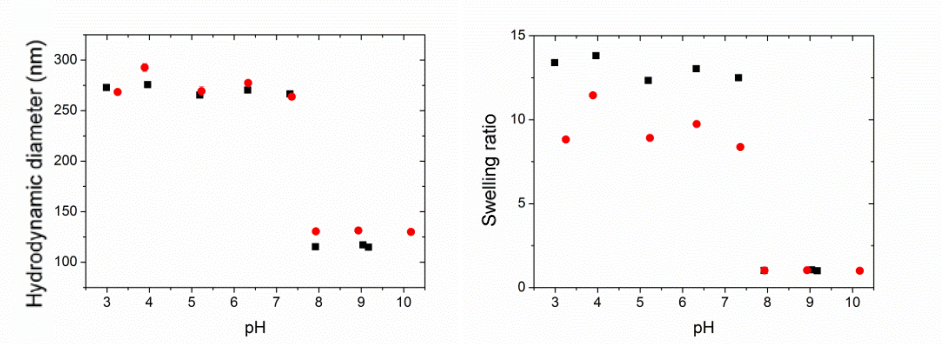


**Figure 3.18.** Hydrodynamic diameters (left) and swelling ratios (right) of nanogels RBAC0.93PM10 (■) and RDM0.93PM10 (●) as a function of pH at an ionic strength of 150 mM in PBS.

However, a small difference could be distinguished in terms of the swelling ratio, since nanogels cross-linked with DSDMA showed lower swelling ratios compared to the ones cross-linked with BAC. As explained before, the difference in swelling capability could arise from three different factors: hydrophilicity of cross-linkers, the length between the two cross-linking points, and the morphology of nanogels. In this case, taking into account that neither the difference in length between the reactive groups nor the difference in water solubility of cross-linkers (1.2 and 4.4 mg/mL for DSDMA and BAC, respectively)[38] was considerable, the differences in swelling ratio may be caused by the different inner structure of nanogel particles. As monomers containing methacrylate groups are more reactive than the ones with acrylamide groups when copolymerizing with monomers with methacrylate groups, nanogels cross-linked with DSDMA would have a more heterogeneous microstructure than the ones cross-linked with BAC. Considering the relation obtained by studying the swelling-de-swelling behavior and morphology of nanogels synthesized by using EG-based cross-linkers, lower swelling ratio would be expected in the case of using DSDMA. In the case of disulfide-based cross-linkers, the difference is swelling capability was not as high as in the case of EG-based cross-linkers, since the cross-linkers did not differ very much in both the solubility and the length between the cross-linking points.

## 3.3.3. Effect of the cross-linker concentration

### 3.3.3.1. Ethylene glycol-based cross-linkers

Different families of nanogels were synthesized by using different cross-linker concentrations, giving the possibility to understand the influence of the amount of the cross-linker used on the pH- and thermo-sensitive swelling-de-swelling behavior of nanogels.

In Figure 3.19 the pH-sensitive swelling-de-swelling behavior of nanogels containing 20 wt%M of PEGMA and cross-linked with PEGDA at different concentrations (PD0.33PM20 and PD0.93PM20) were compared. The VPTpH (6.8 ± 0.1), the hydrodynamic diameter of collapsed nanoparticles and the sharpness of the transition were found to be independent of the cross-linker concentration. Imaz and Forcada[35] also reported that the cross-linker concentration did not affect the final collapsed average diameters of nanogels based on PVCL synthesized by using PEGDA as cross-linker.

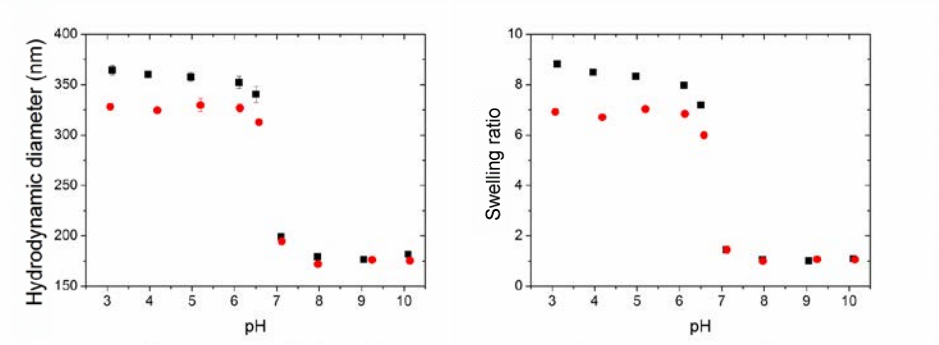


**Figure 3.19.** Hydrodynamic diameters and swelling ratios of nanogels PD0.33PM20 (■) and PD0.93PM20 (●) as a function of pH at an ionic strength of 10 mM.

However, from the decrease in swelling ratio it is foreseeable that an increase in cross-linker concentration hindered the swelling. This result was the expected one, since it is well known that the swelling ratio of nanogels becomes smaller for highly cross-linked nanogels. Other authors reported the same effect in PNIPAM-based,[42,47,59-63] PVCL-based nanogels,[35,64] and carboxymethyl starch-based nanogels.[65]

Furthermore, on the basis of the relation between the swelling-de-swelling behavior and morphology of the nanogels studied comparing different cross-linker types, the inner structure of nanogels cross-linked with a higher cross-linker concentration was expected to be more heterogeneous, showing a lower swelling ratio. This fact would be in agreement with the conclusion reported by Varga *et al.*:[66] an increase in the amount of cross-linker added to the reaction mixture, led to a non-uniform segment density distribution. Schneider *et al.*[14] and Kratz *et al.*[63] also concluded that an increase in the amount of cross-linker caused particles with more heterogeneous morphology.

Moreover, the pH-dependent thermo-sensitivity resulted to be independent of the cross-linker concentration, as can be observed in Figure 3.20 where nanogels PD0.33PM10 (■) and PD0.93PM10 (●) were compared. This result was the expected one, since the difference in cross-linker amount was very low. Other authors also observed that the transition temperature was not affected by the cross-linker concentration at such low cross-linker concentrations.[42,60,67] Imaz and Forcada[35] reported that VPTT values of PVCL-based nanogels

were irrespective of the cross-linker concentration for values lower than about 5 wt%M, but varied at higher concentrations.

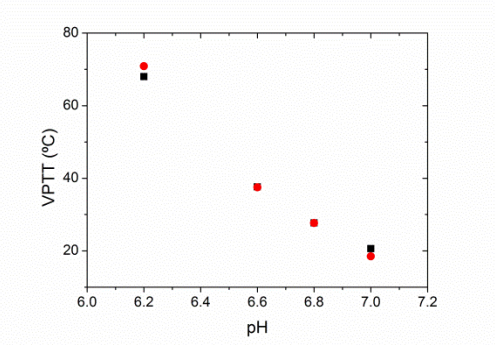


**Figure 3.20.** VPTT values of nanogels PD0.33PM10 (■) and PD0.93PM10 (●) as a function of pH at an ionic strength of 10 mM.

The effect of the cross-linker concentration on stimuli-sensitive swelling-de-swelling behavior of the nanogels is summarized in Appendix II. Interestingly, the effects were found to be very similar regardless of the cross-linker type (EG- and disulfide-based cross-linkers) and PEGMA concentration.

### 3.3.3.2. Disulfide-based cross-linkers

With the aim of increasing the amount of disulfide linkages for future possible degradation of nanogels, new nanogels were synthesized by using 3.2 and 6.3 mol%M of cross-linker DSDMA (see Table 3.2). In Figure 3.21 the pH-dependent swelling-de-swelling behaviors of nanogels RDM0.93PM10, RDM3.2PM10, and RDM6.3PM10 are plotted.

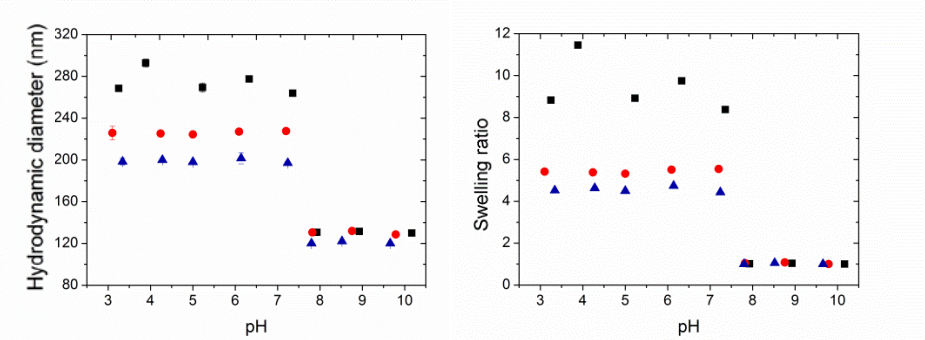


**Figure 3.21.** Hydrodynamic diameters (left) and swelling ratios (right) of nanogels RDM0.93PM10 (■), RDM3.2PM10 (●), and RDM6.3PM10 (▲) as a function of pH at an ionic strength of 150 mM in PBS.

As expected, the increase in cross-linker concentration did not affect the final particle diameter, but the swelling ratio decreased. Füllbrandt *et al.*[60] also reported that the cross-linking degree affected the swelling capability, but the size of collapsed nanogel particle did not show a systematic dependence of the cross-linker concentration comparing to the particle sizes in the swollen state. Additionally, the values of the swelling ratio at pH 3 were calculated and plotted in Figure 3.22 as a function of the amount of DSDMA. It could be seen that the swelling was hindered increasing the amount of cross-linker used but this dependence seemed to decrease exponentially, since at higher concentrations, the swelling-de-swelling behavior was less affected by the cross-linker concentration. These results are in accordance with those obtained in literature.[60,67] Ghugare *et al.*[68] observed the same tendency in dextran-based nanogels: increasing the degree of methacryloyl substitution on dextran chains and thereby the cross-linking degree, the swelling ratio decreased exponentially.

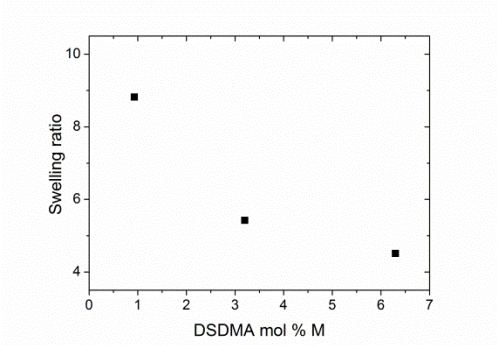


**Figure 3.22.** Swelling ratios of nanogels at pH 3 at an ionic strength of 150 mM in PBS, as a function of DSDMA concentration (mol%M) by using 10 wt%M of PEGMA. Nanogels RDMZPM10 (see Table 3.2).

## 3.3.4. Functionalization of nanogels

In the design of multifunctional nanocarriers, the presence of reactive functional groups, such as polyethylene glycol (PEG), primary amine and epoxide groups are highly desirable for targeted and environmental responsive drug delivery. In general, surface functionalization of nanoparticles plays a critical role to provide novel properties such as further bioconjugation, dimensional control, and biodegradability.[2,69-71] In the present section, the syntheses and characterizations of PEGylated and epoxide- and primary amine-functionalized nanogels are reported.

### 3.3.4.1. PEGylation of nanogels

For the *in vivo* deployment, nanogels are typically protected from the immune system by PEG. PEGylated nanoparticles can escape recognition by immune system responses, such as those of the reticuloendothelial system, resulting in long blood circulation times and preferential accumulation in tumor tissues through the enhanced permeability and retention effect. Moreover, aggregation decreases owing to the increased solubility in buffer and serum of passivated surfaces due to the hydrophilicity of PEG.[18,19,72-75]

In this work PEGMA was used for the PEGylation of the nanogel particles. The terminal end group of this PEG-based compound is an unsaturated reactive polymerizable group, which allows the PEG chains to be covalently incorporated onto the surface of the polymer particles

by copolymerization with the main monomer. Also, PEGMA chains could enhance the colloidal stability of nanogel particles due to the provided steric stabilization and hydrophilicity.

In order to analyze the role of the PEGylation on the pH-response of nanogel particles, their colloidal characteristics were studied at different pHs and at 25 °C. In Figure 3.23, hydrodynamic diameters, swelling ratios, and electrophoretic mobilities of the nanogels E0.93PM0, E0.93PM10, and E0.93PM20 are plotted as a function of pH.

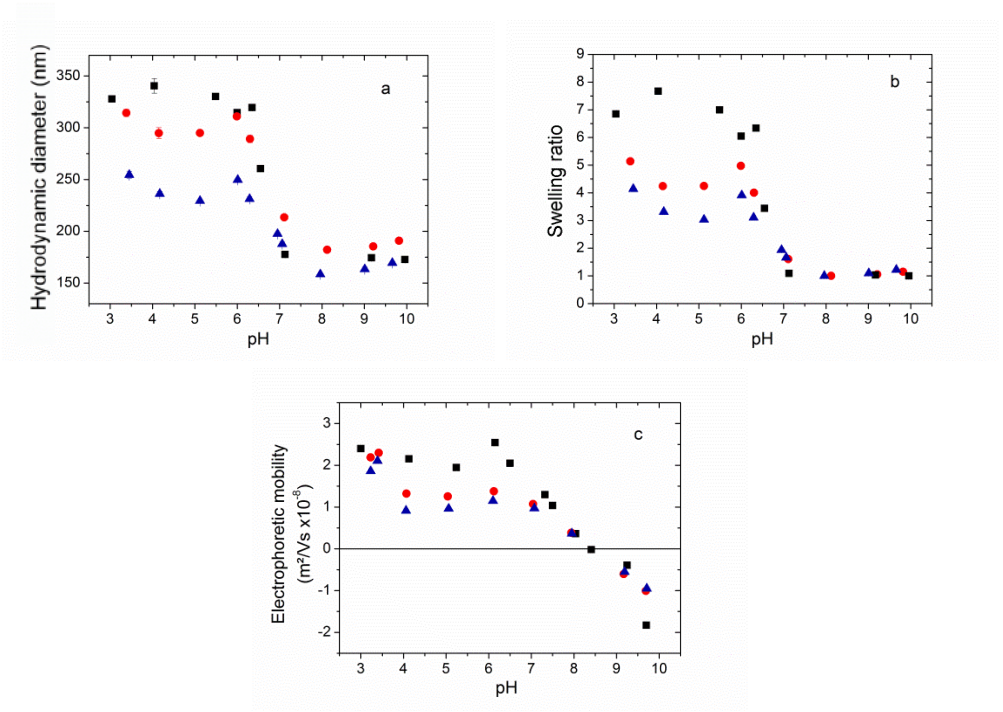


**Figure 3.23.** Hydrodynamic diameters (a), swelling ratios (b), and electrophoretic mobilities (c) of nanogel particles as a function of pH at an ionic strength of 10 mM.
E0.93PM0 (■), E0.93PM10 (●), and E0.93PM20 (▲).

As can be seen, the behavior in response to pH was similar to that of other PDEAEMA-based nanogels reported in previous works.[76-78] As expected, they were highly swollen at acidic pH values due to the electrostatic repulsions between the strongly charged cationic polymeric chains, while they experienced collapse at alkaline conditions, due to the neutralization of the cationic groups. All of them underwent a volume phase transition at around

pH 6-7 (VPTpH). This fact was confirmed by the electrophoretic mobility results shown in Figure 3.23c.

Nevertheless, the PEGylation affected colloidal characteristics. It is noticeable that the addition of PEGMA resulted in lower hydrodynamic diameters of swollen particles and thereby lower swelling ratios. Similar results were reported by Hayashi *et al.,*[78] Serrano-Medina *et al.*,[79] and Beamish *et al.*[80] for nanoparticles stabilized by PEG-based stabilizers. This effect was explained considering that the presence of a PEG-based compound enhanced the network cross-linking *via* the formation of entanglements, which were fixed by extended cross-linking nodes in the networks. These entanglements hindered the movement of PDEAEMA chains, making more difficult the swelling of the nanogel particles. Zhou *et al.*[81] and Fraser *et al.*[82] also reported a decrease in swelling ratio of PEG-based nanogels because of the PEGylation. They attributed to the higher cross-linking density and more heterogeneous structure of the nanogels. Moreover, the transition became broader in the presence of PEGMA chains probably due to the increase in heterogeneity, which was also observed by Zhou *et al.*[81] when analyzing the morphology of PEG-chitosan-based nanogels.

The presence of PEGMA provoked a decrease in electrophoretic mobility values at acidic conditions, due to the shielding of the surface charge originating from cationic groups of the polymer chains. Other authors also observed the charge shielding given by PEG chains in copolymer blocks or nanogels.[13,76,78,83] Moreover, closer attention to Figure 3.23 suggests that the presence of PEGMA provoked an effective shielding of the hydroxide ions at basic pH values, decreasing the absolute electrophoretic mobility values. Thus, PEG chains acted like a molecular brush preventing the adsorption of free hydroxide ions of the buffers onto the polymer surface, as reported by Marek *et al.*[76]

Even all the nanogels underwent a transition at around pH 6-7, the addition of PEGMA chains provoked a shift in VPTpH from 6.5 (E0.93PM0) to 6.9 (E0.93PM10 and E0.93PM20). This result reveals that PEGMA chains hindered the deprotonation of cationic charged groups, making the collapse of nanogel particles more difficult. This fact can be also seen in the electrophoretic mobility values since the decrease in electrophoretic mobility started at more basic conditions in nanogels containing PEGMA chains. At this point it is important to remark that lower electrophoretic mobility values do not mean lower charge density, since the electrophoretic mobility is only affected by the groups located in the outer part.[84] The addition of PEGMA provoked the screening of some positively charged amine groups of polymeric

chains located at the surface of the nanogel particles, while retaining charged groups in the interior.[13] Considering the charge screening, the increase in VPTpH on PEGylating the nanogels could be related to the hindered deprotonation.

It is noticeable that even though nanogels were PEGylated, they showed thermo-sensitivity, increasing their interest for bio-applications. The temperature-dependence of the hydrodynamic diameters at different pHs for nanogels E0.93PM10 and E0.93PM20 are shown in Figures 3.24 and 3.25, respectively. The thermo-sensitivity was pH-dependent as in the case of nanogel E0.93PM0 (see Figure 2.11): nanogel particles were swollen at acidic pH, collapsed at basic conditions and showed thermo-sensitivity in the pH range of pH 6-8. As explained before, the thermal response arose from the possibility of polymeric chains to form H-bonds with water molecules in the pH range of pH 6-8 and the decrease in size increasing the temperature was observed due to the weakening of the H-bonds.

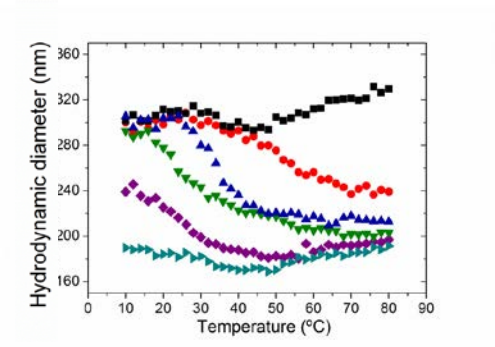


**Figure 3.24.** Hydrodynamic diameters of nanogel E0.93PM10 as a function of temperature at different pHs and in a cationic buffered medium with an ionic strength of 10 mM.

pH 5.2 (■), pH 6.3 (●), pH 6.5 (▲), pH 6.7 (▼), pH 7.1 (◆), and pH 7.9 (►).

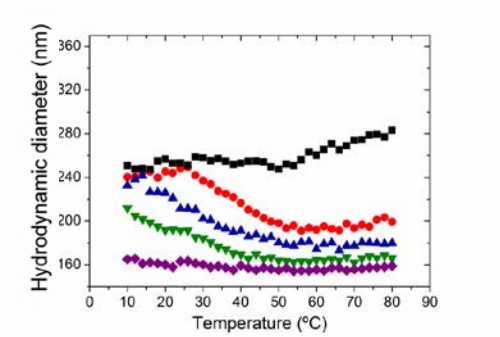


**Figure 3.25.** Hydrodynamic diameters of nanogel E0.93PM20 as a function of temperature at different pHs and in a cationic buffered medium with an ionic strength of 10 mM.

pH 5.2 (■), pH 6.2 (●), pH 6.6 (▲), pH 7.6 (▼), and pH 8.0 (◆).

Above all, remarkable was the huge dependence of the thermo-sensitivity on the pH of the medium, independent of the amount of PEGMA used. With the aim of investigating the role of PEGMA on the thermal response, volume phase transition temperature (VPTT) values for the nanogels E0.93PM0, E0.93PM10, and E0.93PM20 were determined at different pHs and plotted in Figure 3.26. As expected, aside from the amount of PEGMA used, due to the weakening of electrostatic repulsions, lower temperatures were needed to disrupt H-bonds at more basic pHs, decreasing the VPTTs. Nevertheless, closer attention to Figure 3.26 reveals some differences between the nanogels. On the one hand, the pH range where nanogels showed thermo-sensitivity varied depending on the amount of PEGMA used. The presence of PEGMA caused the thermo-sensitivity to occur at slightly more basic conditions (pH range of 6.0-6.8 in the case of E0.93PM0 and pH 6.2-7.0 in the case of E0.93PM10 and E0.93PM20) in accordance with the increase in VPTpH given by the PEGylation. PEGMA shielded the cationic charges and increased the hydrophilicity, making more difficult the deprotonation of the polymeric chains and thus, the collapse. This is the reason why the pH range where nanogels showed thermo-sensitivity was shifted to more alkaline pH values.

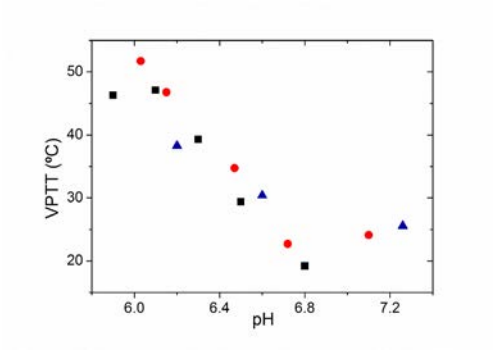


**Figure 3.26.** VPTT values of E0.93PM0 (■), E0.93PM10 (●), and E0.93PM20 (▼) as a function of pH at an ionic strength of 10 mM.

On the other hand, increasing the amount of PEGMA used, the transitions became more discontinuous or in other words, the swelling/collapse occurred over a broader temperature range. This result can be attributed to the heterogeneities in the morphology of the particles, as explained by other authors.[79,85,86] The presence of PEGMA led to a more heterogeneous structure and cross-linking points' distribution in the nanogel particles to such an extent that the sharpness of the transition region was broadened. According to the explanation given by Wu and Zhou,[87] the broadening of the transition was attributed to the fact that different parts of the gel network underwent the phase transition at different temperatures. Moreover, the pH-dependence of VPTT values was lower in the case of E0.93PM20. This low dependency could be understood in terms of its poor swelling-de-swelling behavior. The slight increase in VPTT at more alkaline pHs than 7 in the case of nanogels E0.93PM10 and E0.93PM20 could be related to the fact that nanogel particles were partially collapsed at these conditions (see Figure 3.23a), suggesting higher VPTTs than the expected ones.

With the aim of better studying the effect of the amount of PEGMA on the thermal behavior of nanogels, in Figure 3.27 the thermo-sensitivity curves of nanogels dispersed at pH 6.5 are shown. As expected, remarkable was the decrease in swelling of the nanogels when they were PEGylated. Additionally, the presence of PEGMA in the PDEAEMA-based nanogels caused the shrinking to occur at higher temperatures: the transition temperature shifted from 29.9 °C (E0.93PM0) to 34.8 °C (E0.93PM10). This shift could be caused by the hydrophilicity of PEGMA chains. Serrano-Medina *et al.,*[79] Peng *et al.,*[85] and Trongsatitkul *et al*.[86] observed the

same effect in nanogels based on PNIPAM. They reported that the PEGylation resulted in a shifting of hydrophilic/hydrophobic balance of the nanogel to higher temperatures, due to the hydrophilicity of PEG chains.

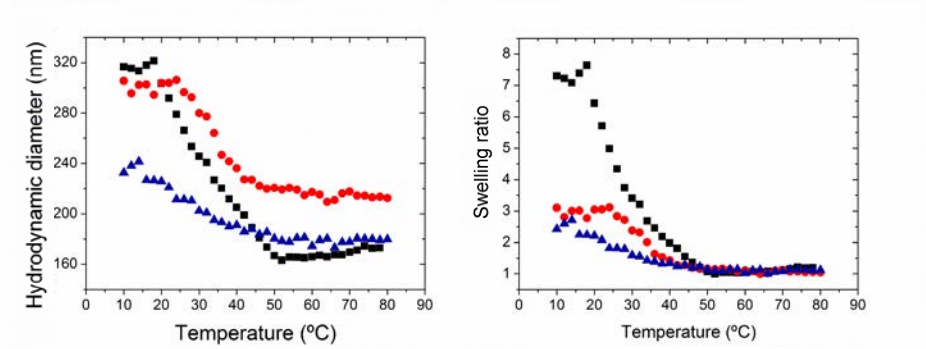


**Figure 3.27.** Hydrodynamic diameters (left) and swelling ratios (right) of nanogels E0.93PM0 (■), E0.93PM10 (●), and E0.93PM20 (▲) as a function of temperature at an ionic strength of 10 mM.

However, adding a 20 wt%M of PEGMA, the transition was given at 32.5 °C. Considering the hydrophilicity of PEGMA, higher transition temperature than that of the E0.93PM10 (34.8 °C) was expected, but the lower swelling of E0.93PM20 should be considered. The fact that the nanogels were not able to swell completely made the nanogel E0.93PM20 to show lower transition temperatures for a given pH.

The concentration of PEGMA affected in the same way regardless of the cross-linker type and concentration used in the syntheses of the nanogels synthesized. Its effect is summarized in Appendix II.

*The content of this section was published in the Journal of Polymer Science, Part A: Polymer Chemistry* ***2015****, DOI: 10.1002/pola.27996.*

### 3.3.4.2. Epoxide-functionalized nanogels

Glydicyl methacrylate (GM) has been commonly selected for the incorporation of epoxide groups in the particles. It has an unsaturated vinyl group for the polymerization and it also contains an epoxide functional group that might be opened to react with a series of

functional groups like carboxyl, amino, and hydroxyl, among others.[89-91] Several works can be found in literature where GM has been used for the preparation of nanogels and hydrogels.[20,21,92,93]

Previous to the colloidal characterization of the new epoxide-functionalized nanogels synthesized, so as to confirm the copolymerization between GM and DEAEMA and to detect the epoxide groups in the nanogel particles synthesized, FTIR analysis was performed.

Figure 3.28 shows the FTIR spectrum of the nanogel E0.93PM10GM10. The inset in Figure 3.28 shows the magnified FTIR spectrum in the range of 800-950 $cm^{-1}$. As can be seen, nanogels show the characteristic adsorption bands of the epoxide group at 845 and 915 $cm^{-1}$.[20,94-96] In this way, the functionalization of PDEAEMA-based nanogels with epoxide groups was validated. Even a minor part of epoxide groups can hydrolyze,[97-99] Ma *et al*.[94] reported that they are sufficiently stable to allow their incorporation into nanogel particles and a major part of the epoxy groups remains intact during emulsion polymerization.

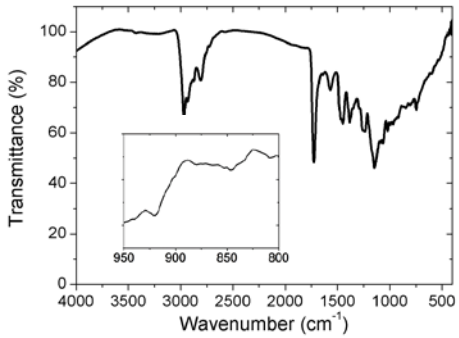


**Figure 3.28.** FTIR spectrum of nanogel E0.93PM10GM10.
Inset: magnified FTIR spectrum in the range of 800-950 $cm^{-1}$.

The colloidal characterization of the nanogels synthesized was carried out and compared with the corresponding nanogel without any epoxide groups (E0.93PM10). Figure 3.29 shows hydrodynamic diameters and swelling ratios of the nanogels E0.93PM10GM10 and E0.93PM10GM20 together with E0.93PM10, as a function of pH.

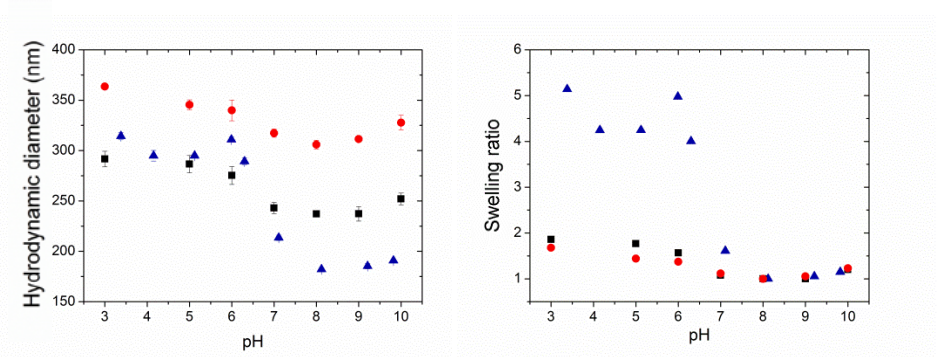


**Figure 3.29.** Hydrodynamic diameters (left) and swelling ratios (right) of nanogels E0.93PM10GM10 (■), E0.93PM10GM20 (●), and E0.93PM10 (▲) as a function of pH at an ionic strength of 10 mM.

It is important to note that the pH-dependent transition was still significant even GM was introduced as comonomer, being swollen at acidic conditions, and collapsing at alkaline conditions. However, the effects of adding GM have to be remarked.

Figure 3.29 shows that the magnitude of the pH-dependent swelling-de-swelling behavior of the nanogels was strongly dependent on the nanogel composition. As the GM content increased, the overall change of the hydrodynamic diameter was smaller as compared to E0.93PM10. The same effect was observed by Häntzschel *et al.*[92] in Poly(VCL-*co*-GM)-based nanogels. As expected, the presence of a non-responsive polymer led to a lower sensitivity.[100] Moreover, it is well known that the pH-responsive swelling-de-swelling behavior of polyelectrolyte-based nanogels is governed by electrostatic interactions between the polymer chains, and therefore, it is determined by their charge density.[101] The addition of GM decreased the charge density of the polymer network, weakening the electrostatic interactions, and thereby, decreasing the swelling capability of nanogel particles. Durmaz and Okay,[102] and Kratz *et al.*[103] reported the same effect varying the amount of an ionic comonomer in poly(acrylamide)-based hydrogels and PNIPAM-based nanogels, respectively.

As mentioned above, another reason that could affect the swelling ratio is the microstructures' heterogeneity.[24] Taking into account the differences in reactivity between the main monomer and the comonomer (GM), a more heterogeneous morphology would be expected.

Furthermore, an increase in GM concentration led to larger collapsed nanogel particles. Being nonionic, the addition of GM decreased the charge density of the nanogel particles and thereby their colloidal stability, leading to a lower number of nanoparticles, which were larger in size.

In spite of undergoing the transition in the pH range from 6 to 7, the addition of GM shifted the VPTpH to slightly more acidic conditions: from 6.9 (E0.93PM10) to 6.3 (E0.93PM10GM10 and E0.93PM10GM20). This shift was also observed in electrophoretic mobility values measured at different pHs, since the copolymerization or the addition of GM to the reaction provoked the decrease in electrophoretic mobility to start at slightly more acidic pHs (see Figure 3.30).

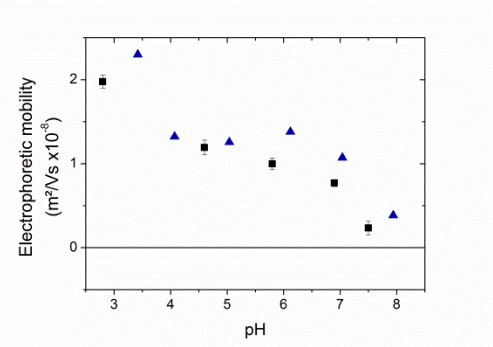


**Figure 3.30.** Electrophoretic mobility of nanogels E0.93PM10GM10 (■) and E0.93PM10 (▲) as a function of pH at an ionic strength of 10 mM.

Additional evidence for the shift in the transition pH range is seen in the potentiometric titration data. Figure 3.31 shows the pH variation as a function of the degree of ionization of nanogels E0.93PM10GM10 and E0.93PM10. In the case of E0.93PM10GM10, the plateau appeared at a lower pH value comparing to the free-GM nanogel, suggesting a lower effective $pK_a$ [6.3 (E0.9.3PM10) > 5.9 (E0.93PM10GM10)], and an easier deprotonation of the charged PDEAEMA polymeric chains. These results can be elucidated considering that nanogels containing GM had a lower charge density. The presence of GM between PDEAEMA polymer chains could weaken the electrostatic repulsions, making the deprotonation and thereby the collapse of particles easier. It was also evident that the width of the plateau decreased by

adding GM as comonomer, since the buffering capacity was lower. Vamvakaki *et al.*[104] also reported that a decrease in DEAEMA content of the copolymer resulted in a narrower plateau.

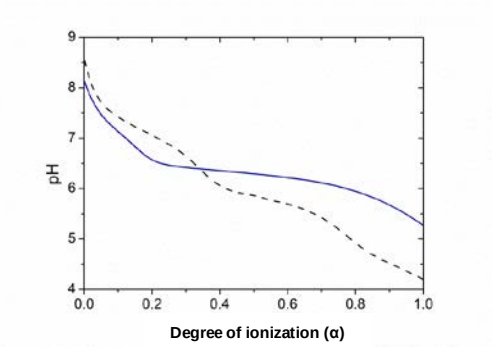


**Figure 3.31.** pH as a function of the degree of ionization (α) of nanogels E0.93PM10GM10 (– –) and E0.93PM10 (—).

### 3.3.4.3. Primary amine-functionalized nanogels

Functionalized groups such as primary amine groups are often incorporated into nanogels to open the possibilities of forming covalent linkages with a wide range of functional groups.[22,105] The most common cationic amino monomer used in emulsion polymerization to prepare primary amine-functionalized nanogels is 2-aminoethyl methacrylate (AEMA).[5,13,106,107] However, in general, primary amine-containing monomers should be protected to avoid unwanted side reactions. For example, AEMA, when it is deprotonated, can give different side reactions: rearrangement due to an acyl migration, Michael addition, or chain transfer reactions.[108,109] To avoid these side reactions, AEMA has to be polymerized at low pH. Taking into account that the main monomer (DEAEMA) is very basic and its emulsion polymerization reaction takes place at pH 9-10, AEMA should be protected when copolymerizing with DEAEMA. Therefore, *t*-Boc (tert-butyloxycarbonyl)-protected AEMA (A-Boc) was used in this work.[110,111]

After the polymerization, Boc groups were removed by using the methodology explained in the experimental part. The complete deprotection of the amine groups was confirmed by the disappearance of the methyl proton signal of the Boc groups at 1.4 ppm (see $^{1}$H-NMR spectra shown in Figure 3.32).[110,111] Overall, this two-step synthesis was useful to obtain nanogels containing primary amine groups.

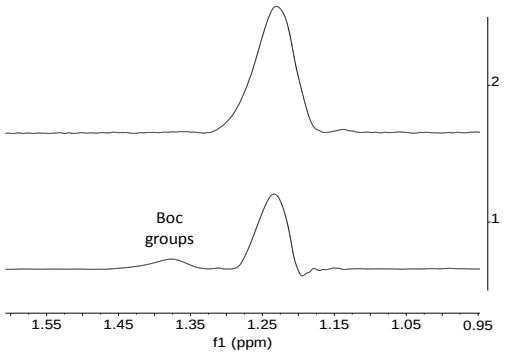


**Figure 3.32.** $^{1}$H-NMR spectra of nanogels E0.93PM10ABoc (1) and E0.93PM10AEMA (2) showing the complete disappearance of Boc groups.

The colloidal characterization of the nanogels was also carried out. Figure 3.33 shows the hydrodynamic diameter and swelling ratio values of the nanogel E0.93PM10AEMA together with the corresponding nanogel without any primary amine groups (E0.93PM10) as a function of pH. As can be observed, the functionalization did not affect the pH-responsive behavior of PDEAEMA-based nanogels.

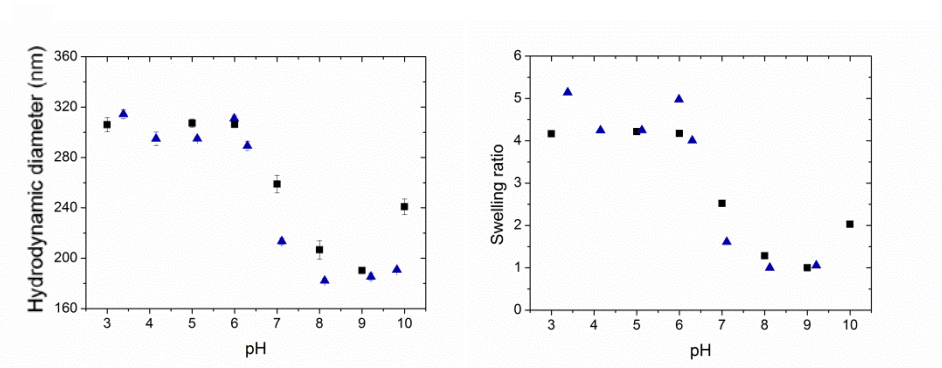


**Figure 3.33.** Hydrodynamic diameters (left) and swelling ratios (right) of nanogels E0.93PM10AEMA (■) and E0.93PM10 (▲) as a function of pH.

The main difference was that functionalized nanogels underwent the volume phase transition in a slightly wider pH range. The heterogeneity in microstructure provoked by the copolymerization could be the reason for a more continuous transition.[87]

Furthermore, in spite of the functionalization with primary amine groups, nanogels showed temperature-dependent swelling-de-swelling behavior, as can be observed in Figure 3.34. Considering the high solubility in water of AEMA (94 mg/mL),[38] one could expect higher VPTT values in the case of nanogel E0.93PM10AEMA, as observed by López-León *et al.*[112] In this case, it has to be taken into account that E0.93PM10 was partially collapsed at pH 7 while E0.93PM10AEMA was swollen (see Figure 3.33). This is the reason why any variation in VPTT values was not observed because of the functionalization (VPTT = 26 °C at pH 7, in both cases).

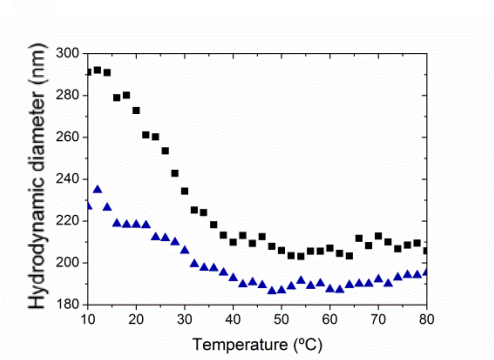


**Figure 3.34.** Hydrodynamic diameters of nanogels E0.93PM10AEMA (■), and E0.93PM10 (▲) as a function of temperature at pH 7 at an ionic strength of 10 mM.

PEGylated, epoxide- and primary-amine functionalized nanogels were synthesized showing dual-stimuli-sensitive swelling-de-swelling behavior, opening new possibilities for bioconjugation, biovectorization, and further functionalization, among others.

## 3.4. Conclusions

New dual stimuli-responsive PDEAEMA-based nanogels were synthesized by surfactant-free emulsion polymerization, and stable pH- and temperature-responsive nanogel particles were obtained. The effects of different variables such as the initiator, cross-linker, and stabilizer concentrations, the cross-linker type, and some functionalizations on the swelling-de-swelling behavior of the nanogels were also studied.

It was observed that an increase in the initiator concentration provoked a decrease in the size of collapsed nanogel particles, but the swelling properties remained constant: neither the transitions nor the swelling capability were affected.

Allowing for the possibility to tune the size and swelling properties of nanogels by varying the cross-linker type, different types of cross-linkers were tried for the synthesis of PDEAEMA-based nanogels. Two main families of nanogels could be distinguished: the one synthesized by using EG-based cross-linkers (EGDMA and PEGDA) and the one synthesized by using disulfide-based cross-linkers (BAC and DSDMA).

Regarding the family of nanogels synthesized by using EG-based cross-linkers, the swelling-de-swelling behavior and morphology of the nanogels were analyzed. On the one hand, the cross-linker type had any effect neither on the VPTpH and VPTT values nor on the size of nanogels. However, the swelling capability was noticeably affected: nanogel synthesized by using PEGDA as cross-linker showed much higher swelling ratio values comparing to the ones obtained by using EGDMA, due to the higher hydrophilicity and larger length between the cross-linking points of PEGDA comparing to EGDMA. On the other hand, the inner structure of nanogels was studied through $^{1}$H transverse relaxation NMR experiments confirming a core-shell type heterogeneous morphology for the nanogels. It was also concluded that the cross-linker type affected the cross-linking points' distribution and thus the heterogeneity in morphology of nanogels: the ones obtained by using EGDMA had more heterogeneous morphology than the ones cross-linked with PEGDA, due to the higher reactivity of the former with the main monomer (DEAEMA). In addition, the swelling ratios and the different cross-linking points' distributions were related, concluding that the nanogel with the most homogeneous morphology achieved the highest swelling ratio.

According to the nanogels synthesized by using disulfide-based cross-linkers, the initiator system was firstly optimized since a low final conversion was achieved when using a

thermal initiator. This low conversion was attributed to the side reactions of the disulfide group. A redox initiator system was used to reduce the possibility of side reactions of the disulfide groups since it enables the reaction polymerizations to carry out at lower temperatures. Regarding the effect of the cross-linker (BAC and DSDMA) on the nanogels swelling-de-swelling behavior, nanogels obtained by using DSDMA showed slightly lower swelling than in the case of using BAC. This result was related to the cross-linkers reactivity with the main monomer and the morphology of the nanogels.

Regarding the effect of the cross-linker concentration on the swelling-de-swelling behavior, there was not any effect on the VPTpH and VPTT values, the sharpness of the transitions and the size of the nanogel particles. Nevertheless, it was found that a decrease in the cross-linker amount provoked an increase in the swelling ratio.

Moreover, owing to the advantages of PEGylation for bio-applications, a new family of nanogels was synthesized by adding different amounts of PEGMA, and their colloidal characterization was carried out. Nanogels still showed dual-stimuli-sensitivity but the swelling capability decreased. In addition, being PEG hydrophilic, the VPTT was shifted toward higher temperatures and as the presence of PEGMA screened the charges, the VPTpH shifted to higher pH values. The results suggest a more heterogeneous inner structure of PEGylated nanogel particles than the nanogels without any PEGMA.

In addition, considering the crucial role of nanogels functionalization to provide novel properties such as bioconjugation, epoxide- and primary amine-functionalized nanogels were obtained. The functionalization of nanogels was validated only qualitatively because of the low amount of functional groups. Then, the stimuli-responsive swelling-de-swelling behavior of the nanogels was also studied. Functionalized nanogels also showed significant stimuli-responsive behavior.

In summary, the syntheses and characterizations of new dual-stimuli-responsive nanogels were reported in this Chapter. The broad selection of stimuli-sensitive swelling-de-swelling behaviors offers some benefits towards the nanogels across the multidisciplinary field of biomedical applications.

## 3.5. References


1. S. Wellert, A. Radulescu, A. Carl, R. von Klitzing, K. Gawlitza, *Macromolecules* **2015**, *48*, 4901-4909.
2. C. Dispenza, S. Rigogliuso, N. Grimaldi, M. A. Sabatino, D. Bulone, M. L. Bondì, G. Ghersi, *React. Funct. Polym.* **2012**, *73*, 1103-1113.
3. X. Zhou, J. Nie, B. Du, *ACS Appl. Mater. Interfaces* **2015**, *7*, 21966-21974.
4. R. Contreras-Cáceres, L. Schellkopf, C. Fernández-López, I. Pastoriza-Santos, J. Pérez-Juste, M. Stamm, *Langmuir* **2015**, *31*, 1143-1149.
5. N. C. Dubey, B. P. Tripathi, M. Stamm, L. Ionov, *Biomacromolecules* **2014**, *15,* 2776-2783.
6. M. H. Smith, E. S. Herman, L. A. Lyon, *J. Phys. Chem. B* **2011**, *115*, 3761-3764.
7. M. Asadian-Birjand, A. Sousa-Herves, D. Steinhilber, J. C. Cuggino, M. Calderón, *Curr. Med. Chem*. **2012**, *19*, 5029-5043.
8. N. Sanson, J. Rieger, *Polym. Chem.* **2010**, *1*, 965-977.
9. S. Mura, J. Nicolas, P. Couvreur, *Nat. Mater.* **2013**, *12*, 991-1003.
10. W. Cheng, G. Wang, J. N. Kumar, Y. Liu, *Macromol. Rapid Commun.* **2015**, *36*, 2102-2106.
11. V. Sáez Martínez, L. Pérez Álvarez, E. Hernáez, T. Herrero, I. Katime, *J. Polym. Sci., Part A: Polym. Chem.* **2007**, *45*, 3833-3842.
12. A. Imaz, J. Forcada, *Eur. Polym. J.* **2009**, *45*, 3164-3175.
13. K. Chen, J. Xu, J. C. Luft, S. Tian, J. S. Raval, J. M. DeSimone, *J. Am. Chem. Soc.* **2014**, *136*, 9947-9952.
14. F. Schneider, A. Balaceanu, A. Feoktystov, V. Pipich, Y. Wu, J. Allgaier, W. Pyckhout-Hintzen, A. Pich, G. J. Schneider, *Langmuir* **2014**, *30*, 15317-15326.
15. N. M. B. Smeets, T. Hoare, *J. Polym. Sci., Part A: Polym. Chem*. **2013**, *51*, 3027-3043.
16. M. Mackiewicz, K. Kaniewska, J. Romanski, E. Augustin, Z. Stojek, M. Karbarz, *J. Mater. Chem. B* **2015**, *3*, 7262-7270.
17. G. Soni, K. S. Yadav, *Saudi Pharm. J.* **2014**, DOI:10.1016/j.jsps.2014.04.001.
18. S. Moffat, *MOJ Proteomics Bioinform*. **2015**, *2*, 37/3.
19. H. Wang, L. Yang, G. L. Rempel *Macromol. Biosci.* **2014**, *14*, 166-172.

20. P. Li, R. Xu, W. Wang, X. Li, Z. Xu, K. W. K. Yeung, P. K. Chu, *Colloids Surf., B* **2013**, *101*, 251-255.
21. Y. Ma, L. He, A. Pan, C. Zhao, *J. Mater. Sci.* **2015**, *50*, 2158-2166.
22. S. Thaiboonrod, A. H. Milani, B. R. Saunders, *J. Mater. Chem. B* **2014**, *2*, 110-119.
23. W. Ji, D. Panus, R. N. Palumbo, R. Tang, C. Wang, *Biomacromolecules* **2011**, *12*, 4373-4385.
24. A. Pikabea, G. Aguirre, J. I. Miranda, J. Ramos, J. Forcada, *J. Polym. Sci., Part A: Polym. Chem*. **2015**, *53*, 2017-2025.
25. Balaceanu, D. E. Demco, M. Möller, A. Pich, *Macromolecules* **2011**, *44*, 2161–2169.
26. Balaceanu, D. E. Demco, M. Möller, A. Pich, *Macromol. Chem. Phys*. **2011**, *212*, 2467–2477.
27. T. Hoare, R. Pelton, *Langmuir* **2004**, *20*, 2123-2133.
28. S. Kawaguchi, A. Yekta, M. A. Winnik, *J. Colloid Interface Sci.* **1995**, *176*, 362-369.
29. G. Aguirre. *Advanced Design of Biocompatible Stimuli-responsive Nanocapsules and Nanogels for Antitumor Drug and Gene Delivery.* PhD Thesis, The University of the Basque Country, **2015**.
30. P. Hazot, Th. Delair, A. Elaissari, C. Pichot, J. P. Chapel, J. Davenas, *Macromol. Symp.* **2000**, *150*, 291-296.
31. J. Ramos, J. Forcada, R. Hidalgo-Alvarez, *Chem. Rev.* **2014**, *114*, 367–428.
32. S. Lally, T. J. Freemont, F. Cellesi, B. R. Saunders, *Colloid. Polym. Sci.* **2011**, *289*, 647-658.
33. K. Kratz, A. Lapp, W. Eimer, T. Hellweg, *Colloids Surf., A* **2002**, 197, 55-67.
34. P. Hazot, J. P. Chapel, C. Pichot, A. Elaissari, T. Delair, *J. Polym. Sci., Part A: Polym. Chem.* **2002**, *40*, 1808-1817.
35. A. Imaz, J. Forcada, *J. Polym. Sci., Part A: Polym. Chem.* **2008**, *46*, 2766-2775.
36. G. Patras, G. G. Qiao, D. H. Solomon, *Macromolecules* **2001**, *34*, 6396-6401.
37. K. W. Dixon, Chapter II, *Polymerization and Depolymerization,* In *Polymer Handbook*, 4th ed., Eds. J. Brandrup, E. H. Immergut, E. A. Grulke, John Wiley & Sons, ISBN: 978-0-471-47936-9, **1999**, pp. 181-308.
38. Calculated using Advanced Chemistry Development (ACD/Labs) Software V11.02 (© 1994-2015 ACD/Labs).

39. A. Imaz, *New Biocompatible Intelligent Microgels: Synthesis, Characterization, and Applications.* PhD Thesis, The University of the Basque Country, **2007**.
40. R. Acciaro, T. Gilányi, I. Varga, *Langmuir* **2011**, *27*, 7917–7925.
41. R. Saunders, *Langmuir* **2004**, *20*, 3925–3932.
42. Obeso-Vera, J. M. Cornejo-Bravo, A. Serrano-Medina, A. Licea-Claverie, *Polym. Bull.* **2013**, *70*, 653-664.
43. J. Ramos, A. Imaz, J. Callejas-Fernández, L. Barbosa-Barros, J. Estelrich, M. Quesada-Pérez, J. Forcada, *Soft Matter* **2011**, *7*, 5067–5082.
44. G. Aguirre, J. Ramos, J. Forcada, *Soft Matter* **2013**, *9*, 261-270.
45. S. Schachschal, A. Balaceanu, C. Melian, D. E. Demco, T. Eckert, W. Richtering, A. Pich, *Macromolecules* **2010**, *43*, 4331–4339.
46. *CRC Handbook of Chemistry and Physics,* Eds. R. C. Weast, CRC Press, Inc.: Boca Raton, Florida, ISBN: 0-84930470-9, **1989.**
47. A. Guillermo, J. P. Cohen Addad, J. P. Bazile, D. Duracher, A. Elaissari, C. Pichot, *J. Polym. Sci. Part B: Polym. Phys.* **2000**, *38*, 889–898.
48. H. Y. Cho, A. Srinivasan, J. Hong, E. Hsu, S. Liu, A. Shrivats, D. Kwak, A. K. Bohaty, H.-j. Paik, J. O. Hollinger, K. Matyjaszewski, *Biomacromolecules* **2011**, *12*, 3478-3486.
49. Y.-J. Pan, Y.-Y. Chen, D.-R. Wang, C. Wei, J. Guo, D.-R. Lu, C.-C. Chu, C.-C. Wang, *Biomaterials* **2012**, *33*, 6570-6579.
50. Y. Wang, J. Nie, B. Chang, Y. Sun, W. Yang, *Biomacromolecules* **2013**, *14*, 3034-3046.
51. Z.-Q. Yu, J.-T. Sun, C.-Y. Pan, C.-Y. Hong, *Chem. Commun.* **2012**, *48*, 5623-5625.
52. Y. Wang, M. Zheng, F. Meng, J. Zhang, R. Peng, Z. Zhong, *Biomacromolecules* **2011**, *12*, 1032-1040.
53. J. C. Gaulding, M. H. Smith, J. S. Hyatt, A. Fernandez-Nieves, *Macromolecules* **2012**, *45*, 39-45.
54. Duracher, A. Elaïssari, C. Pichot, *J. Polym. Sci., Part A: Polym. Chem.* **1999**, *37*, 1823-1837.
55. V. Koval, *Rus. Chem. Rev.* **1994**, *63*, 735-750.
56. X. Hu, Z. Tong, L. A. Lyon, *Langmuir* **2011**, *27*, 4142-4148.
57. H. Yu, Y. Fang, L. Chen, S. Chen, *Polym. Int.* **2009**, *58*, 851-857.
58. G. R. Deen, J. S. Pedersen, *Cogent Chemistry* **2015**, *1*, 1012658-1012672.

59. S. Petrusic, P. Jovancic, M. Lewandowski, S. Giraud, B. Bugarski, J. Djonlagic, V. Koncar, *J. Polym. Res*. **2012**, *19*, 11 pp.
60. M. Füllbrandt, R. von Klitzing, A. Schönhals, *Soft Matter* **2013**, *9*, 4464-4471.
61. C-L. Lin, W-Y. Chiu, C-F. Lee, *Polymer* **2005**, *4*6, 10092-10101.
62. M. Karg, S. Prévost, A. Brandt, D. Wallacher, R. von Klitzing, T. Hellweg, *Prog. Colloid Polym. Sci.* **2013**, *140*, 63-75.
63. K. Kratz, T. Hellweg, W. Eimer, *Polymer* **2001**, *42*, 6631-6639.
64. A. Imaz, J. Forcada, *J. Polym. Sci.; Part A: Polym. Chem*. **2008**, *46*, 2510-2524.
65. B. Zhang, B. Wei, X. Hu, Z. Jin, X. Xu, *Carbohydr. Polym.* **2015**, *124*, 245-253.
66. Varga, T. Gilányi, R. Mészáros, G. Filipscsei, M. Zrínyi, *J. Phys. Chem. B* **2001**, *105*, 9071-9076.
67. L. A. Shah, Z. H. Farooqi, H. Naeem, S. M. Shah, M. Siddiq, *J. Chem. Soc. Pak.* **2013**, *35*, 1522-1529.
68. S. V. Ghugare, E. Chiessi, B. Cerroni, M. T. F. Telling, V. G. Sakai, G. Paradossi, *Soft Matter* **2012**, *8*, 2494-2502.
69. S. Lou, S. Gao, W. Wang, M. Zhang, J. Zhang, C. Wang, C. Li, D. Kong, Q. Zhao, *Nanoscale* **2015**, *7*, 3137-3146.
70. V. Shirshahi, F. Shamsipour, A. H. Zarnani, J. Verdi, R. Saber, *Cancer Nano.* **2013**, *4*, 27-37.
71. J. K. Oh, S. A. Bencherif, K. Matyjaszewski, *Polymer* **2009**, *50*, 4407-4423.
72. Y. Ikeda, Y. Nagasaki, *J. Appl. Polym. Sci.* **2014**, *31*, 10 pp.
73. G. Tamura, Y. Shinohara, A. Tamura, Y. Sanada, M. Oishi, I. Akiba, Y. Nagasaki, K. Sakurai, Y. Amemiya, *Polym. J.* **2012**, *44*, 240-244.
74. J. V. Jokerst, T. Lobovkina, R. N. Zare, S. S. Gambhir, *Nanomedicine* **2011**, *6*, 715-728.
75. Naeye, K. Raemdock, K. Ramut, B. Sproat, J. Demeester, S. C. De Smedt, *Eur. J. Pharm. Sci.* **2010**, *40*, 342-351.
76. S. R. Marek, C. A. Conn, N. A. Peppas, *Polymer* **2010**, *51*, 1237-1243.
77. A. Pikabea, J. Ramos, J. Forcada, *Part. Part. Syst. Char.* **2014**, *31*, 101–109.
78. H. Hayashi, M. Iijima, K. Kataoka, Y. Nagasaki, *Macromolecules* **2004**, *37*, 5389–5396.
79. A. Serrano-Medina, J. M. Cornejo-Bravo, A. Licea-Claveríe, *J. Colloid Interface Sci.* **2012**, *369*, 82-90.

80. J. A. Beamish, J. Zhu, K. Kottke-Marchant, R. E. Marchant, *J. Biomed. Mat. Res., Part A* **2009**, *92A*, 441-450.
81. T. Zhou, C. Xiao, J. Fan, S. Chen, J. Shen, W. Wu, S. Zhou, *Acta Biomater.* **2013**, *9*, 4546-4557.
82. A. K. Fraser, C. S. Ki, C.-C. Lin, *Macromol. Chem. Phys*. **2014**, *215*, 507-515.
83. S. Liu, J. V. M. Weaver, Y. Tang, N. C. Billingham, S. P. Armes, *Macromolecules* **2002**, *35*, 6121-6131.
84. I. Tsoneva, T. Tomov, *Bioelectrochem. Bioenerg.* **1984**, 12, 253-258.
85. J. Peng, T. Qi, J. Liao, M. Fan, F. Luo, H. Li, Z. Qian, *Nanoscale* **2012**, *4*, 2694-2704.
86. T. Trongsatitkul, B. M. Budhlall, *Colloids Surf. B* **2013**, *103*, 244-252.
87. C. Wu, S. Zhou, *Macromolecules* **1997**, *30*, 574–576.
88. A. Pikabea, J. Ramos, N. Papachristos, D. Stamopoulos, J. Forcada, *J. Polym. Sci., Part A: Polym. Chem.* **2015**, DOI: 10.1002/pola.27996.
89. E. Pollert, K. Knížek, M. Maryško, K. Závěta, A. Lančok, J. Boháček, D. Horák, M. Babič, *J. Magn. Magn. Mater.* **2006**, *306*, 241-247.
90. S. Mishra, J. Singh, V. Choudhary, *J. Appl. Polym. Sci.* **2010**, *115*, 549-557.
91. H. J. Zhou, M. Z. Rong, M. Q. Zhang, B. Lehmann, K. Friedrich, *Polym. J.* **2005**, *37*, 677-685.
92. N. Häntzschel, F. Zhang, F. Eckert, A. Pich, M. A. Winnik, *Langmuir* **2007**, *23*, 10793-10800.
93. X. Jiang, D. Xiong, Y. An, P. Zheng, W. Zhang, L. Shi, *J. Polym. Sci., Part A: Polym. Chem*. **2007**, *45*, 2812-2819.
94. Z. Ma, Y. Guan, H. Liu, *J. Polym. Sci., Part A: Polym. Chem*. **2005**, *43*, 3433-3439.
95. Horák, N. Chekina, *J. Appl. Polym. Sci.* **2006**, *102*, 4348-4357.
96. Y. Liu, W. Hu, Z. Lu, C. M. Li, *Med. Chem. Commun.* **2010**, *1*, 132-135.
97. J. M. Geurts, P. E. Jacobs, J. G. Muijs, J. J. G. S. Van Es, A. L. German, *J. Appl. Polym. Sci.* **1996**, *61*, 9-19.
98. H. Bakhshi, M. J. Zohuriaan-Mehr, H. Bouhendi, K. Kabiri, *Polym. Test.* **2009**, *28*, 730-736.
99. M. H. Nasirtabrizi, S. Mohebalizadeh, A. P. Jadid, *Iran. Polym. J.* **2011**, *20*, 579-586.
100. Gürdag, B. Kurtuluş, *Ind. Eng. Chem. Res.* **2010**, *49*, 12675-12684.
101. K. Kratz, T. Hellweg, W. Eimer, *Ber. Bunsenges. Phys. Chem.* **1998**, *102*, 1603-1608.

102. K. Kratz, T. Hellweg, W. Eimer, *Colloids Surf., A.* **2000,** *170*, 137-149.
103. S. Durmaz, O. Okay, *Polymer* **2000**, *41*, 3693–3704.
104. M. Vamvakaki, L. Papoutsakis, V. Katsamanis, T. Afchoudia, P. G. Fragouli, H. Iatrou, N. Hadjischristidis, S. P. Armes, S. Sidorov, D. Zhirov, V. Zhirov, M. Kostylev, L. M. Bronstein, S. H. Anastasiadis, *Faraday Discuss.* **2005**, *128*, 129-147.
105. X. Hu, Z. Tong, A. Lyon, *Colloid. Polym. Sci.* **2011**, *289*, 333-339.
106. N. Bhuchar, R. Sunasee, K. Ishihara, T. Thundat, R. Narain, *Bioconjugate Chem.* **2012**, *23*, 75-83.
107. J. Ramos, A. Martín-Molina, M. P. Sanz-Izquierdo, A. Rus, L. Borque, R. Hidalgo-Álvarez, F. Galisteo-González, J. Forcada, *J. Polym. Sci., Part A: Polym. Chem.* **2003**, *41*, 2404-2411.
108. J. Ramos. *New Biomaterials for Biomedical Applications: Cationic Latexes and Microgels.* PhD Thesis, The University of the Basque Country, **2005**.
109. A. H. Alidedeoglu, A. W. York, C. L. McCormick, S. E. Morgan, *J. Polym. Sci., Part A: Polym. Chem.* **2009**, 47, 5405-5415.
110. K. P. Kumar, R. V. Søndergaard, B. Windschiegl, K. Almdal, T. L. Andresen, *J. Mater. Chem. B* **2014**, *2*, 6652-6659.
111. R. P. Tang, R. N. Palumbo, L. Nagarajan, E. Krogstad, C. Wang, *J. Controlled Release* **2010**, *142*, 229-237.
112. T. López-León, J. L. Ortega-Vinuesa, D. Basto-González, A. Elaïssari, *J. Phys. Chem. B.* **2006**, *110*, 4629-4636.

# 4

# Multi-stimuli-responsive Magneto-nanogels

# 4.1. Introduction

Nanogels can be labeled with inorganic nanoparticles such as quantum dots, silver, gold, or magnetic nanoparticles (MNPs) to yield multifunctional hybrid materials with additional highly and tunable properties, extending their applications to the biomedical field as theranostic agents. The combination between the organic and the inorganic components establishes a symbiotic relation in which the nanogels give colloidal stability as well as stimuli-responsive features, while the inorganic counterparts provide quantum properties such as photoluminescence, surface plasmon resonance, or magnetism.[1-6]

Particularly, the introduction of MNPs into nanogels brings significant advantages due to MNPs' biocompatibility, biodegradability, facile synthesis, easy functionalization along with extraordinary properties in presence of a magnetic field. The use of MNPs in biomedical applications has been recently reviewed by many authors.[7-14] Incorporating MNPs in the nanogel particles provides a number of benefits making the magneto-labeled nanogels a powerful tool for biomedical applications such as Magnetic Resonance Imaging (MRI) for clinical diagnosis,[15-19] magnetically guidable drug/gene delivery,[20] cell separation,[21] hyperthermia anticancer therapy,[22] enzyme immobilization,[23] and magnetically assisted hemodialysis.[24-27] Thus, owing to both the ability to undergo reversible volume-phase transitions in response to environmental stimuli and magnetic properties, remarkable is the suitability of these hybrid nanogels for theranostics (diagnosis and therapy in a single system). The tremendous interest in such systems is reflected on the large number of works on magneto-nano/microgels suitable for biomedical applications since the last two years.[28-35]

Base on the abovementioned, magnetic labeled hybrid nanogels were prepared by using PDEAEMA-based dual-stimuli-responsive nanogels. For that purpose, firstly, different types of MNPs of magnetite were synthesized. After characterizing their chemical composition and morphological, colloidal, crystallographic and magnetic properties, they were encapsulated into the previously synthesized nanogels, obtaining a variety of magneto-nanogels (MNGs). Three different families of MNGs were prepared by changing variables such as type and concentration of MNPs, type of nanogel, and the preparation method used.

The first MNG family was obtained by physical encapsulation of citric acid-coated MNPs (CA-MNPs) into the PDEAEMA-based nanogels. The second family was prepared by using primary amine-functionalized nanogels and different initial amount of MNPs, giving the

opportunity to study the effect of the MNPs' concentration on the final properties of the MNG particles. In addition, the use of EDC/NHS [*N*-(3-Dimethylaminopropyl)-*N*′-ethylcarbodiimide hydrochloride/*N*-Hydroxysuccinimide] coupling to form amide linkages between primary amine groups of nanogels and carboxylate groups of MNPs resulting from the citric acid (CA) was investigated. The third family of MNGs was prepared by combining MNPs containing hydroxide groups and epoxide-functionalized nanogels. Different pHs were used for the preparation, obtaining MNGs with significantly different properties from each other.

After the preparation of MNGs, their colloidal, morphological, and magnetic characterizations were carried out together with the thermogravimetric analysis, opening the opportunity to study the interactions and attachments between the MNPs and nanogels in each case. These studies provide important information to understand the final properties of MNGs. In summary, a variety of multi-stimuli-responsive hybrid nanoparticles combining pH-, temperature- and magnetic response was prepared and thoroughly characterized.

## 4.2. Experimental

### 4.2.1. Materials

- Nanogels PM0, PM10, and PM20 were previously synthesized as described in Chapters 2 and 3 (E0.93PM0, E0.93PM10, and E0.93PM20, respectively) and used for the preparation of MNGs through electrostatic interactions.
- Nanogel AEMA was previously synthesized as described in Chapter 3 (E0.93PM10AEMA) and used for the preparation of MNGs from primary amine-functionalized nanogels.
- Nanogel GM10 was previously synthesized as described in Chapter 3 (E0.93PM10GM10) and used for the preparation of MNGs from epoxide-functionalized nanogels.

All the following materials were used as received:

- Ferric chloride hexahydrate ($FeCl_3 \cdot 6H_2O$) and ferrous chloride tetrahydrate ($FeCl_2 \cdot 4H_2O$), both supplied by Sigma-Aldrich, were used for the syntheses of the MNPs.

- Ammonium hydroxide solution ($NH_4OH$, 28 % (w/w)) and citric acid (CA), both supplied by Sigma-Aldrich, were used to prepare citric acid-coated MNPs.
- Sodium hydroxide (NaOH) was used in the synthesis of MNPs.
- *N*-(3-Dimethylaminopropyl)-*N′*-ethylcarbodiimide hydrochloride (EDC) and *N*-Hydroxysuccinimide (NHS), both supplied by Sigma-Aldrich, were used for the preparation of MNGs from primary amine-functionalized nanogels.
- Glycine, γ-aminobutyric acid, pyridine, bis-tris, sodium phosphate monobasic, and dibasic, Trizma®, triethylamine and sodium chloride (NaCl), supplied by Sigma-Aldrich, were used to prepare the buffer solutions.
- Double deionized (DDI) water was used throughout the work.

## 4.2.2. Synthesis of Magnetic Nanoparticles (MNPs)

Different types of MNPs were synthesized by the well-known co-precipitation method. In this method, $Fe^{2+}$ and $Fe^{3+}$ aqueous salt solutions are co-precipitated by the addition of a base. Since it must be carried out in an oxygen-free environment,[36] nitrogen flux was used during the synthesis reactions. MNPs were obtained without using any stabilizer[37] and also by using CA to coat them with carboxylic groups.[38] In both cases, the obtained $Fe_3O_4$ nanoparticles (MNPs) were washed with ethanol and DDI water and separated by a permanent magnet. Then, they were dried in an oven under vacuum. All the synthesis procedures and characterizations are reported in Appendix III.

## 4.2.3. Preparation of Magneto-nanogels (MNGs)

### 4.2.3.1. Preparation of MNGs through electrostatic interactions

The preparation of MNGs was carried out by physical encapsulation of the citric acid-coated MNPs (CA-MNPs) into the previously synthesized nanogels E0.93PM0, E0.93PM10, and E0.93PM20 presented in Chapters 2 and 3. In this Chapter, nanogels are named PM0, PM10, and PM20, respectively.

Briefly, 0.01 g of previously lyophilized nanogel and 0.01 g of CA-MNPs were dispersed in 20 mL of a bis-tris (pH 6) buffer solution at an ionic strength of 10 mM. After sonication

during 30 min, the obtained dispersions were centrifuged twice (10,000 rpm, 20 min) in order to separate the MNGs from the non-encapsulated MNPs. The final precipitate was redispersed in buffer solutions at different pHs prior to characterization. In Table 4.1, the different nanogels synthesized by using different amounts of poly(ethylene glycol) methacrylate (PEGMA) as stabilizer and the corresponding MNGs produced together with the preparation conditions, are shown.

| Nanogels | MNGs |
|---|---|
| PM0 | PM0m |
| PM10 | PM10m |
| PM20 | PM20m |
| **Reaction conditions:** 30′ sonication, 25 °C<br>0.01 g nanogel, 0.01 g CA-MNPs, 20 mL buffer (pH 6, 10 mM)<br>**Variable:** the nanogel used (obtained varying the amount of PEGMA wt%M) | |

**Table 4.1.** Recipes and preparation conditions used for the preparation of MNGs through electrostatic interactions.

### 4.2.3.2. Preparation of MNGs from primary amine-functionalized nanogels

The preparation of these MNGs was carried out by combining the primary amine functionalized nanogel E0.93PM10AEMA (see section 3.3.4.3 in Chapter 3) and CA-coated MNPs described in Appendix III. In this Chapter, nanogel E0.93PM10AEMA is named AEMA. Briefly, a certain amount of CA-coated MNPs was dispersed in 40 mL of a buffer solution of bis-tris at pH 7 at an ionic strength of 10 mM in a sonication bath for 15 min. 0.01 g of nanogel was also dispersed in 10 mL of a buffer solution of bis-tris under the same conditions.

In the case of using EDC and NHS for the formation of amide linkages between carboxylic groups of the MNPs and primary amine groups of the nanogels, 0.4 mg of EDC and 0.8 mg of NHS were added to the MNPs' dispersion in order to activate the carboxylate groups of the CA-MNPs. They were mixed for 10 min, before mixing with nanogels' dispersion.

The obtained dispersions were mixed and placed into a 50-mL glass reactor. The reaction content was stirred at 300 rpm for 1 h at 25 °C. The final dispersion was centrifuged twice (15,000 rpm, 30 min) in order to separate the MNGs from the non-attached MNPs. Then, a magnet was used to separate the MNGs from the MNPs-free nanogels. Part of the final

precipitate was redispersed in buffer solutions at different pHs prior to colloidal and morphological characterizations and the other part was dried in an oven under vacuum prior to thermogravimetric and magnetic characterizations. In Table 4.2 the recipes for the preparation of MNGs by using AEMA nanogel, along with the preparation conditions, are shown.

| Nanogel | MNPs | MNPs (wt% AEMA) | EDC/NHS | MNGs |
|---|---|---|---|---|
| AEMA | CA-MNPs | 100 | NO | AEMAm1 |
| | | 200 | | AEMAm2 |
| | | 200 | YES | AEMAm2C |

**Reaction conditions:** - 300 rpm, 25 °C, 1 h
- 0.01 g AEMA, 50 mL buffer (pH 7, 10 mM)
**Variables:** - Amount of MNPs used with respect to AEMA (wt% AEMA)
- Use of EDC and NHS: YES/NO

**Table 4.2.** Recipes and preparation conditions used for the preparation of MNGs from primary amine-functionalized nanogels.

### 4.2.3.3. Preparation of MNGs from epoxide-functionalized nanogels

This nanogel family was prepared by using nanogel E0.93PM10GM10 with epoxide groups described in Chapter 3 (see section 3.3.4.2) and MNPs with hydroxyl groups. The nanogel is named GM10 in this Chapter. Briefly, 0.01 g of nanogel GM10 and 0.01 g of uncoated MNPs were dispersed in 25 mL of buffer solutions of glycine and bis-tris at an ionic strength of 10 mM by sonication (30 min). Different pHs were tried to carry out the reactions between nanogel and MNPs: pH 3 and pH 6. The obtained dispersions were mixed and placed into a 100-mL jacketed glass reactor. The reaction content was heated to 50 °C, stirred at 300 rpm, and purged with nitrogen. Then, the reaction was carried out for 12 h. Table 4.3 shows the nomenclature used for the MNGs obtained.

The final dispersion obtained was centrifuged twice (15,000 rpm, 30 min) in order to separate the MNGs from the free MNPs, and MNPs-free nanogels were separated by using a magnet. Part of the final precipitate was redispersed in buffer solutions at different pHs and the other part was dried in an oven under vacuum prior to the different characterizations.

| Nanogel | MNPs | pH | MNGs |
|---|---|---|---|
| GM10 | Uncoated MNPs | 3 | GM10m3 |
| | | 6 | GM10m6 |
| 0.01 g GM10 in 25 mL buffer (10 mM) and 0.01 g MNPs in 25 mL buffer (10 mM)<br>**Reaction conditions: 1.** 30' sonication of both dispersions, **2.** 300 rpm, 50 °C, 12 h<br>**Variable:** pH used for the synthesis | | | |

**Table 4.3.** Recipes and reaction conditions used for the preparation of MNGs from epoxide-functionalized nanogels.

## 4.2.4. Characterization of the different nanoparticles

### 4.2.4.1. Colloidal characterization

Photon Correlation Spectroscopy (PCS) measurements were performed to obtain the pH- and thermo-sensitivity of the different nanoparticles. For that purpose, samples were dispersed at different pHs at an ionic strength of 10 or 150 mM at a concentration of 0.005 wt%. Measurements were carried out at 25 °C from pH 3 to pH 10 (3 measurements every pH unit) for studying the pH-sensitivity, and at different pHs from 10 to 80 °C (every 2 °C) for investigating the thermal behavior. The optimized stabilizing time of the measurements was 2 min. Since no hysteresis between heating and subsequent cooling cycles was observed, only the heating cycles of the thermo-sensitivity curves are shown.

Volume phase transition pH and temperature (VPTpH and VPTT) were determined and established as the pH and temperature corresponding to the inflection point in the average hydrodynamic diameter versus pH or temperature curves, respectively.

The swelling ratio was calculated by using the following equation:

$$\text{Swelling ratio} = \left(\frac{dp_X}{dp_S}\right)^3 \qquad (4.1)$$

where $dp_X$ is the hydrodynamic diameter at a given pH or temperature (for pH- and temperature-responsive curves, respectively), and $dp_S$ is the smallest hydrodynamic diameter in all the pH or temperature range.

Electrophoretic mobility measurements were conducted by Electrophoretic Light Scattering (ELS, Zetasizer Nano ZS, Malvern Instruments) as explained in Chapter 2. Besides,

with the aim of studying the pH-dependent ionization degree of nanogels, potentiometric titrations were performed by using T90 titrator (Metter Toledo). The same procedure as the one described in Chapter 2 was used for the titrations and analyzing the data obtained.[39] Once calculating the value of degree of ionization/protonation (α),[40] the pH/α curves were obtained (see section 2.2.3.2).

#### 4.2.4.2. Thermogravimetric characterization

Thermogravimetric analysis (TGA) was used to determine the average $Fe_3O_4$ content of representative MNP and MNG samples. TGA was carried out on a thermogravimetric analyzer (TGA Q500, TA instruments) with a heating rate of 10 °C/min from 40 to 800 °C under nitrogen atmosphere. The magnetite, $Fe_3O_4$ content in the MNPs and MNGs was given according to the weight percentage of the residue remaining after thermal analysis.[41]

#### 4.2.4.3. Magnetic characterization

Preliminary studies were performed on the magnetic properties of the MNPs and MNGs by means of a Vibrating Sample Magnetometer (VSM, Quantum Design PPMS). A VSM measures the magnetization of the sample placed in an external magnetizing field by converting the dipole field of the sample into an AC electrical signal. Magnetic properties of the materials were studied as a function of magnetic field, obtaining magnetization (M) vs. applied magnetic field (H) hysteresis loops. Parameters extracted from the hysteresis loops include the saturation magnetization $M_S$ (the maximum M at high H values, reflecting the magnetizability of magnetic materials), the remanence $M_r$ (it reflects the remaining magnetization of magnetic materials when an external magnetic field is removed) and the coercivity $H_C$ (it characterizes the ability of magnetic materials to retain magnetization when the external magnetic field is removed).

#### 4.2.4.4. FTIR analysis

Some drops of the aqueous dispersions of MNPs and MNGs synthesized were placed in a sheet made of Thallium Bromoiodide (KSR-5) for obtaining Fourier Transform Infrared (FTIR) spectra. They were analyzed after evaporating the water.

### 4.2.4.5. X-ray characterization

X-ray diffraction measurements were performed by a Bruker D8 Advance powder X-ray diffractometer (BRUKER axs) with monochromatic Cu $K_\alpha$ incident radiation ($\lambda$ = 0.154 nm) and using Bragg-Brentano geometry. The measurements were achieved 2$\theta$ in the 15-95° range with 0.05° step size and a step time of 10 s.

### 4.2.4.6. Morphological characterization

Various, conventional and advanced, microscopy techniques such as Optical Microscopy (OM), Atomic Force Microscopy (AFM), and Transmission Electron Microscopy (TEM), were employed to investigate the morphology of the obtained MNPs and MNGs. Energy-Dispersive X-ray Spectroscopy (EDS) was used for the elemental analysis of the samples, as well.

**Optical Microscopy (OM).**

Prior to the investigation with AFM, a conventional optical microscope (OM) was employed to evaluate the produced specimens of MNGs obtained through electrostatic repulsions. OM images were recorded in reflection mode with a LEICA DMRXP (Leica, Wetzlar, Germany).

**Atomic Force Microscopy (AFM).**

Atomic Force Microscopy (AFM) was employed to acquire data on the morphological and geometrical characteristics of the MNGs obtained through electrostatic repulsions by means of a scanning probe microscope (Solver PRO; NT-MDT Co, Moscow, Russia) with a 100x100x5 $\mu m^3$ XYZ scanner hosted on an active vibration isolation table (MOD-1M plus; Halcyonics GmbH, Goettingen, Germany). Measurements were performed in the semi-contact scanning mode with NCH (Non-Contact/tapping mode-High resonance frequency) cantilevers that end with silicon nitride tips (Nano and More GmbH, Wetzlar, Germany) and have the nominal parameters, spring constant = 42 N/m and resonance frequency = 320 kHz. The optimum imaging results were obtained with the following scanning parameters: line frequency 1.5-4 Hz, area = 0.5x0.5 - 30x30 $\mu m^2$, and lines per image = 256-512. In the AFM observations the 'phase' signal was recorded during each single scan, which provides information referring to the viscoelasticity/adhesion/friction of the imaged sample.[42] In addition, referring to the study of

MNGs with AFM, the semi-contact mode was used, being the optimum mode of operation for soft biomaterials since any problems caused by tip deformation are minimized in this mode.[43]

**Transmission Electron Microscopy (TEM).**

Samples of MNPs were prepared redispersing the MNPs in ethanol at a concentration of 0.33 mg/mL, after grinding the sample by using a mortar and pestle. Then, they were sonicated at low temperature in order to avoid overheating.

Two different preparation techniques were used for the samples of MNGs:

a. Samples of MNGs were dispersed in a buffer of pH 6 at a concentration of 0.05 mg/mL and sonicating for 1-1.5 h at low temperature, so as to avoid overheating. All the samples were placed onto a Formvar-coated copper grid, which has been previously hydrophilized by a glow discharge process and dried at room temperature.

b. Samples of MNGs were sonicated for 3 min at low temperature so as to avoid overheating, diluted to 0.05 wt% and placed in a carbon grid. Then, samples were rotated at 2,000 rpm for 120 s in order to dry quickly at room temperature by a spinning process (Spin Coater P6700, Specialty Coating Systems, Inc.).

TEM images were obtained by using a high-resolution transmission electron microscope (TECNAI G2 20 TWIN, 200 kV, filament LaB6).

**Energy-Dispersive X-ray Spectroscopy (EDS).**

Elemental analysis was performed by means of Energy Dispersive X-ray Spectroscopy (EDS). The built-in energy-dispersive X-ray ability of the Scanning Transmission Electron Microscopy (STEM) was used.

# 4.3. Results and discussion

## 4.3.1. Magnetic Nanoparticles (MNPs)

The co-precipitation method was used for the synthesis of the MNPs. Even though numerous methods have been established for the synthesis of MNPs of magnetite, the co-precipitation of iron salts is the common methodology used, being environmentally friendly, non-toxic, easy, economic, and scalable for bulk commercial applications.[44] As explained in the experimental part, different types of MNPs were synthesized as described in Appendix III. The characterization of these MNPs is also described in Appendix III.

## 4.3.2. Magneto-nanogels (MNGs)

### 4.3.2.1. MNGs through electrostatic interactions

As reported in literature, positively charged nanogels can be useful for the encapsulation of negatively charged inorganic nanoparticles.[31] In this work, MNGs were formed by loading negatively charged CA-MNPs into the positively charged PDEAEMA-based nanogels PM0, PM10, and PM20. The encapsulation of CA-MNPs into nanogels was carried out in a buffer solution of pH 6 at an ionic strength of 10 mM. These conditions were chosen in order to ensure maximum electrostatic interactions between CA-MNPs and nanogels. As can be observed in Figure 4.1, the surface of CA-MNPs was negatively charged and the one of nanogels was positively charged in almost all the pH range, but the maximum difference between the electrophoretic mobility values was given at pH 6, suggesting the strongest electrostatic interactions. Sauzedde *et al*.[45] used similar methodology for the encapsulation of MNPs on polymer latexes. Moreover, Tuncer *et al.*[46] reported the synthesis of a multi-responsive microgel with MNPs through electrostatic interactions between the different nanoparticles.

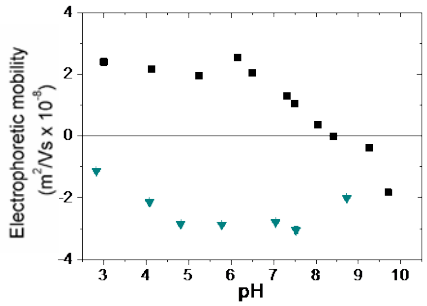


**Figure 4.1.** Electrophoretic mobilities of nanogel PM0 (■) and CA-MNPs (▼) as a function of pH at 25 °C and at an ionic strength of 10 mM.

In Figure 4.2, pictures of a bare nanogel, PM0 (a), and a magnetic nanogel, PM0m (b), are shown. As can be observed, the color of the dispersion changed due to the encapsulation of MNPs, which yielded a black-brownish dispersion. MNGs aqueous dispersion showed good colloidal stability: after several days staying at room temperature, only a very small amount of sediment was observed at the bottom of the glass container. This was likely an indication of the entrapment of MNPs within the polymer networks, confirming that the preparation of MNGs by electrostatic self-assembly was successful. As reported by other authors, this preparation method was simple and effective, and could be extended to other negatively charged nanoparticles.[31]

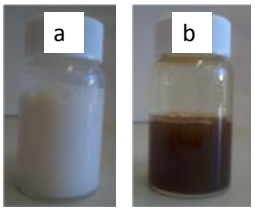


**Figure 4.2.** Pictures of nanogel PM0 (a) and MNG PM0m (b).

Once preparing the MNGs, different characterizations were carried out. The sensitivity of MNGs to pH and temperature was firstly analyzed in order to study the stimuli-responsive behavior.

As can be seen in Figure 4.3, all the nanogels were stable in all the pH range since no agglomeration was detected by PCS measurements,[47] except for pH 8, at which MNGs agglomerated. This agglomeration could arise from the decrease in charge of the particles. However, this could not be the only reason for the agglomeration, since it was only observed when MNPs were encapsulated into the nanogels. Before the encapsulation, nanogels were colloidally stable in all the pH range. Therefore, it can be said that it was promoted by the attractive magnetic forces between MNPs. Pich *et al.*[48] reported that some MNPs could be weakly connected to other MNGs, leading to the flocculation of hybrid nanogels.

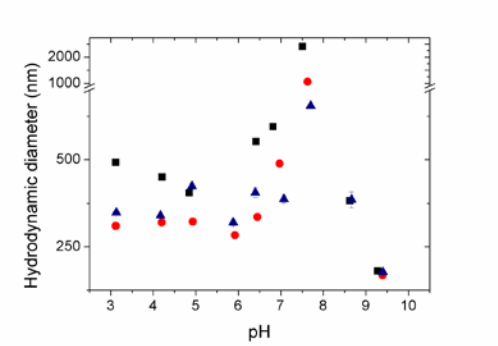


**Figure 4.3.** Hydrodynamic diameters of MNGs: PM0m (■), PM10m (●), and PM20m (▲) as a function of pH at an ionic strength of 10 mM.

In order to analyze the effect of MNPs absorption on the MNGs' pH-responsiveness, in Figure 4.4 the pH-dependences of the hydrodynamic diameters, swelling ratios, and electrophoretic mobilities of nanogel PM0 and the corresponding MNG PM0m, are shown.

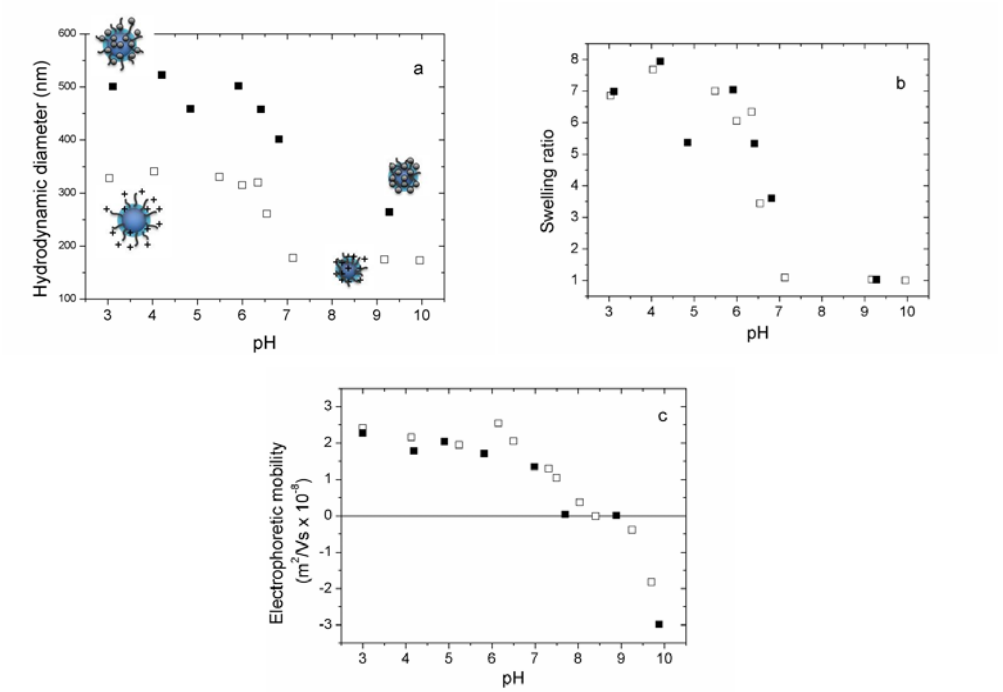


**Figure 4.4.** Hydrodynamic diameters (a), swelling ratios (b), and electrophoretic mobilities (c) of nanogel PM0 (□) and MNG PM0m (■) as a function of pH at an ionic strength of 10 mM.

It is noticeable the increase in size of the nanogel particles after the encapsulation of CA-MNPs. Several factors should be considered to analyze this effect. At a first stage, the nanogels were lyophilized, sonicated and redispersed. So as to see if these processes affected the final particle size, the temperature-dependences of hydrodynamic diameters of sample PM0 before and after the lyophilization process and sample PM0m dispersed at pH 6.4, were compared (see Figure 4.5). Nanogels were larger in size after the lyophilization process. But the encapsulation of MNPs also had an effect, increasing even more the size of the nanogel particles, likely because the repulsion forces between charged MNPs dominated. Backes *et al.*[49] also observed an increase in size of poly(*N*-isopropylacrylamide) (PNIPAM)-based microgels after the encapsulation of $CoFe_3O_4$ nanoparticles, due to the increase in the osmotic pressure inside the nanoparticles. Pich *et al.*[50] reported that since the distance between

nanoparticles included in microgels was small at large loading amounts, the repulsion forces between charged nanoparticles dominated, increasing the size of the composite microgels.

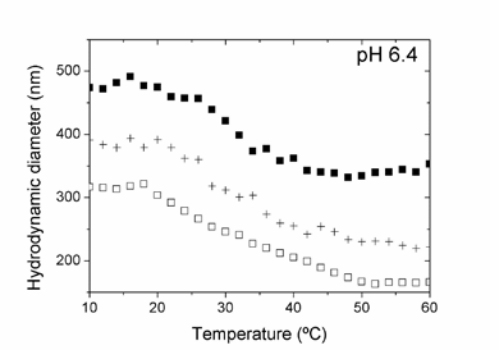


**Figure 4.5.** Hydrodynamic diameters of nanogel PM0 (before lyophilization) (□), after lyophilization (+), and MNG PM0m (■) dispersed at pH 6.4 as a function of temperature at an ionic strength of 10 mM.

However, surprisingly, the swelling curve of the MNG as a function of pH (Figure 4.4b) showed a similar trend to that of the empty nanogel particles, showing a broadening of the transition. This broadening could be explained by the higher heterogeneity of the MNGs than that of the nanogels. The increase in heterogeneity was also seen in the polydispersity index (PDI) values obtained by PCS measurements (data not shown). Anyway, these MNGs showed pH-sensitivity and a significant volume change useful for the release of drugs, if necessary.

Figure 4.4c shows that the electrophoretic mobility was not affected by the absorption of MNPs despite their negative charge: the electrophoretic mobility was positive in the acidic region, decreased at pH 6 due to the neutralization of amine groups, and the isoelectric point (IEP) was given at around pH 8. This observation could be understood in terms of the low contribution of MNPs to the electrophoretic mobility of the MNGs comparing to the one of PDEAEMA polymeric chains. MNPs incorporated into the nanogels did not contribute to the electrophoretic mobility and besides, the contribution of the MNPs located at the surface of the MNGs would be very low comparing to the one of positively charged PDEAEMA chains of the nanogel. This hypothesis will be confirmed after calculating the amount of charged groups coming from CA-coated MNPs and PDEAEMA polymeric chains.

Closer attention to Figure 4.4c indicates that the encapsulation of the MNPs made the IEP to shift to more acidic pHs. The reason for this variation could be the neutralization of some

cationic amine groups by the CA-MNPs. In this scenario, MNPs contributed decreasing the electrophoretic mobility.

Similar results and effects were observed in the case of PM10 and PM20 nanogels (see Figure 4.6).

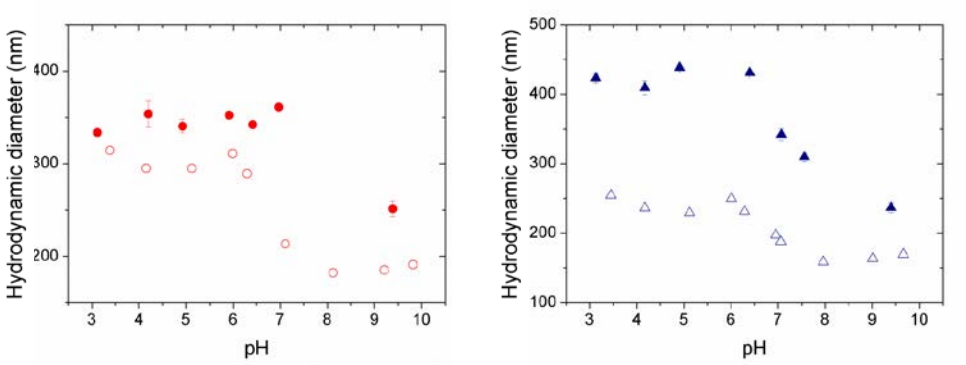


**Figure 4.6.** Hydrodynamic diameters of PM10 (○), PM10m (●), PM20 (Δ), and PM20m (▲) as a function of pH at an ionic strength of 10 mM.

With the aim of studying the response to temperature of the prepared MNGs, their swelling ratios dispersed in a buffer of pH 5.9 were calculated as a function of temperature by using equation 4.1 (see Figure 4.7). The first observation was that in spite of the encapsulation of MNPs, all the MNGs exhibited thermo-responsive volume phase-transitions. This means that besides the interaction of MNPs with the polymer chains of the nanogel, the polymer network still had enough freedom to swell and collapse in water at different temperatures. However, as expected, PEGMA affected the swelling-de-swelling behavior of the MNGs: the higher the concentration of the stabilizer used, the more hindered the chains' movement was, decreasing the ability to swell.

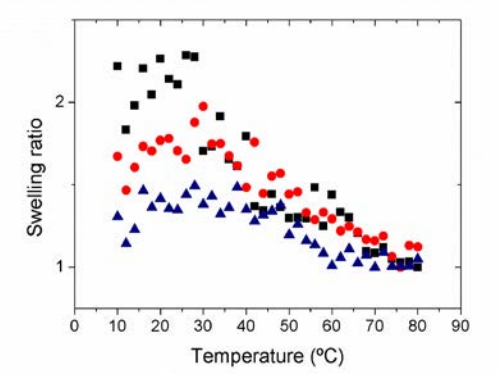


**Figure 4.7.** Swelling ratios of the MNGs PM0m (■), PM10m (●), and PM20m (▲) dispersed at pH 5.9 at an ionic strength of 10 mM as a function of temperature.

In addition, as explained in Chapters 2 and 3, pH is an important parameter controlling the hydrophilic/hydrophobic interactions' balance of the PDEAEMA-based nanogels. Thus, the thermal response of PM0m MNG was studied at different pHs, in order to distinguish clearly the influence of the charges originating from the protonation of amine groups on PDEAEMA chains. Figure 4.8a shows the thermo-sensitivity curves of PM0m MNG at pH 5.9 and 6.4. It was observed that the VPTT for the MNG shifted to lower values varying the pH from 5.9 to 6.4. Deprotonation of the amine groups resulted in the ability to form H-bonds with water molecules, which were weakened by increasing the temperature, causing the collapse of nanogels more easily. As expected, the thermo-sensitivity of PM10m and PM20m also showed similar pH-dependency (data not shown). These results confirmed the tunable and dual-stimuli-sensitive swelling-de-swelling behavior of the MNGs prepared through electrostatic interactions.

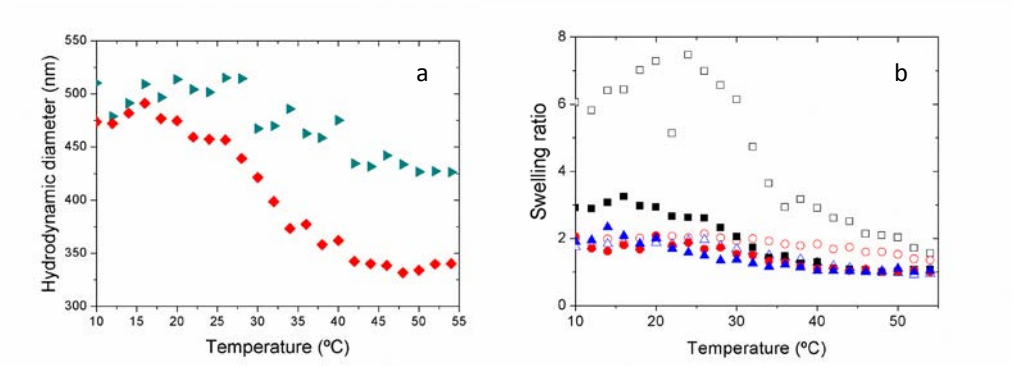


**Figure 4.8.** (a) Hydrodynamic diameters of PM0m MNG at pH 5.9 (▶) and pH 6.4 (♦) at an ionic strength of 10 mM as a function of temperature. (b) Swelling ratios of nanogels PM0 (□), PM10 (○), and PM20 (Δ) and MNGs PM0m (■), PM10m (●), and PM20m (▲) dispersed at pH 6.4 at an ionic strength of 10 mM as a function of temperature.

With the aim of studying the effect of MNPs' incorporation on thermo-sensitivity, the swelling ratios of the bare nanogels and those of the corresponding MNGs were plotted as a function of temperature (Figure 4.8b). Remarkable was the decrease in swelling ratio caused by the incorporation of MNPs in nanogel PM0. This could be caused by the physical barrier introduced by MNPs that hindered the polymer chains' movements, decreasing the swelling capacity. According to Rubio-Retama *et al*.,[51] this effect was attributed to the strong interactions between nanoparticles and polymer chains, increasing the rigidity of the polymer matrix. Regmi *et al*.[52] also observed a much smaller change in volume in the presence of MNPs due to the steric effects arising from the MNPs. On the other hand, the swelling ratio of the nanogels containing PEGMA was not almost affected by the encapsulation of MNPs. As observed in Chapter 3 (see Figure 3.4b), the swelling ratio of the nanogels with PEGMA was lower due to the PDEAEMA chain movement restriction. The slight effect produced by the encapsulation of the MNPs could be related to this low sensitivity.

Analyzing the results observed in Figure 4.8b, it is also interesting to note that the incorporation of magnetite influenced the transition temperature. As reported by Pich *et al*.,[48] there are two major different interactions within the nanogel network which influence the transition temperature in the opposite way. One is the strong interaction between magnetite and polymer network at low magnetite loads, which leads to lowering of the transition

temperature. The other is the dominant magnetite-magnetite interaction at higher loads of inorganic particles, which may shift the transition temperature to higher values, as additional energy is needed to overcome these interparticle forces inside the network. Since the VPTTs were shifted to lower values, interactions between MNPs and polymeric chains dominated. Boularas *et al.*[53] also reported a decrease in VPTT of oligo(ethylene glycol)-based hybrid microgels loaded with MNPs.

Moreover, the incorporation of MNPs into the nanogels structure had a strong influence on the particle morphology. Due to the inorganic load, MNGs were analyzed without any dye, the electronic contrast being already provided by MNPs. Figure 4.9a shows TEM microphotographs of the produced PM0m MNG. Taking into account that the dark regions are the MNPs,[54] TEM pictures reveal a relatively homogeneous distribution of the MNPs inside of the MNGs. In addition, it could be seen that MNPs were adsorbed on the shell of the nanogels and also encapsulated inside them. The microscopy images indicate that nearly all the magnetite particles were encapsulated into the nanogels and a small amount of free magnetite was located out of them. The presence of MNPs outside the nanogels could be justified considering that samples were sonicated for a long time (1-1.5 h) for the TEM observations. The drying process could result in a deformation and shrinkage of the nanogel particles, spreading the MNPs. The MNGs maintained a nearly spherical morphology despite the presence of the hard magnetite inclusions.

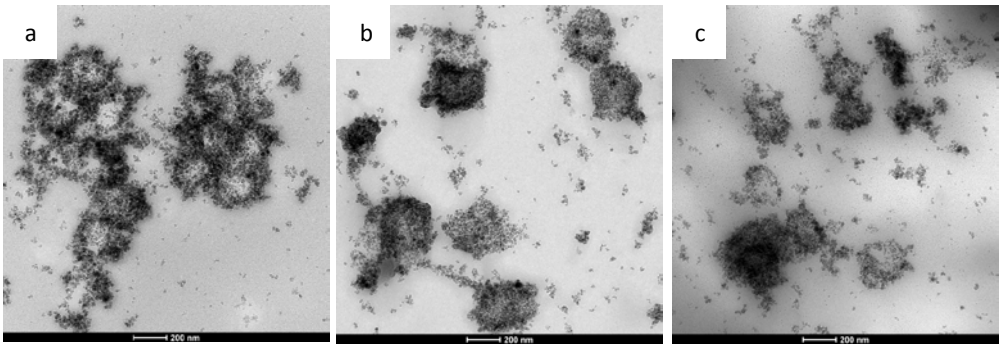


**Figure 4.9.** TEM microphotographs of PM0m (a), PM10m (b), and PM20m (c). Scale bar: 200 nm. TEM samples prepared by technique a.

Furthermore, TEM image in Figure 4.9a shows the formation of MNGs' agglomerates. This could arise from the magnetic interactions between the particles when drying at room temperature.[55] We assume that such agglomeration of MNGs occurred during water evaporation, as observed by Pich *et al*.[48] Furthermore, it is necessary to note that the TEM images were taken in the dry state of the samples provoking the shrinkage of the polymer network. Therefore, these sizes were not comparable with the sizes obtained by PCS in water.[48,56]

Figure 4.9(b,c) shows the TEM microphotographs of PM10m and PM20m MNGs. As can be seen, the morphology of these MNGs was also well defined, being spherical, uniform in size and loaded with MNPs. Comparing to the morphological characteristics of PM0m, it seemed that in this case the MNPs were mostly located on the surface of the nanogels, while in the nanogels containing PEGMA (PM10 and PM20), the MNPs were more prone to get inside the nanogels. This hypothesis could be understood in terms of the driving forces for the encapsulation: electrostatic interactions between positively charged nanogels and negatively charged MNPs. Taking this into account, it is foreseeable that the charge of the nanogels must affect the encapsulation. The encapsulation was carried out at a pH at which the cationic charge of PEGMA-containing nanogels was shielded by the PEGMA chains (see Figure 3.4c). In the case of PM0m, the more charged shell of PM0 is the reason why the MNPs were more prone to locate at the surface.

Moreover, AFM analysis of MNGs prepared was carried out. Firstly, a uniform and good distribution of the particles in the films was confirmed by OM. OM pictures of PM10m and PM20m films are shown in Figure 4.10.

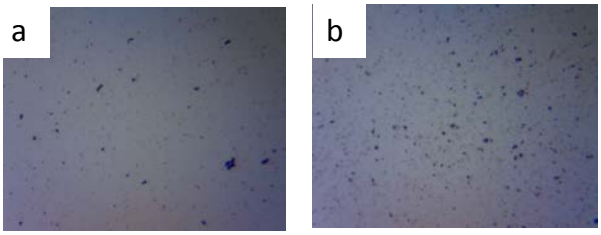


**Figure 4.10.** OM pictures (x 200, reflection mode) of PM10m (a) and PM20m (b).

Figure 4.11a presents an AFM image of the PM0m sample. It could be seen that some of the MNG particles (vertical white arrows) exhibited a dark core and a bright shell that referred to two different phases in respect to the viscoelasticity/adhesion/friction properties. We ascribed this feature to the presence of magnetite MNPs (hard phase denoted by the dark core) inside the MNGs (soft phase denoted by the bright shell).

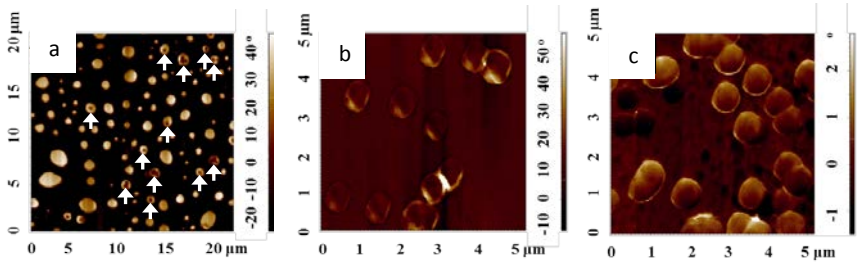


**Figure 4.11.** Representative AFM images ("phase signal") of MNGs PM0m (a, 20x20 µm$^2$), PM10m (b, 5x5 µm$^2$), and PM20m (c, 5x5 µm$^2$).

Figure 4.11 (b,c) shows AFM images ("phase signal") of PM10m and PM20m MNGs, respectively. Comparing to PM0m (Figure 4.11a), it seems that PM10m and PM20m MNGs were relatively single-phase, since it was difficult to distinguish the core-shell structure observed in a significant population of the PM0m particles. The reason for not distinguishing the magnetic part could be that MNPs were located inside the nanogel particles in the case of PM10m and PM20m. The hypothesis is confirmed after TEM images' observation, which was that PEGMA chains enhanced the encapsulation of MNPs inside the nanogels instead of locating them onto the surface.

In order to determine the magnetic content in the MNGs prepared, a TGA analysis was carried out. By using this technique, the polymer should be degraded completely when the temperature is high enough, but if there are inorganic materials in the sample, they should remain. Therefore, at the end of the TGA analysis, the residue obtained is only due to the inorganic material, in this case, the MNPs. Considering that the measurements were carried out under nitrogen atmosphere, no oxidation from $Fe_3O_4$ to $Fe_2O_3$ was expected (see Figure 4.12).

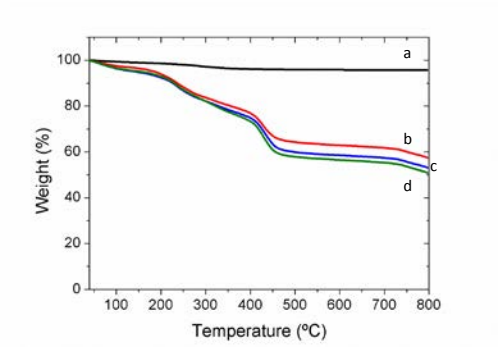


**Figure 4.12.** TGA curves of CA-MNPs (a), PM0m (b), PM10m (c), and PM20m (d).

CA-MNPs had little weight loss attributed to the decomposition of CA, whereas MNGs showed appreciable weight loss due to the degradation of PDEAEMA chains. Taking the content of CA grafted on MNPs into account, the amount of charges in moles per gram of $Fe_3O_4$ coming from MNPs could be calculated. Comparing with the amount of charged groups per weight of nanogel, it was obtained that approximately there were 10 times more charged groups coming from PDEAEMA chains. In this way, the hypothesis given to justify the unaffected electrophoretic mobility of the MNG PM0m (see Figure 4.4c) was corroborated, since the bare nanogels would have much higher contribution on the electrophoretic mobility comparing to the CA-MNPs.

Furthermore, the magnetic content in MNGs PM0m, PM10m, and PM20m was obtained from the values of the residual weight percentage: 57.4, 53.1, and 50.9 %, respectively. Even the differences were not remarkable, it can be said that increasing the amount of PEGMA the content of MNPs decreased. This could be explained by analyzing the synthesis strategy. The encapsulation of MNPs occurred through electrostatic interactions between positively charged nanogels and negatively charged MNPs. As explained in the experimental part, 0.01 g of nanogel was used to encapsulate the MNPs in all the cases. However, the amount of PDEAEMA chains and thus the charge density was affected by the amount of PEGMA used. In the presence of PEGMA, the relative amount of PDEAEMA chains was slightly lower, suggesting that the amount of charged groups would be lower increasing the concentration of PEGMA. This could be the reason why a slightly lower amount of magnetite was encapsulated in the nanogels containing PEGMA.

To examine the magnetic behavior of the MNGs synthesized, magnetic measurements were also carried out at 25 °C. The magnetic hysteresis loop in Figure 4.13 shows the response ability of CA-MNPs and PM0m to an external magnetic field. The magnetization curve of the PM0m clearly shows that the superparamagnetic behavior was kept even when the MNPs were incorporated into the nanogel, since no hysteresis was observed. As expected, due to the lower magnetic content, there was a decrease in saturation magnetization ($M_S$) from the pure MNPs (57.2 emu/g) to the MNG (40.4 emu/g). This decrease was in agreement with the magnetic loading obtained by TGA measurements (95.8 wt% for CA-MNPs and 57.4 wt% for PM0m).

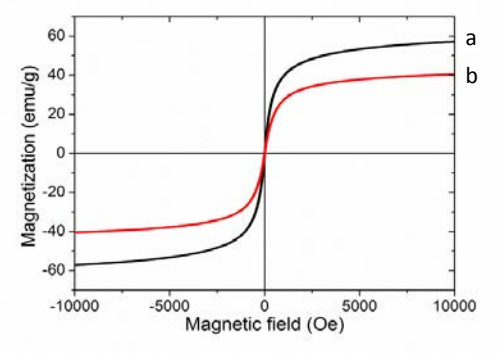


**Figure 4.13.** Magnetization curves of CA-MNPs (a) and PM0m (b) at 25 °C.

Furthermore, the magnetic response of the MNGs could be visually probed by using a magnet. Pictures in Figure 4.14 show the magnetic response of PM0m MNG, as it was attracted suddenly by the magnet, forming a film on the flask wall close to the magnet (see the arrow in Figure 4.14b). In addition, the MNGs were magnetized solely under the action of the external magnetic field losing their magnetization when it ceased to apply, confirming in this way their superparamagnetic behavior.

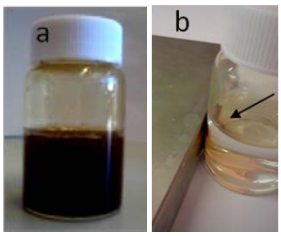


**Figure 4.14.** Sample PM0m dispersed in water (a) and attracted to a magnet (b).

*The content of this section was published in the Journal of Polymer Science, Part A: Polymer Chemistry **2015**, DOI: 10.1002/pola.27996.*

### 4.3.2.2. MNGs from primary amine-functionalized nanogels

It is well known that different strategies can be exploited so as to encapsulate inorganic nanoparticles into polymeric nanogels. However, among them, covalent linkage is perhaps the most appropriate and interesting procedure, since it enables a well-defined and more stable coupling between the particles, as reported in literature.[57-62]

Primary amine groups could provide to the nanogels new possibilities for additional interactions with MNPs. Therefore, primary amine-functionalized PDEAEMA-based nanogels described in Chapter 3 (see section 3.3.4.3., nanogel E0.93PM10AEMA) were used for the preparation of this family of MNGs, with the aim of strengthening the attachment of MNPs with the nanogels. In this Chapter, the nanogel is named AEMA. The recipes and preparation conditions of the MNGs are described in Table 4.2.

Two different MNGs were obtained. MNGs AEMAm1 and AEMAm2 were prepared by physically binding nanogel AEMA and CA-MNPs and by using 100 and 200 wt% of MNPs with respect to the nanogel weight, respectively.

One of the best methods for the formation of amide linkages between carboxyl and amine groups *via* carbodiimide activation is the use of EDC (*N*-(3-Dimethylaminopropyl)-*N*′-ethylcarbodiimide hydrochloride) and NHS (*N*-Hydroxysuccinimide).[63] Many authors have reported the use of EDC and NHS for the formation of hybrid particles through covalent bonding between MNPs and polymer chains.[57,64-67] The reaction mechanism is illustrated in Figure 4.15. As can be seen, EDC activates carboxylate groups, forming highly reactive and unstable intermediates. The addition of NHS stabilizes the amine-reactive intermediate by

converting it to an amine-reactive NHS ester, thus considerably increasing the efficiency of EDC-mediated coupling reactions. Then, primary amine attacks the carbonyl group of the NHS-ester, forming an amide group.

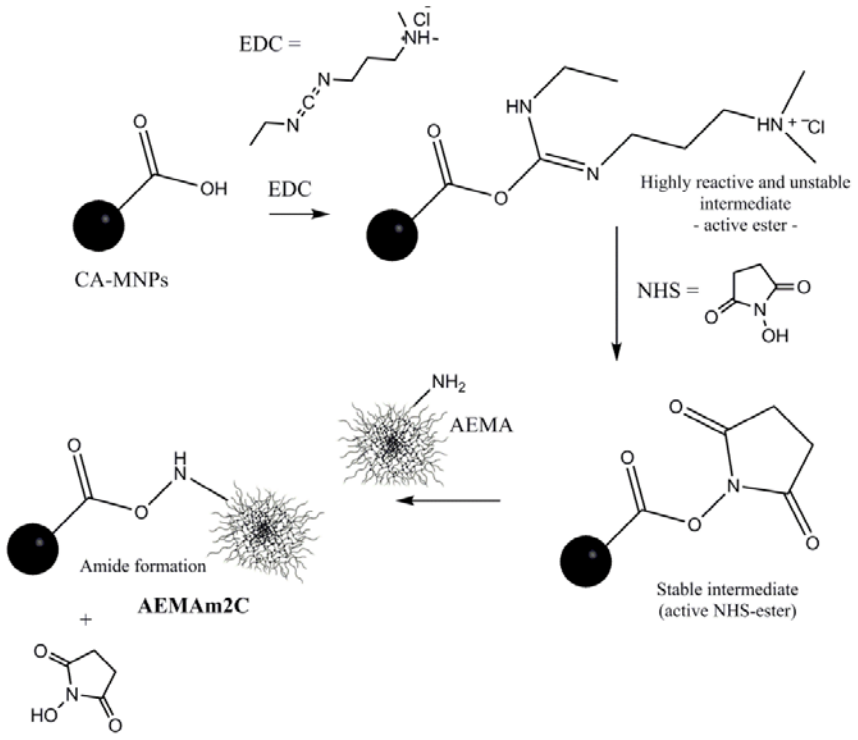


**Figure 4.15.** Reaction mechanism of the amide linkages formation between the primary amine groups of nanogel AEMA and carboxylate groups of CA-MNPs by using EDC and NHS.

Taking this into account, both particles types (MNPs and nanogel AEMA) were covalently linked through the amidation reaction between the carboxylic groups of CA-MNPs and primary amine groups of AEMA, by using EDC/NHS coupling, obtaining the MNG AEMAm2C.

When using EDC, the choice of pH for the coupling reactions is important since the coupling efficiency to carboxylic groups is affected by pH. The commonly reported optimal pH range for EDC is from 4 to 5. However, it has been shown that EDC is still effective in a pH

range of 6-8, even more in presence of NHS, which increases the efficiency of EDC-mediated coupling reactions.[64-66,68,69] In this work, pH 7 was used for the preparation of MNGs because deprotonated primary amine groups were needed to attack the carboxylic groups, and form the amide linkages.

Once the MNGs were prepared, their colloidal, morphological, thermogravimetric, and magnetic characteristics were investigated and compared.

Figure 4.16 shows the pH-sensitive swelling-de-swelling behavior of MNGs AEMAm1, AEMAm2, and AEMAm2C.

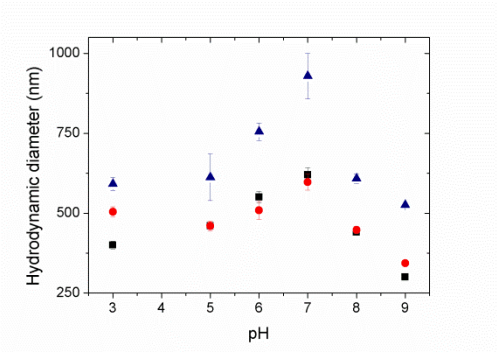


**Figure 4.16.** Hydrodynamic diameters of MNGs AEMAm1 (■), AEMAm2 (●), and AEMAm2C (▲) as a function of pH at an ionic strength of 150 mM.

The slight increase in hydrodynamic diameters of the MNGs at pH 7 could be attributed to the weakened electrostatic repulsions that caused the MNGs to agglomerate. This fact was confirmed by the low electrophoretic mobility values of the MNGs in the pH range of 6-7 shown in Figure 4.17. In addition, it has to be taken into account the high ionic strength (150 mM) used for the measurements. The presence of large amount of salts could cause both charge shielding and loss of steric stability due to shrinking of polymeric chains that act as stabilizer. Gui and Jin[28] reported that the addition of NaCl induced the shielding effect of the electrostatic stabilization in hybrid nanospheres with magnetic cores and thermo/pH-sensitive nanogel shells. The formation of agglomerates could also be elucidated in terms of the large amount of MNPs into the nanogels that could lead to colloidal destabilization of the system, as reported in literature.[70,71]

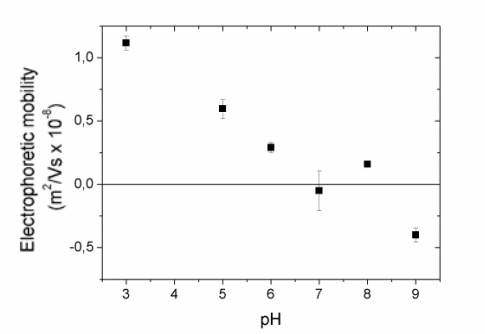


**Figure 4.17.** Electrophoretic mobilities of MNG AEMAm1 as a function of pH at an ionic strength of 150 mM.

Moreover, the morphological characterization of the MNGs was carried out. Figure 4.18 shows some TEM microphotographs of MNG AEMAm1. All the MNGs had a spherical shape and were monodisperse in size (80 nm, approximately). Remarkable was the absence of free MNPs outside MNGs, confirming the strong attachment of MNPs into the nanogel network. Moreover, MNGs with core-shell type morphology were obtained, in which almost all the MNPs was located inside the nanogels and there was no MNPs at the surface. Different sizes from the ones obtained by PCS measurements were expected since TEM images were taken in the dry state of the samples, and the polymer network shrank at these conditions.[50]

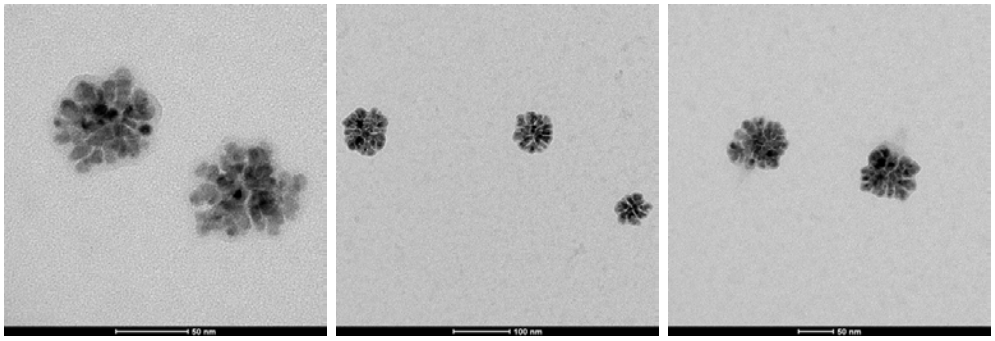

**Figure 4.18.** TEM microphotographs of MNG AEMAm1. TEM samples prepared by using technique b.

Figure 4.19 shows TEM microphotographs of MNG AEMAm2. MNGs had a spherical shape and were monodisperse in size (~ 200 nm). Interestingly, all of them contained MNPs, which were homogeneously dispersed into the nanogel particles and almost no unattached MNPs were observed outside the MNGs, confirming the strong attachment of the MNPs to the nanogel particles. Moreover, it seems that the amount of MNPs in each MNG particle was similar.

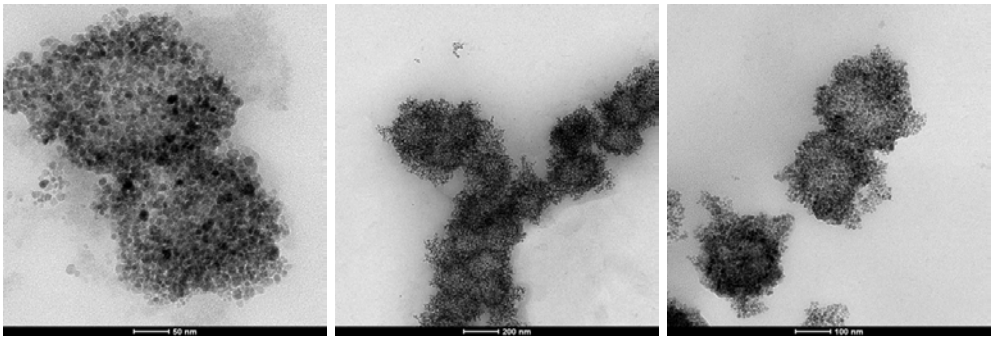

**Figure 4.19.** TEM microphotographs of MNG AEMAm2.
TEM samples prepared by using technique b.

Comparing to MNG AEMAm1 more MNPs were encapsulated into the nanogels, as larger initial amount of MNPs was used for the preparation. Attractive interactions between the MNPs provoked nanogels to agglomerate after the evaporation of water while preparing the samples for TEM measurements. This tendency was more pronounced since there were more MNPs. Even the size of AEMAm2 could not be exactly obtained from TEM images due to the agglomeration of MNG particles, it seemed that AEMAm2 was larger in size compared to AEMAm1. MNPs could make the water exclusion and the shrinking of MNG particles more difficult due to their rigidity, as reported by Fang *et al.*[72] in magneto-responsive nanocapsules. Moreover, in the case of AEMAm1 there were not any MNPs at the surface of the MNGs, while in the case of AEMAm2, MNPs were also found at the surface. In summary, larger amount of MNPs into the nanogels led to higher tendency to agglomerate, larger sizes, and different MNPs distribution.

To study the stability of the MNGs and specially the strength of the MNPs' attachment, samples were redispersed at different pHs (pH 7 and pH 3) and investigated by TEM (see

Figure 4.20 for MNG AEMAm2). MNPs remained attached to the nanogels even when they were redispersed at pH 3 but some MNPs were detached from the nanogel particles after redispersing the MNG sample at pH 7. The partial detachment of MNPs at pH 7 could be attributed to the weakened electrostatic attractive interactions between MNPs and nanogels due to the deprotonation of amine groups of PDEAEMA in the nanogel.

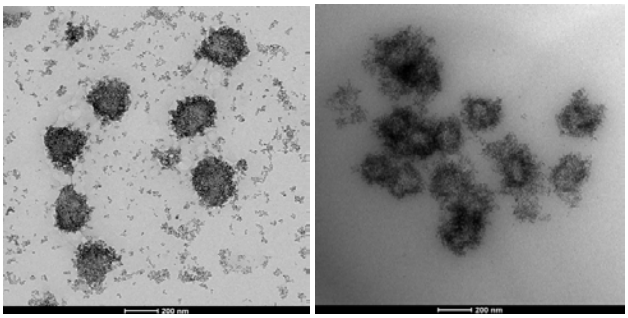

**Figure 4.20.** TEM microphotographs of MNGs AEMAm2 after redispersion at pH 7 (left) and at pH 3 (right). TEM samples prepared by using technique b.

As explained before, with the purpose of enhancing the attachment of MNPs, covalent bonding was aimed. For that, EDC/NHS coupling was used, obtaining MNG AEMAm2C (see TEM microphotographs in Figure 4.21). Large amount of MNPs was encapsulated into the nanogels. Comparing to the respective MNPs obtained without covalently coupling the MNPs (MNG AEMAm2), it seems that now the distribution of the MNPs was slightly more heterogeneous into the nanogels and that the tendency to agglomerate was also higher.

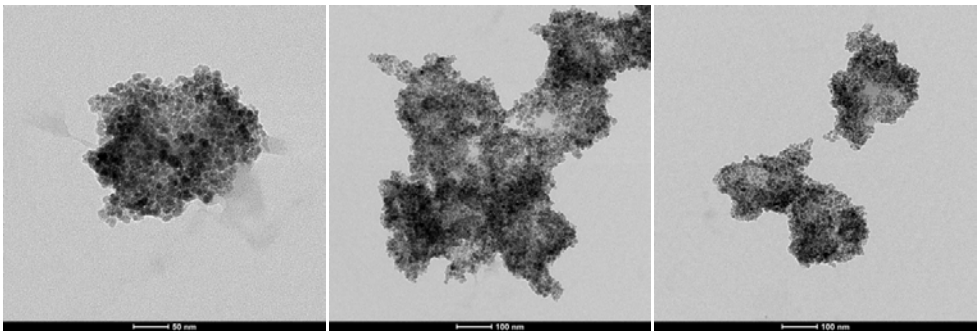

**Figure 4.21.** TEM microphotographs of MNG AEMAm2C. TEM samples prepared by using technique b.

In order to verify the attachment strengthening of MNPs to the nanogel through covalent bonding, MNG AEMAm2C was redispersed at different pHs and samples were observed by TEM (see Figure 4.22a and b for the sample redispersed at pH 7 and pH 3, respectively). MNPs remained inside the nanogels and they did not detach from the nanogels, confirming the formation of covalent bonding between MNPs and nanogels.

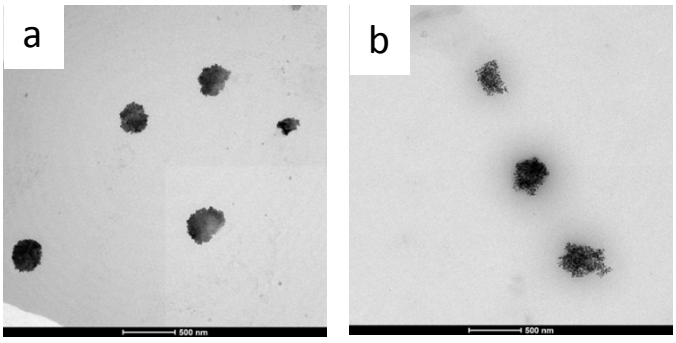


**Figure 4.22.** TEM microphotographs of MNGs AEMAm2C after redispersing at pH 7 (a) and pH 3 (b). TEM samples prepared by using technique b.

Moreover, the magnetic loading of MNGs could be quantified by TGA measurements. Figure 4.23 shows the TGA curves of CA-MNPs, and MNGs AEMAm1, AEMAm2, and AEMAm2C. All of them indicate high content of MNPs inside the MNGs: 60-70 wt%. In the case of AEMAm1, a value of 60 % was obtained, which was close to the amount of MNPs used for the preparation of MNGs (50 wt% with respect to the total amount). The slightly higher magnetic content than the used one means that MNGs were separated from some nanogels without any MNPs by using a magnet.

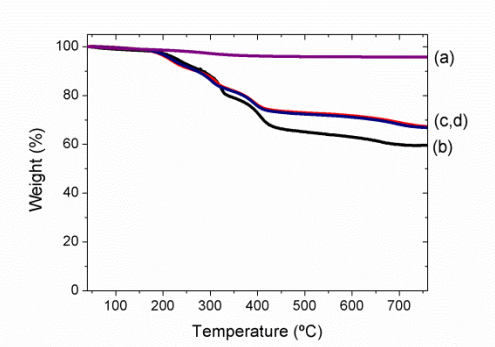


**Figure 4.23.** TGA curves of CA-MNPs (a), and MNGs AEMAm1 (b), AEMAm2 (c), and AEMAm2C (d) at 25 °C.

As expected, the inorganic content was higher increasing the initial amount of MNPs used for the preparation of MNGs. In the case of AEMAm2 and AEMA2C, an initial amount of 66.7 wt% of MNPs was used with respect to the total weight of the sample (200 wt% of MNPs with respect to the amount of nanogel, see Table 4.2), which was in accordance with the obtained magnetic loading of the MNGs. These results indicate that by adding 200 wt% of MNPs with respect to the weight of nanogel, the encapsulation was 100 % efficient, since all the MNPs were introduced in all the nanogel particles and undesirable bare nanogels were avoided.[73] Moreover, the addition of EDC and NHS did not affect the magnetic content, as can be observed in the TGA curves of AEMAm2 and AEMAm2C (Figure 4.23c and d).

In addition, the magnetic response of MNG AEMAm1 was studied by VSM measurements at 25 °C and compared with the magnetization results of CA-MNPs (see Figure 4.24). As expected, due to the lower magnetic content of AEMAm1 (60 wt%, see Figure 4.23), the value of $M_S$ (saturation magnetization) was lower than the one of the MNPs. Interestingly, the magnetization was not screened by the polymeric chains of the nanogel, since the superparamagnetic behavior of the MNPs remained after the encapsulation into the nanogel particles (neither remanence nor coercivity was observed in the magnetization curve) and $M_S$ directly depended on the magnetic content. Chen *et al.*[74] established a linear relationship between the amount of polymer coating and $M_S$ in PNIPAM-$Fe_3O_4$ hybrid microgels. Taking this and the $M_S$ values obtained for CA-MNPs and AEMAm1 into account, a $M_S$ of 43 emu/g for MNGs AEMAm2 was calculated.

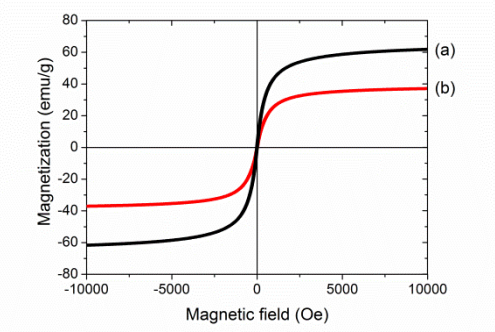


**Figure 4.24.** Magnetization curve of CA-MNPs (a) and AEMAm1 (b) at 25 °C.

The high sensitivity to external magnetic field could be confirmed visually by the instantaneous and full attachment of the MNGs to an external magnet (see Figure 4.25).

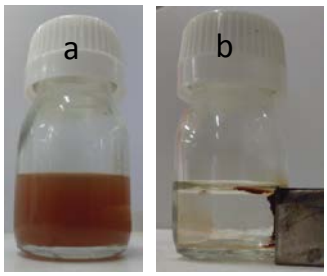


**Figure 4.25.** Sample of MNG AEMAm1 dispersed in water (a) and attracted to the magnet (b).

At this point, even though the method and nanogels used for the preparation of the MNGs were different, a quick comparison between the MNGs AEMAm1 and PM0m could be interesting, since the same initial amount of MNPs was used in both cases. Firstly, they did not differ in magnetic content (60 % approximately) and magnetic response ($M_S$ of 40 emu/g, approximately). However, even though the preparation techniques of the samples for TEM observations were different [see the different preparation techniques (a and b) in the experimental part], TEM images of both MNGs suggest that the attachment and encapsulation of MNPs was stronger in the case of AEMAm1. This fact was also visualized after the

centrifugation process, since no presence of MNPs was observed in the supernatant in the case of AEMAm1. There are two possible reasons to explain this observation.

The presence of primary amine groups could improve the attachment of MNPs into the nanogels, due to the higher possibility of primary amine groups to form H-bonds compared to the tertiary amine groups. As illustrated in the schematic representation of Figure 4.26, primary amine groups are able to form H-bonds from two hydrogen atoms, strengthening the attachment of MNPs to nanogel particles. Therefore, apart from the electrostatic interactions between the positively charged amine groups of PDEAEMA chains and negatively charged carboxylate groups of CA-MNPs, the H-bonds formed by the primary amine groups enhanced the encapsulation of MNPs into the nanogels.

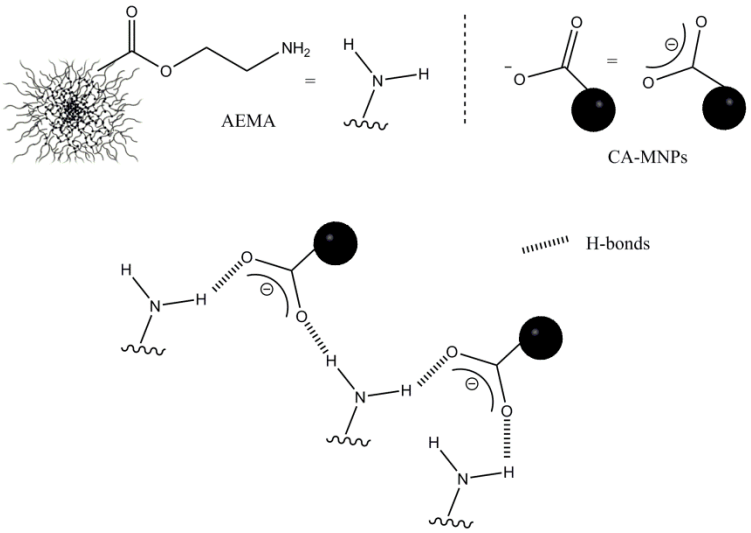


**Figure 4.26.** Schematic representation of possible H-bonds between primary amine groups of nanogel AEMAm1 and carboxylate groups of CA-MNPs.

The procedure to prepare the MNGs could also affect the interaction between MNPs and nanogel particles (see sections 4.2.3.1 and 4.2.3.2 for MNGs PM0m and AEMAm1, respectively). Briefly, the preparation of PM0m was carried out by sonicating both the CA-MNPs and the nanogel together for 30 min. However, in the case of AEMAm1, both CA-MNPs and nanogel (AEMA) were dispersed separately and then, both dispersions were mixed for one

hour. In the latter case, since they were dispersed in water before being in contact, they were prone to interact with each other, comparing to MNG PM0m where nanogels and the MNPs were mixed in solid state. In this way, together with the higher possibility of forming H-bonds due to the primary amine groups, the attachment was enhanced in the case of AEMAm1 comparing to that of PM0m.

#### 4.3.2.3. MNGs from epoxide-functionalized nanogels

As commented before, there are different strategies to incorporate inorganic nanoparticles into polymeric nanogels but the covalent linkage is the most appropriate to obtain stable coupling between them, as seen in the case of MNGs prepared from primary amine-functionalized nanogels.

Covalent linkage between the nanogels and MNPs was aimed also in the case of the third family of MNGs, but for that purpose epoxide-functionalized nanogels (GM10) and MNPs containing hydroxide groups at the surface were used. The reactions were carried out at pH 6 and pH 3, obtaining the MNGs named GM10m6 and GM10m3, respectively (see Table 4.3). The idea of using two different pHs was to optimize the preparation conditions.

Considering that nanogel GM10 is swollen at both pHs (see Figure 3.29), it could be said that the incorporation of MNPs into the nanogels was promoted in both cases. But the optimum pH for the reactions has to be also considered. According to the literature, the epoxide group of glycidyl methacrylate could react with hydroxide groups by two different mechanism routes: epoxide ring-opening and transterification.[75-77] Taking this into account, three different reaction mechanisms were expected for the reaction between the nanogel GM10 and uncoated MNPs, as depicted in Figure 4.27. The common reaction for an epoxide group with an alcohol is the epoxide ring-opening reaction, where a hydroxyl group attacks at the methylene carbon of the epoxide group, but it can also react with hydroxyl groups by the transterification route. Notwithstanding, in all the cases covalent bonds between nanogel particles and MNPs would be formed through the nucleophilic attack of the hydroxide groups. At pH 6, MNPs were expected to have stronger nucleophilicity because more hydroxide groups were deprotonated. Thus, the optimum pH for these reactions would be six. Comparing MNGs GM10m6 and GM10m3, and understanding the effect of the pH to prepare the MNGs, the role of the covalent binding on MNPs incorporation could be understood.

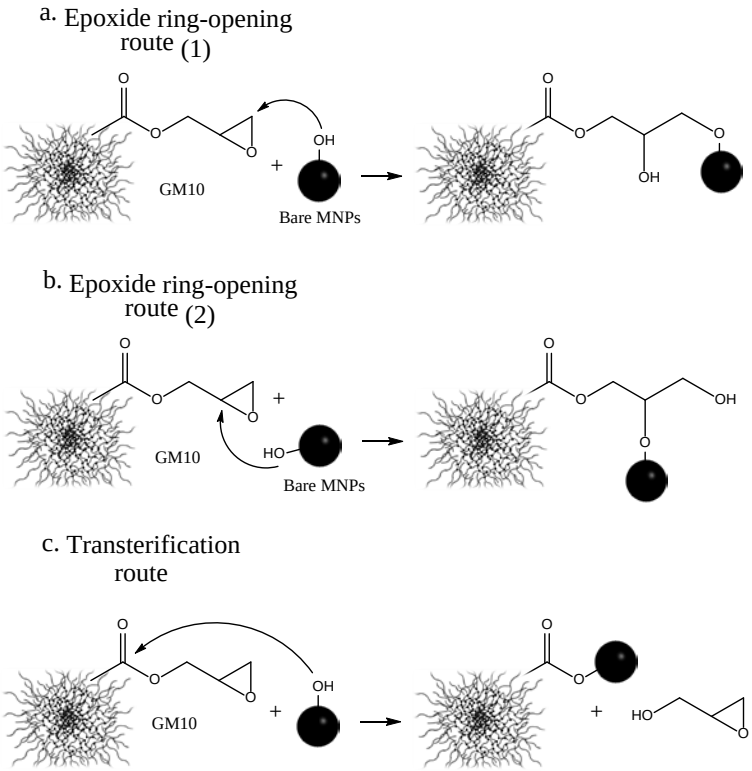


**Figure 4.27.** Scheme of the chemical reactions between the epoxide groups of nanogel GM10 and hydroxyl groups of the MNPs by way of epoxide ring-opening (a, b) and transterification (c) reaction mechanisms.

So as to confirm the covalent bonding between epoxide groups of GM10 and hydroxyl groups of the uncoated MNPs, FTIR analysis was carried out. FTIR spectra of nanogel GM10, MNPs, and MNG GM10m6 are shown in Figure 4.28, together with the magnified FTIR spectra in the range of 950-850 $cm^{-1}$. The comparison between the spectra of nanogel GM10 and MNG GM10m6 revealed the presence of MNPs in the MNG sample, due to the new peaks relative to MNPs of magnetite at 3400 $cm^{-1}$ (O-H v) and 590 $cm^{-1}$ (Fe-O v). Moreover, the disappearance of the peak at 910 $cm^{-1}$ relative to the epoxide group of the nanogel indicated that the reaction between epoxide groups of the nanogel particles and hydroxyl groups of the MNPs was successful.[78] The comparison between the spectrum of MNPs and the one of the MNGs

suggests the presence of polymeric chains based on P(DEAEMA-glycidyl methacrylate), since many new peaks appeared apart from the ones coming from $Fe_3O_4$ MNPs: at 2900 $cm^{-1}$ (C-H ν), at 1740$cm^{-1}$ (C=O ν), 1460 $cm^{-1}$ (C-H δ), 1400 $cm^{-1}$ ($CH_3$ δ), 1300-1250 $cm^{-1}$ (C-O-C asymmetric ν), 1160-1050 $cm^{-1}$ (C-O-C symmetric ν), and 1070 $cm^{-1}$ (C-N ν).[79,80]

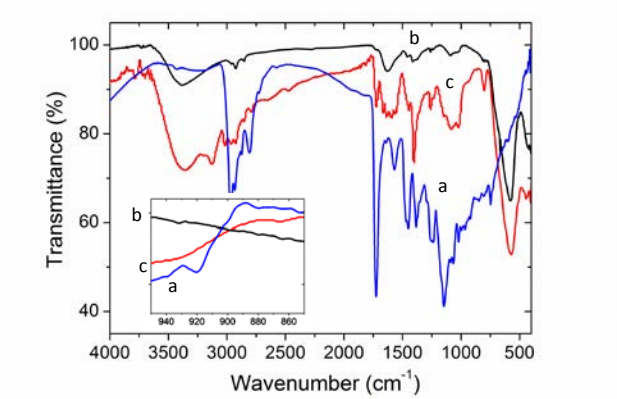


**Figure 4.28.** FTIR spectra of nanogel GM10 (a), MNPs (b), and MNG GM10m6 (c). Inset: magnified FTIR spectra in the wavenumber range of 950-850 $cm^{-1}$.

After confirming the reaction between MNPs and nanogel particles, the colloidal properties of the MNGs were characterized. Figure 4.29 shows the hydrodynamic diameters of GM10m6 and GM10m3 as a function of pH. The results of nanogel GM10 are also shown. It is noteworthy the high impact of the pH used in the preparation. In the case of GM10m6, the incorporation of magnetite into the nanogels did not affect the hydrodynamic diameters' values and pH-responsive swelling-de-swelling behavior, being swollen at acidic conditions and collapsing at around pH 7.5. Nevertheless, MNG GM10m3 did not show the typical pH-responsiveness: MNG particles agglomerated in the pH range of 5-8, and recovered their size at higher pHs (8-9). Related to these results, remarkable was the difference in polydispersity indices (PDIs) of the particle size distribution, being at around 0.25 and 0.4 for GM10m6 and GM10m3, respectively, which means that GM10m3 was more polydisperse in size than GM10m6.

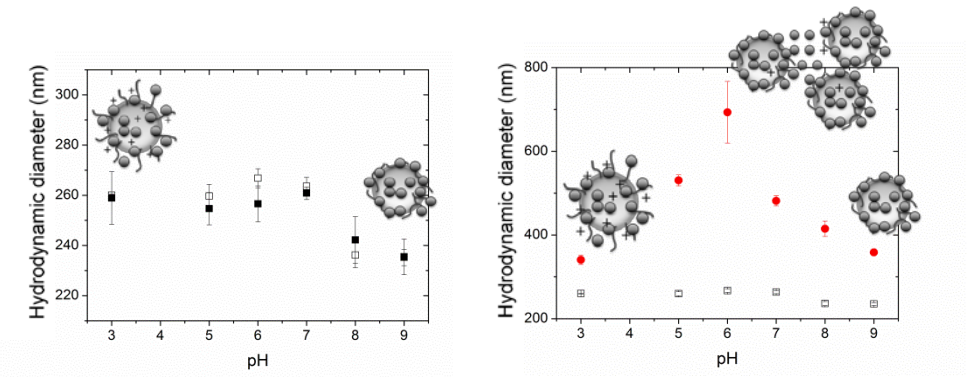


**Figure 4.29.** Hydrodynamic diameters of nanogel GM10 (□) and MNGs GM10m6 (■) and GM10m3 (●) as a function of pH at an ionic strength of 150 mM. Schematic representations of the MNGs are also shown.

The loading of a large amount of inorganic particles could influence over the interactions between polymer chains, reducing the colloidal stability of the system.[70,71] However, GM10m6 did not show any agglomeration in the pH range studied. The incorporation of MNPs into the nanogels could provoke charge shielding of the polymeric chains and weakening of electrostatic repulsions, resulting in MNGs agglomeration. Nevertheless, there must be additional reasons for the agglomeration of MNG GM10m3, since both nanogels showed very similar electrophoretic mobility values (see Figure 4.30), suggesting similar electrostatic stability. Backes *et al.*[49] also reported that there was not a simple relation between the electrophoretic mobility and interactions between $CoFe_2O_4$ nanoparticles and PNIPAM-based microgels. Pich *et al*.[50] also observed that the stabilization of composite microgels was not only given by an electrostatic mechanism.

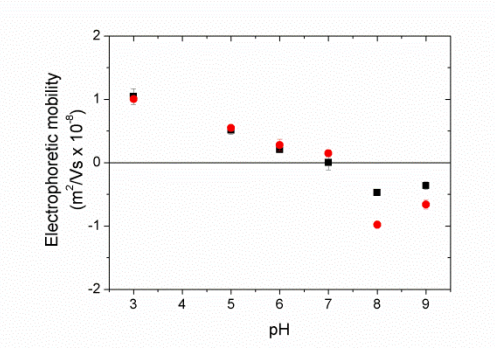


**Figure 4.30.** Electrophoretic mobilities of MNGs GM10m6 (■) and GM10m3 (●) as a function of pH at an ionic strength of 10 mM.

With the aim of understanding this behavior, the morphology of the MNGs was analyzed by TEM. The incorporation of MNPs into the nanogels forming MNGs GM10m6 and GM10m3 can be observed in the representative TEM microphotographs shown in Figures 4.31 and 4.32, respectively.

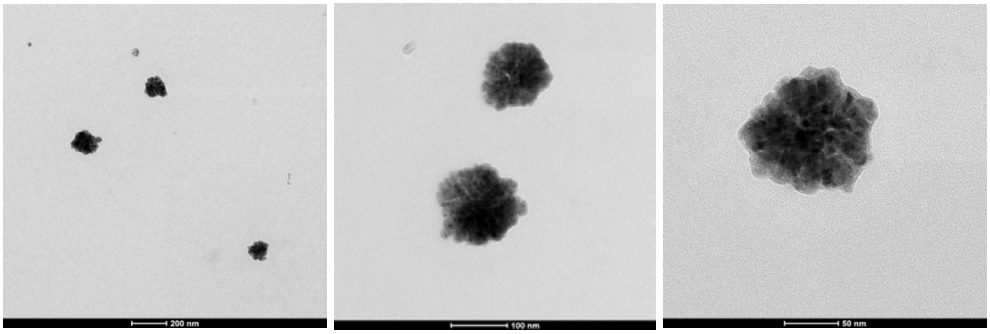

**Figure 4.31.** TEM microphotographs of GM10m6. TEM samples prepared by using technique b.

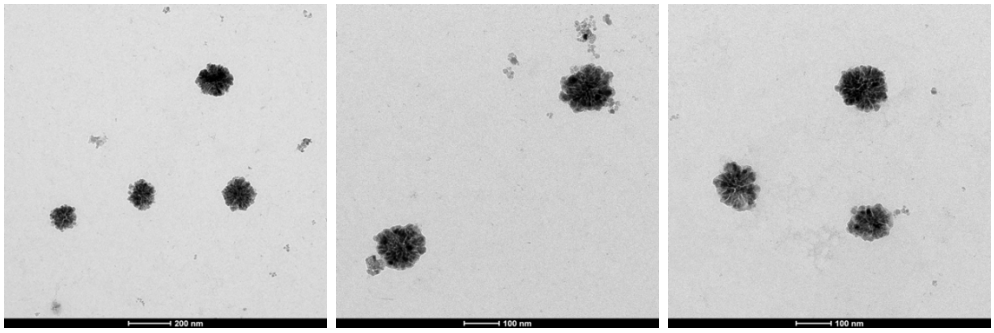

**Figure 4.32.** TEM microphotographs of GM10m3. TEM samples prepared by using technique b.

Both types of MNGs had a spherical shape with an average diameter of about 150 nm and MNPs were uniformly attached onto the surface and also located inside the nanogel particles. At first sight there was not any significant difference in morphology between both MNGs but the presence of a small part of MNPs outside the nanogel particles in the case of GM10m3 suggests a weaker attachment of MNPs onto the nanogels when the reaction was carried out at pH 3. This fact was also observed visually, since after the centrifugation process, more MNPs remained in the supernatant in the case of GM10m3: the non-covalently bound MNPs were mostly separated while centrifuging the sample, but some of them precipitated, as seen by TEM. The presence of those MNPs could be the reason for the agglomeration of MNGs prepared at pH 3.

Uncoated MNPs (free MNPs) are known to agglomerate due to van der Waals and dipole interactions between them, and also the high surface energy of the MNPs.[81-83] These interactions dominating between the weakly connected MNPs could be the responsible for enhancing the interactions occurring between individual MNGs GM10m3. Echeverria and Mijangos[84] also reported that MNPs provoked an increase in the interactions occurring between individual microgels, as a result of the magnetic forces between MNPs. Pich *et al.*[48] also described that at high magnetite content, MNPs that are weakly connected to the microgel or located beside the template lead to the flocculation of hybrid microgels. Moreover, the weakly attached MNPs could also cause the compression of the chains that stabilize the nanogel particles, leading to the agglomeration of MNGs. This idea was reported by Pich *et al.*[50] with high loading of polypyrrole particles in microgels based on poly(*N*-vinyl caprolactam-*co*-acetoacetoxyethylmethacrylate).

However, in the pH range of 8-9, MNPs were negatively charged, enhancing the electrostatic repulsive interactions between MNGs and weakly connected MNPs. Also, being more hydrophilic, they had lower tendency to agglomerate and the interactions between MNPs became weaker. Because of the separation of single MNG particles, the average hydrodynamic diameters decreased.

The pH-dependent behavior of GM10m3 is schematized in Figure 4.33. Electrostatic repulsions between MNGs dominated in the pH range of 3-5 and MNGs were separated from one another. In the pH range of 5-8, MNGs formed agglomerates because of the weaker electrostatic repulsions between MNGs along with the attractive interactions between weakly attached MNPs and their tendency to agglomerate. Meanwhile, at pH 8-9, MNGs were separated from each other, since the attractive interactions between MNPs became weaker.

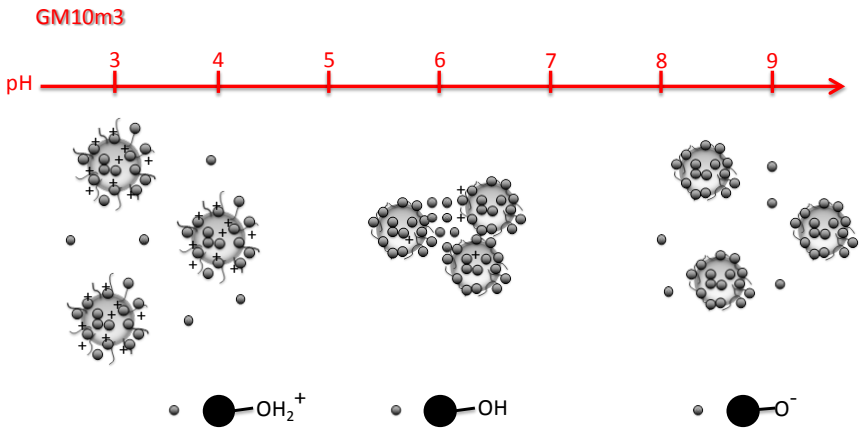


**Figure 4.33.** Schematic representations of MNG GM10m3 and an uncoated MNP at different pH ranges.

Nevertheless, in the case of preparing the MNGs at pH 6, it seems that MNPs were covalently bound to the nanogel particles, and so, the attractive interactions were screened by the polymeric chains. The interactions, being weaker, were not sufficient to provoke agglomeration of individual MNGs. Even the high magnetic content in the nanogels provoked charge shielding in both cases, the presence of weakly attached MNPs led to the agglomeration of MNGs in the case of using pH 3 for their preparation.

Moreover, the magnetic loading of the MNGs can be quantified by TGA measurements. As can be seen in the TGA curves shown in Figure 4.34 (left), the magnetic contents in MNGs GM10m6 and GM10m3 were found to be 61 and 41 wt%, respectively, being highly satisfactory values for easy separation by a magnet.[85] These results indicate that the optimum pH for the preparation of MNGs was six. Both magnetic content values were close to the amount of MNPs used for the preparation of MNGs (50 wt%) but some differences have to be mentioned. In the case of GM10m6, the nanogels without any MNPs were separated from the MNGs by using a magnet as larger amount of magnetite than the initial one was obtained. However, in the case of GM10m3, some MNPs were not encapsulated into the nanogels, since the final amount of MNPs was lower than the initial one. The lower encapsulation of MNPs inside the nanogel particles at pH 3 was observed on sight while centrifuging the samples, since some MNPs remained in the supernatant.

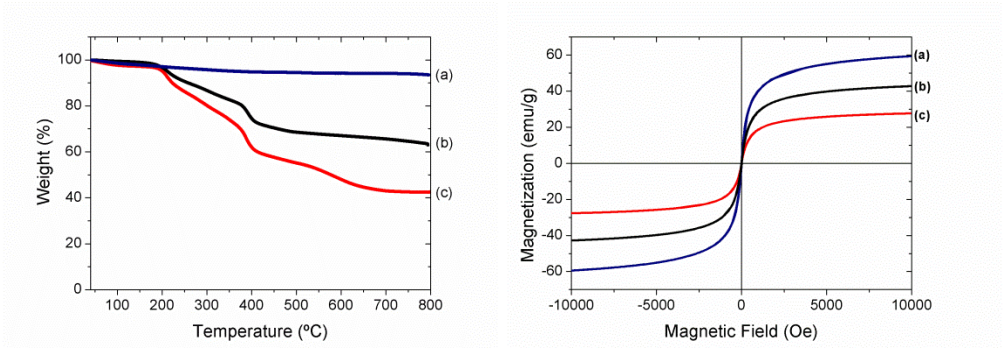


**Figure 4.34.** TGA (left) and magnetization (right) curves of the MNPs (a) and MNGs GM10m6 (b) and GM10m3 (c).

Furthermore, with the aim of studying the magnetic response of the MNGs obtained, their magnetization was measured by VSM at 25 °C. Figure 4.34 (right) shows the magnetic hysteresis loops of uncoated MNPs, and MNGs GM10m6 and GM10m3. Even though both MNGs showed lower $M_S$ values than the MNPs due to the contribution of the non-magnetic part (nanogel GM10), they showed high enough Ms values, as required for biomedical applications.[86-88] These values were higher than those reported in the literature for magneto-nano/microgels.[47,62,63,74,89] Relatively high magnetization values means that the procedure

described for the preparation of MNGs was successful for the encapsulation of a relatively high fraction of MNPs into the PDEAEMA-based nanogels.

The magnetization results could be related to the TGA measurements, as previously explained.[74] Considering that MNPs had 94 wt% of inorganic content and a $M_S$ of 60 emu/g, magnetization values for the MNGs containing 61 (GM10m6) and 41 wt% of MNPs (GM10m3) were calculated to be 38 and 26 emu/g, respectively, which were close to the obtained $M_S$. Since the expected $M_S$ values of the MNGs considering their magnetic content were in good agreement with the measured values, a linear relationship between the magnetic content and $M_S$ of the MNGs was confirmed also in this case. The fact that the magnetic properties were maintained even after the encapsulation, *i.e.*, the polymer chains did not shield the magnetic properties of MNPs, suggests that the MNPs were highly exposed to the surface.[90]

These results indicate that the covalent linkage did not provoke any loss of the magnetization, supporting that the covalent binding is the best option for the incorporation of MNPs into the nanogels. These results also suggest that the magnetic properties would not be affected by the covalent binding to the nanogels neither in the case of MNG AEMAm2C.

Concerning the *in vitro* and *in vivo* applications, the superparamagnetic behavior of the MNGs is critical, since they do not retain any magnetism and can be redispersed after removal of magnetic field. The MNGs prepared exhibited superparamagnetic properties, as evidenced by the zero coercivity and remanence on the magnetization loops at low applied magnetic field (see Figure 4.34).[86,91,92]

The magnetic properties were also demonstrated by using a magnet. Figure 4.35 illustrates the magnetic response of MNGs GM10m3 and GM10m6. MNGs were attracted suddenly by the magnet, forming a film on the flask wall close to the magnet. In agreement with VSM results, the sample GM10m6 was approached more quickly to the magnet, leading to a more transparent dispersion due to its higher magnetic response.

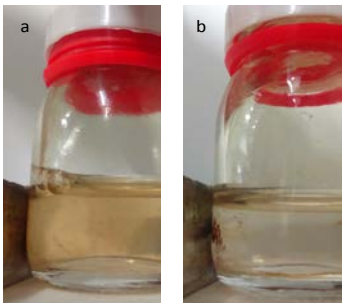


**Figure 4.35.** Samples GM10m3 (a) and GM10m6 (b) attracted to the magnet.

At this point it should be highlighted the importance of the pH on the preparation of the MNGs, since much higher content of MNPs was incorporated when the reaction was carried out at pH 6 comparing to pH 3. Undoubtedly, the optimum pH for the preparation of MNGs was six. Different aspects have to be considered for the understanding of this result.

It is well known that magnetite ($Fe_3O_4$) can suffer from oxidation at acidic conditions, forming maghemite ($\gamma Fe_2O_3$):[93]

$$Fe_3O_4 + 2H^+ \rightarrow \gamma Fe_2O_3 + Fe^{2+} + H_2O$$

Even though the reaction was carried out under nitrogen atmosphere, first of all, to confirm that the MNPs of magnetite $Fe_3O_4$ did not suffer from oxidation at the reaction conditions used, the obtained MNPs were dispersed at pH 6 and pH 3, stirred for 12 h at 50 °C simulating the reaction conditions, and analyzed by XRD. Figure 4.36 shows the XRD patterns of the MNPs without any treatment (a), MNPs after 12 h dispersed at pH 3 (b), and MNPs after 12 h dispersed at pH 6 (c). The comparison between all the XRD patterns confirmed that MNPs of magnetite maintained their structure and did not suffer from oxidation at the reaction conditions used. From the absence of (219) and (300) peaks in the XRD pattern, it could be stated that the magnetite was not oxidized to maghemite.

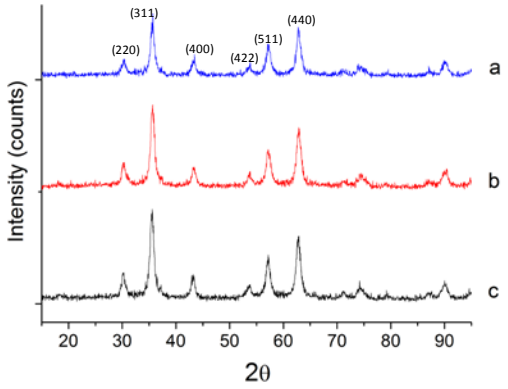


**Figure 4.36.** XRD patterns of the uncoated MNPs without any treatment (a), dispersed at pH 3 (b), and dispersed at pH 6 (c) for 12 h at 50 °C.

Therefore, with the aim of understanding the difference in magnetic content between both MNGs, aspects such as the preparation methodology, the interactions between the different nanoparticles, and the reaction mechanisms must be considered.

At a first stage, being the mixing of the different nanoparticles for the subsequent reactions compulsory, the water dispersibility of MNPs could have an effect. Magnetite is an amphoteric solid that can be subjected to changes in surface charge upon varying the pH, as explained in Appendix III. At low pH values, the surface of the MNPs becomes protonated and hydrophobic, whereas at high pH values, negative charges are generated onto the surface, rendering them hydrophilic. On the basis of the aforementioned, a hydrophilic surface could enhance the dispersibility and availability in water of MNPs. This could be one possible reason for obtaining higher inorganic content in the case of preparing the MNGs at pH 6, as the interaction with nanogels and the encapsulation are more favorable.[94]

The interactions between MNPs and nanogels had to be also considered. Even though nanogel particles GM10 were swollen and positively charged at both pH values (see Figure 3.29), the electrophoretic mobility values and pH/α curve (Figures 3.51 and 3.52, respectively) suggest that the surface of the nanogel particles dispersed at pH 6 was less positively charged comparing to the ones dispersed at pH 3. On the other hand, the protonation of hydroxide groups was less pronounced at pH 6, being its IEP at pH 7 (see Appendix III). Thus, weaker electrostatic repulsions between MNPs and GM10 were expected at pH 6, implying a lower

hindrance to the interaction between them. Sauzedde *et al.*[45] concluded that the adsorption of MNPs onto various cationic latexes was limited by repulsive interactions between them. Zhang *et al.*[57] also reported the importance of the electrostatic interactions and surface properties between microspheres and MNPs, affecting the combination between two types of particles for further covalent bonding.

Apart from the interactions between the different nanoparticles, the reaction mechanisms for the covalent bonding must be studied in depth. As explained before, the reaction was based on the nucleophilic attack of the hydroxide group of uncoated MNPs to the epoxide-containing groups of GM10 (electrophile). It is well known that the nucleophilicity increases with the electron intensity, because a nucleophilic attack is given through unpaired electron pairs. Taking these concepts into account, the protonated hydroxide is not able to act as a nucleophile, while hydroxide groups in form of (-OH) and ($-O^-$) can attack an electrophile. Being larger the amount of the latter at pH 6, the reaction was more favorable, leading to the encapsulation of larger amount of MNPs. In this way, the role of the covalent bonding on the encapsulation was confirmed.

Zhang *et al*.[57] also reported the role of the pH on the preparation of magnetic P(NIPAM-*co*-acrylic acid) microcontainers. In that case, the amino-modified $Fe_3O_4$@$SiO_2$ particles could not be assembled onto the surface of the core/shell microspheres at pH 9 due to the electrostatic repulsions between the two particles and the unsuccessful amide formation, but the assemblies could be formed at pH 6. Differences in magnetic properties have been also observed by other authors by varying the pH of the preparation of composite and hybrid particles, since the pH strongly influenced the efficacy and rate of the chemical reactions.[95-98]

The interaction between MNPs and nanogels was easier at pH 6 due to the higher dispersibility of MNPs in water and weaker repulsive electrostatic repulsions between them. Apart from this, as the nucleophilicity of the MNPs was stronger at pH 6, the formation of covalent bonding was more favorable, demonstrating that the optimum pH for the preparation of MNGs from epoxide-functionalized nanogels was six.

## 4.4. Conclusions

In this Chapter, the incorporation of MNPs into the previously synthesized dual-stimuli-responsive PDEAEMA-based nanogels yielding multi-responsive MNGs is described. For that

purpose, different preparation methods were used and a variety of magnetic-labelled nanogels' families were obtained. They were thoroughly characterized by means of their colloidal, morphological, thermogravimetric, and magnetic properties.

The preparation of the first family of MNGs was carried out by incorporating CA-coated MNPs into PEGylated PDEAEMA-based nanogels taking advantage of electrostatic interactions. The MNGs obtained were found to undergo significant pH- and thermo-responsive volume changes as well as showing high magnetic response. Their preparation is schematically represented in Figure 4.37.

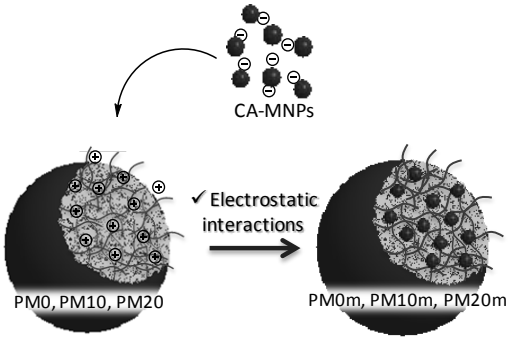


**Figure 4.37.** Schematic representation of the formation of MNGs PM0m, PM10m, and PM20m by means of the electrostatic interactions between CA-MNPs and PDEAEMA-based nanogels.

The second family of MNGs was prepared by encapsulating different concentrations of CA-coated MNPs into primary-amine functionalized PDEAEMA-based nanogels. Superparamagnetic MNGs with high magnetic loading and magnetizations were obtained also in this case. Even some agglomeration was observed in the pH range from 7 to 8 due to the large amount MNPs, the attachment of MNPs to the nanogel particles was strengthened because of the presence of primary amine groups in the nanogels able to form H-bonds with the MNPs. Some MNGs were also obtained by covalently binding the MNPs to the nanogels, strengthening even more the attachment. The preparation of MNGs from primary amine-functionalized nanogels is represented in Figure 4.38.

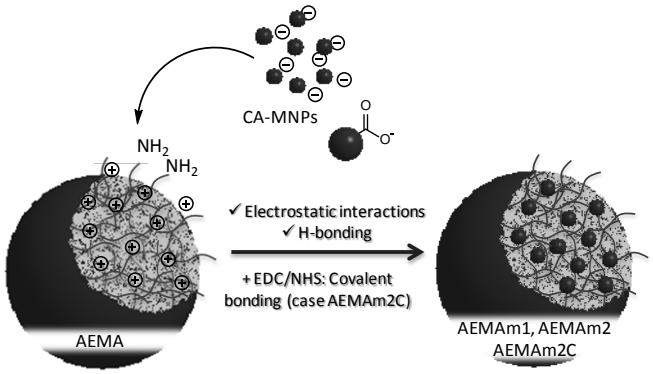


**Figure 4.38.** Schematic representation of the formation of MNGs AEMAm1, AEMAm2, and AEMAm2C by means of electrostatic interactions, H-bonding, and covalent bonding between CA-MNPs and primary amine-functionalized PDEAEMA-based nanogels.

The third family of MNGs was prepared by binding uncoated MNPs to the previously synthesized epoxide-functionalized PDEAEMA-based nanogels. Two different pHs were used for the preparation of the MNGs so as to optimize the reaction conditions, giving the opportunity to understand the attachment of MNPs to the nanogels. First of all, the formation of covalent bonding between the MNPs and nanogel particles was confirmed by FTIR analysis. The magnetic loading and thereby the magnetic response were found to be much higher when a pH of 6 was used for the preparation. This result was attributed to the favoured reactions between epoxide and hydroxide groups at pH 6, as well as the easier interaction between the different nanoparticles due to the weaker repulsive interactions and higher dispersibility of MNPs in water at pH 6. These MNGs showed the typical pH-responsiveness together with high magnetic response and superparamagnetic behavior. Figure 4.39 represents the preparation of this family of MNGs.

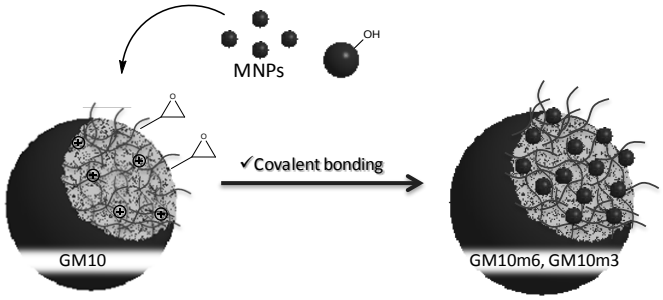


**Figure 4.39.** Schematic representation of the formation of MNGs GM10m3 and GM10m6 by means of covalent bonding between uncoated MNPs and epoxide-functionalized PDEAEMA-based nanogels.

In summary, syntheses and characterizations of a series of new dual-stimuli-responsive MNGs were reported in this Chapter. Owing to both the stimuli-responsive behavior together with the high magnetic response of magnetic nanoparticles, the resultant hybrid nanogels exhibit such advantageous features for biomedical applications such as stimuli-mediated MRI, hyperthermia, magnetically guided controlled drug delivery, and cellular uptake, among others. Figure 4.40 summarizes the properties of the MNGs prepared.

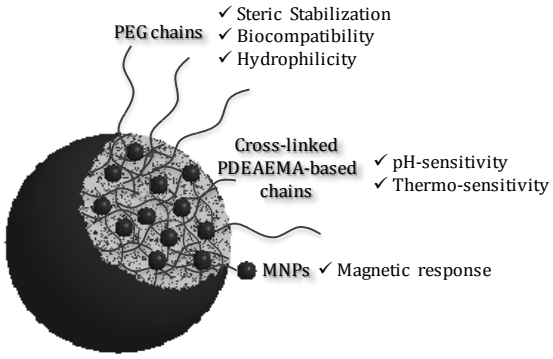


**Figure 4.40.** Schematic representation that summarizes the properties of the MNGs prepared.

Although the evaluation of the *in vitro* and *in vivo* performance of MNGs against tumor growth is obviously required, this work demonstrates the great potential of the MNGs obtained as a theranostic system.

## 4.5. References


1. R. Ladj, A. Bitar, M. M. Eissa, H. Fessi, Y. Mugnier, R. Le Dantec, A. Elaissari, *Int. J. Pharm.* **2013**, *458*, 230-241.
2. B. Sierra-Martin, A. Fernandez-Barbero, *Soft Matter* **2015**, *11*, 8205-8216.
3. R. Contreras-Cáceres, S. Abalde-Cela, P. Guardia-Girós, A. Fernández-Barbero, J. Pérez-Juste, R. A. Alvarez-Puebla, L. M. Liz-Marzán, *Langmuir* **2011**, *27*, 4520-4525.
4. V. Fischer, M. B. Bannwarth, G. Jakob, K. Landfester, R. Muñoz-Espí, *J. Phys. Chem. C* **2013**, *117*, 5999-6005.
5. H. Wang, J. Yi, S. Mukherjee, P. Banerjee, S. Zhou, *Nanoscale* **2014**, *6*, 13001-13011.
6. M. J. Sailor, J.-H. Park, *Adv. Mater.* **2012**, *24*, 3779–3802.
7. R. A. Revia, M. Zhang, *Mater. Today* **2015**, DOI: 10.1016/j.mattod.2015.08.022.
8. M. Mahdvai, M. B. Ahmad, M. J. Haron, F. Namvar, B. Nadi, M. Z. A. Rahman, J. Amin, *Molecules* **2013**, *18*, 7533-7548.
9. B. Issa, I. M. Obaidat, B. A. Albiss, Y. Haik, *Int. J. Mol. Sci.* **2013**, *14*, 21266-21305.
10. M. Colombo, S. Carregal-Romero, M. F. Casula, L. Gutiérrez, M. P. Morales, I. B. Böhm, J. T. Heverhagen, D. Prosperi, W. J. Parak, *Chem. Soc. Rev.* **2012**, *41*, 4306-4334.
11. S. Bucak, B. Yavuztürk, A. D. Sezer, *Magnetic Nanoparticles: Synthesis, Surface Modifications and Application in Drug Delivery* In *Pharmacology, Toxicology and Pharmaceutical Science, Pharmacology, "Recent Advances in Novel Drug Carrier Systems"*, Eds. A. D. Sezer, ISBN 978-953-51-0810-8, DOI: 10.5772/52115, **2012**.
12. A. Aggarwal, P. Chhajer, S. Maheshwari, *Int. J. Pharm. Sci. Res.* **2012**, *3*, 4670-4680.
13. M. Mahmoudi, S. Sant, B. Wang, S. Laurent, T. Sen, *Adv. Drug Delivery Rev.* **2011**, *63*, 24-46.
14. J. Estelrich, E. Escribano, J. Queralt, M. A. Busquets, *Int. J. Mol. Sci.* **2015**, *16*, 8070-8101.

15. Y. Gong, M. Fan, F. Gao, J. Hong, S. Liu, S. Luo, J. Yu, J. Huang, *Colloids Surf., B* **2009**, *71*, 243-247.
16. H. M. Kim, Y.-W. Noh, H. S. Park, M. Y. Cho, K. S. Hong, H. Lee, D. H. Shin, J. Kang, M.-H. Sung, H. Poo, Y. T. Lim, *Small* **2012**, *8*, 666-670.
17. C. Sanson, O. Diou, J. Thévenot, E. Ibarboure, A. Soum, A. Brûlet, S. Miraux, E. Thiadière, S. Tan, A. Brisson, V. Dupuis, O. Sandre, S. Lecommandoux, *ACS Nano* **2011**, *5*, 1122-1140.
18. D. Hao, T. Ai, F. Goerner, X. Hu, V. M. Runge, M. Tweedle, *J. Magn. Reson. Imaging* **2012**, *36*, 1060-1071.
19. W. Xu, K. Kattel, J. Y. Park, Y. Chang, T. J. Kim, G. H. Lee, *Phys. Chem. Chem. Phys.* **2012**, *14*, 12687-12700.
20. A. Curcio, R. Marotta, A. Riedinger, D. Palumberi, *Chem. Commun.* **2012**, *48*, 2400-2402.
21. W. Wu, J. Shen, Z. Gai, J. Hong, P. Banerjee, S. Zhou, *Biomaterials* **2011**, *32*, 9876-9887.
22. I. Rabias, D. Tsitrouli, E. Karakosta, T. Kehagias, G. Diamantopoulos, M. Fardis, D. Stamopoulos, T. G. Maris, P. Falaras, N. Zouridakis, N. Diamantis, G. Panayotou, D. A. Verganelakis, G. I. Drossopoulou, E. C. Tsilibari, G. Papavassiliou, *Biomicrofluidics* **2010,** *4,* 024111, 8 pp.
23. J. Hong, D. Xu, P. Gong, J. Yu, H. Ma, S. Yao, *Microporous Mesoporous Mater.* **2008**, *109*, 470-477.
24. D. Stamopoulos, P. Bouziotis, D. Benaki, C. Kotsovassilis, P. N. Zirogiannis, *Nephrol. Dial. Transpl.* **2008,** *23,* 3234-3239.
25. D. Stamopoulos, P. Bouziotis, D. Benaki, P. N. Zirogiannis, K. Kotsovassilis, V. Belessi, V. Dalamgas, K. Papadopoulos, *Ther. Apheresis Dial.* **2009,** *13,* 34-41.
26. D. Stamopoulos, D. Benaki, P. Bouziotis, P. N. Zirogiannis, *Nanotechnology* **2007**, *18*, 495102, 14 pp.
27. D. Stamopoulos, E. Manios, V. Gogola, D. Benaki, P. Bouziotis, D. Niarchos, M. Pissas, *Nanotechnology* **2008,** *19,* 505101, 13 pp.
28. R. Gui, H. Jin, *RCS Adv.* **2014**, *4*, 2797-2806.
29. C. A. Demarchi, A. Debrassi, F. de Campos Buzzi, R. Corrêa, V. C. Filho, C. A. Rodrigues, N. Nedelko, P. Demchenko, A. Ślawska-Waniewska, P. Dłużewski, J.-M. Greneche, *Soft Matter* **2014**, *10*, 3441-3450.

30. Liu, C. Detrembleur, A. Debuigne, M.-C. De Pauw-Gillet, S. Mornet, L. Vander Elst, S. Laurent, E. Duguet, C. Jérôme, *J. Mater Chem. B.* **2014**, *2*, 1009-1023.
31. G. Liu, D. Wang, F. Zhou, W. Liu, *Small* **2015**, *23*, 2807-2816.
32. J. Zhu, C. Peng, W. Sun, Z. Yu, B. Zhou, D. Li, Y. Luo, L. Ding, M. Shen, X. Shi, *J. Mater. B* **2015**, *3*, 8684-8693.
33. M. Sun, A. Zhou, Q. Zhang, M. Ye, Q. Liu, *Eur. Polym. J.* **2015**, *66*, 569-576.
34. H. Tabani, K. Khodaei, Y. Bide, F. D. Zare, S. Mirzaei, A. R. Fakhari, *J. Chromatogr. A* **2015**, *1407*, 21-29.
35. K. Jaiswal, M. De, S. S. Chou, S. Vasavada, R. Bleher, P. V. Prasad, D. Bahadur, V. P. Dravid, *ACS Appl. Mater. Interfaces* **2014**, *6,* 6237-6247.
36. L. F. Cótica, V. F. Freitas, G. S. Dias, I. A. Santos, S. C. Vendrame, N. M. Khalil, R. M. Mainardes, M. Staruch, M. Jain, *J. Magn. Magn. Mater.* **2012**, *324*, 559-563.
37. C. Mascolo, Y. Pei, T. A. Ring, *Materials* **2013**, *6*, 5549-5567.
38. R. A. Frimpong, J. Z. Hilt, *Nanotechnology* **2008**, *19*, 175101, 7 pp.
39. T. Hoare, R. Pelton, *Langmuir* **2004**, *20*, 2123-2133.
40. S. Kawaguchi, A. Yekta, M. A. Winnik, *J. Colloid Interface Sci.* **1995**, *176*, 362-369.
41. S. Lu, J. Ramos, J. Forcada, *Langmuir* **2007**, *23*, 12893-12900.
42. B. Bhushan, J. Qi, *Nanotechnology* **2003**, *14*, 886-895.
43. D. Losic, K. Short, J. J. Gooding, J. G. Shapter, *J. Serb. Chem. Soc.* **2004**, *69*, 93–106.
44. M. Kokate, K. Garadkar, A. Gole, *J. Mater Chem. A*, **2013**, *1*, 2022-2029.
45. F. Sauzedde, A. Elaïssari, C. Pichot, *Colloid Polym. Sci.* **1999**, *277*, 846-855.
46. C. Tuncer, Y. Samav, D. Ülker, S. B. Baker, V. Bütün, *J. Appl. Polym. Sci.* **2015**, DOI: 10.1002/app.42072.
47. S. Bhattacharya, F. Eckert, V. Boyko, A. Pich, *Small* **2007**, *3*, 650-657.
48. A. Pich, S. Bhattacharya, Y. Lu, V. Boyko, H.-J. P. Alder, *Langmuir* **2004**, *20*, 10706-10711.
49. S. Backes, M. U. Witt, E. Roeben, L. Kuhrts, S. Aleed, A. M. Schmidt, R. von Klitzing, *J. Phys. Chem. B* **2015**, *119*, 12129-12137.
50. A. Pich, Y. Lu, V. Boyko, K.-F. Arndt, H.-J. P. Adler, *Polymer* **2003**, *44*, 7651-7659.
51. J. Rubio-Retama, N. E. Zafeiropoulos, B. Frick, T. Seydel, E. López-Cabarcos, *Langmuir* **2010**, *26*, 7101-7106.

52. R. Regmi, S. R. Bhattarai, C. Sudakar, A. S. Wani, R. Cunningham, P. P. Vaishnava, R. Naik, D. Oupicky, G. Lawes, *J. Mat. Chem.* **2010**, *2*0, 6158-6163.
53. M. Boularas, E. Gombart, J-F. Tranchant, L. Billon, M. Save, *Macromol. Rapid Commun.* **2015**, *36*, 76-83.
54. L. Zhou, J. Yuan, W. Yuan, X. Sui, S. Wu, Z. Li, D. Shen, *J. Magn. Magn. Mat*. **2009**, *321*, 2799-2804.
55. P. Gong, H. Sun, J. Hong, D. Xu, S. Yao, *Sci. China, Ser. B: Chem.* **2007**, *50*, 217-223.
56. B. Luo, X.-J. Song, F. Zhang, A. Xia, W.-L. Yang, J.-H. Hu, C.-C. Wang, *Langmuir* **2010**, *26*, 1674-1679.
57. F. Zhang, C.-C. Wang, *Langmuir* **2009**, *25*, 8255-8262.
58. A. Riedinger, M. P. Leal, S. R. Deka, C. George, I. R. Franchini, A. Falqui, R. Cingolani, T. Pellegrino, *Nano Lett.* **2011**, *11*, 3136-3141.
59. M. A. Hood, M. Mari, R. Muñoz-Espí, *Materials* **2014**, *7*, 4057-4087.
60. C. Hartmann, R. D. Sanderson, *Macromol. Symp.* **2007**, *255*, 24-35.
61. L. Roeder, M. Reckenthäler, L. Belkoura, S. Roitsch, R. Strey, A. M Schmidt, *Macromolecules* **2014**, *47*, 7200-7207.
62. M. Rahimi, M. Yousef, Y. Cheng, E. I. Meletis, R. C. Eberhart, K. Nguyen, *J. Nanosci. Nanotechnol.* **2009**, *9*, 4128-4134.
63. L. Wang, J. Sun, *J. Mater. Chem.* **2008**, *18*, 4042-4049.
64. A. López-Cruz, C. Barrera, V. L. Calero-DdelC, C. Rinaldi, *J. Mater. Chem.* **2009**, *19*, 6870-6876.
65. A. Sahoo, K. S. P. Devi, R. Banerjee, T. K. Maiti, P. Pramanik, D. Dhara, *ACS Appl. Mater. Interfaces* **2013**, *5*, 3884-3893.
66. Q. Wu, X. Wang, C. Liao, Q. Wei, Q. Wang, *Nanoscale* **2015**, *7*, 16578-16582.
67. M. Lattuada, T. A. Hatton, *Langmuir* **2007**, *23*, 2158-2168.
68. H. Mohammad-Beigi, S. Yaghmaei, R. Roostaazad, A. Arpanaei, *Physica E* **2013**, *49*, 30-38.
69. J. Hong, D. Xu, P. Gong, H. Sun, L. Dong, S. Yao, *J. Mol. Cattal. B: Enzym.* **2007**, *45*, 84-90.
70. M. Laurenti, P. Guardia, R. Contreras-Cáceres, J. Pérez-Juste, A. Fernandez-Barbero, E. Lopez-Cabarcos, J. Rubio-Retama, *Langmuir* **2011**, *27*, 10484-10491.
71. A. Z. Pich, H-J. P. Adler, *Polym. Int.* **2007**, *56*, 291-307.

72. J.-H. Fang, Y.-T. Lee, W.-H. Chiang, S.-H. Hu, *Small* **2015**, *11*, 2417-2428.
73. Lu, J. Ramos, J. Forcada, *Macromol. Symp*. **2009**, *281,* 89-95.
74. Chen, Z. Cao, X. Guo, J. Nie, J. Xu, Z. Fan, B. Du, *Polymer* **2011**, *52*, 172-179.
75. A. V. Reis, A. R. Fajardo, I. T. A. Schuquel, M. R. Guilherme, G. J. Vidotti, A. F. Rubira, E. C. Muniz, *J. Org. Chem.* **2009**, *74*, 3750-3757.
76. W. N. E. van Dijk-Wolthuis, J. J. Kettenes-van den Bosch, A. van der Kerk-van Hoof, W. E. Hennink, *Macromolecules* **1997**, *30*, 3411-3413.
77. G. Aguirre. *Advanced Design of Biocompatible Stimuli-responsive Nanocapsules and Nanogels for Antitumor Drug and Gene Delivery.* PhD Thesis, The University of the Basque Country, **2015**.
78. Z. Ma, Y. Guan, H. Liu, *J. Polym Sci., Part A: Polym Chem.* **2005**, *43*, 3433-3439.
79. Y. Liu, W. Hu, Z. Lu, C. M. Li, *Med. Chem. Commun.* **2010**, *1*, 132-135.
80. P. Li, R. Xu, W. Wang, X. Li, Z. Xu, K. W. K. Yeung, P. K. Chu, *Colloids Surf., B* **2013,** 101, 251-255.
81. R. Turcu, I. Craciunescu, V. M. Garamus, C. Janko, S. Lyer, R. Tietze, C. Alexiou, L. Vekas, *J. Magn. Magn. Mater.* **2015***, 380,* 307-314.
82. Y. Lalatonne, J. Richardi, M. P. Pileni, *Nat. Mater.* **2004**, *3*, 121-125.
83. R. Turcu, I. Craciunescu, V. M. Garamus, C. Janko, S. Lyer, R. Tietze, C. Alexiou, L. Vekas, *J. Magn. Magn. Mater.* **2015***, 380,* 307-314.
84. C. Echeverria, C. Mijangos, *Langmuir* **2011**, *27*, 8027-8035.
85. M. Rahman, A. Elaissari, *Sep. Purif. Technol.* **2011**, *81*, 286-294.
86. F. Medeiros, A. M. Santos, H. Fessi, A. Elaissari, *Int. J. Appl. Pharm.* **2011**, *403*, 139-161.
87. J. Huang, Y. Xue, N. Cai, H. Zhang, K. Wen, X. Luo, S. Long, F. Yu, *Mater. Sci. Eng. C* **2015**, *46*, 41-51.
88. C. F. Adams, A. Rai, G. Sneddon, H. H. P. Yiu, B. Polyak, D. M. Chari, *Nanomedicine: NMB* **2015**, *11*, 19-29.
89. L. Tan, H. Pu, M. Jin, Z. Chang, D. Wan, J. Yin, *Colloids Surf.* **2010**, *360*, 137-141.
90. J.-M. Shen, L. Xu, Y. Lu, H.-M. Cao, Z.-G. Xu, T. Chen, H.-X. Zhang, *Int. J. Pharm.* **2012**, *427*, 400-409.
91. Z. Yuan, Y. Wang, D. Chen, *J. Mater. Sci.* **2014**, *4*9, 3287-3296.
92. C. S. S. R. Kumar, F. Mohammad, *Adv. Drug Delivery Rev.* **2011**, *63*, 789-808.
93. N. Singh, G. J. S. Jenkins, R. Asadi, S. H. Doak, *Nano Rev.* **2010**, *1,* 5358-5372.

94. P. Papaphilippou, M. Christodoulou, O.-M. Marinica, A. Taculescu, L. Vekas, K. Chrissafis, T. Krasia-Cristoforou, *ACS Appl. Mater. Interfaces* **2012**, *4*, 2139-2147.
95. M. Srivastava, J. Singh, M. Yashpal, D. K. Gupta, R. K. Mishra, S. Tripathi, A. K. Ojha, *Carbohydr. Polym.* **2012**, *89*, 821-829.
96. K. H. Wu, W. C. Huang, G. P. Wang, T. R. Wu, *Mater. Res. Bull.* **2005**, *40*, 1822-1831.
97. M. Srivastava, A. K. Ojha, S. Chaubey, P. K. Sharma, A. C. Pandey, *Mater. Sci. Eng.*, *B* **2010**, *175*, 14-21.
98. C. Zhang, J. Shi, X. Yang, L. De, X. Wang, *Mater. Chem. Phys.* **2010**, *123*, 551-556.

# 5

# Biomedical Applications of PDEAEMA-based Multi-responsive Nanogels

# 5.1. Introduction

Recent advances in the design of new nanoparticles have attracted a great deal of interest from the point of view of applications in biomedicine. Particularly, nanogels and magnetic labeled nanogels have gained significant momentum due to their remarkable advantages for theranostics. The large number of interactions of nanoparticles with cells, as well as the intensity of the adverse physiological outcome, makes an examination of the biocompatibility with cells one of the major issues surrounding the safety and efficacy of materials to be used in biomedical applications.[1-3] Therefore, preliminary studies on the biocompatibility of the multi-responsive poly(2-diethylaminoetyl methacrylate) (PDEAEMA)-based nanogels and magneto-nanogels (MNGs) prepared were carried out. Different biocompatibility tests have been performed for that purpose.

On the one hand, the examination of the interactions of nanogels with blood cells is essential since a direct contact could occur between them. Even the determination of haemolysis is one of the most common tests to evaluate the cytotoxicity of nanoparticles against human blood cells,[4] this is not the only indicator of blood cells health. It has been reported that microscopy techniques provide further evidence and additional information about the hemocompatibility.[5] Among them, Atomic Force Microscopy (AFM) has appeared to be adequate for the analysis of biological samples, being non-destructive and enabling both analysis of the overall cell shape and high resolution imaging.[6-11] Taking this into account, preliminary studies on the biocompatibility of a PDEAEMA-based magneto-nanogel (MNG) with peripheral human blood cells were carried out by microscopy techniques. Even many works on the study of the effect of magnetic nanoparticles (MNPs) on the blood cells have been reported,[12,13] to the best of our knowledge, this is the first time that MNGs interactions with human blood cells have been examined by microscopy.

On the other hand, in order to know the suitability of the nanoparticles for clinical use, cell viability must be examined. Hence, *in vitro* cytotoxicity experiments of two nanogels based on PDEAEMA with cervical cancer cells (HeLa cells) were carried out. Looking for biocompatibility, being most of the surfactants potentially toxic to organisms due to their surface activity allowing reactions with biological membranes, it is interesting to remark that these nanogels were synthesized by surfactant-free emulsion polymerization. Moreover, PEGylation of nanoparticles has appeared to improve their biocompatibility.[14] Being the

difference between both nanogels the presence of a stabilizer, poly(ethylene glycol methacrylate) (PEGMA), the effect of the PEGylation on the nanogels cytotoxicity was also addressed.

Nanogels have found to be specially attractive in the field of drug delivery owing potential advantages such as tunable size, large surface area, ability to entrap bioactive molecules and also to improve the pharmacological profiles of drugs and thereby therapeutic efficacy.[15-17]

Doxorubicin hydrochloride (DOXO) is one of the most potent and commonly used anticancer drug, being valuable in the treatment of a variety of malignancies such as some leukaemias, and stomach, lung, ovaries, and breast cancers.[18-21] However, its clinical usage is hampered due to its dose-dependent cytotoxicity against normal cells, limited solubility, and low bioavailability.[22,23] To mitigate this problematic issue and improve its biodistribution and bioavailability, intense research efforts have focused on the design and implementation of carrier systems such as the abovementioned nanogels.[24-26]

An ideal drug delivery system should target only the desired cells and tissues, and release their cargo at a well-defined time at the intracellular space, responding to specific stimuli such as pH, temperature, and redox microenvironments.[27] pH-responsiveness can be exploited for selective drug release at the slightly acidic pH of tumors and/or cellular compartments endosome/lisosome.[27-29] Particularly, polymers based on monomers containing tertiary amines such as 2-(diethylamino)ethyl methacrylate (DEAEMA) have been widely studied since they are able to prevent premature burst drug release being pH-responsive at physiological conditions,[30,31] to interact with the negatively charged cell membranes being positively charged, and to induce endosomal escape.[32,33] Hence, interestingly, PDEAEMA-based nanogels could be potentially useful as drug delivery systems.

In this Chapter, the potential application as cargo delivery systems of two PDEAEMA-based nanogels was analyzed. For that purpose, the anticancer drug DOXO was used. After examining the encapsulation efficiency and drug loading capacity of the nanogels, the colloidal stability of DOXO-loaded nanogels in cell culture media was investigated. Moreover, the DOXO release kinetics was studied by *in vitro* experiments and in order to understand the delivery mechanism, the release profiles were fitted to the theoretical model Peppas-Sahlin. In addition, the cellular uptake and intracellular distribution in breast cancer MDA-MB-231 cell lines of the nanogels were studied by confocal fluorescence microscopy.

In summary, the suitability of nanogels and MNGs for biomedical applications was studied in this Chapter. Apart from performing preliminary studies on the biocompatibility of nanogels and MNGs with HeLa and blood cells, the nanogels potential as drug delivery systems was addressed.

## 5.2. Experimental

### 5.2.1. Materials

- Nanogels E0.93PM0 and E0.93PM10 (named PM0 and PM10 in this Chapter) and magneto-nanogel (MNG) PM0m presented in Chapters 2, 3, and 4 were used for the experiments.
- The anticancer drug Doxorubicin hydrochloride (DOXO), supplied by Sigma-Aldrich, was used.
- Breast cancer MDA-MB-231 and cervical cancer HeLa cell lines were supplied by Cell Biolabs.
- 4'-6'-diamidino-2-phenylindole dihydrochloride (DAPI), supplied by Invitrogen, was used to stain the cell nuclei.
- Fetal bovine serum (FBS) was used to simulate blood serum conditions.
- Sodium acetate/acetic acid (SA), phosphate buffered saline (PBS), bis-tris, and sodium chloride (NaCl), all of them supplied by Sigma-Aldrich, were used to prepare the buffer solutions.
- Whole blood was drawn by venipuncture from a volunteer donor.
- Vacutainer test tubes (BD, Franklin Lakes, NJ, USA) containing ethylenediaminetetraacetic acid (EDTA) as an anticoagulant of blood were used for temporary blood storage.
- Double deionized (DDI) water was used throughout the work.

## 5.2.2. *In vitro* biocompatibility tests of PDEAEMA-based nanogels and magneto-nanogels

### 5.2.2.1. *In vitro* cytotoxicity tests of some PDEAEMA-based nanogels

*In vitro* cell toxicity tests of nanogels with HeLa cells were performed with the CCK-8 cytotoxicity assay[34,35] and by using nanogel concentrations in the range of 0.005-0.5 mg/mL. The absorbance of viable cells was measured by UV-VIS microplate absorbance reader (Bio Rad model 689, USA) at 450 nm. Relating it to the absorbance of a blank sample, cell viability values were calculated.

### 5.2.2.2. *In vitro* biocompatibility tests of MNGs with blood cells

Preliminary *in vitro* experiments on the biocompatibility of the MNGs with cells of peripheral blood [red blood cells (RBCs), white blood cells (WBCs), and platelets (Plts)] were performed. The experiments were based on the incubation of blood cells with the MNGs under standardized conditions.

#### 5.2.2.2.1. Incubation of MNGs with blood cells

The incubation procedure of MNGs with blood cells was performed as described by Stamopoulos *et al*.[36] Whole blood was withdrawn by venipuncture from one donor and placed in standard anticoagulant-containing diaminoethanetetraacetic acid (EDTA) Vacutainer test tubes (BD, Franklin Lakes, NJ, USA). The blood sample was used fresh, as the subsequent processing was accomplished within two hours after collection.

In the first protocol (Sample Series I), blood cells were dispersed in autologous plasma. 120 μL of whole blood was directly diluted with 400 μL of autologous plasma isolated from whole blood with centrifugation at appropriate conditions (x120 g for 10 min).

In the second protocol (Sample Series II), blood cells were dispersed in physiological saline. The pristine whole blood was initially washed with physiological saline (NaCl 0.9 %) to completely reject the autologous plasma. To completely reject the supernatant, 120 μL of whole blood was subjected to three consecutive rounds of addition of 1 mL of NaCl dispersion, mild manual homogenization, and centrifugation (x 1200 g for 2 min). At the end, the precipitated blood cells were redispersed in 400 μL of physiological saline.

In the third protocol (Sample Series III), blood cells obtained from the second protocol were redispersed in autologous plasma right after a short term (t < 10 min) of incubation with MNGs. 120 μL of initially washed blood cells were diluted with 400 μL of autologous plasma also in this series.

Thus, in all the cases the concentration of blood cells in the final sample was identical. Then, 50 μL of MNGs dispersion (at a concentration 0.05 wt% in buffer at pH 6) was also added. The samples were mildly incubated for 2 h, using a homemade 45°-inclined incubator, at 20-30 rpm and room temperature. Aliquots were withdrawn at the following times: 0, 5, 10, 15, 30, 60, and 120 min.

#### 5.2.2.2.2. Preparation of MNGs-incubated blood cells films

After the incubation experiments, films of the MNGs-incubated blood cells were prepared for the imaging and elemental analysis by microscopy. To perform microscopy experiments and obtain reliable information, the MNGs-incubated blood cells should be prepared in a single-layered film form with appropriate characteristics.[11,37] The employed procedure was originally presented for the case of pristine blood cells by Stamopoulos *et al.* [8,38]

Single-layered films of MNGs-incubated blood cells were prepared on standard microscope glass slides (Corning, NY, USA) thoroughly cleaned with ethanol. 50 μL of the MNGs-incubated blood cells dispersion was deposited onto the glass slide, near one of its corners, that is placed onto the centrifugal spinner, an electronically controlled platform (Headway Research INC MOTOR CONTROL-101) that can rotate at prefixed conditions (angular speed and duration). The centrifugal force exerted onto the sample produced a dry film in the sense that the plasma or saline evaporated during the rotation process when the sample was left in air environment after the deposition. Most important, by careful adjustment of the angular speed (2,000 rpm) and rotation duration (10 s), single layered films of uniformly distributed and closely packed cells were produced onto the glass slide.

#### 5.2.2.2.3. Analysis by microscopy techniques

All the samples of MNGs-incubated blood cells were analyzed by microscopy to attain information on the morphological and geometrical characteristics and elemental composition.

**Optical Microscopy (OM).** Prior to any analysis by Atomic Force Microscopy (AFM), optical microscope (OM) was employed to evaluate the films of MNGs-incubated blood cells. OM images were recorded with a LEICA DMRXP (Leica, Wetzlar, Germany).

**Atomic Force Microscopy (AFM).** AFM was employed to acquire data on the morphological and geometrical characteristics of the MNGs-incubated blood cells by means of a scanning probe microscope (Solver PRO; NT-MDT Co, Moscow, Russia) with a 100x100x5 $\mu m^3$ XYZ scanner hosted on an active vibration isolation table (MOD-1M plus; Halcyonics GmbH, Goettingen, Germany). Measurements were performed in the semi-contact scanning mode with NCH (Non-Contact/tapping mode-High resonance frequency) cantilevers that end with silicon nitride tips (Nano and More GmbH, Wetzlar, Germany) and have the nominal parameters, spring constant = 42 N/m and resonance frequency = 320 kHz. The optimum imaging results were obtained with the following scanning parameters: line frequency 1.5-4 Hz, area = 0.5x0.5 - 30x30 $\mu m^2$, and lines per image = 256-512. In the AFM observations the 'height' signal was recorded during each single scan, which provides information referring to the standard morphology of the imaged sample.[39] In addition, the semi-contact mode was used being the optimum mode of operation for soft biomaterials since the problems caused by tip deformation are minimized by this mode.[40]

**Scanning Electron Microscopy (SEM).** For Scanning Electron Microscopy (SEM) analyses, the MNGs-incubated blood cells were deposited on ultra-smooth silicon substrates that were precoated with a relatively thick (100 nm) underlayer of Niobium (Nb) by means of a sputtering Edwards 306A unit (Edwards, Sanborn, NY, USA). The SEM data were acquired by using an Inspect microscope (FEI, Hillsboro, OR, USA) working with W (tungsten) filament. Regarding the sample preparation stage, the Nb-precoated silicon substrate hosting the single-layered film of blood cells was glued with silver paste onto conventional pin stubs with extra care to short-circuit the holder (pin stub) with the surface of the film at, at least, two different corners of the silicon substrate. Then a thin overlayer (5-20 nm) of gold (Au) was deposited under vacuum ($10^{-1}$ Torr) by means of a typical SEM sputtering unit (E5100; Quorum Technologies Ltd, East Sussex, UK). Au overlayer serves to make the sample conductive and to adequately protect it from possible cumulative heating and ultimate evaporation originating from the exposition to

the electronic beam. During SEM imaging, an acceleration voltage of 20-30 kV, a working distance of 10 mm, and spot size of 3 were employed.

**Energy-dispersive X-ray Spectroscopy (EDS).** Elemental analysis was performed by means of Energy Dispersive X-ray Spectroscopy (EDS), the built-in energy-dispersive X-ray ability of the SEM was used. The contribution of Au was excluded by subtracting the EDS spectrum obtained from a free space of the sample, since it was expected to be very high related to the other elements in the MNGs.

## 5.2.3. *In vitro* DOXO loading inside the PDEAEMA-based nanogels

The loading of DOXO onto the nanogels was determined by a depletion method.[41] Briefly, a stock solution of DOXO (10 mg/mL) was prepared in DDI water. Nanogels were dispersed by magnetic stirring at pH 5.5-6 at a concentration of 2 mg/mL and then, samples were sonicated for homogenization. DOXO-loaded nanogels were prepared by adding an appropriate amount of DOXO to the nanogel dispersions obtaining samples with DOXO concentrations from 0.5 mM to 2.5 mM. After storing the samples in a refrigerator for 48 h, DOXO-loaded nanogels were separated from free (non-encapsulated) DOXO by centrifugation. The amount of free DOXO was determined by taking the aqueous dispersion of the supernatant and by using a UV-VIS spectrophotometer (Cary 50 spectrophotometer, Agilent Technologies, Germany) at 488 nm. The drug loading (D.L.) and entrapment efficiency (E.E.) values were calculated by using the equations 5.1 and 5.2, respectively.

$$\mathrm{D.L.\%} = \frac{w_{\mathrm{DOXO\ loaded}}}{w_{\mathrm{DOXO+polymer}}} \mathrm{x}\ 100 \qquad (5.1)$$

$$\mathrm{E.E.\%} = \frac{w_{\mathrm{DOXO\ loaded}}}{w_{\mathrm{Total\ DOXO}}} \mathrm{x}\ 100 \qquad (5.2)$$

where $w_{\mathrm{Total\ DOXO}}$ = total weight of DOXO in feeding

$w_{\mathrm{DOXO\ loaded}} = w_{\mathrm{Total\ DOXO}}$ (in feeding) – $w_{\mathrm{free\ DOXO}}$ (in supernatant)

$w_{\mathrm{DOXO+polymer}}$ = total weight of DOXO loaded nanogels = $w_{\mathrm{DOXO\ loaded}} + w_{\mathrm{polymer}}$

## 5.2.4. Colloidal stability of the DOXO-loaded PDEAEMA-based nanogels in cell culture media

The colloidal stability of DOXO-loaded nanogels in cell culture media was studied by measuring the hydrodynamic diameters of nanogels during 17 days of incubation with cells. Measurements were carried out by using Dynamic Light Scattering (DLS, (ALV-5000F, ALV-6GmbH, Germany)). For that purpose, nanogels containing DOXO at a concentration of 0.5 mM were used. Samples were diluted (1/200) in cell culture media supplemented with 10 % of FBS at 37 °C and at pH 7.4 (PBS buffer) and pH 5.2 (SA buffer) under slow stirring.

## 5.2.5. *In vitro* DOXO release from the PDEAEMA-based nanogels

The *in vitro* DOXO release was examined by a dialysis method. DOXO-loaded nanogels were placed into dialysis tubes (MWCO 3500) and dialyzed in cell culture media supplemented with 10 % of FBS at 37 °C and at pH 7.4 and 5.2. The released amount of DOXO was determined spectrophotometrically at 480 nm. The cumulative DOXO release was calculated by using the following equation:

$$\text{Cumulative DOXO release} = \frac{w_{\text{DOXO released}}}{w_{\text{DOXO loaded}}} \text{ x } 100 \qquad (5.3)$$

Furthermore, drug release profiles were fitted to Peppas-Sahlin model described by the following equation:[42]

$$\frac{M_t}{M_\infty} = k_1 t^m + k_2 t^{2m} \qquad (5.4)$$

where $M_t$ and $M_\infty$ represent the drug amount at a drug release time (t) and the total amount of loaded drug, respectively. $k_1$ is the Fickian kinetic constant and $k_2$ is the relaxational/dissolution rate constant (*i.e.* anomalous transport). The coefficient m is the Fickian diffusional exponent that depends on the geometry of the particles.

### 5.2.6. Cellular uptake of the PDEAEMA-based nanogels

Fluorescence microscopy (Leica DMI6000B, Leica Microsystems, Germany) was used to follow the cellular uptake of the DOXO-loaded nanogels. The DOXO-loaded nanogels were incubated with MDA-MB-321 cells and fluorescence images were obtained at different incubation times (2 and 6 h) using the blue channel for cell nuclei stained by DAPI ($\lambda_{exc.}$ 350nm), the red channel for DOXO ($\lambda_{exc.}$ 488nm), and transmitted light in Differential Interference Contrast (DIC) mode.[43]

## 5.3. Results and discussion

### 5.3.1. Biocompatibility of the PDEAEMA-based nanogels and MNGs

Considering the significant concern of the potential toxicity of new materials developed for biomedical applications, the biocompatibility of nanogels and MNGs prepared was studied.

#### 5.3.1.1. *In vitro* cytotoxicity of the PDEAEMA-based nanogels

In order to know the suitability of these nanogel particles for clinical use, their cytotoxicity must be studied. The cell toxicity of nanogels PM0 and PM10 was studied at different nanogel concentrations and incubation times (24 and 48 h) in HeLa cell line (see Figure 5.1). Cell viability values above 50% for both nanogels after 24 h of incubation indicate their cytocompatibility.[44]

The difference between both nanogels must be highlighted. On the one hand, PM0 showed cell viability values above 75 % in the nanogel concentration range of 0.005-0.05 mg/mL. However, viabilities of nanogel PM10 were somehow a bit lower but still above 60 % in the nanogel concentration range of 0.005-0.01 mg/mL. Oishi *et al.*[45] obtained similar cell viability values with PDEAEMA-based nanogels for an incubation time of 24 h, but using lower nanogel concentrations.

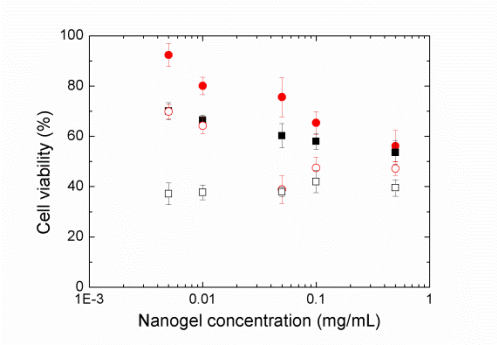


**Figure 5.1.** Cell viability upon incubation for nanogels PM0 [24 h (●) and 48 h (○)] and PM10 [24 h (■) and 48 h (□)] at 37 °C in HeLa cells culture.

The differences between PM0 and PM10 were further confirmed by the results obtained at longer incubation times (48 h). As can be observed, cell viabilities using both nanogels decreased, only being cytocompatible (with cell viabilities above 50 %) nanogel PM0 at the lowest concentrations (ca. 70 and 65 % at 0.01 and 0.005 mg/mL, respectively). In contrast, nanogel PM10 was toxic to cells in the whole range of concentration tested at incubation times of 48 h. At first sight, the increased cytotoxicity of PM10 was surprising, since PEGylated systems are known to be more biocompatible.[46] However, the concentration of the added PEGylated compound has to be considered. According to Peng *et al.*,[16] the concentration of PEGMA should not be too low neither too high for the sake of improving cell viability.

It is well known that the cationic surface charge could exhibit toxic and harmful haemolytic activity and risk of opsonization.[33,47] Although further studies are required to confirm this point, the results suggest that the positive surface charge was not the reason for increasing the cytotoxicity, since the surface charge of the PEGylated nanogels (PM10) was screened by PEGMA chains and a higher cytocompatibility would be expected in this case.

These experiments indicate the suitable concentration range of the PDEAEMA-based nanogels for biomedical applications for blood circulation times of 24 h.

### 5.3.1.2. Biocompatibility of MNGs with blood cells

Biocompatibility experiments on the MNGs with blood cells were accomplished with many microscopy techniques such as OM, SEM, and AFM. They were focused on the possible

changes that could occur in the morphological and geometrical characteristics of red blood cells (RBCs) and platelets (Plts) upon incubation with the MNGs. Mostly, the attention was focused on RBCs because of their comparatively large population[48] and their important role in the oxygen-carrying processes.[11] Possible lysis of RBCs observed in the *in vitro* experiments would definitely prohibit the use of MNGs in future *in vivo* applications.[2,37] Therefore, side effects and possible haemolysis processes were studied. Plts were also examined after the incubation with MNGs, considering their central role in the homeostatic processes. Their aggregation could be affected by the presence of the MNGs[49] ultimately leading to thrombotic complications.[50] Preliminary studies were performed by using different dispersion media. In this way, the impact of the media on the interactions between MNGs and blood cells was also evaluated.

In Figure 5.2, a well formed film of closely packed RBCs is shown, evidencing appropriate characteristics for the subsequent analysis with AFM and SEM. The image is of Sample Series I, but in all the cases RBCs were well distributed.

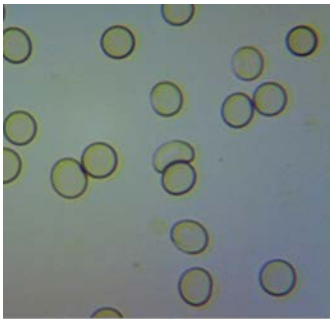

**Figure 5.2.** Representative OM image (x200) of RBCs incubated with MNGs in autologous plasma. (Sample Series I)

In Figures 5.3a-c, representative images of a RBC from Sample Series I for incubation times 0, 10, and 120 min are shown, respectively. These data prove that MNGs were not attached onto the membrane of RBCs even for extended incubation times. This can be easily explained considering that Sample Series I refers to RBCs dispersed in autologous plasma. It was expected that the rich species of proteins, lipids, and carbohydrates that exists in blood plasma could interact with the introduced MNGs and thus block any biochemically active sites

that could interact with the proteins, lipids, and carbohydrates of the RBC membrane. MNGs did not alter the morphological and geometrical characteristics of the RBCs even for such extended times. Also, from measurements with higher magnification coming from subareas of the RBCs membrane –not shown here–, no changes in their characteristics were evidenced. Laurencin *et al*.[51] also reported that proteins and salts could be the responsible for inhibiting the interactions between MNPs and RBCs. Schwalbe *et al*.[52] also reported that plasma was able to block the interactions between MNPs and leukocytes.

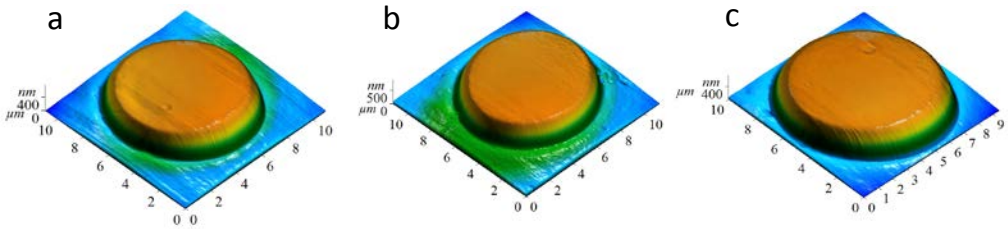


**Figure 5.3.** Representative AFM images (12x12 μm$^2$) of RBCs that were incubated with MNGs in autologous plasma (Sample Series I) for (a) t = 0 min, (b) t = 10 min, and (c) t = 120 min.

Figures 5.4a-5.4c show representative data from Sample Series II. Blood cells were 'washed' with physiological saline prior to incubation with the MNGs, isolating the plasma from the sample. These images indicate that a significant part of MNGs were attached to the RBCs, especially at their periphery. In Figure 5.4c, the EDS spectrum of the big crystal designated by the white arrow in Figure 5.4b is shown. Some NaCl crystals originating from the physiological saline appeared around the RBCs, but apart from the standard electrolytes (Na, Cl, Mg, etc), a small amount of Fe could be identified at around 6.4 keV, indicating the presence of MNGs in the cluster. The relative amount of Fe is small related to the other elements, because a dilute solution of 0.05% w/w of MNGs was used in the experiments. The presence of the other non-standard elements (Si, Nb and Au) can be explained considering the sample preparation protocol employed for the SEM measurements; Si refers to the substrate, Nb to the conducting underlayer deposited onto the surface of Si and Au to the conducting overlayer that among others is needed to increase the imaging quality. Therefore, when the RBCs were formerly washed with physiological saline prior to the incubation with MNGs, a noticeable adsorption

was observed, with MNGs mainly located at the periphery of RBCs. These microscopy data prove that, in contrast to sample prepared by dispersing with plasma (Sample Series I), when plasma was isolated from the sample (Sample Series II) MNGs could interact with the electrolytes of physiological saline and the proteins, lipids, and carbohydrates of the RBC membrane. In fact, Stamopoulos *et al*.[9,53] have reported that media such as saline could interfere with blood cells, modifying the morphological characteristics of the membrane of the RBCs. Baumann *et al.*[54] also reported that the interactions between nanoparticles with different cells are highly influenced by plasma proteins.

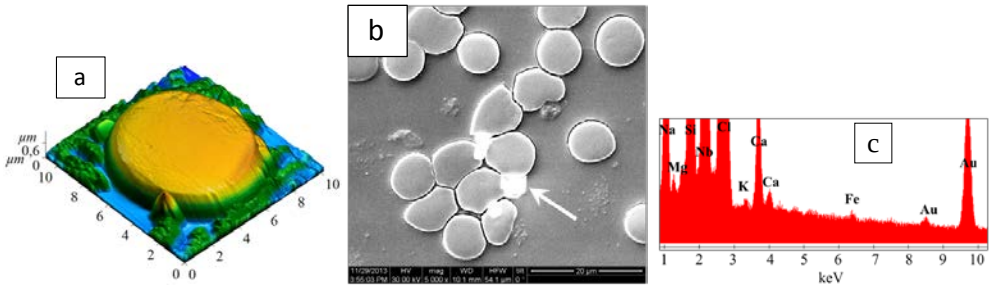


**Figure 5.4.** Representative (a) AFM (10x10 μm$^2$) and (b) SEM images of RBCs that initially were washed with saline and then incubated with MNGs for 15 min in saline. (c) EDS spectrum for the crystal designated with the white arrow in (b). (Sample Series II).

The attachment of nanoparticles to the surface of the RBCs has been suggested for prolonging the circulation time of nanoparticles,[55,56] for the delivery of therapeutic agents,[57,58] and for MRI,[51,59-61] among others. However, such attachment could affect the properties of the membrane and thereby, functions of the RBCs. Zhao *et al*.[48] observed that the attachment of mesoporous silica nanoparticles to the surface of the RBCs restricts the flexibility of the membrane, affecting the deformability of the RBCs and thus effective blood circulation. Creangă *et al.*[62] evidenced a haemolytic effect of magnetic nanoparticles. Therefore, the possible adverse effects must be considered.

In Figure 5.5, an image of the RBCs of Sample Series II is shown. It is observed the presence of 'ghost' ones (RBCs that have lost significant part of their cytoplasm and contain lower haemoglobin concentration),[63] confirming the lysis of the RBCs after being incubated for extended time into saline. Specifically, this sample has been incubated for 15 min into saline.

Other authors have also observed 'ghost' RBCs by microscopy after the addition of nanoparticles, indicating the haemolysis caused by the addition of them.[64-66]

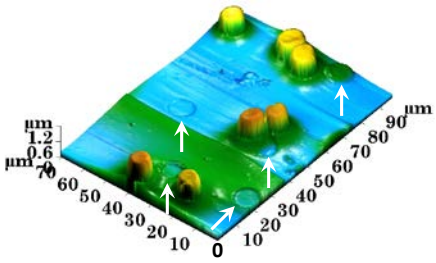


**Figure 5.5.** Representative AFM image (70x100 µm$^2$) of RBCs that initially were washed with saline and then were incubated with MNGs for 15 min in saline (Sample Series II). 'Ghost' RBCs are designated with white arrows.

Representative data for Sample Series III are shown in Figures 5.6a-5.6c. In this case, the blood cells were 'washed' with physiological saline prior to incubation with the MNGs, then short term (t < 10 min) incubation was performed and finally the blood cells were isolated and redispersed in autologous plasma. The images present RBCs that have been incubated with MNGs for times up to 120 min. In contrast to the lysis observed in Sample Series II, in Series III the MNGs did not alter the morphological and geometrical characteristics of the RBCs even at extended times of *in vitro* incubation. Moreover, no changes in the characteristics of the membrane were evidenced from measurements with higher magnifications of the RBCs membrane subareas –not shown here–. Thus, even when RBCs were washed by physiological saline, the subsequently added autologous plasma was able to protect RBCs from being damaged or even lysed after their incubation with MNGs. Moreau *et al.*[67] also concluded that plasma was able to protect RBCs from the agglutination and haemolysis after the addition of polycations.

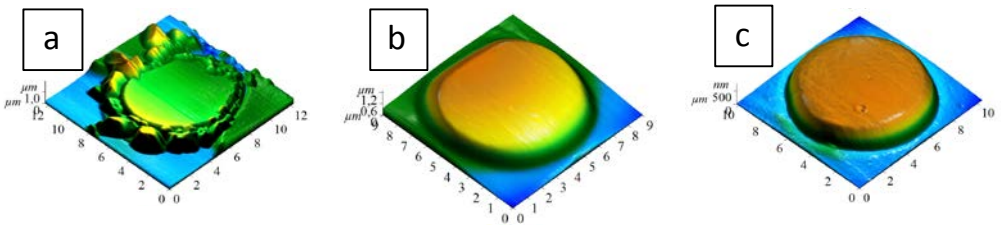


**Figure 5.6.** Representative AFM images of RBCs incubated with MNGs (Sample Series III) for (a) t = 0 min, (b) t = 10 min, and (c) t = 120 min.

To confirm the blood compatibility, the effect of MNGs incubation on the platelets (Plts) was also studied, being the Plts aggregation the most widely studied functional response of clinical relevance.[49] Nanoparticles are known to induce platelet aggregation under *in vitro* conditions, but this aggregation should be minimized. In this work, no significant interaction with MNGs was evidenced. Notably, any change in the adhesive/coagulation properties of Plts was observed, and they were randomly distributed in the sample even after extended incubation times with MNGs up to 120 min (see white arrows marking the Plts in Figure 5.7).

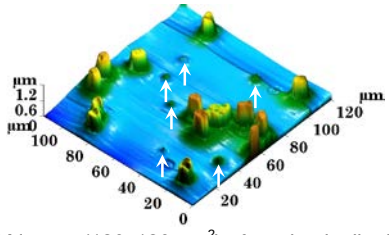

**Figure 5.7.** Representative AFM image (120x120 $\mu m^2$) of randomly distributed Plts in a sample of blood cells that was saline-washed, MNGs incubated for 120 min and plasma-redispersed (Sample Series III).

Summarizing, these preliminary results give evidence that MNGs could be well tolerated by human blood cells, specifically when autologous plasma was used. Artificial media such as physiological saline could complicate the situation since they did not protect blood cells in the absence of plasma. MNGs were attached onto their membrane at short times of incubation, immediately after the introduction of MNGs, and some lysis also took place at extended times of incubation. The former could be probably an advantage in the case where such 'magnetically-modified' RBCs are to be used in MRI as 'cellular contrast agents.[59] However, the latter is surely an unwanted side effect that must be avoided, since haemolysis activity is an

indicator of lower biocompatibility with blood cells.[68] More experiments are needed to clarify these issues but it can be stated that the MNGs prepared are potentially useful for biomedical applications.

*This section has been published in the Journal of Polymer Science Part A: Polymer Chemistry* ***2015****, DOI: 10.1002/pola.27996.*

## 5.3.2. PDEAEMA-based nanogels as drug delivery systems

The potential of some PDEAEMA-based nanogels (PM0 and PM10) to be used as anticancer drug delivery systems was studied. More specifically, the drug loading capacity and drug release kinetics of the nanogels were studied, together with the colloidal stability in cell culture media and cellular uptake of the DOXO-loaded nanogels. The difference between both nanogels was the presence of the PEG-based stabilizer PEGMA (10 wt% with respect to DEAEMA) in the case of PM10. In this way, the effect of PEGMA chains on the usefulness of nanogels as drug delivery systems was also investigated.

### 5.3.2.1. DOXO loading

The therapeutic efficiency of any chemotherapeutic drug largely depends upon its bioavailability at a particular site. DOXO is a potent chemotherapeutic drug used in the treatment of various cancers. However, as commented before, its efficacy is limited due to its toxicity, short life-time and low solubility. Therefore, drug carriers such as nanogels with sustainable bioavailability and permitting slow release of drugs may augment the therapeutic efficiency.[69]

The capacity of nanogels PM0 and PM10 to load the anticancer drug DOXO was firstly evaluated. To study the effect of the DOXO amount on the loading efficiency, drug loading (D.L.) and the entrapment efficiency (E.E.) values for the nanogels were calculated for different DOXO concentrations by using equations 5.1 and 5.2, respectively (see Figure 5.8). For that purpose, the required minimum DOXO concentration to be potentially cytotoxic *in vitro* was taken into account.

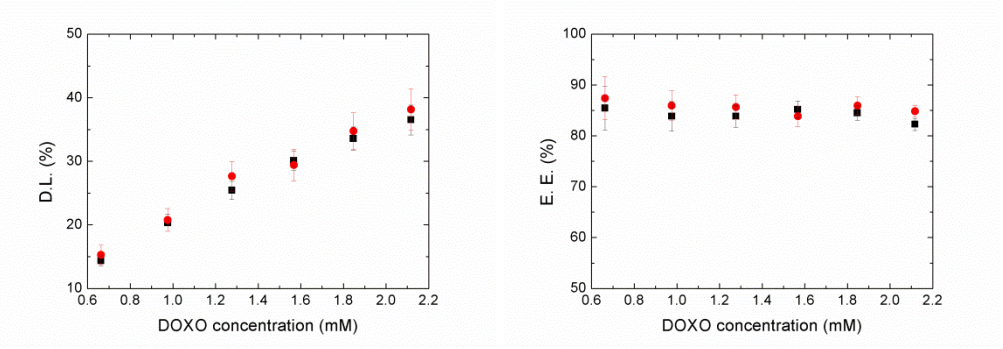


**Figure 5.8.** Drug loading (D.L., right) and entrapment efficiency (E.E., left) values as a function of DOXO concentration for nanogels PM0 (●) and PM10 (■).

A linear increase in D.L. was observed by increasing the initial DOXO concentration and a D.L. of 40 % was achieved in the studied DOXO concentration range. Moreover, E.E. values were independent of the DOXO concentration, and an increase in the DOXO amount did not decrease the encapsulation values. Interestingly, a high value of E.E. was obtained in all the cases (85-90 %, approximately), suggesting that almost all the amount of DOXO used was adequately encapsulated inside the nanogel particles. Aguirre *et al.*[43] observed similar D.L. and E.E. values for poly(*N*-vinylcaprolactam)-based and PDEAEMA-based nanogels by using the same procedure to encapsulate DOXO. The obtained D.L. and E.E. values were higher compared to other drug delivery systems,[30,70-72] suggesting the success of the encapsulation methodology used and the high loading capacity of the nanogels synthesized.

The chemical structure of the uncharged DOXO molecule could be seen in Appendix I. It is well known that DOXO molecules can form H-bonds or interact by electrostatic and hydrophobic interactions.[73]

The pH used for the encapsulation (~ pH 5.5) has to be taken into account. At this point, PDEAEMA-based nanogel particles were swollen, as the VPTpH was appeared to be at around 7.5 at physiological conditions (see Chapters 2 and 3). Swollen nanogel particles allowed the encapsulation of DOXO. However, both polymeric chains of nanogel particles and DOXO molecules ($pK_a \approx 8.2$)[74] were positively charged, indicating possible electrostatic repulsions between them, and thereby, hindering the drug loading. Gui *et al.*[75] studied the effect of pH used in the encapsulation and observed that at more alkaline pHs the

encapsulation efficiency was increased. This increase was attributed to the minimal electrostatic interactions between the polymer chains and DOXO molecules, since the net charge of DOXO molecules was around zero ($pK_a$ = 8.2). Consequently, in the present case, even there were electrostatic repulsions between positively charged of PDEAEMA chains and DOXO molecules, pretty high E.E. values were obtained, confirming the role of the diffusion in overcoming the electrostatic barrier.

DOXO could also form H-bonds with polymeric chains.[22] In this case, protonated amine groups and hydroxyl hydrogens of DOXO would be able to form H-bonds with H-bond acceptors of the polymeric chains, which are the carbonyl and ether groups of PDEAEMA, the cross-linker ethylene glycol dimethacrylate (EGDMA), and the stabilizer PEGMA.

The results shown in Figure 5.8 suggest that the presence of PEGMA chains (10 wt% with respect to the main monomer DEAEMA) did not almost affect the drug loading and the differences observed held in the limits of the experimental error at least at the used PEGMA concentration and the studied DOXO concentration. At this point, opposite effects have to be taken into account. PEGMA contains groups that could form H-bonds with DOXO enhancing the loading capacity of nanogel particles. So, more encapsulation would be expected for the nanogel PM10. However, PEGMA chains could cause an increase in cross-linking density, leading to a hindered diffusion of DOXO molecules inside the nanogel particles in the case of PM10. Quinto *et al.*[76] reported a similar effect by studying the effect of PEG chains length on the DOXO loading. Anyway, the impact of PEGMA was not evidenced.

It can be stated that the diffusion force of the drug upon swelling of the nanogels could overcome the electrostatic repulsions between the drug and the nanogel particles, and once inside the nanogels, the formation of H-bonds between them is the driving force for the encapsulation.

The anticancer drug DOXO was successfully encapsulated into the nanogel particles synthesized, as high drug loading and entrapment efficiency values were obtained.

### 5.3.2.2. Colloidal stability of the DOXO-loaded PDEAEMA-based nanogels

The adequate colloidal stability and size of the polymeric nanoparticles is one of the most important practical challenges for clinical use. Nanoparticles can massively interact with the biological components in the blood stream after injected into the body, provoking

dissociation or aggregation, and thus, leading to premature drug release, indefinite biodistribution, and low drug accumulation in tumor sites.[17] Thereby, the colloidal stability of the DOXO-loaded nanogels was studied by means of their average sizes.

As average hydrodynamic diameter values shown in Table 5.1 demonstrate, bare nanogels had sizes lower than 300 nm what is accepted as an adequate size for drug carriers according to The National Cancer Institute (USA).[77] Moreover, nanogels were swollen at pH 5.2 while collapsed at pH 7.4. This pH-responsive swelling-de-swelling behavior could be interesting for the selective drug release at the slightly acidic pH of tumors and/or at more acidic cellular compartments (endosomes/lysosomes).

| Nanogel | Hydrodynamic diameter (nm) | |
|---|---|---|
| | pH 5.2 | pH 7.4 |
| **PM0** | 266 | 180 |
| **PM10** | 286 | 162 |

**Table 5.1.** Hydrodynamic diameter of the bare nanogels PM0 and PM10 at 37 °C and an ionic strength of 150 mM (PBS), at different pHs.

Moreover, drug incorporation could increase the nanogel size due to either the enlargement of the core and/or the fusion of drug-containing particles into larger ones. As can be observed in Figure 5.9, DOXO loaded-nanogels underwent a size increase after the incorporation of the drug. For a better understanding of the drug loading effect on the nanogel size, swelling ratio was calculated for different DOXO concentrations by using the following equation:

$$\text{Swelling ratio} = \left(\frac{\mathrm{dp_{DOXO}}}{\mathrm{dp_0}}\right)^3 \qquad (5.5)$$

where $dp_{DOXO}$ and $dp_0$ are the hydrodynamic diameters at any DOXO concentration and without DOXO, respectively.

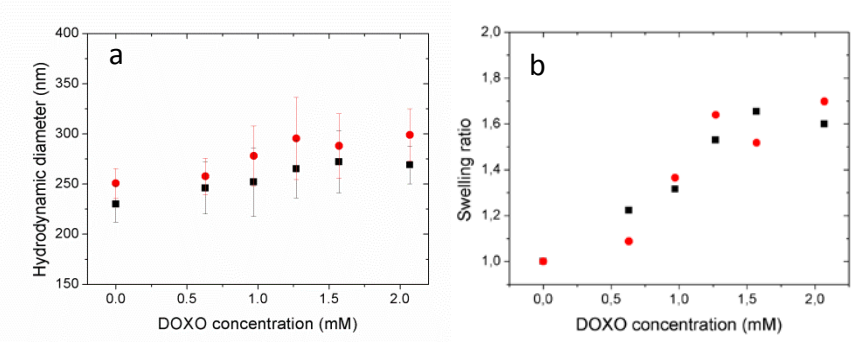


**Figure 5.9.** Average hydrodynamic diameters (a) and swelling ratios (b) of nanogels PM0 (●) and PM10 (■) at pH 7 and at 20 °C as a function of the DOXO concentration loaded.

As can be observed, DOXO loaded provoked only a slight increase in the swelling ratio (up to 1.6). Amjadi *et al.*[78] also reported a slight increase in the size of poly(lactide-*co*-glycolide) nanoparticles by loading different amounts of DOXO. Murphy *et al.*[79] observed that the loading of different drugs into the cores did not affect the hydrodynamic diameter of the nanogels.

Furthermore, as many biological components in the blood stream can interact with nanogels, a key issue is the colloidal stability of DOXO-loaded nanogels in the medium used for incubation with cells. In order to test it, the hydrodynamic diameters of the nanogels were measured during the incubation at high dilution conditions (1/200) and in cell culture medium containing 10 % (v/v) of Fetal Bovine Serum (FBS), being the most commonly used supplement for cell culture.[80] Moreover, with the aim of mimicking *in vivo* administration, two different pHs were used: pH 5.2 (simulating the immediate extracellular and intracellular environment of tumor cancer cells and within the lysosomes of normal cells) and pH 7.4 (simulating blood serum conditions).[70,71]

In Figure 5.10, the temporal evolution of hydrodynamic diameter of DOXO-loaded nanogels PM0 and PM10 upon incubation can be observed. At first sight, a high influence of pH on the colloidal stability was evidenced. At pH 5.2, PM0 and PM10 nanogel particles showed slightly larger sizes at the beginning of the incubation process, being swollen. They were colloidally stable for many days of incubation, since their size was almost constant. However, at pH 7.4, the nanogel size increased abruptly after 2 days of incubation, probably

due to the formation of agglomerates. Many factors have to be considered in order to understand this difference and the possible formation of agglomerates at pH 7.4.

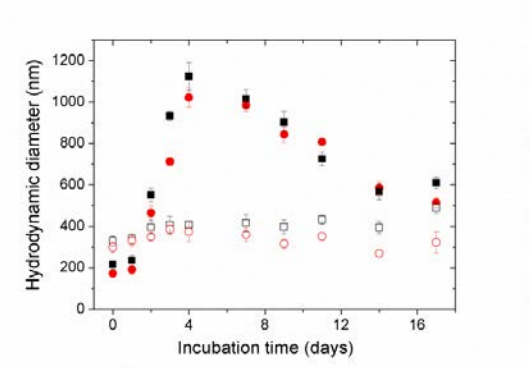


**Figure 5.10.** Temporal evolution of the average hydrodynamic diameter of the DOXO-loaded nanogels PM0 and PM10 at 37 °C in biological mimicking media. Nanogel PM0 at pH 7.4 (●) and at pH 5.2 (○) and nanogel PM10 at pH 7.4 (■) and at pH 5.2 (□).

The surface of the nanogel particles was positively charged at pH 5.2 but it was reduced at pH 7.4 due to the deprotonation of amine groups in PDEAEMA chains (see Chapters 2 and 3). Thus, the lack of electrostatic repulsions between polymeric chains could be one of the reasons for the agglomeration, since the colloidal stability was weaker.

The interactions with the biological components present in the cell culture medium must be also taken into account, since when a polymer surface is in contact with blood, plasma proteins are rapidly adsorbed onto it.[82] The adsorption of proteins is mainly governed by electrostatic and hydrophobic interactions in a process known as opsonization[83,84] and could change the surface properties of the nanogels, altering their cellular interactions. As reported by Legros *et al.*,[85] nanogel-protein interactions strongly depend on nanogel surface characteristics such as functionalities, hydrophobicity or charges.

The possible interactions of Bovine Serum Albumin (BSA), being the main constitutive plasma protein in FBS, with nanogel particles were studied.[86] Considering that the $pK_a$ of BSA is located at pH 4.7, BSA is negatively charged at both pHs, promoting charge-based attractions with the cationic nanogel particles and hence, provoking large agglomerates. Comparing both pHs, BSA is more negatively charged at pH 7.4 than at pH 5.2.[82,87] However,

the surface charge of nanogels is less positive at 7.4, as presented in other Chapters. Thus, similar electrostatic interactions between BSA and nanogels were expected regardless of the pH.

Moreover, as mentioned above, hydrophobic interactions could lead to the adsorption of BSA molecules.[88] As reported in Chapters 2 and 3, PDEAEMA-based nanogel particles are hydrophilic at acidic conditions (swollen nanogels), albeit the hydrophobicity increased at higher pHs (collapsed nanogels). Therefore, stronger hydrophobic interactions between BSA and nanogel particles were expected at pH 7.4, leading to the adsorption of BSA molecules onto the nanogel surfaces.[83] In this case, the hydrophobic domains of PDEAEMA chains could be the responsible for interacting with proteins. In addition, the charge neutralization that can cause the adsorption of BSA molecules in the incubating media could lead to the formation of larger particles.[80]

The agglomeration observed at pH 7.4 was caused by the favored adsorption of BSA onto the nanogels together with the weakened electrostatic repulsions between the polymeric chains of the nanogels. The agglomeration behavior of cationic nanogels in serum due to the adsorption of proteins has already been demonstrated elsewhere.[43,87,89] A possible picture describing the observed behavior could be the formation of aggregates composed of 3-4 nanogel particles stabilized by a corona of proteins.

Additionally, when comparing the diameters of both nanogels at different incubation times, no significant differences were observed. It has been reported that PEG-based chains could prevent the interactions of nanogels with proteins, since they migrate to the aqueous interface, rendering protein adsorption resistance at the surface.[88] However, from the results obtained, it can be thought that a 10 wt% of PEGMA with respect to DEAEMA was not enough to prevent the adsorption. Moreover, as seen in Chapter 3, the presence of PEGMA provoked charge shielding of nanogel particles, reducing electrostatic repulsions between charged polymeric chains, being a possible reason for the agglomeration of the nanogel particles. Most important, both nanogels were colloidally stable up to two days of incubation at both pHs.

#### 5.3.2.3. DOXO release kinetics

The dialysis method was used to study DOXO release kinetics from the PDEAEMA-based nanogels, avoiding nanogel diffusion to the dialysate medium. To that end, DOXO-loaded nanogel dispersions were dialyzed at 37 °C against different serum-containing (10 %

(v/v) FBS) buffer solutions. In order to simulate extracellular and intracellular environment of tumor cancer cells, sodium acetate/acetic acid (SA) buffer solution (pH 5.2) was used and phosphate buffer saline (PBS) solution (pH 7.4) was used to mimic blood serum conditions. The *in vitro* cumulative cargo release under both pHs could be observed in Figure 5.11.

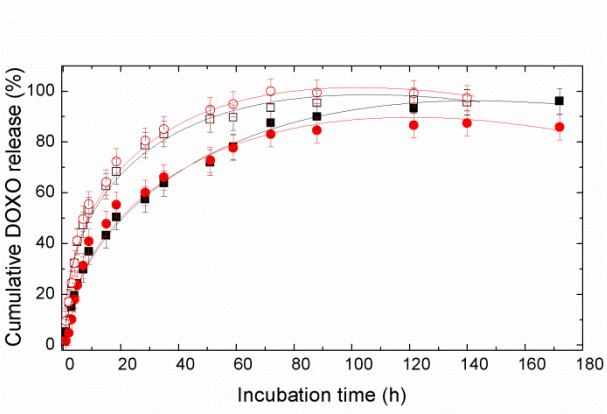


**Figure 5.11.** Evolution of cumulative DOXO release at 37 °C in solutions containing 10 % (v/v) FBS. Nanogel PM0 at pH 7.4 (●) and at pH 5.2 (○) and nanogel PM10 at pH 7.4 (■) and at pH 5.2 (□). Solid lines are the fittings to the experimental points by using the Sahlin and Peppas model.

Both nanogels showed a burst release within the first 20 h of incubation at pH 5.2 and pH 7.4, but after 20 h, a sustained release was observed, achieving a DOXO release of 85-100 %, approximately. Sadighian *et al*.[90] reported that commonly, there is a high extent of burst drug release in drug delivery systems such as nanogels. The rate of drug release from the nanogels is theoretically affected by many factors such as the diffusion of the drug through the nanogel particles, and the extent of swelling of nanogels. It is believed that the drug located in the inner part releases more slowly and in a sustainable way, because of the hindered diffusion from the highly cross-linked inner part of the nanogels. Manchun *et al*.[70] reported that DOXO in the outer layer of nanogels released at the first pulse (burst release), while the more sustainable release was controlled by the rate of DOXO release from the core of the nanogel particles.

Additionally, being pH-responsive nanogels and considering that the swelling extent affects drug release, the effect of the pH on the release kinetics should be studied. To reflect the changes on the nanogel particles' size and morphology at different pH values more

intuitively, Figure 5.12 shows a schematic representation of nanogels PM0 and PM10 at different pHs together with the hydrodynamic diameters values. As can be observed, even the sizes were slightly different from one another, both nanogels were swollen at pH 5.2, while collapsed at pH 7.4.

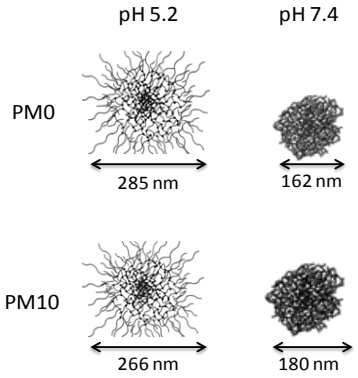


**Figure 5.12.** Schematic representation together with the hydrodynamic diameters of nanogels PM0 and PM10 at pH 5.2 and at pH 7.4 at 37 °C, and an ionic strength of 150 mM.

The release kinetics results indicate that the burst release phase was even more abrupt at acidic conditions (pH 5.2) than at pH 7.4, achieving released cargo levels of up to 70 % within the first 20 h of incubation. The main reason for the differences in the release kinetics of DOXO observed could be attributed to the pH-responsive swelling-de-swelling behavior, since the cargo diffusion out of the gel network would be favoured when nanogel particles are swollen. Moreover, the extended PDEAEMA chains could also favour the release.

Another possible reason for the faster release of the cargo at acidic conditions could be the electrostatic repulsions between the positively charged PDEAEMA-based nanogels and DOXO. At pH 5.2, both nanogels and DOXO molecules were more positively charged than at pH 7.4, enhancing the electrostatic repulsions and favouring the drug expulsion. However, considering that the driving force for the encapsulation was the formation of H-bonds between the polymeric chains and DOXO, it can be stated that electrostatic interactions affect only slightly on the pH-responsive swelling-de-swelling behavior of nanogels. Hence, the faster release kinetics of DOXO at acidic conditions was mostly caused by the favoured cargo diffusion from swollen nanogel particles. Sadighian *et al*.[90] also observed an increase in the drug diffusion rate from nanogels at acidic medium due to the swelling of the nanogel particles

and the related increase in pore size. Sousa-Herves *et al*.[27] also reported an accelerated DOXO release from multi-responsive nanogels containing a pH-responsive comonomer.

Because of the pH-induced drug release mechanism, the nanogels synthesized would have potential applications in anticancer drug delivery. Compared to the normal tissue pH (7.4), pH values of intracellular compartments and tumor tissues lie at more acidic conditions. Being the release of DOXO faster at acidic conditions, the nanogels synthesized would be able to reduce the undesirable toxicity associated with the free drug in normal tissue.[70]

Furthermore, no remarkable differences in DOXO release kinetics were observed between PM0 and PM10, suggesting that the PEG-based chains did not have any impact on the release kinetics, at least at the used concentration (10 wt% with respect to the main monomer DEAEMA). So as to study the effect of the swelling capability on the release, swelling ratio values at 37 °C and an ionic strength of 150 mM were calculated by using equation 3.2, obtaining the values of 1.2 and 1.1 for nanogels PM0 and PM10, respectively. As the interactions were not covalent, it was expected that the delivery would be governed by diffusion.[91] One factor affecting the drug diffusion is the cross-linking density.[92] In Chapter 3, a direct relationship between the swelling capability and the cross-linking density ratio was remarked. Therefore, considering that both nanogels showed very similar swelling-de-swelling behavior, it was expected also a similar cross-linking density.[93] This could be the reason why analogous DOXO release kinetics was observed in both nanogels.

In order to understand the release mechanism, the obtained release profiles were fitted to Peppas-Sahlin theoretical model.[42] Both nanogels appeared to obey this model. A superposition of two apparently independent mechanisms of drug transport could be elucidated from this model: a Fickian controlled drug release mechanism and a case-II transport related to the relaxation of polymer chains. Table 5.2 shows the obtained $k_1$ and $k_2$ values from the fitting to Peppas-Sahlin model for nanogels PM0 and PM10 at pH 5.2 and 7.4. The positive $k_1$ values confirmed the existence of a diffusion process, and the negative $k_2$ values were interpreted in terms of a insignificant relaxation process compared to the diffusion mechanism.[94]

| pH | Nanogel | Parameters | | |
|---|---|---|---|---|
| | | $K_1$ | $K_2$ | m |
| 7.4 | PM0 | 0.098 ± 0.035 | -0.026 ± 0.007 | 0.60 ± 0.04 |
| | PM10 | 0.093 ± 0.007 | -0.022 ± 0.003 | 0.61 ± 0.02 |
| 5.2 | PM0 | 0.20 ± 0.02 | -0.092 ± 0.018 | 0.51 ± 0.03 |
| | PM10 | 0.19 ± 0.02 | -0.092 ± 0.019 | 0.50 ± 0.03 |

**Table 5.2.** Fitting parameters for Peppas-Sahlin model for nanogels PM0 and PM10.

First of all, $k_1$ values were one order of magnitude greater than $k_2$ ones indicating that the predominant release mechanism was the Fickian diffusion in both nanogels. This result was in accordance with the non-covalent nature of interaction between DOXO and nanogels. Many authors have confirmed that the main release mechanism was diffusion in nanogels and hydrogels.[24,43,90] Furthermore, comparing the values obtained at different pHs, remarkably larger $k_1$ and $k_2$ values were seen at pH 5.2 that at pH 7.4, regardless of the nanogel. These results confirmed the faster release under acidic conditions, at which nanogels are completely swollen. Xu *et al.*[94] also used the Peppas-Sahlin model to understand the release of DOXO from porous silicon nanoparticles with polymeric coatings and observed higher $k_1$ values at acidic conditions.

Concerning the effect of PEGylation, the differences observed were within the statistical uncertainty. However, the results suggest that the presence of 10 wt% of PEGMA slowed down to some extent the diffusion of DOXO from the nanogel particles. Further studies are needed in order to confirm this fact, but one could expect a slower DOXO release by increasing the amount of PEGMA used in the syntheses, since nanogels would have lower swelling capabilities and a higher cross-linking density, hindering the drug delivery. Saito *et al*.[92] reported that the release of DOXO could be adjusted by means of the pH and cross-linking density in the case of PEG-based hydrogels. As expected, a higher cross-linking density resulted in a slower DOXO release.

In addition, m in equation 5.4 is the purely Fickian diffusion exponent. Values between 0.50-0.60, being in the range of 0.43 and 0.85, confirmed that the diffusion also contained a contribution of non-Fickian behavior (relaxational phenomena).[42]

In summary, regardless of the nanogel used, DOXO was mainly released by diffusion and this release was faster at acidic conditions, increasing the interest of the nanogels synthesized for anticancer drug delivery.

#### 5.3.2.4. Cellular uptake

The analysis of the cellular uptake and intracellular distribution of the nanogels is also critical to assess the biological activities of chemotherapeutic formulations.[17] DOXO-loaded nanogel PM0 was incubated into a breast cancer MDA-MB-231 cell line and the nuclei were selectively stained in blue with DAPI. Then, the cellular uptake of the DOXO-loaded nanogel PM0 was examined by fluorescence microscopy. Figure 5.13 shows Differential Interference Contrast (DIC) images (a), DOXO fluorescence in cells (red) (b), cell nuclei stained by DAPI (blue) (c), and merged images (d) for nanogel PM0 in a breast cancer MDA-MB-231 cell line after 2 and 6 h of incubation. At this point it is important to point out that DOXO fluorescence was only observable when it was released from nanogels, because of the self-quenching effect of DOXO inside the nanogel particles.[69,95,96]

Images of Figure 5.13 from a2 to d2 demonstrate that DOXO released from the nanogel particles at incubation time of 2 h, progressively diffusing into the cell cytoplasm. The low fluorescence intensity at 2 h of incubation could be related to the low amount of DOXO released at 2 h (see Figure 5.11). Nevertheless, the fluorescence intensity was enhanced after 6 h of incubation, confirming that more amount of DOXO was released from the nanogel particles, entering the cell nuclei by diffusion from the cytoplasm. This result was in agreement with the one obtained analyzing the DOXO release kinetics (Figure 5.11), since more DOXO was released after 6 h of incubation. These observations demonstrate that the nanogels could effectively deliver DOXO into the cell nuclei. In this regard, it is well known that DOXO is able to enter and accumulate into cellular nuclei only after 1 h of incubation, achieving a more sustainable release of the cargo from the nanogel.[97,98]

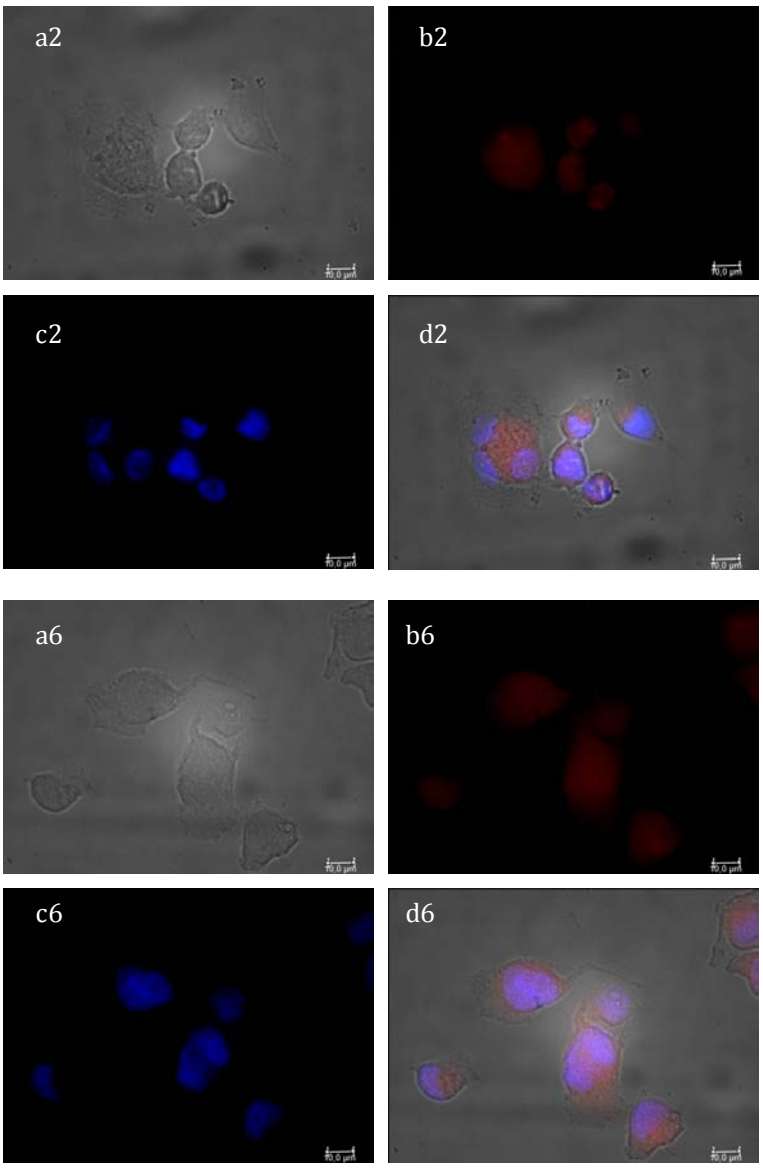


**Figure 5.13.** Fluorescence microscopy images of DOXO-loaded PM0 in MDA-MB-321 cells. Differential interference contrast (DIP) images (a), DOXO fluorescence in cells (red) (b), cell nuclei stained with DAPI (blue) (c), and the superposition of the previous three images (d). The number close to the letters refers to the incubation time: 2 (2 h) and 6 (6 h).

## 5.4. Conclusions

In this Chapter, the potential application of some multi-responsive PDEAEMA-based nanogels was analyzed. Apart from testing their biocompatibility with cells, the suitability of the nanogels as drug delivery systems was analyzed.

First of all, cytotoxicity tests of some PDEAEMA-based nanogels using a HeLa cell line were performed, concluding the concentration range at which nanogels are cytocompatible: nanogels were cytocompatible at the concentration range of 0.005-0.05 mg/mL at 24 h, but at 48 h only nanogel PM0 was cytocompatible at the lowest concentrations used (0.01 and 0.005 mg/mL).

Preliminary *in vitro* experiments on the biocompatibility of MNGs with human blood cells were also carried out, by using different media to disperse the whole blood. A tolerable biochemical compatibility of the MNGs with human blood cells was evidenced in the presence of autologous plasma, since plasma was able to protect RBCs and Plts from any damages and adverse effects. These results suggest that MNGs could be potentially useful for biomedical applications by using plasma. However, when plasma was isolated and physiological saline was used to disperse the blood, MNGs attached to the RBCs membrane and some haemolysis occurred, hampering the clinical use of the MNGs synthesized.

Apart from the biocompatibility tests, the applicability of the selected nanogels as cargo release systems was studied. It was observed that the selected nanogels PM0 and PM10 were able to efficiently load a high DOXO content up to 40 %. The diffusion of the drug upon swelling of the nanogels favoured the uptake and the cargo was encapsulated by means of H-bonds between the drug and the polymeric chains. After the encapsulation of DOXO, nanogels were slightly larger in size.

Moreover, the colloidal stability of DOXO-loaded nanogels was analyzed in cell culture media at different pHs, mimicking biological conditions: pH 5.2 (in the endosomes/lysosomes) and pH 7.4 (in the bloodstream). Nanogels were colloidally stable for many days at pH 5.2, but some agglomerates were formed at pH 7.4 after few days of incubation with cells. Nanogels were colloidally stable since the electrostatic repulsions between polymeric chains were strong and the adsorption of BSA was not favoured. However, nanogels agglomerated at pH 7.4 because of the weakened electrostatic repulsions between polymeric chains, together with the favoured adsorption of BSA on the nanogels.

Furthermore, the DOXO release kinetics was examined at different pHs: pH 5.2 mimicking the acidic tumor cells and pH 7.4 mimicking the normal cells. Regardless of the pH, nanogels showed a burst release within the first 20 h of incubation and then a sustainable release up to 85-100 % of the total loading amount. Interestingly, the release of DOXO was faster at acidic conditions, as the nanogel particles were swollen and the extended PDEAEMA chains favoured the release of the drug. Additionally, by fitting the release profiles to the Peppas-Sahlin model, the faster release at acidic conditions was corroborated and it was concluded that diffusion was the main mechanism governing the drug release.

Likewise, the cellular uptake of DOXO-loaded nanogels and the progressive release of drug from the nanogels to the cell nuclei were demonstrated by spectrofluorimetric measurements.

In summary, biocompatibility of the PDEAEMA-based multi-responsive nanogels with HeLa and human blood cells was confirmed and the suitability of the nanogels as potential carriers of DOXO was also validated.

## 5.5. References


1. X. Li, L. Wang, Y. Fan, Q. Feng, F.-Z. Cui, *J. Nanomater.* **2012**, *2012,* ID 548389, 19 pp.
2. E. M. Múzquiz-Ramos, D. A. Cortés-Hernández, J. C. Escobedo-Bocardo, A. Zugasti-Cruz, X. S. Ramírez-Gómez, J. G. Osuna-Alarcón, *J. Mater. Sci.: Mater. Med.* **2013**, *24*, 1035-1041.
3. M. M. Yallapu, M. C. Ebeling, N. Chauhan, M. Jaggi, S. C. Chauhan, *Int. J. Nanomed.* **2011**, *6*, 2779-2790.
4. M. A. Dobrovolskaia, P. Aggarwal, J. B. Hall, S. E. McNeil, *Mol. Pharm.* **2008**, *5*, 487-495.
5. R. A. Roggers, M. Joglekar, J. S. Valenstein, B. G. Trewyn, *ACS Appl. Mater. Interfaces* **2014**, *6*, 1675-1681.
6. S. H. Jung, D. Park, J. H. Park, Y.-M. Kim, K.-S. Ha, *Exp. Mol. Med.* **2010**, *42*, 9, 597-605.
7. D. A. Lamprou, V. Venkatpurwar, M. N. V. R. Kumar, *PloS One* **2013**, *8*, e64490, 1-5.
8. D. Stamopoulos, N. Bakirtzi, E. Manios, E. Grapsa, *Int. J. Nanomedicine* **2013**, *8,* 3887-3894.

9. D. Stamopoulos, E. Grapsa, E. Manios, V. Gogola, N. Bakirtzi, *Nanotechnology* **2012**, *23*, 485101, 8 pp.
10. E. Y. Parshina, A. S. Sarycheva, A. I. Yusipovich, N. A. Brazhe, E. A. Goodilin, G. V. Maksimov, *Laser Phys. Lett.* **2013**, *10*, 075607, 6 pp.
11. M. Girasole, S. Dinarelli, G. Boumis, *Micron* **2012**, *43*, 1273-1286.
12. L. F. Cótica, V. F. Fritas, G. S. Dias, I. A. Santos, S. C. Vendrame, N. M. Khalil, R. M. Mainardes, M. Staruch, M. Jain, *J. Magn. Magn. Mater.* **2012**, *324*, 559-563.
13. D. Stamopoulos, E. Manios, V. Gogola, D. Benaki, P. Bouziotis, *Nanotechnology* **2008**, *19*, 505101, 13 pp.
14. K. Chen, J. Xu, J. C. Luft, S. Tian, J. S. Raval, J. M. Desimone, *J. Am. Chem. Soc.* **2014**, *136*, 9947-9952.
15. J. Ramos, J. Forcada, R. Hidalgo-Alvarez, *Chem. Rev.* **2014,** *114,* 367-428.
16. J. Peng, T. Qi, J. Liao, M. Fan, F. Luo, H. Li, Z. Qian, *Nanoscale* **2012**, *4*, 2694-2704.
17. H. Qian, X. Wang, K. Yuan, C. Xie, W. Wu, X. Jiang, L. Hu, *Biomater. Sci.* **2014**, *2*, 220-232.
18. N. G. Yabbarov, G. A. Posypanova, E. A. Vorontsov, O. N. Popova, E. S. Severin, *Biochemistry (Moscow)* **2013**, *78*, 884-894.
19. H. A. Jambi, *World Appl. Sci. J.* **2015**, *33*, 1267-1278.
20. X. Yao, L. Chen, X. Chen, Z. Zhang, H. Zheng, C. He, J. Zhang, X. Chen, *ACS Appl. Mater. Interfaces* **2014**, *6*, 7816-7822.
21. D. Hynek, L. Krejcova, O. Zitka, V. Adam, L. Trnkova, J. Sochor, M. Stiborova, T. Eckschlager, J. Hubalek, R. Kizek, *Int. J. Electrochem. Sci.* **2012**, *7*, 13-33.
22. K. Karatasos, *J. Phys. Chem. B* **2013**, *117*, 2564-2575.
23. J.-O. You, P. Guo, D. T. Auguste, *Angew. Chem. Int. Ed.* **2013**, *52*, 1-7.
24. M. Casolaro, I. Casolaro, S. Bottari, B. Del Bello, E. Maellaro, K. D. Demadis, *Eur. J. Pharm. Biopharm.* **2014**, *88*, 424-433.
25. F. Zhan, W. Chen, Z. Wang, W. Lu, R. Cheng, C. Deng, F. Meng, H. Liu, Z. Zhong, *Biomacromolecules* **2011**, *12*, 3612-3620.
26. T. R. Arunraj, N. S. Rejinold, N. A. Kumar, R. Jayakumar, *Colloids Surf., B* **2014**, *113*, 394-402.
27. A. Sousa-Herves, S. Wedepohl, M. Calderón, *Chem. Commun.* **2015**, *51*, 5264-5267.

28. W.-H. Chiang, W.-C. Huang, Y.-J. Chang, M.-Y. Shen, H.-H. Chen, C.-S. Chern, H.-C. Chiu, *Macromol. Chem. Phys.* **2014**, *215*, 1332-1341.
29. S. Mura, J. Nicolas, P. Couvreur, *Nat. Mater.* **2013**, *12*, 991-1003.
30. Y. Q. Yang, B. Zhao, Z. D. Li, W. J. Lin, C. Y. Zhang, X. D. Guo, J. F. Wang, L. J. Zhang, *Acta Biomater.* **2013**, *9*, 7679-7690.
31. A. Pikabea, J. Ramos, J. Forcada, *Part. Part. Syst. Charact.* **2014**, *31*, 101-109.
32. A. S. M. Wong, S. K. Mann, E. Czuba, A. Sahut, H. Liu, T. C. Suekama, T. Bickerton, A. P. R. Johnston, G. K. Such, *Soft Matter* **2015**, *11*, 2993-3002.
33. A. Tamura, M. Oishi, Y. Nagasaki, *J. Controlled Release* **2010**, *146*, 378-387.
34. J. S. Park, S. W. Yi, H. J. Kim, K.-H. Park, *Carbohydr. Polym.* **2016**, *136*, 791-802.
35. P. Cao, X. Sun, Y. Liang, X. Gao, X. Li, W. Li, Z. Song, W. Li, G. Liang, *Nanomedicine* **2015**, *10*, 1585-1597.
36. D. Stamopoulos, E. Manios, V. Gogola, D. Benaki, P. Bouziotis, *Nanotechnology* **2008**, *19*, 505101, 13 pp.
37. M. O'Reilly, L. McDonnell, J. O'Mullane, *Ultramicroscopy* **2001**, *86*, 107-112.
38. D. Stamopoulos, D. Benaki, P. Bouziotis, P. N. Zirogiannis, *Nanotechnology* **2007***, 18,* 495102, 14 pp.
39. B. Bhushan, J. Qi, *Nanotechnology* **2003**, *14***,** 886-895.
40. D. Losic, K. Short, J. J. Gooding, J. G. Shapter, *J. Serb. Chem. Soc.* **2004**, *69*, 93-106.
41. G. Aguirre. *Advanced Design of Biocompatible Stimuli-responsive Nanocapsules and Nanogels for Antitumor Drug and Gene Delivery.* PhD Thesis, The University of the Basque Country, **2015**.
42. N. A. Peppas, J. J. Sahlin, *Int. J. Pharm.* **1989**, *57*, 169-172.
43. G. Aguirre, E. Villar-Alvarez, A. González, J. Ramos, P. Taboada, J. Forcada, *J. Polym. Sci., Part A: Polym. Chem.* DOI: 10.1002/pola.28025, **2016**.
44. M. E. Cavet, K. L. Harrington, K. R. VanDerMeid, K. W. Ward, J.-Z. Zhang, *Cont. Lens Anterior Eye* **2009,** *32*, 171-175.
45. M. Oishi, H. Hayashi, K. Itaka, K. Kataoka, Y. Nagasaki, *Colloid. Polym. Sci.* **2007**, *285*, 1055-1060.
46. J. V. Jokerst, T. Lobovkina, R. N. Zare, S. S. Gambhir, *Nanomedicine* **2011**, *6*, 715-728.
47. Y. Zhou, J. Li, F. Lu, J. Deng, J. Zhang, P. Fang, X. Peng, S.-F. Zhou, *Drug Des., Dev. Ther.* **2015**, *9*, 2635-2645.

48. Y. Zhao, X. Sun, G. Zhang, B. G. Trewyn, I. I. Slowing, V. S.-Y. Lin, *ACS Nano* **2011**, *5*, 1366-1375.
49. S. Manju, K. Sreenivasan, *Langmuir* **2011**, *27*, 14489-14496.
50. C. V. Hussey, V. M. Bernhard, M. R. McLean, J. E. Fobian, *Ann. Clin. Lab. Sci.* **1979**, *9*, 487-493.
51. M. Laurencin, N. Cam, T. Georgelin, O. Clément, G. Autret, J.-M. Siaugue, C. Ménager, *Adv. Healthcare Mater.* **2013**, *2*, 1209-1212.
52. M. Schwalbe, C. Jörke, N. Buske, K. Höffken, K. Pachmann, J. H. Clement, *J. Magn. Magn. Mater.* **2005**, *293*, 433-437.
53. D. Stamopoulos, E. Manios, E. Gourni, V. Gogola, D. Benaki, M. Pissas, P. Bouziotis, *Cell. Physiol. Biochem.* **2009**, *24*, 33-44.
54. D. Baumann, D. Hofmann, S. Nullmeier, P. Panther, C. Dietze, A. Musyanovych, S. Ritz, K. Landfester, V. Mailänder, *Nanomedicine* **2013**, *8*, 699-713.
55. E. Chambers, S. Mitragotri, *Exp. Biol. Med.* **2007**, *232*, 958-966.
56. A. C. Anselmo, V. Grupta, B. J. Zern, D. Pan, M. Zakrewsky, V. Muzykantov, S. Mitragotri, *ACS Nano* **2013**, *7*, 11129-11137.
57. E. Chambers, S. Mitragotri, *J. Controlled Release* **2004**, *100*, 111-119.
58. S. S. Hall, S. Mitragotri, P. S. Daugherty, *Biotechnol. Prog.* **2007**, *23*, 749-754.
59. A. Antonelli, C. Sfara, E. Manuali, I. J. Bruce, M. Magnani, *Nanomedicine* **2011**, *6*, 211-223.
60. A. Boni, D. Ceratti, A. Antonelli, C. Sfara, M. Magnani, E. Manuali, S. Salamida, A. Gozzi, A. Bifone, *Contrast Media Mol. Imaging* **2014**, *9*, 229-236.
61. M. Brähler, R. Georgieva, N. Buske, A. Müller, S. Müller, J. Pinkernelle, U. Teichgräber, A. Voigt, H. Bäumler, *Nano Lett.* **2006**, *6*, 2505-2509.
62. D. E. Creangă, M. Culea, C. Nădejde, S. Oancea, L. Curecheriu, M. Racuciu, *J. Phys.: Conf. Ser.* **2009**, *170*, 012019, 5 pp.
63. S. V. Jansen, I. Müller, N. Kiesendahl, T. Schmitz-Rode, U. Steinseifer, *Cardiovasc. Eng. Technol.* **2015**, *6*, 376-382.
64. Y. Teow, P. V. Asharani, M. P. Hande, S. Valiyaveettil, *Chem. Commun.* **2011**, *47*, 7025-7038.
65. O. V. Samsonova, A. S. Arseniev, M. P. Kirpichnikov, A. V. Feofanov, *Advanced approaches of confocal microscopy to study interactions of membrane active peptides*

*with living cells: hemolytic activity of latarcin Ltc1,* In *Microscopy: Science, Technology, Applications and Education,* Eds. A. Méndez-Vilas, J. Díaz, *Vol. 1*, pp. 627-632, Formatex, Spain, **2010**.

66. E. Baumann, G. Stoya, A. Völkner, W. Richter, C. Lemke, W. Linss, *Acta Histochem.* **2000**, *102*, 21-35.
67. E. Moreau, M. Domurado, P. Chapon, M. Vert, D. Domurado, *J. Drug Targeting* **2002**, *10*, 161-173.
68. S. Luo, S. Song, C. Zheng, Y. Wang, X. Xia, B. Lian, G. Feng, *J. Evidence-Based Complementary Altern. Med.* **2015**, ID 840896, 11 pp.
69. R. Venkatesan, A. Pichaimani, K. Hari, P. K. Balasubramanian, J. Kulandaivel, K. Premkumar, *J. Mater. Chem. B* **2013**, *1*, 1010-1018.
70. S. Manchun, K. Cheewatanakornkool, C. R. Dass, *Carbohydr. Polym.* **2014**, *114*, 78-86.
71. M. Oishi, Y. Nagasaki, *React. Funct. Polym.* **2007**, *67*, 1311-1329.
72. M. Oishi, H. Hayashi, M. Iijima, Y. Nagasaki, *J. Mater. Chem.* **2007**, *17*, 3720-3725.
73. F. Shi, J. Ding, C. Xiao, X. Zhuang, C. He, L. Chen, X. Chen, *J. Mater. Chem.* **2012**, *22*, 14168-14179.
74. J. Qi, P. Yao, F. He, C. Huang, *Int. J. Pharm.* **2010**, *393*, 176-184.
75. R. Gui, R. Wang, J. Sun, *Colloids. Surf., B* **2014**, *116*, 518-525.
76. C. A. Quinto, P. Mohindra, S. Tong, G. Bao, *Nanoscale* **2015**, *7*, 12728-12736.
77. S. K. Sahoo, T. K. Jain, M. K. Reddy, V. Labhasetwar, *Nano-Sized Carriers for Drug Delivery* In *NanoBioTechnology: BioInspired Devices and Materials of the Future*, 1st edn , Eds. O. Shoseyov, I. Levy, Humana Press, Totowa, New Jersey, ISBN: 978-1-59745-218-2 **, 2007**, *329*.
78. I. Amjadi, M. Rabiee, M. S. Hosseini, M. Mozafari, *Appl. Biochem. Biotechnol.* **2012**, *168*, 1434-1447.
79. E. A. Murphy, B. K. Majeti, R. Mukthavaram, L. M. Acevedo, L. A. Barnes, D. A. Cheresh, *Mol. Cancer Ther.* **2011**, *10*, 972-982.
80. H. Katas, Z. Hussain, S. A. Awang, *J. Nanomater.* **2013**, *2013*, ID 536291, 9 pp.
81. A. Ponta, S. Akter, Y. Bae, *Pharmaceuticals* **2011**, *4*, 1281-1292.
82. S. Ge, K. Kojio, A. Takahara, T. Kajiyama, *J. Biomater. Sci., Polym. Ed.* **1998**, *9*, 131-150.
83. D. Huo, Y. Li, Q. Qian, T. Kobayashi, *Colloids Surf., B* **2006**, *50*, 36-42.

84. M. C. C. Ferrer, P. Sobolewski, R. J. Composto, D. M. Eckmann, *J. Nanotechnol. Eng. Med.* **2013**, *4*, 01002, 8 pp.
85. C. Legros, A.-L. Wirotius, M.-C. De Pauw-Gillet, K. C. Tam, D. Taton, S. Lecommandoux, *Biomacromolecules* **2015**, *16*, 183-191.
86. G. L. Francis, *Cytotechnology* **2010**, *62*, 1-16.
87. L. Nuhn, S. Gietzen, K. Mohr, K. Fischer, K. Toh, K. Miyata, Y. Matsumoto, K. Kataoka, M. Schmidt, R. Zentel, *Biomacromolecules* **2014**, *15*, 1526-1533.
88. T. Trongsatitkul, B. M. Budhlall, *Colloids Surf., B* **2013**, *103*, 244-252.
89. A. Zubareva, A. Ilyina, A. Prokhorov, D. Kurek, M. Efrenov, V. Varlamov, S. Senel, P. Ignatyev, E. Svirshchevskaya, *Molecules* **2013**, *18*, 7848-7864.
90. S. Sadighian, H. Hosseini-Monfared, K. Rostamizadeh, M. Hamidi, *Adv. Pharm. Bull.* **2015**, *5*, 115-220.
91. I. Altimari, U. G. Spizzirri, F. Iemma, M. Curcio, F. Puoci, N. Picci, *J. Appl. Polym. Sci.* **2012**, *125*, 3006-3013.
92. H. Saito, A. S. Hoffman, H. I. Ogawa, *J. Bioact. Compact. Polym.* **2007**, *22*, 589-601.
93. A. Pikabea, G. Aguirre, J. I. Miranda, J. Ramos, J. Forcada, *J. Polym. Sci., Part A: Polym. Chem.* **2015**, *53*, 2017-2025.
94. W. Xu, R. Thapa, D. Liu, T. Nissinen, S. Granroth, A. Närvänen, M. Suvanto, H. A. Santos, V.-P. Lehto, *Mol. Pharmaceutics* **2015**, *12*, 4038-4047.
95. D. Park, Y. Cho, S.-H. Goh, Y. Choi, *Chem. Commun.* **2014**, *50*, 15014-15017.
96. Z. S. Al-Ahmady, W. T. Al-Jamal, J. V. Bossche, T. T. Bui, A. F. Drake, A. J. Mason, K. Kostarelos, *ACS Nano* **2012**, *6*, 9335-9346.
97. Y. Chen, Y. Chen, J. Nan, C. Wang, F. Chu*, J. Appl. Polym. Sci.* **2012**, *124*, 4678-4685.
98. M. B. Thomas, K. Radhakrishnan, D. P. Gnanadhas, D. Chakravortty, A. M. Raichur, *Int. J. Nanomed.* **2013**, *8*, 267-273.

# 6

# Conclusions

# 6.1. Conclusions

**1.** New PDEAEMA-based monodisperse nanogels were successfully prepared by batch emulsion polymerization presenting both temperature- and pH-sensitivity:

**a.** The heterogeneity of PDEAEMA-based nanogel morphology was demonstrated by using high-resolution transverse $^{1}$H-NMR measurements.

**b.** Their dual and tunable sensitivity was studied thoroughly. As well as investigating the swelling-de-swelling behavior of the nanogels in response to pH, their buffering capacity was confirmed by potentiometric titrations, suggesting the ability to disrupt endosomes *via* an osmotic pressure buildup (proton sponge hypothesis). Apart from the pH-sensitivity, nanogels showed a tunable pH-dependent thermo-sensitivity: an increase in the pH value led to a significant decrease in VPTT, which could be adjusted as desired close to human body temperature (37 °C).

**c.** The effect of the ionic strength of the medium on the response to different stimuli was studied. It is remarkable that the transition temperature of the nanogel particles dispersed in PBS was given at physiological conditions (38 °C and pH 7.1), demonstrating the potential use of these nanoparticles in several bio-applications.

**d.** The tunable and dual sensitivity at physiological conditions makes the nanogels attractive and potentially applicable in drug delivery, as they can be tailored to suit the needs of a particular bio-application.

**2.** New dual stimuli-responsive PDEAEMA-based nanogels were synthesized by surfactant-free emulsion polymerization, and stable pH- and temperature-responsive nanogel particles were obtained. The effects of different variables such as the initiator, cross-linker and stabilizer concentrations, the cross-linker type and some functionalizations on the swelling-de-swelling behavior of the nanogels were also studied:

**a.** An increase in the initiator concentration provoked a decrease in the size of collapsed nanogel particles, but the swelling properties remained constant: neither the transitions nor the swelling capability were affected.

**b.** Allowing for the possibility to tune the size and swelling properties of nanogels by varying the cross-linker type, different types of cross-linkers were tried for the synthesis of PDEAEMA-based nanogels. Two main families of nanogels could be distinguished: the one synthesized by using EG-based cross-linkers (EGDMA and PEGDA) and the one synthesized by using disulfide-based cross-linkers (BAC and DSDMA).

**c.** Regarding the family of nanogels synthesized by using EG-based cross-linkers, the swelling-de-swelling behavior and morphology of nanogels were analyzed. On the one hand, the cross-linker type had any effect neither on the VPTpH and VPTT values nor on the size of nanogels. However, the swelling capability was noticeably affected: nanogel synthesized by using PEGDA as cross-linker showed much higher swelling ratio values comparing to the ones obtained by using EGDMA, due to the higher hydrophilicity and larger length between the cross-linking points of PEGDA comparing to EGDMA. On the other hand, the inner structure of nanogels was studied through $^{1}H$ transverse relaxation NMR experiments confirming a core-shell type heterogeneous morphology for the nanogels. It was also concluded that the cross-linker type affected the cross-linking points' distribution and thus the heterogeneity in morphology of nanogels: the ones obtained by using EGDMA had more heterogeneous morphology than the ones cross-linked with PEGDA, due to the higher reactivity of the former with the main monomer (DEAEMA). In addition, the swelling ratios and the different cross-linking points' distributions were related, concluding that the nanogel with the most homogeneous morphology achieved the highest swelling ratio.

**d.** According to the nanogels synthesized by using disulfide-based cross-linkers, the initiator system was firstly optimized since a low final conversion was achieved when using a thermal initiator. This low conversion was attributed to the side reactions of the disulfide group. A redox initiator system was used to reduce the possibility of side reactions of the disulfide groups since it enables the reaction polymerizations to carry out at lower

temperatures. Regarding the effect of the cross-linker (BAC and DSDMA) on the nanogels swelling-de-swelling behavior, nanogels obtained by using DSDMA showed slightly lower swelling than in the case of using BAC. This result was related to the cross-linkers reactivity with the main monomer and the morphology of the nanogels.

**e.** Regarding the effect of the cross-linker concentration on the swelling-de-swelling behavior, there was not any effect on the VPTpH and VPTT values, the sharpness of the transitions and the size of the nanogel particles. Nevertheless, it was found that a decrease in the cross-linker amount provoked an increase in the swelling ratio.

**f.** Owing to the advantages of PEGylation for bio-applications, a new family of nanogels was synthesized by adding different amounts of PEGMA, and their colloidal characterization was carried out. Nanogels still showed dual-stimuli-sensitivity but the swelling capability decreased. In addition, being PEG hydrophilic, the VPTT was shifted toward higher temperatures and as the presence of PEGMA screened the charges, the VPTpH shifted to higher pH values. The results suggest a more heterogeneous inner structure of PEGylated nanogel particles than the nanogels without any PEGMA.

**g.** Considering the crucial role of nanogels functionalization to provide novel properties such as bioconjugation, epoxide- and primary amine-functionalized nanogels were obtained. The functionalization of nanogels was validated only qualitatively because of the low amount of functional groups. Then, the stimuli-responsive swelling-de-swelling behavior of the nanogels was also studied. Functionalized nanogels also showed significant stimuli-responsive behavior.

**h.** The syntheses and characterizations of new dual-stimuli-responsive nanogels were reported in this Chapter. The broad selection of stimuli-sensitive swelling-de-swelling behaviors offers some benefits towards the nanogels across the multidisciplinary field of biomedical applications.

**3.** The incorporation of MNPs into the previously synthesized dual-stimuli-responsive PDEAEMA-based nanogels yielding multi-responsive MNGs is described. For that purpose,

different preparation methods were used and a variety of magnetic-labelled nanogels' families were obtained. They were thoroughly characterized by means of their colloidal, morphological, thermogravimetric, and magnetic properties.

**a.** The preparation of the first family of MNGs was carried out by incorporating CA-coated MNPs into PEGylated PDEAEMA-based nanogels taking advantage of electrostatic interactions. The MNGs obtained were found to undergo significant pH- and thermo-responsive volume changes as well as showing high magnetic response.

**b.** The second family of MNGs was prepared by encapsulating different concentrations of CA-coated MNPs into primary-amine functionalized PDEAEMA-based nanogels. Superparamagnetic MNGs with high magnetic loading and magnetizations were obtained also in this case. Even some agglomeration was observed in the pH range of 7-8 due to the large amount MNPs, the attachment of MNPs to the nanogel particles was strengthened because of the presence of primary amine groups in the nanogels able to form H-bonds with the MNPs. Some MNGs were also obtained by covalently binding the MNPs to the nanogels, strengthening even more the attachment.

**c.** The third family of MNGs was prepared by binding uncoated MNPs to the previously synthesized epoxide-functionalized PDEAEMA-based nanogels. Two different pHs were used for the preparation of the MNGs so as to optimize the reaction conditions, giving the opportunity to understand the attachment of MNPs to the nanogels. First of all, the formation of covalent bonding between the MNPs and nanogel particles was confirmed by FTIR analysis. The magnetic loading and thereby the magnetic response were found to be much higher when a pH of 6 was used for the preparation. This result was attributed to the favoured reactions between epoxide and hydroxide groups at pH 6, as well as the easier interaction between the different nanoparticles due to the weaker repulsive interactions and higher dispersibility of MNPs in water at pH 6. These MNGs showed the typical pH-responsiveness together with high magnetic response and superparamagnetic behavior.

**d.** Syntheses and characterizations of a series of new dual-stimuli-responsive MNGs were reported in this Chapter. Owing to both the stimuli-responsive behavior together with the

high magnetic response of magnetic nanoparticles, the resultant hybrid nanogels exhibit such advantageous features for biomedical applications such as stimuli-mediated MRI, hyperthermia, magnetically guided controlled drug delivery, and cellular uptake, among others. Although the evaluation of the *in vitro* and *in vivo* performance of MNGs against tumor growth is obviously required, this work demonstrates the great potential of the MNGs obtained as a theranostic system.

**4.** The potential application of some multi-responsive PDEAEMA-based nanogels was analyzed.

a. Cytotoxicity tests of some PDEAEMA-based nanogels using a HeLa cell line were performed, concluding the concentration range at which nanogels are cytocompatible: nanogels were cytocompatible at the concentration range of 0.005-0.05 mg/mL at 24 h, but at 48 h only nanogel PM0 was cytocompatible at the lowest concentrations used (0.01 and 0.005 mg/mL).

b. Preliminary *in vitro* experiments on the biocompatibility of MNGs with human blood cells were also carried out, by using different media to disperse the whole blood. A tolerable biochemical compatibility of the MNGs with human blood cells was evidenced in the presence of autologous plasma, since plasma was able to protect RBCs and Plts from any damages and adverse effects. These results suggest that MNGs could be potentially useful for biomedical applications by using plasma. However, when plasma was isolated and physiological saline was used to disperse the blood, MNGs attached to the RBCs membrane and some haemolysis occurred, hampering the clinical use of the MNGs synthesized.

c. The applicability of the selected nanogels as cargo release systems was also studied. It was observed that the selected nanogels PM0 and PM10 were able to efficiently load a high DOXO content up to 40 %. The diffusion of the drug upon swelling of the nanogels favoured the uptake and the cargo was encapsulated by means of H-bonds between the drug and the polymeric chains. After the encapsulation of DOXO, nanogels were slightly larger in size.

d. The colloidal stability of DOXO-loaded nanogels was analyzed in cell culture media at different pHs, mimicking biological conditions: pH 5.2 (in the endosomes/lysosomes) and pH 7.4 (in the bloodstream). Nanogels were colloidally stable for many days at pH 5.2, but some agglomerates were formed at pH 7.4 after few days of incubation with cells. Nanogels were colloidally stable since the electrostatic repulsions between polymeric chains were strong and the adsorption of BSA was not favoured. However, nanogels agglomerated at pH 7.4 because of the weakened electrostatic repulsions between polymeric chains, together with the favoured adsorption of BSA on the nanogels.

e. The DOXO release kinetics was examined at different pHs: pH 5.2 mimicking the acidic tumor cells and pH 7.4 mimicking the normal cells. Regardless of the pH, nanogels showed a burst release within the first 20 h of incubation and then a sustainable release up to 85-100 % of the total loading amount. Interestingly, the release of DOXO was faster at acidic conditions, as the nanogel particles were swollen and the extended PDEAEMA chains favoured the release of the drug. Additionally, by fitting the release profiles to the Peppas-Sahlin model, the faster release at acidic conditions was corroborated and it was concluded that diffusion was the main mechanism governing the drug release.

f. The cellular uptake of DOXO-loaded nanogels and the progressive release of drug from the nanogels to the cell nuclei were demonstrated by spectrofluorimetric measurements.

g. Biocompatibility of the PDEAEMA-based multi-responsive nanogels with HeLa and human blood cells was confirmed and the suitability of the nanogels as potential carriers of DOXO was also validated.

# Appendix I

## Chemical Structures of the Reagents Used and List of Symbols

# I.1. Reagents

## I.1.1. Monomers

2-(diethylamino)ethyl methacrylate (DEAEMA)

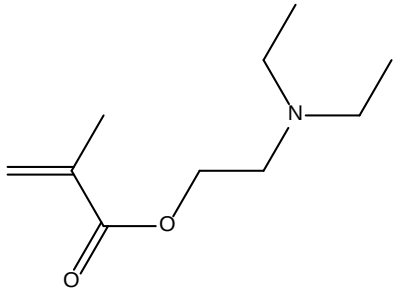


Glycidyl methacrylate (GM)

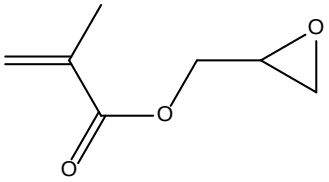


(2-Boc-amino)ethyl methacrylate (A-Boc)

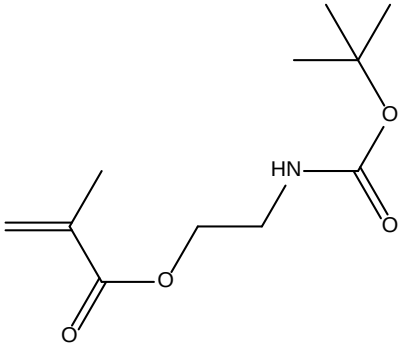

## I.1.2. Cross-linkers

Ethylene glycol dimethacrylate (EGDMA)

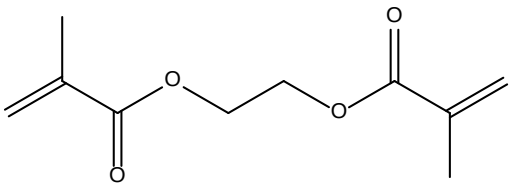

Poly(ethylene glycol) diacrylate (PEGDA)

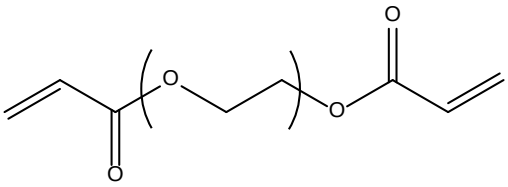

*N,N'*-Bis(acryloyl)cystamine (BAC)

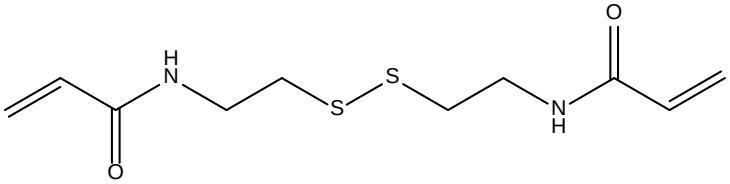

Bis(2-methacryloyl)oxyethyl disulfide (DSDMA)

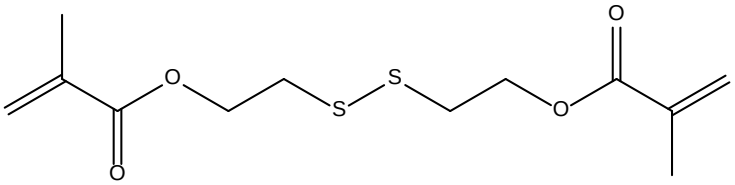

## I.1.3. Initiators

2,2′-azobis (*N,N′*-dimethyleneisobutyramidine) dihydrochloride (ADIBA)

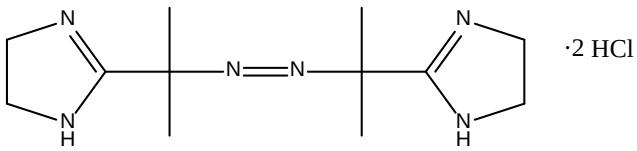


·2 HCl

Tetramethylethylenediamine (TEMED)

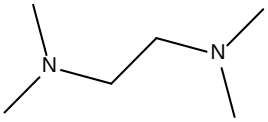


Potassium persulfate (KPS)

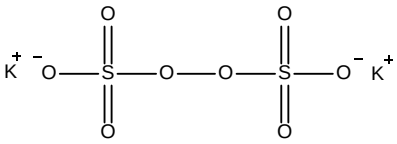


## I.1.4. Stabilizer

Poly(ethylene glycol) methacrylate (PEGMA, $M_n$=526)

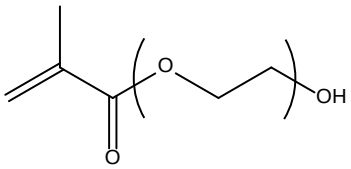

## I.1.5. Drug

Doxorubicin hydrochloride (DOXO)

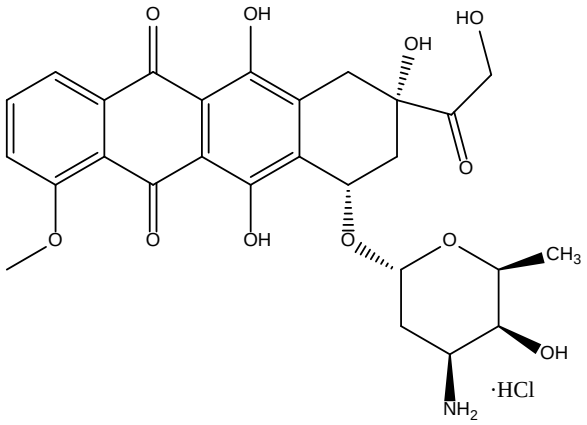

## I.1.6. Other reagents

*N*-(3-Dimethylaminopropyl)-*N*′-ethylcarbodiimide hydrochloride (EDC)

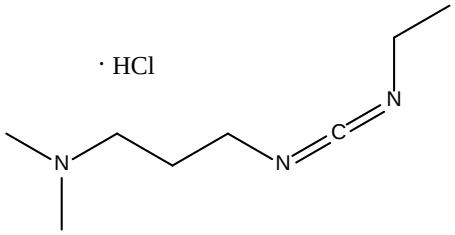


*N*-Hydroxysuccinimide (NHS)

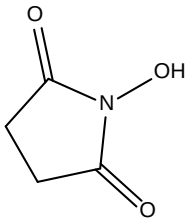


Citric acid (CA)

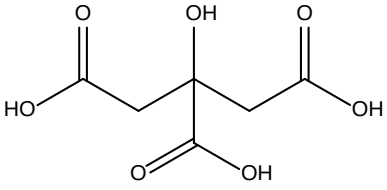

## I.2. List of Symbols

ADIBA 2,2′-azobis (N,N′-dimethyleneisobutyramidine) dihydrochloride

A-Boc (2-Boc-amino)ethyl methacrylate

AEMA 2-aminoethyl methacrylate

AFM Atomic Force Microscopy

BAC Bis(acryloyl)cystamine

Boc tert-butyloxycarbonyl

BSA Bovine Serum Albumin

CA Citric acid

CLD Cross-linking density

$D_2O$ Deuterium oxide

DAPI 4'-6'-diamidino-2-phenylindole dihydrochloride

DCl Deuterium chloride

DDI Double deionized water

DEAEMA 2-(diethylamino)ethyl methacrylate

DIC Differential Interference Contrast

D.L. Drug loading

DLS Dynamic Light Scattering

DOXO Doxorubicin hydrochloride

DSDMA Bis(2-methacryloyl)oxyethyl disulfide

EDC *N*-(3-Dimethylaminopropyl)-*N′*-ethylcarbodiimide hydrochloride

EDS Energy-dispersive X-ray Spectroscopy

EDTA Ethylenediaminetetraacetic acid

E.E. Encapsulation Efficiency

EG Ethylene glycol

EGDMA Ethylene glycol dimethacrylate

ELS Electrophoretic Light Scattering

FBS Fetal bovine serum

$FeCl_2 \cdot 4H_2O$ Ferrous chloride tetrahydrate

$FeCl_3 \cdot 6H_2O$ Ferric chloride hexahydrate

FTIR Fourier Transform Infrared

GM Glycidyl methacrylate
KSR-5 Thallium Bromoiodide
KPS Potassium persulfate
$H_C$ Coercivity
HCl Hydrochloric acid
IEP Isoelectric point
MNGs Magneto-nanogels
MNPs Magnetic nanoparticles
MRI Magnetic Resonance Imaging
$M_r$ Magnetic remanence
$M_S$ Saturation magnetization
MWCO Molecular weight Cut-off
NaCl Sodium chloride
NaOH Sodium hydroxide
NCH Non-Contact/tapping mode-High resonance frequency
NHS *N*-Hydroxysuccinimide
$NH_4OH$ Ammonium hydroxide
NIPAM *N*-isopropylacrylamide
NMR Nuclear Magnetic Resonance
OM Optical Microscopy
PBS Phosphate Buffered Saline
PCS Photon Correlation Spectroscopy
PDEAEMA Poly(diethylaminoethyl) methacrylate
PDMAEMA Poly(dimethylaminoethyl) methacrylate
PDI Polydispersity Index
PEG Poly(ethylene glycol)
PEGDA Poly(ethylene glycol) diacrylate
PEGMA Poly(ethylene glycol) methacrylate
Plts Platelets
PMMA Poly(methyl methacrylate)
PNIPAM Poly(*N*-isopropylacrylamide)
PVCL Poly(*N*-vinyl caprolactam)

PZC Point of zero charge
RBCs Red blood cells
SA Sodium acetate/acetic acid
SEM Scanning Electron Microscopy
siRNA Small interfering ribonucleic acid
STEM Scanning Transmission Electron Microscopy
TEM Transmission Electron Microscopy
TEMED Tetramethylethylenediamine
TFA Trifluoroacetic acid
TGA Thermogravimetric Analysis
VCL *N*-vinylcaprolactam
VPTpH Volume phase transition pH
VPTT Volume phase transition temperature
VSM Vibrating Sample Magnetometer
WBCs White blood cells
XRD X-ray diffraction

# Appendix II

## pH- and thermo-sensitivity of functionalized PDEAEMA-based nanogels and different effects on their swelling-de-swelling behaviors

# II.1. pH- and thermo-sensitivity of the nanogels

## II.1.1. Nanogels synthesized by using EGDMA as cross-linker

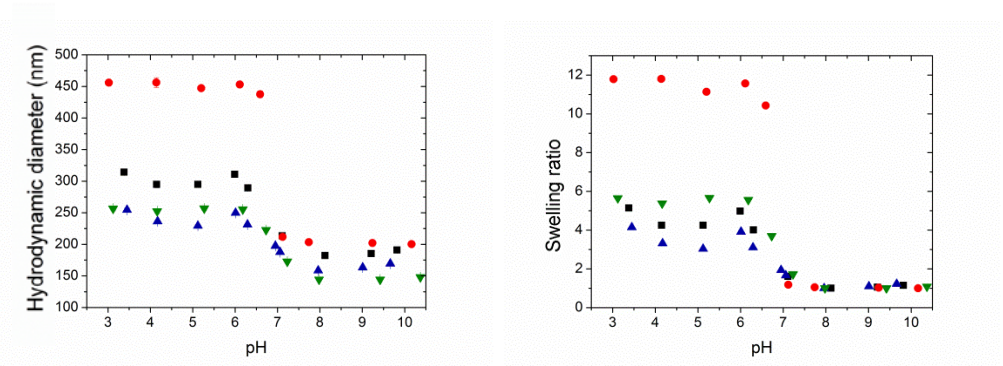


**Figure II.1.** Hydrodynamic diameters (left) and swelling ratios (right) of nanogels as a function of pH at 25 °C and an ionic strength of 10 mM. E0.93PM10 (■), E0.93PM20 (▲), E0.33PM10 (●), and E0.33PM20 (▼).

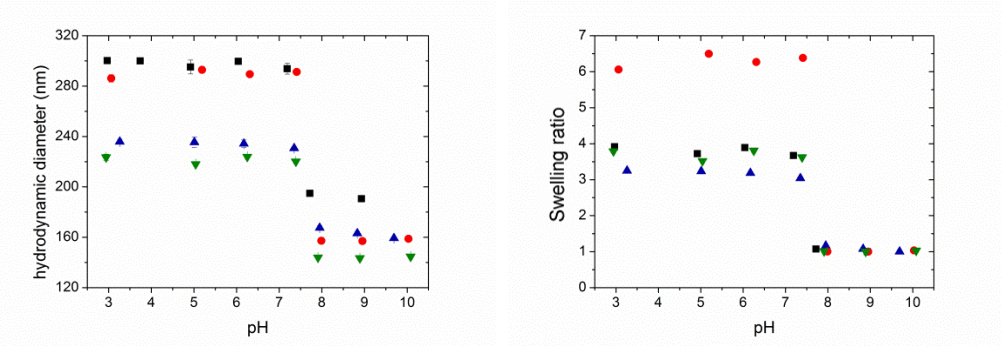


**Figure II.2.** Hydrodynamic diameters (left) and swelling ratios (right) of nanogels as a function of pH At 25 °C and an ionic strength of 150 mM in PBS.
E0.93PM10 (■), E0.93PM20 (▲), E0.33PM10 (●), and E0.33PM20 (▼).

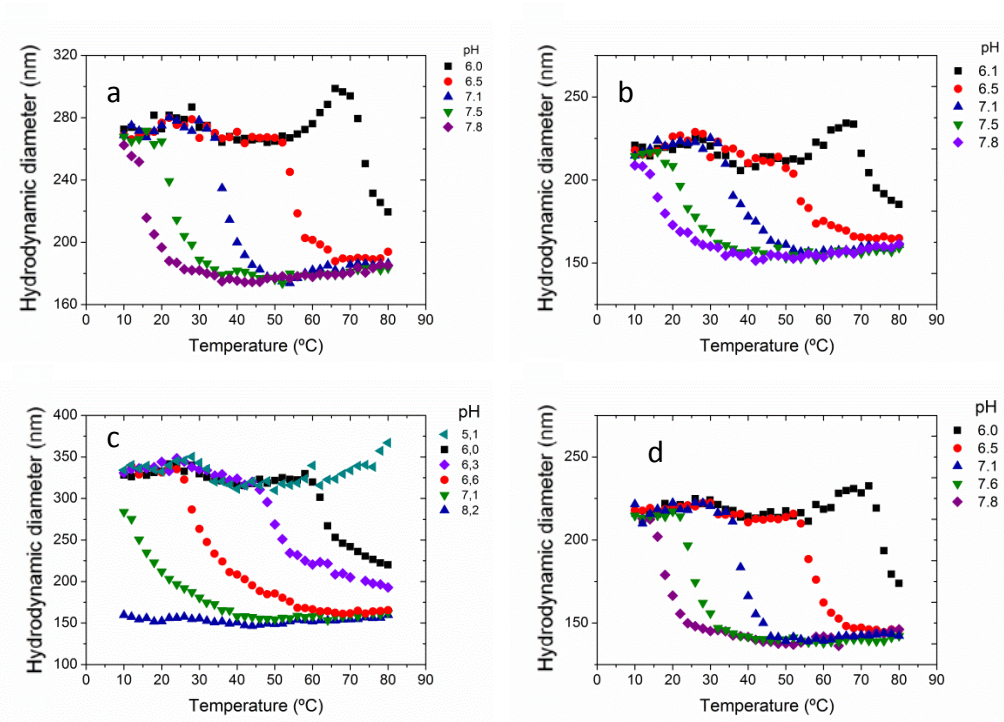


**Figure II.3.** Hydrodynamic diameters of nanogels as a function of temperature at different pHs at an ionic strength of 150 mM in PBS. E0.93PM10 (a), E0.93PM20 (b), E0.33PM10 (c), and E0.33PM20 (d).

## II.1.2. Nanogels synthesized by using PEGDA as cross-linker

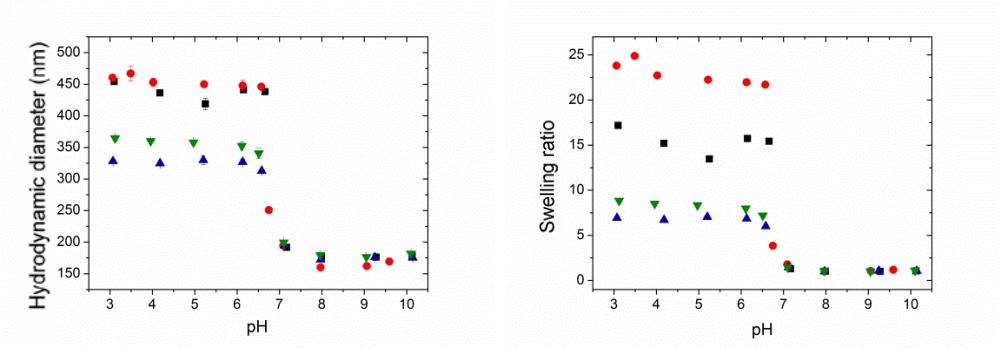


**Figure II.4.** Hydrodynamic diameters (left) and swelling ratios (right) of nanogels as a function of pH at 25 °C and an ionic strength of 10 mM.
PD0.93PM10 (■), PD0.93PM20 (▲), PD0.33PM10 (●), and PD0.33PM20 (▼).

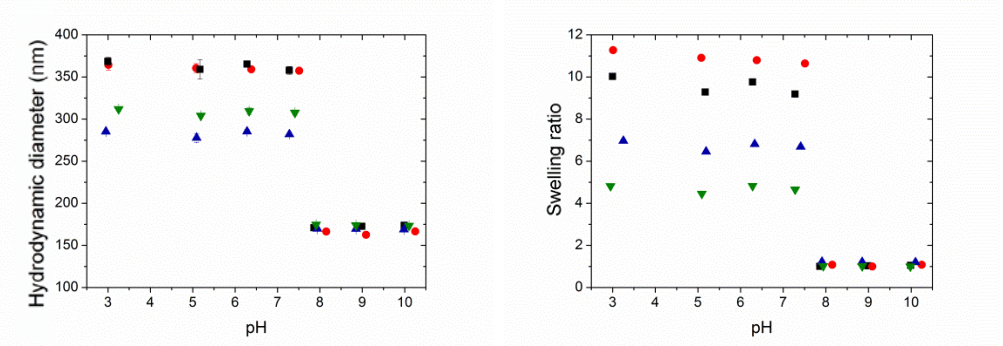


**Figure II.5.** Hydrodynamic diameters (left) and swelling ratios (right) of nanogels as a function of pH at 25 °C and an ionic strength of 150 mM in PBS.
PD0.93PM10 (■), PD0.93PM20 (▲), PD0.33PM10 (●), and PD0.33PM20 (▼).

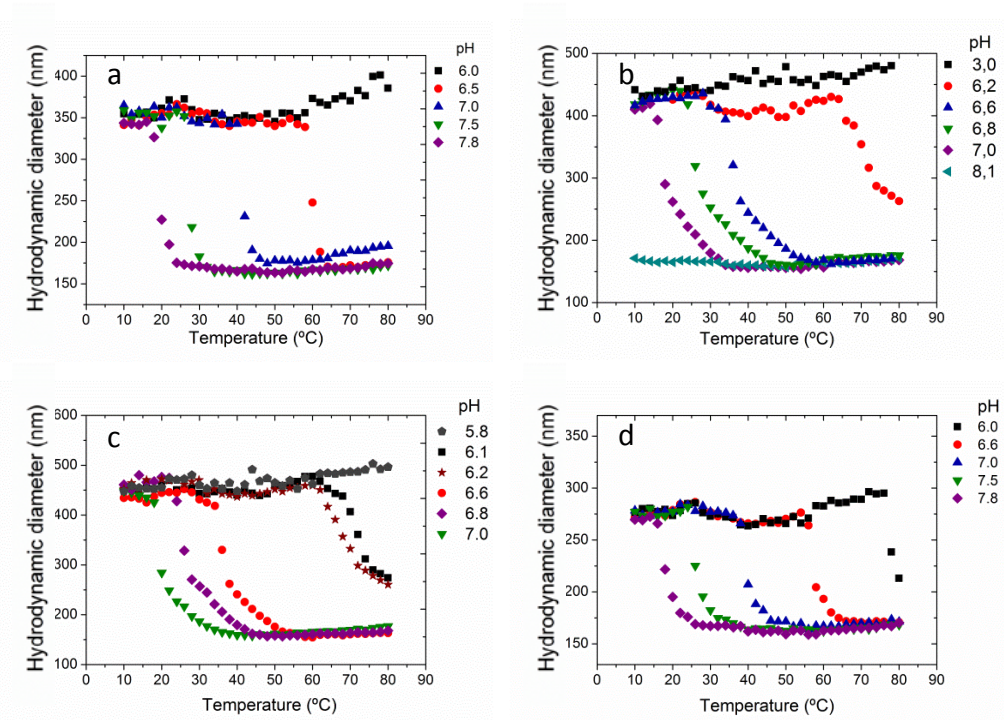


**Figure II.6.** Hydrodynamic diameters of nanogels as a function of temperature at different pHs at an ionic strength of 150 mM in PBS. PD0.93PM10 (a), PD0.93PM20 (b), PD0.33PM10 (c), and PD0.33PM20 (d).

## II.1.3. Nanogels synthesized by using BAC as cross-linker

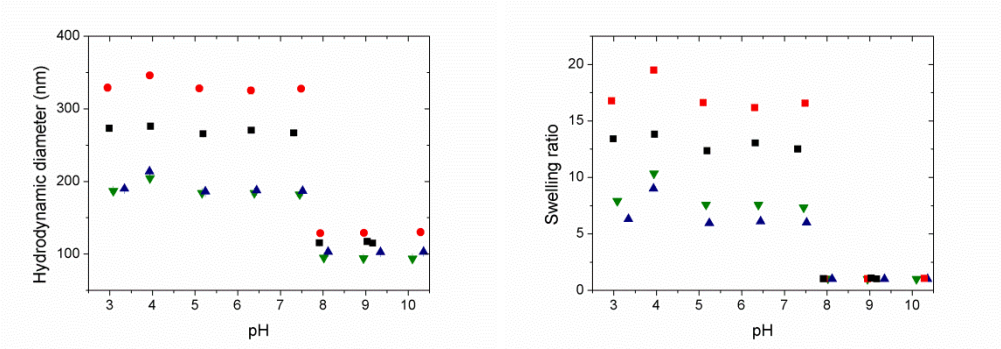


**Figure II.7.** Hydrodynamic diameters (left) and swelling ratios (right) of nanogels as a function of pH at 25 °C and an ionic strength of 150 mM in PBS.
RBAC0.93PM10 (■), RBAC0.93PM20 (▲), RBAC0.33PM10 (●), and RBAC0.33PM20 (▼).

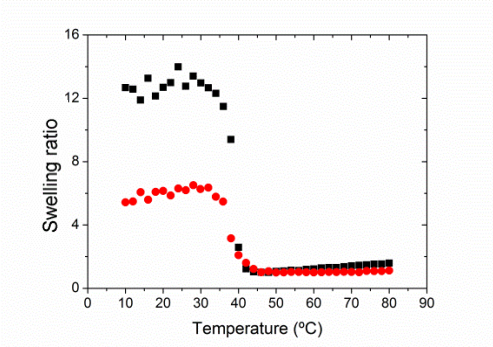


**Figure II.8.** Swelling ratio of nanogels RBAC0.33PM10 (■) and RBAC0.33PM20 (●) as a function of temperature at pH 7.4 and at an ionic strength of 150 mM in PBS.

# II.2. Different effects on the swelling-de-swelling behavior of nanogels

## II.2.1. Effect of the cross-linker type

Regarding the effect of the cross-linker type (EGDMA and PEGDA), the same tendency was observed regardless of the concentration of cross-linker and PEGMA used:

- VPTpH and size of collapsed nanogel particles were not affected by the cross-linker type.
- The transition sharpness of nanogels cross-linked with EGDMA was broader than that of the ones cross-linked with PEGDA, since the former had more heterogeneous inner structure.
- The swelling ratio was much lower in the case of using EGDMA compared to PEGDA, due to the higher hydrophobicity of EGDMA and the shorter distance between the cross-linking points on the one hand, and more heterogeneous inner structures obtained in the case of using EGDMA as cross-linker, on the other hand.
- Nanogels cross-linked with PEGDA underwent the transition at higher temperatures for a given pH. Being PEGDA more hydrophilic, higher temperatures were needed to disrupt H-bonds and thereby, to collapse the nanogel particles. This result is reflected in Figure II.9, which shows the pH-dependence of VPTT of some nanogels synthesized. VPTT values for nanogels cross-linked with EGDMA are visualized with solid symbols, while the ones for nanogels cross-linked with PEGDA are visualized with open symbols.

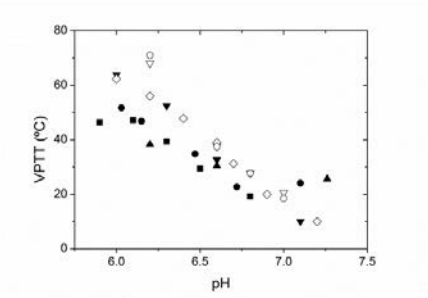


**Figure II.9.** VPTT values for nanogels E0.93PM0 (■), E0.93PM10 (●), E0.93PM20 (▲), E0.33PM10 (▼), PD0.93PM10 (○), PD0.33PM10 (▽), and PD0.33PM20 (◇) as a function of pH at an ionic strength of 10 mM.

## II.2.2. Effect of the cross-linker concentration

Independent of the cross-linker type (EGDMA, PEGDA, and BAC) and concentration of the stabilizer (PEGMA), increasing the cross-linker concentration from 0.33 to 0.93 mol%M:

- The size of collapsed nanogel particles did not vary.
- VPTpH and VPTT values were not affected.
- The sharpness of the transition was not influenced.
- An increase in cross-linker concentration provoked a decrease in swelling degree.

## II.2.3. Effect of the stabilizer (PEGMA) concentration

With regard to the stabilizer concentration on the dual-stimuli-responsive swelling-de-swelling behavior of nanogels, the same effects were seen irrespective of the type and concentration of the cross-linker used. Increasing the concentration of PEGMA from 10 to 20 wt%M:

- No variation in the size of collapsed nanogel particles was observed.
- No changes in VPTpH and VPTT values were observed.
- A decrease in the swelling ratio was observed because of an increase in cross-linking density *via* the formation of entanglements between the polymeric chains.
- The formation of nanogels with a more heterogeneous microstructure, and thereby broader pH- and temperature-dependent volume transitions, were observed.

## II.2.4. Effect of the ionic strength

The effect of the ionic strength and type of buffer on the stimuli-sensitivity of all the nanogels was studied. For that purpose, nanogels dispersed at an ionic strength of 10 mM and 150 mM (PBS) were compared. First of all, it is remarkable the high stability of all the nanogels even at high salt concentrations. Irrespective of the nanogel, by increasing the ionic strength, the transition was shifted to more alkaline conditions due to the increase in $pK_a$, the transition was sharper and the swelling of nanogel particles was hindered because of the electrostatic and osmotic screening. As an example, in Figure II.10, pH-sensitivities of nanogel PD0.33PM20 dispersed at 10 mM (cationic buffer) and at 150 mM (PBS) were shown and are useful to corroborate the observation.

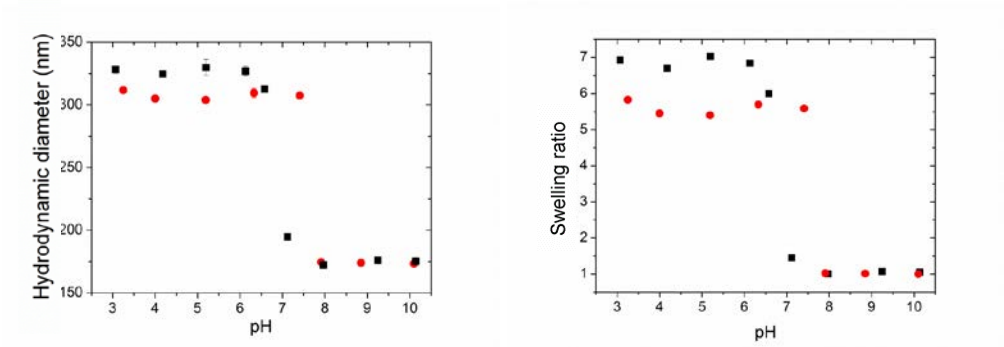


**Figure II.10.** Hydrodynamic diameters and swelling ratios of nanogel PD0.33PM20 dispersed at an ionic strength of 10 mM (■), and 150 mM (PBS) (●) as a function of pH.

The pH-dependent thermal behavior was also influenced by the salt concentration and type of buffer. Nanogels dispersed in PBS at 150 mM underwent sharper transitions, and the temperatures were higher for a given pH, due to the increase in $pK_a$ and the hindered deprotonation. Figure II.11 shows the VPTT values as a function of pH for nanogel PD0.33PM20 dispersed at 10 mM in a cationic buffer and in PBS at 150 mM.

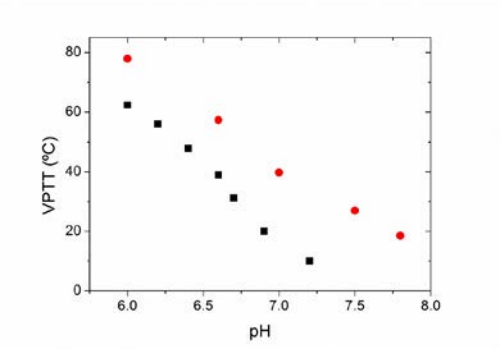


**Figure II.11.** VPTT values for nanogel PD0.33PM20 dispersed at an ionic strength of 10 mM (■) and 150 mM (PBS) (●) as a function of pH.

# Appendix III

## Synthesis and Characterization of Magnetic Nanoparticles

The synthesis and characterization of the MNPs used to prepare the MNGs reported in Chapter 4 are described here.

# III.1. Synthesis of Magnetic Nanoparticles

## III.1.1. Synthesis of uncoated Magnetic Nanoparticles (MNPs)

$Fe_3O_4$ MNPs were synthesized by the coprecipitation method.[1] 10.8 g of $FeCl_3 \cdot 6H_2O$ and 4.0 g of $FeCl_2 \cdot 4H_2O$ (2:1 molar ratio) were dispersed in 200 mL DDI water. 6.4 g of NaOH was also dispersed in 200 mL DDI water. They were mixed together and placed into a 500-mL jacketed glass reactor. The reactor content was stirred at 500 rpm, and purged with nitrogen. The reaction was carried out for 3 h.[2]

## III.1.2. Synthesis of citric acid-coated Magnetic Nanoparticles (CA-MNPs)

Surface coating with citric acid (CA) was used to confer carboxylic groups to the surface of the MNPs, providing in this way the required hydrophilic properties and colloidal stability in water to the MNPs. CA-coated MNPs of magnetite, $Fe_3O_4$, were obtained in the following way: a 0.4 M $FeCl_3 \cdot 6H_2O$ solution (21.6 g in 200 mL of DDI water) and a 0.2 M $FeCl_2 \cdot 4H_2O$ solution (8.0 g in 200 mL of DDI water) (2:1 molar ratio) were mixed together and placed into a 500-mL jacketed glass reactor, the reactor content was heated at 80 °C, stirred at 300 rpm, and purged with nitrogen. Then, 50 mL of $NH_4OH$ solution was added dropwise during 10 min. Subsequently, 40 mL of 2 M CA solution were immediately added into the suspension, and the reaction was carried out for 1 h.[3]

# III.2. Characterization of Magnetic Nanoparticles

## III.2.1. Uncoated Magnetic Nanoparticles (MNPs)

Since the aim was to obtain hydroxide groups at the surface of MNPs, NaOH was used as alkaline base, and no steric stabilizer was used in the synthesis of MNPs.

First of all, XRD analysis was performed to analyze the phase of the synthesized MNPs (see Figure III.1). The XRD profile reveals that MNPs consisted of highly crystalline particles of magnetite and matched with the theoretical one. From the absence of (219) and (300) peaks in the XRD profile, it was confirmed the absence of maghemite.[4-8]

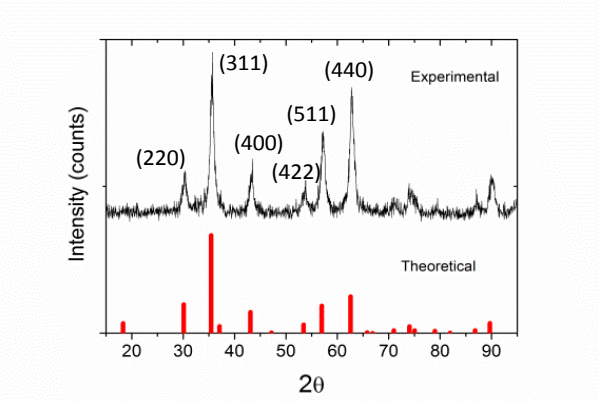


**Figure III.1.** X-ray diffraction profile of the MNPs synthesized (experimental) and the theoretical one for MNPs of magnetite. The numbers in parentheses indicate the (*hkl*) planes.

FTIR analysis was further used with the aim of analyzing the functional groups of the synthesized MNPs (see Figure III.2). The peak around 3376 $cm^{-1}$ was assigned to the stretching (v) vibrations and the one at 1620 $cm^{-1}$ to the bending (δ) vibrations of the –OH groups due to adsorbed water on the surface of MNPs. The peak at 560 $cm^{-1}$ corresponds to Fe-O stretching vibrations.[4-10] From these results, it was confirmed the presence of hydroxide groups at the surface of the MNPs synthesized, as illustrated in the schematic representation of an uncoated MNP (Figure III.2).

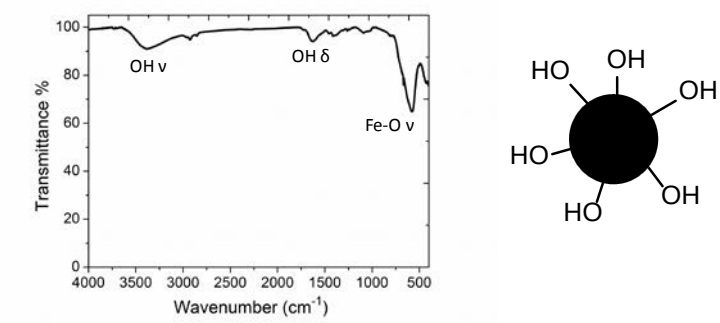


**Figure III.2.** FTIR spectrum of uncoated MNPs (left)
and schematic representation of an uncoated MNP (right).

It is well known that the charge density is a predominant factor affecting the interactions between particles and varies greatly with pH. Figure III.3 shows the electrophoretic mobility values of uncoated MNPs and schematic representations of an uncoated MNP as a function of pH. The IEP was located at pH 7, in agreement with the values reported in literature.[5-7,11,12] Magnetite is an amphoteric solid which can develop charges by protonation (Fe-$OH_2^+$) and deprotonation (Fe-$O^-$) of Fe-OH sites on surface, due to the adsorption of $H^+$ and $OH^-$ ions at the hydrated interface of the MNPs.[13] As shown in the schematic representations of an uncoated MNP as a function of pH, MNPs were protonated (Fe-$OH_2^+$) at lower pHs than pH 6, while they were negatively charged (Fe-$O^-$) at more alkaline pHs than pH 6.

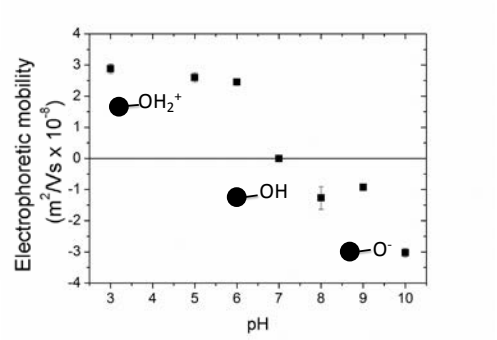


**Figure III.3.** Electrophoretic mobility values of uncoated MNPs and schematic representations of an uncoated MNP as a function of pH at an ionic strength of 10 mM.

Potentiometric titrations were also carried out, and the degree of ionization (α) was calculated as a function of pH (see Figure III.4). The point of zero charge (PZC) could be determined as the pH where the degree of ionization (α) = 0. For the MNPs, the PZC was found to be at around pH 7.0, which was the same as the IEP.

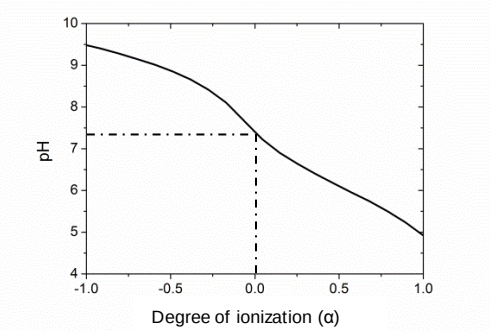


**Figure III.4.** pH/α curve of uncoated MNPs.

Moreover, the morphology of the MNPs' samples was determined by TEM. As Figure III.5 displays, the majority of the $Fe_3O_4$ particles were nearly monodisperse in size and spherical in shape. Even though some magnetite nanoparticles were partially superimposed onto the agglomerate core and the average particle size could not be determined precisely, it was found to be between 10-20 nm. The formation of large agglomerates was attributed to the reduction of surface energy and also to the magnetic dipole-dipole interactions and the van der Waals forces between $Fe_3O_4$ nanoparticles.[7,14] However, with the hydroxyl groups, the obtained MNPs had good stability and dispersibility in water.[15]

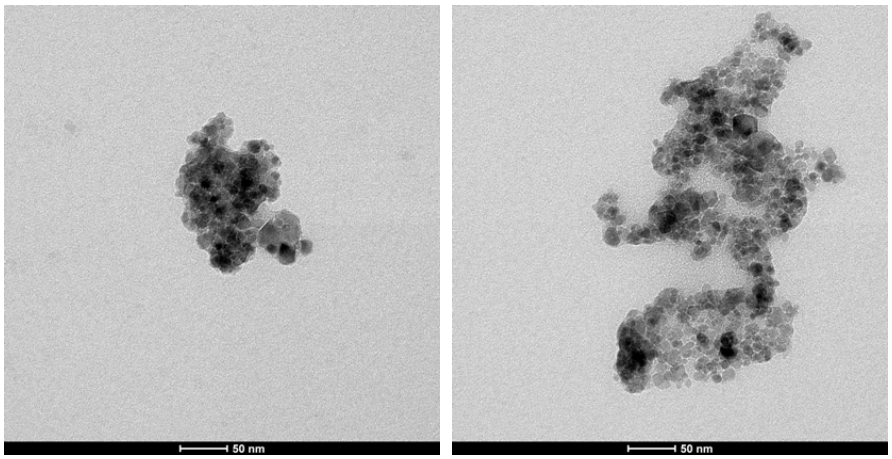


**Figure III.5.** TEM microphotographs of uncoated MNPs.

Furthermore, EDS analyses were carried out to ensure the chemical composition of the MNPs synthesized. The spectrum shown in Figure III.6 verified the high amount of Fe in the MNPs.

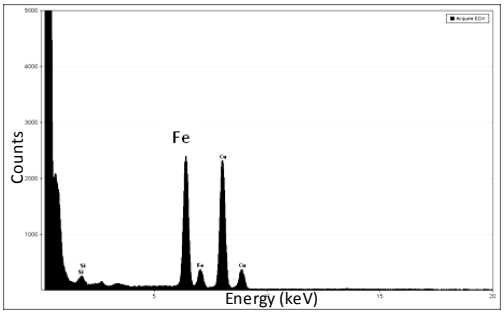


**Figure III.6.** EDS analysis of uncoated MNPs.

In addition, Figure III.7 shows the TGA curve of the MNPs obtained by using a thermogravimetric analyzer. As the analysis was performed under $N_2$ atmosphere, the oxidation of MNPs of magnetite was avoided. The weight loss of 6 % occurring was ascribed to the dehydration of the hydroxyl groups on the nanoparticles surface, in agreement with other works in literature.[16]

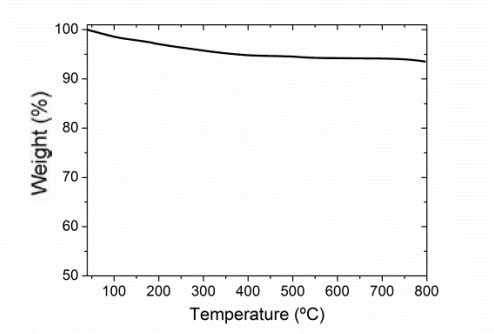


**Figure III.7.** TGA curve of uncoated MNPs.

Additionally, the magnetic properties of the $Fe_3O_4$ nanoparticles synthesized were analyzed by using a VSM. The magnetization curve shown in Figure III.8 was obtained by plotting the magnetization of the sample with the applied magnetic field. The $M_S$ value of uncoated MNPs was about 60 emu/g at 25 °C, which was in agreement with the values obtained in literature.[17] Moreover, the hysteresis curves indicated the superparamagnetic behavior of the MNPs synthesized, since almost negligible coercivity or remanence existed.

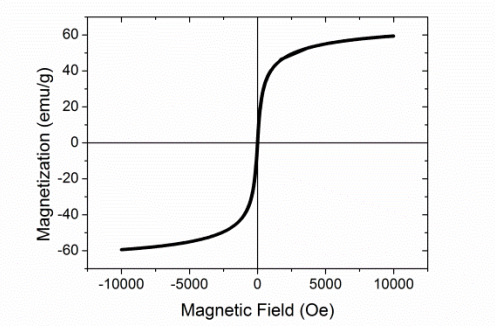


**Figure III.8.** Magnetization curve of uncoated MNPs at 25 °C.

## III.2.2. Citric acid-coated Magnetic Nanoparticles (CA-MNPs)

Functionalization of the surface of MNPs using small molecules that gives electrosteric stabilization to the MNPs has gained great interest. In this work, as commented in

the experimental part, MNPs were stabilized using citric acid (CA), which provided a charged surface resulting from the carboxylic groups. CA is a small molecule containing three carboxyl groups and one hydroxyl group (see Figure III.9a) and it is able to chemisorb onto iron oxide nanoparticles by forming a carboxylate group with the Fe-OH molecules present onto the nanoparticle surface, leaving one or two negatively charged carboxyl groups that can be used for other purposes.[18,19] The MNPs synthesized are named CA-MNPs.

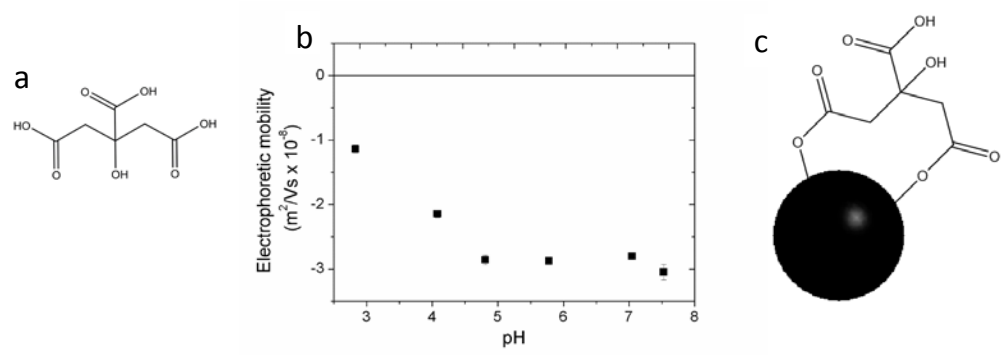


**Figure III.9.**The chemical structure of citric acid (a), electrophoretic mobilities of the MNPs as a function of pH at an ionic strength of 10 mM (b), and the possible schematic representation of a citric acid-coated MNP (citric acid coating on the surface of MNPs) (c).

Electrophoretic mobility measurements shown in Figure III.9b confirmed that the adsorption of CA onto the surface of MNPs resulted in a highly negative surface charge, due to the presence of negatively charged carboxylate groups on the surface of MNPs. The isoelectric point (IEP) was not observed in the pH range of pH 3-8. Moreover, the electrostatic repulsive forces among the highly negatively charged MNPs in aqueous suspension are known to play an important role in their water stabilization, as reported by Kumar *et al*.[20] and Nigam *et al*.[21] with CA-coated iron oxide nanoparticles.

In addition, XRD analysis was performed to investigate the phase of the synthesized CA-MNPs (see the XRD profile in Figure III.10). The XRD profile reveals that CA-MNPs consisted of highly crystalline particles of magnetite. The main characteristic peaks were obtained with the (*hkl*) values of (220), (311), (400), (422), (511), and (440). As can be seen in Figure III.10, the XRD profile obtained matched with the theoretical one. From the absence of

(219) and (300) peaks in the XRD profile, it can be stated that no maghemite was present in the sample,[4-8] confirming the successful synthesis of MNPs of magnetite.

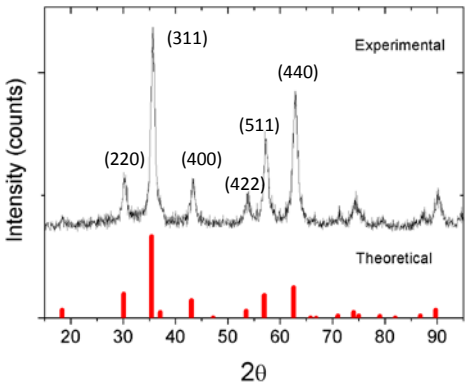


**Figure III.10.** X-ray diffraction profile of CA-MNPs synthesized (experimental) and the theoretical one for MNPs of magnetite. The numbers in parentheses indicate the (*hkl*) planes.

TEM microphotographs of the CA-MNPs in Figure III.11 show that the obtained MNPs were spherical, monodisperse in size and of about an average size of 10 nm. As the magnetite particle size was less than 15 nm it was expected for them to exhibit superparamagnetic behavior. In this work, CA was used in order to ensure colloidal stability and the results indicate that CA performed as an effective stabilizer. As reported by various authors, iron oxide nanoparticles are usually coated with biocompatible organic or inorganic materials to ensure biocompatibility and prevent agglomeration.[22-25] However, as confirmed by TEM measurements, some of them formed large particulate clusters of about 40-100 nm in size due to the attractive dipole-dipole and van der Waals interactions between the MNPs. These attractive interactions were weaker than in the case of uncoated MNPs because of the coating by CA.

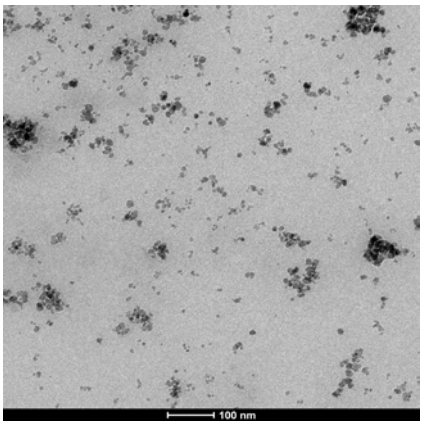


**Figure III.11.** TEM microphotographs of CA-MNPs.

Moreover, hydrodynamic diameters of around (160 ± 5) nm were obtained by PCS measurements in the range of pH 3-8, suggesting the formation of MNP clusters of smaller nanoparticles. In order to understand this difference in size, it should be taken into account that the sizes measured by TEM and PCS are not comparable, since the particles are dry in the case of using TEM while they are dispersed in water in the case of using PCS.[26,27]

Furthermore, EDS analyses were carried out to ensure the chemical composition of the MNPs synthesized. The spectrum shown in Figure III.12 verifies that CA-MNPs contained a large amount of Fe.

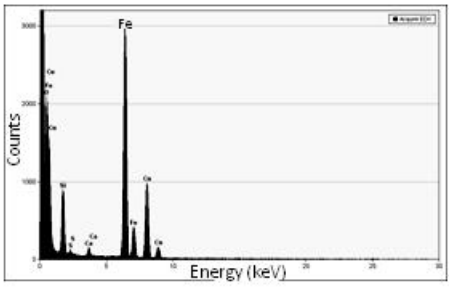


**Figure III.12.** EDS analysis of CA-MNPs.

Moreover, the thermogravimetric analysis of the CA-MNPs was carried out. From the TGA curve shown in Figure III.13, it can be stated that CA-MNPs had little weight loss

attributed to the decomposition of CA: 4.25 wt%. The content of CA grafted on MNPs was estimated to be 0.22 mmol/g.

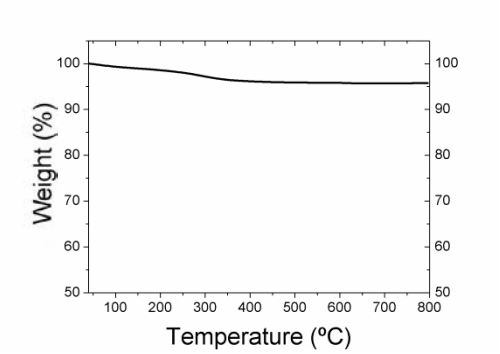


**Figure III.13.** TGA curve of CA-MNPs.

To examine the magnetic behavior of the MNPs synthesized, magnetic measurements were carried out at 25 °C. The magnetic hysteresis loop shown in Figure III.14 reflects the response ability of magnetic materials to an external magnetic field. The saturation magnetization ($M_S$) value was 57.2 emu/g at 10 kOe, which is enough for bio-medical applications.[28-31] This value was slightly lower than uncoated MNPs (60 emu/g) obtained by co-precipitation method,[32] because of the coating by CA. Moreover, it was seen that the nanoparticles had very low coercivity and no hysteresis, confirming their superparamagnetic behavior. This feature was actually in accordance with what was expected from their particle size. Taking the equation given by Yamaura *et al*.[33] and the $M_S$ obtained for the MNPs (57.2 emu/g), a critical diameter of 15 nm was obtained for the MNPs, which was similar to that obtained by TEM.

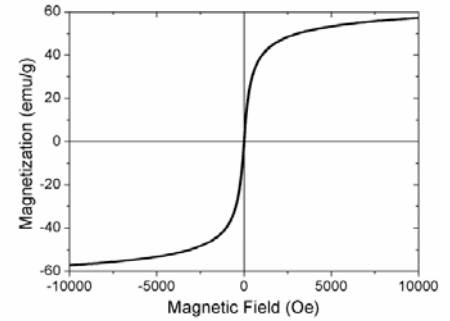


**Figure III.14.** Magnetization curve of CA-MNPs.

Summarizing, due to the coating by CA, CA-MNPs were more uniformly distributed and had negative surface charge in all the pH range arising from the carboxylic groups, while uncoated MNPs showed an IEP and/or PZC at pH 7, due to the protonation/deprotonation of hydroxyl groups of MNPs. Comparing the magnetization curves of different MNPs, both of them showed a $M_S$ of around 60 emu/g, even though the coating by CA made the $M_S$ to decrease to some extent.

These aqueous stable and superparamagnetic MNPs having high magnetic response show potential for magnetic drug targeting, hyperthermia treatment, and Magnetic Resonance Imaging (MRI), among other biomedical applications.

## III.3. References

1. J. Ugelstad, P. Stenstad, L. Kilaas, W. S. Prestvik, R. Herje, A. Bererge, E. Hornes, *Blood Purif.* **1993**, *11*, 349-369.
2. M. C. Mascolo, Y. Pei, T. A. Ring, *Materials* **2013**, *6*, 5549-5567.
3. R. A. Frimpong, J. Z. Hilt, *Nanotechnology* **2008**, *19*, 175101, 7 pp.
4. M. Kokate, K. Garadkar, A. Gole, *J. Mater Chem. A*, **2013**, *1*, 2022-2029.
5. S. J. Iyengar, M. Joy, C. K. Ghosh, S. Dey, R. K. Kotnala, S. Ghosh, *RCS Adv.* **2014**, *4*, 64919-64929.
6. R. M. Patil, P. B. Shete, N. D. Thorat, S. V. Otari, K. C. Barick, A. Prasad, R. S. Ningthoujam, B. M. Tiwale, S. H. Pawar, *RCS Adv.* **2014**, *4*, 4515-4522.

7. P. B. Shete, R. M. Patil, R. S. Ningthoujam, S. J. Ghosh, S. H. Pawar, *New J. Chem.* **2013**, *37*, 3784-3792.
8. Z. Ma, Y. Guan, H. Liu, *J. Polym Sci., Part A: Polym Chem.* **2005**, *43*, 3433-3439.
9. J. Zhang, Z. Lu, M. Wu, Q. Wu, J. Yang, *RCS Adv.* **2015**, *5*, 58889-58894.
10. N. Puvvada, D. Mandal, P. Kumar Panigrahi, A. Pathak, *Toxicol. Res.* **2012**, *1*, 196-200.
11. Q. Zhang, F. Yang, F. Tang, K. Zeng, K. Wu, Q. Cai, S. Yao, *Analyst* **2010**, *135*, 2426-2433.
12. T. J. Daou, S. Begin-Colin, J. M. Grenche, F. Thomas, A. Derory, P. Bernhardt, P. Legar, G. Pourroy, *Chem. Mater.* **2007**, *19*, 4494-4505.
13. E. Tombácz, A. Majzik, Zs. Horvát, E. Illés, *Rom. Rep. Phys.* **2006**, *58*, 281-286.
14. L. F. Cótica, V. F. Freitas, G. S. Dias, I. A. Santos, S. C. Vendrame, N. M. Khalil, R. M. Mainardes, M. Staruch, M. Jain, *J. Magn. Magn. Mater.* **2012**, *324*, 559-563.
15. T. Chen, Z. Cao, X. Guo, J. Nie, J. Xu, Z. Fan, B. Du, *Polymer* **2011**, *52*, 172-179.
16. D. Serrano-Ruiz, S. Rangou, A. Avgeropoulos, N. E. Zafeiropoulos, E. López-Cabarcos, J. Rubio-Retama, *J. Polym. Sci., Part B: Polym. Phys.* **2010**, *48*, 1668-1675.
17. M. Yamaura, R. L. Camilo, L. C. Sampaio, M. A. Macêdo, M. Nakamura, H. E. Toma, *J. Magn. Magn. Mat.* **2004**, *279*, 210-217.
18. L. Li, K. Y. Mak, C. W. Leung, K. Y. Chan, W. K. Chan, W. Zhong, P. W. T. Pong, *Microelectron. Eng.* **2013**, *110*, 329-334.
19. M. E. De Sousa, M. B. Fernández van Raap, P. C. Rivas, P. Mendoza Zélis, P. Girardin, G. A. Pasquevich, J. L. Alessandrini, D. Muraca, F. H. Sánchez, *J. Phys. Chem. C* **2013**, *117*, 5436-5445.
20. S. Nigam, K. C. Barick, D. Bahadur, *J. Magn. Magn. Mat.* **2011**, *323*, 237-243.
21. S. Kumar, C. Ravikumar, R. Bandyopadhyaya, *Langmuir* **2010**, *26*, 18320-18330.
22. L. Li, K. Y. Mak, C. W. Leung, K. Y. Chan, W. K. Chan, W. Zhong, P. W. T. Pong, *Microelectron. Eng.* **2013**, *110*, 329-334.
23. A.-H. Lu, E. L. Salabas, F. Schüth, *Angew. Chem. Int. Ed.* **2007**, *46*, 1222-1244.
24. M. Mahmoudi, S. Sant, B. Wang, S. Laurent, T. Sen, *Adv. Drug Delivery Rev.* **2011**, *63*, 24-46.
25. M. Mahdavi, M. B. Ahmad, M. J. Haron, F. Namvar, B. Nadi, M. Z. A. Rahman, J. Amin, *Molecules* **2013**, *18*, 7533-7548.

26. B. Luo, X.-J. Song, F. Zhang, A. Xia, W.-L. Yang, J.-H. Hu, C.-C. Wang, *Langmuir* **2010**, *26*, 1674-1679.
27. A. Pich, S. Bhattacharya, Y. Lu, V. Boyko, H.-J. P. Alder, *Langmuir* **2004**, *20*, 10706-10711.
28. Z.-P. Xiao, K.-M. Yang, H. Liang, J. Lu, *J. Polym. Sci., Part A: Polym. Chem.* **2010**, *48*, 542-550.
29. H. Lu, G. Yi, S. Zhao, D. Chen, L.-H. Guo, J. Cheng, *J. Mat. Chem.* **2004**, *14*, 1336-1341.
30. K. Xu, H. Gu, R. Zheng, H. Liu, X. Zhang, Z. Guo, B. Xu, *J. Am. Chem. Soc.* **2004**, *126*, 9938-9939.
31. X. Lu, R. Jiang, M. Yang, Q. Fan, W. Hu, L. Zhang, Z. Yang, W. Deng, Q. Shen, Y. Huang, X. Liu, W. Huang, *J. Mat. Chem. B* **2014**, *2*, 376-386.
32. Y.-Q. Zhang, X.-W. Wei, R. Yu, *Catal. Lett.* **2010**, *135*, 256-262.
33. M. Yamaura, R. L. Camilo, L. C. Sampaio, M. A. Macêdo, M. Nakamura, H. E. Toma, *J. Magn. Magn. Mat.* **2004**, *279*, 210-217.

# Laburpena

Gaur egun medikuntzan sekulako garrantzia lortu duen alorra da nanomedikuntza, diagnostiko zehatzagoak egiteko eta terapiak hobetzeko balio duela ikusi baita. Errate baterako, sendagai ugariren eraginkortasun terapeutikoa murriztua dago hainbat arrazoirengatik; disolbagarritasun mugatua, egonkortasun txikia, eta zitotoxikotasuna, bertzeak bertze. Arazo honen aitzinean, minbiziaren aurkako tratamenduen eraginkortasuna handitu eta botiken banaketa gorputzean zehar hobetu asmoz, garraiatzaile sistemen diseinua ezinbertzekoa bilakatu da. Agertoki honetan, kate polimeriko gurutzatuez osatutako partikula koloidalek, nanogel bezala ezagunak, arreta handia erakarri dute.

Nanopartikula hauek, uretan egonkorrak izateaz gain, daukaten egitura porotsua dela medio, botika kantitate handiak gorde eta modu kontrolatuan askatzeko gauza dira. Gainera biobateragarriak badira, tamaina nanometrikoari esker oztopo biologikoak gainditzeko eta organismo barruan askatasunez mugitzeko gai direnez, organismoko edozein tokitara heltzen ahal dira. Alabaina, kanpo-eragile baten aitzinean ematen duten bolumen-aldaketa azkarragatik lortu dute batez ere berebiziko arrakasta. Bolumen-aldaketaren trantsizio horiek polimero kateetan eragiten duten aldarapen (elektrostatikoak eta osmotikoak) eta erakarpen (hidrogeno-loturak, van der Waals indarrak eta indar hidrofoboak) indarren arteko balantzak arautzen ditu. Kanpo-estimuluak orotarikoak izan daitezke: fisikoak (tenperatura, eremu magnetikoa, erradiazioa…), kimikoak (pH-a, indar ionikoa…) edota biologikoak (entzimak, ligandoak…).

Nanogelak proteinen absortzioan, terapia genikoan, eta ehun-ingeniaritzan ere erabilgarriak izan daitezkeen arren, botiken garraiatzaile gisa duten potentziala agerikoa da. Minbiziaren aurkako tratamenduari dagokionez, odolean eta ehun osasuntsuetan botikari eusteko gai izan beharko luke garraiatzaileak, eta ehun gaixoetan askatu egin beharko luke, bertako seinale jakinei erantzunez. Ehun eta zelula gaixoetako pH-a (pH 5,2) ehun osasuntsuekiko ezberdina denez (pH 7,4), pH-arekiko sentikorrak diren nanogelak nabarmentzen dira. Horien artean, batik bat, pH azidoetan hazten direnak, zelula eta ehun gaixoetan puztu eta bertan medikamentuak askatuko bailituzkete. pH-ari erantzuten dioten nanogelak sortzeko, batez ere, amina tertziarioak dauzkaten polibaseak erabiltzen dira, pH azidoetan puzteaz landa, sendagaia zelularen nukleoan askatuta endosoma hausteko gai baitira. Hauen artean poli(dietilaminoetil) metakrilatoa (PDEAEMA) azpimarra daiteke, biobateragarria delako eta baldintza fisiologikoetan ematen baititu bolumen-aldaketak.

Gainera, nanogelei propietate erakargarriak emanen dituzten partikula ez-organikoak eransten ahal zaizkie; errate baterako, puntu kuantikoak, nanopartikula magnetikoak (NPMak), urrezko eta zilarrezko nanopartikulak, eta karbonozko nanoegiturak. Nanogelen kanpo-eragileekiko sentikortasuna eta nanopartikula ez-organikoen propietate kuantikoen (magnetismoa eta fotoluminiszentzia, kasu) arteko konbinazioari esker, biomedikuntzarako baliagarriak eta interesgarriak diren ezaugarrien jabe dira nanogel hibridoak.

NPMek, konparazio batera, sekulako garrantzia hartu dute, erraz sintetiza eta funtzionaliza daitezkeelako, biobateragarriak, biodegradagarriak, eta egonkorrak direlako, eta batez ere, erantzun superparamagnetikoa erakusten dutelako. NPMek abantaila anitzez hornitzen dituzte nanogelak, MNGak hainbat aplikazio biomedikoetan erabilgarri eginez; hala nola, erresonantzia magnetiko bidezko irudigintza, hipertermia magnetikoa, magnetikoki gidatutako farmakoen askatzea, eta magnetikoki lagunduriko hemodialisia.

Tesi honen helburu nagusia sentikortasuna anizkoitza duten nanogelen sintesia, karakterizazioa eta aplikazioetarako erabilera ikertzea dela erran daiteke.

Hasteko, lan honetan, PDEAEMAn oinarritutako nanogel partikula berriak sintetizatu dira emultsio polimerizazio bidez, baina emultsionatzailerik erabili gabe, hauen izaera toxikoa dela eta. Hori lortzearren, dietilaminoetil metakrilatoa (DEAEMA) erabili da monomero nagusi gisa, eta etilenglikol dimetakrilatoa (EGDMA) gurutzatzaile moduan. Lehenik eta behin, kanpo-eragileen aitzinean ematen dituen bolumen-aldaketak sakonki ikertu dira. Nanogel honek pH-a 7,5 denean ematen du bolumen-aldaketaren trantsizioa; pH horren azpitik nanogela hazita dago positiboki kargatutako amina taldeen arteko aldarapen elektrostatikoak tarteko, eta pH horren gainetik, indar hidrofoboak gailentzen direnez, nanogela uzkurtu egiten da. pH-ari erantzuteaz gain, pH-aren araberako termosentikortasuna ere badu nanogelak pH-a 6-8 den tartean, polimero kateak hidrogeno-loturak sortzeko gai baitira eta hauek tenperaturarekin apurtzen direnean nanogela uzkurtu egiten delako. Tarte horretan, pH-a zenbat eta azidoagoa izan, orduan eta tenperatura altuagoetan ematen dute bolumen-aldaketaren trantsizioa, aldarapen elektrostatikoek uzkurtzea zailtzen baitute. Aldakortasun hau interesgarria izan liteke, beharren arabera erregulatzeko aukera emanen lukeelako. Nanogelak kargatutako kate polimerikoez osatuta daudenez, beraien indar ionikoaren baitakoa da. Hori dela eta, indar ionikoak nanogelaren bolumen-aldaketetan duen eragina ere ikertu da: indar ionikoa handitzeak haztea murriztu eta bolumen-aldaketaren trantsizioak pH eta tenperatura altuagoetara mugiarazten dituela ikusi da. Gainera, Erresonantzia Magnetiko Nuklear (EMN) bidez nanogelak morfologia heterogeneoa duela frogatu da.

Nanogelen hazte/uzkurtze jokaerak aplikazio bakoitzaren eskakizunetara egokitua egon behar duenez, garrantzitsua da bertan eraginen duten sintesi-aldagaiak kontrolatzea. Horregatik, aitzinetik sintetizatutako nanogela eredu gisa hartuz, hainbat erreakzio-aldagairen efektuak aztertu dira, hala nola, hasarazle, gurutzatzaile eta egonkortzailearen kontzentrazioak, gurutzatzaile mota, eta funtzionalizazio ezberdinak.

Erabilitako hasarazle kantitateak partikulen tamainan eragin handia dauka emultsio polimerizazioan. Hori aintzat hartuz, lehenik eta behin, hasarazlearen kontzentrazioak duen eragina aztertu da. Espero bezala, hasarazle kantitatea handitzeak nanogel partikulen tamaina txikitzen duela ikusi da, baina pH-arekiko erantzunean ez da aldaketarik ikusi.

Gainera, jakina denez, poli(etilenglikol) (PEG) bidezko modifikazioak nanogelak egonkortzen ditu aglomerazioa ekidinez, eta opsonizaziotik babesten ditu, odol-zirkulazioan duten biziraupena luzatuz. Nanogelei PEGdun konposatuak eranstea bioaplikazioetarako onuragarria izan daitekeela kontuan hartuz, poli(etilenglikol metakrilato) (PEGMA) kantitate ezberdinak gehituz nanogel familia berri bat sintetizatu da. Aipagarria da, PEGilatuta ere, pH-aren eta tenperaturaren arabera bolumena aldaketak jasaten dituztela. Hala eta guztiz ere, PEGMA eransteak nanopartikulen hazte ahalmena txikitzen duela ondorioztatu da. Gisa berean, hidrofiloa izanik, PEGMAk trantsizio tenperatura igoarazten du eta kargak estaltzen dituenez, trantsizio pH-a pH azidoagoetara mugitzen du, indar elektrostatikoak ahultzen direlako.

Horrez gain, aukera zabalagoa edukitze aldera, gurutzatzaile mota ezberdinei erreparatu zaie. Erabilitako gurutzatzailearen arabera, bi nanogel familia bereiz daitezke. Alde batetik, biobateragarriak direla aprobetxatuz, etilenglikolean oinarritutako gurutzatzaileak [EGDMA eta poli(etilenglikol) diakrilatoa (PEGDA)] erabili dira eta bertze aldetik, disulfuroan oinarritutako gurutzatzaileak [*N,N'*-Bis(akriloil)zistamina (BAC) eta Bis(2-metakriloil)oxietil disulfuroa (DSDMA)]. Izan ere, disulfuro lotura zelulaz kanpoko eremu erreduzitzaileetan hausten ahal da, nanogelari propietate degradagarriak emanez. Honela, botikaren askatzearen gaineko kontrol handiagoa edukiko lukete nanogelek. Bidenabar, gurutzatzaile motak eta kontzentrazioak nanogelen bolumen-aldaketetan eta tamainan duten eragina ere ikertu da.

Lehenbiziko familiari dagokionez, PEGDArekin gurutzatutako nanogelak anitzez ere gehiago hazten direla egiaztatu da, EGDMA baino hidrofiloagoa delako eta gainera, talde erreaktiboen arteko luzera anitzez handiagoa delako PEGDAren kasuan. Halaber, EMN bidez nanogelen morfologia aztertu da eta barne-egiturarik heterogeneoena EGDMArekin

gurutzatutako nanogelek dutela ikusi da, gurutzatzaile honek baitu monomero nagusiarekin (DEAEMA) erreaktibitaterik handiena. Era berean, emaitza hauek kanpo-estimuluekiko bolumen-aldaketekin erlazionatuz, gehien hazten direnak morfologiarik homogeneoena duten nanogelak direla ondorioztatu da. Gurutzatzaile kontzentrazioaren igoera batek, berriz, nanogelak haztea zailtzen duela baieztatu da. Hala ere, gurutzatzaile kantitateak ez du kanpo-eragileekiko sentikortasunetan eragiten, erabilitako kontzentrazioan behinik behin.

Disulfuroan oinarritutako gurutzatzaileak erabili diren kasuan, hasarazle sistema optimizatu behar izan da lehendabizi, disulfuro taldeek ematen dituzten albo-erreakzioak direla eta. Erreakzio hauek gutxituta etekina igotzen ahal da. Horretarako, erredox-sistema bat erabili da hasarazle gisa, erreakzioak tenperatura baxuagoetan egiteko aukera ematen duelako. Horrela, sentikortasun anitza duten nanogel egonkorrak lortu dira. Kasu honetan ere, gurutzatzaile motak nanogelen haztean duen efektua aztertu da, gurutzatzaileen propietateetan eta nanogelen esperotako morfologian oinarrituz. Gurutzatzaile kantitateak hazte ahalmena esponentzialki txikitzen duela ikusi da, gainera.

Jakina denez, funtzionalizazioak ezaugarri berriez hornitzen ahal luke nanogela; adibidez, funtzionalizatuz gero, nanogela gai izanen litzateke botiken askatzea jomugara zuzentzeko edota proteinak geldiarazi, babestu eta askatzeko. Honen interesa aintzat hartuz, amina primario eta epoxido taldeekin funtzionalizatutako nanogelak ekoitzi dira. Funtzionalizatuta ere, pH-aren eta tenperaturaren aitzinean bolumena aldatzen zaiela egiaztatu da.

Nanogel sorta honek beharren arabera egokitzeko abagunea ematen du, kanpo-eragileen aitzinean era ezberdinetan erantzuten baitute. Halaber, parametro anitzen eragina ezagutzeak sintesi-bide espezifikoak diseinatzeko aukera zabaltzen du material arrakastatsuen garapenerako bidean.

Bertzalde, NPMak erantsi zaizkie aitzinetik ekoitzitako nanogelei, kanpo-eragileekiko sentikorrak diren MNG superparamagnetikoak erdietsiz. Guztira hiru MNG familia lortu dira, prestaketa baldintzak, eta NPM eta nanogel motak aldatuz. Lehenik, azido zitrikoz estalitako NPMak funtzionalizaziorik gabeko nanogel partikuletan barneratzea lortu da, negatiboki kargaturiko NPMen eta positiboki kargatutako nanogelen arteko indar elektrostatikoei esker. Erantzun magnetiko handia izateaz gain, MNGek pH-aren eta tenperaturaren aitzinean bolumen-aldaketa adierazgarriak ematen dituztela frogatu da. Gainera, NPMak barneratuta ere, pH-aren araberako termosentikortasuna agertzen dute.

NPMen eta kate polimerikoen arteko lotura indartzeko asmoz, azido zitrikoz estalitako NPMak amina primarioarekin funtzionalizatutako nanogelekin konbinatu dira, indar elektrostatikoez at, hidrogeno-loturak sortuz. Horrez gain, prestaketa baldintza leunagoak erabili direnez, partikula ez-organikoak hobeki atxiki dira. Lortutako MNGek pH-aren aitzinean bolumen-aldaketa jasaten dute eta erantzun magnetiko altua erakusten dute. Hori gutxi ez balitz, NPMak oraindik gehiago atxikitzeko asmoz, partikula magnetikoen karboxilo talde eta nanogelen amina primarioen artean amida lotura kobalenteak eratu dira. Gisa honetan ere izaera superparamagnetiko altuko MNGak lortu dira eta gainera, partikula ez-organikoen eta nanogelen arteko lotura sendotu da.

Hirugarren MNG familia, berriz, egonkortzailerik gabeko NPMak epoxido taldeekin funtzionalizatutako nanogeletan sartuz eratu da. Lehenik eta behin, Fourier Transform Infragorri Espektroskopia (FTIR) bidez, lotura kobalentea sortu dela baieztatu da. Ondotik, NPMak nola barneratu diren ikertu da. Prestaketan erabilitako pH-aren eragina aipagarria da; izan ere, pH 6-a erabiliz anitzez partikula magnetiko gehiago barneratzea lortu da, pH 3-arekin alderatuz. Ezberdintasun hau faktore anitzekin azaltzen ahal da. Alde batetik, NPMak hidrofiloagoak direnez, uretan hobeki dispertsatzen dira elkarrekintza erraztuz eta gainera, nukleofiloagoak direnez, erreakzionatzeko joera handiagoa dute. Bertze aldetik, pH 6-ean NPMen eta nanogelen arteko aldarapen elektrostatikoak ahulagoak dira, eta hidrogeno-lotura indartsuagoak osatzen ahal dira, pH 3-ko egoerarekin konparatuta. Hau guztia dela eta, pH 6-a erabiliz, erantzun magnetiko eta egonkortasun altuagoko MNGak erdietsi dira. MNG familia honetan ere NPMak sendo lotuta daude, lotura kobalenteari eta interakzio hidrofiloei esker. Erantzun magnetiko hagitz altua izateaz gain, MNG hauek pH-aren aitzinean bolumen aldaketa ematen dute.

Azkenik, aplikazio bioteknologikoei dagokienez, erdietsitako nanogelak farmakoen garraiatzaile gisa erabil daitezkeenetz ikertu da. Horretarako, PDEAEMAn oinarritutako bi nanogel aukeratu dira, PEGMArik gabekoa bata eta PEGMAduna bertzea. Botika gisa, doxorubizina (DOXO) hautatu da, minbizia mota batzuen aurkako medikamenturik eraginkorrena delako. Beraien egitura porotsuari esker, nanogelak DOXO kantitate handiak hartzeko gai direla ikusi da, erabilitako prozedura hagitz eraginkorra dela egiaztatzearekin batera. Nanogel partikulak hazita egoteak DOXO botika barneratzea laguntzen du, eta indar hidrofilo eta hidrofoboen eraginez egonkortzen da behin nanogelen barrenean dagoela. Gainera, partikulek zelulen hazkuntza-ingurunean dauden osagai biologikoekin izan ditzaketen

elkarrekintzak kontuan hartu behar dira. Errate baterako, nanopartikulak odolarekin kontaktuan daudenean, plasmako proteinak azkar absorba daitezkeela ikusi izan da. Hori dela eta, behi-fetuaren seruma erabili da DOXOz betetako nanogelen egonkortasuna aztertzeko. Bi pH ezberdin erabili dira: 5,2-a (zelula gaixoak antzeratuz) eta 7,4-a (zeluloa osasuntsuak imitatuz). Nanogelak pH 5,2-an pH fisiologikoan (pH 7,4) baino egonkorragoak direla egiaztatu da, hain segur, behi-serumeko albumina (behi-fetuaren serumeko osagai nagusia) ez delako hainbertze atxikitzen nanogelen gainazalera eta kargatutako kate polimerikoen arteko aldarapen elektrostatikoek ematen duten egonkortasunagatik ere bai.

Behin nanogelen barrenean sartuta, pH 5,2-an botikaren askatzea ikertu da, endosomak, lisosomak eta zelula gaixoak antzeratuz, eta pH 7,4-an zelula osasuntsuak eta odola imitatuz. Ondotik, askatzearen mekanismoa hobeki ulertu ahal izateko, Peppas Sahlin eredura doitu dira lortutako kurbak. DOXO difusio bidez eta era kontrolatu batean askatzen dela egiaztatzeaz gain, baldintza azidoetan sendagaia azkarrago askatzen dela frogatu da. Emaitza hau nanogelen pH-arekiko sentikortasunari dagokio; izan ere, nanogelak pH azidoetan puztu egiten dira, barrenean dagoen medikamentuaren askatzea erraztuz. Honek minbiziaren aurkako borrokan nanogel hauek eduki dezaketen garrantzia azpimarratzen du, botika ehun eta zelula gaixoetan azkarrago askatuko bailukete.

Honetaz gain, zelulak nanogelak absorbatzeko gai direla eta sendagaia pixkanaka zelularen nukleora askatzen dela balioztatu da espektrofluorimetria bidez. Hondarrean, nanogelen zitobateragarritasuna aztertu da HeLa (utero-lepoko minbizia) zelulak erabiliz. Hala, nanogel bakoitzaren kontzentrazio tarte erabilgarria zein den ikasi da. Harrigarria bada ere, PEGilatu gabeko nanogelak zitotoxikotasun baxuagoa agertu du.

Bertze aldetik, material berrien segurtasuna eta eraginkortasuna ziurtatu behar da bioaplikazioetan erabilgarriak izan daitezen. Nanopartikulek anitzetan odol-zeluletan ondorio fisiologikoak eragiten dituztela gogoan hartuz, lan honetan, MNGen eta odol-zelulen arteko elkarrekintzak ikertu dira mikroskopio bidez. MNGak odolarekin inkubatu aitzinetik, odol laginak dispertsio ingurune ezberdinak erabiliz prestatu dira. Alde batetik, plasma autologoa globulu gorriak eta plaketak MNGengandik babesteko gai dela egiaztatu da, edozein eragin kaltegarri ekidinez. Alabaina, serum fisiologikoarekin odola garbitu eta plasma isolatutakoan, MNGak globulu gorrietara itsatsi direla eta hemolisia gertatu dela ikusi da, beraien erabilgarritasun klinikoa galaraziz. Dena den, plasmari esker MNGak odol zelulekin bateragarriak direla erran daiteke.

Laburbilduz, alde batetik, minbiziaren aurkako botika garraiatzeko eta zeluletan askatzeko gai diren nanogel biobateragarriak erdietsi dira. Bertzalde, kanpo-estimuluekiko sentikorrak diren nanogel magnetikoak lortu dira. Gainera, azken hauek odol-zelulengan ez dutela ondorio negatiborik eragiten ikusi da.